AD-A182 949 FATIGUE BEHAVIOR OF LONG AND SHORT CRACKS IN ALUMINUM ALLOYS..(U) CALIFORNIA UNIV BERKELEY DEPT OF MATERIALS SCIENCE AND MINERA.. R O RITCHIE ET AL. 01 MAY 87 1/3

UNCLASSIFIED UCB/RP/87/A1047 AFOSR-TR-87-0072 F/G 11/6.1 NL

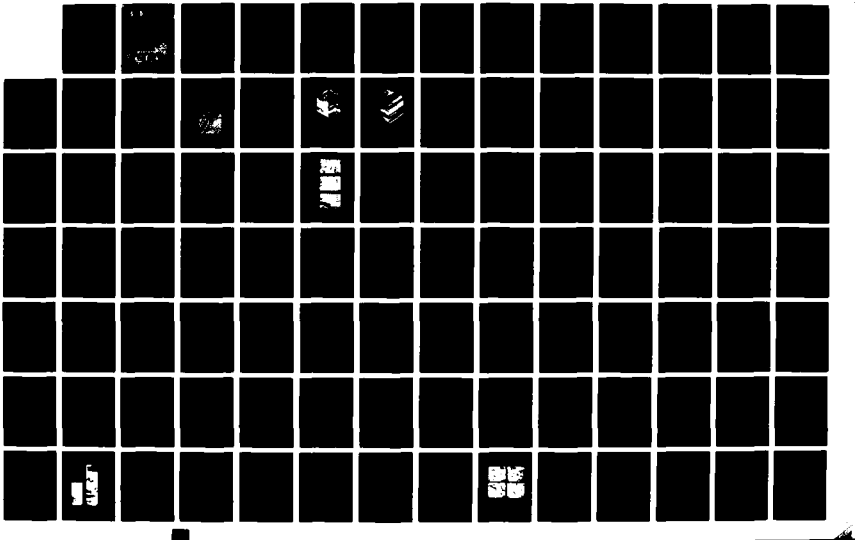

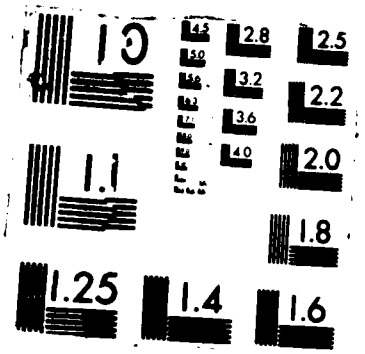
1.0
1.1
1.25
1.4
1.6
1.8
2.0
2.2
2.5
2.8
3.2
3.6
4.0
4.5
5.0
5.6

AFOSR-TR- 87-0872

Final Report
to
U.S. Air Force Office of Scientific Research

on

FATIGUE BEHAVIOR OF LONG AND SHORT CRACKS IN ALUMINUM ALLOYS

Grant AFOSR-82-0181

for period 15 April 1984 to 14 April 1987

by
R. O. Ritchie and W. Yu

May 1987

Report No. UCB/RP/87/A1047

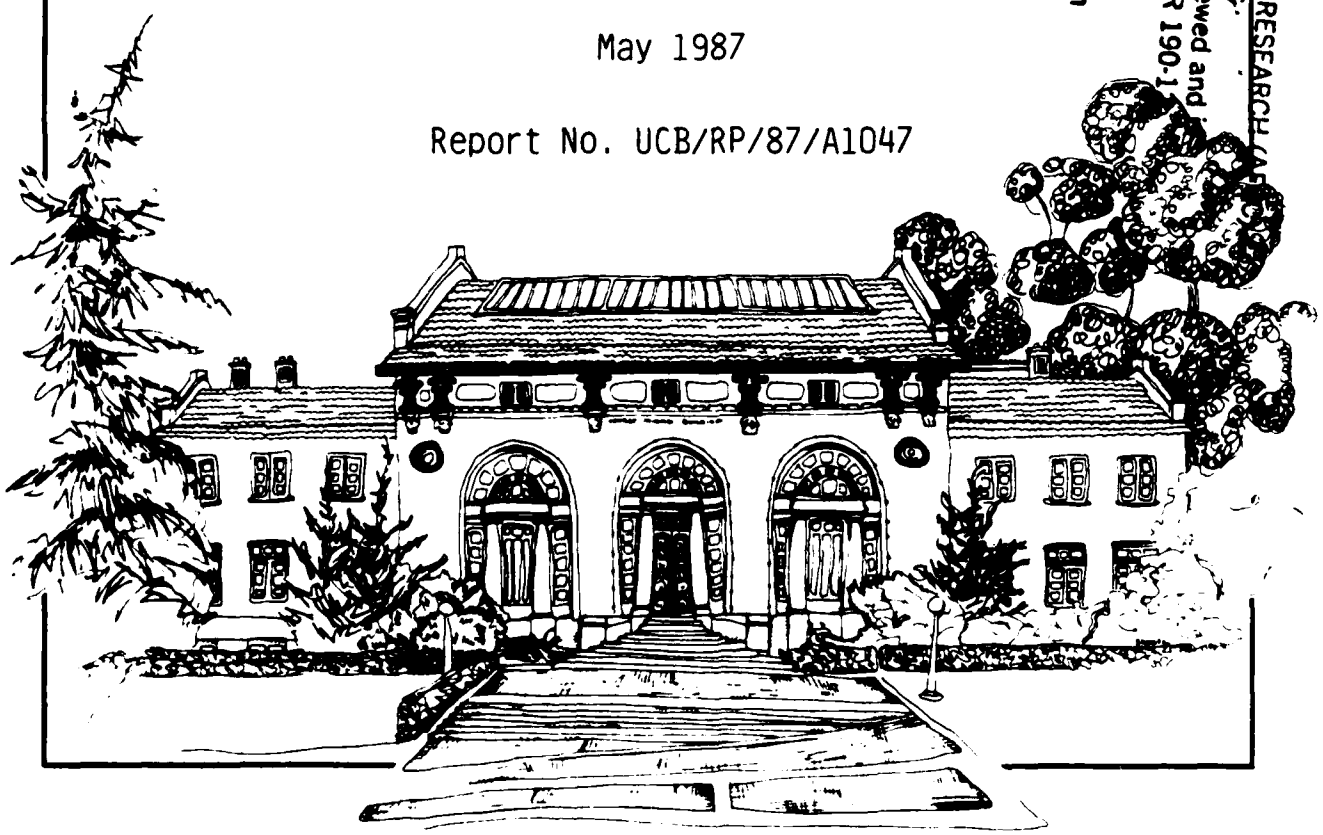

Department of Materials Science and Mineral Engineering
University of California, Berkeley, CA 94720

UNCLASSIFIED

SECURITY CLASSIFICATION OF THIS PAGE

REPORT DOCUMENTATION PAGE

1a. REPORT SECURITY CLASSIFICATION Unclassified	1b. RESTRICTIVE MARKINGS None
2a. SECURITY CLASSIFICATION AUTHORITY Not Applicable	3. DISTRIBUTION/AVAILABILITY OF REPORT Not Applicable Approved for public release; distribution unlimited.
2b. DECLASSIFICATION/DOWNGRADING SCHEDULE Not Applicable	
4. PERFORMING ORGANIZATION REPORT NUMBER(S) UCB/RP/87/A1047	5. MONITORING ORGANIZATION REPORT NUMBER(S) AFOSR-TR- 87-0872
6a. NAME OF PERFORMING ORGANIZATION Robert O. Ritchie, Dept. of Mat. Sci. & Minl. Eng.	6b. OFFICE SYMBOL (If applicable)
7a. NAME OF MONITORING ORGANIZATION Air Force Office of Scientific Research AFOSR/NE	
6c. ADDRESS (City, State, and ZIP Code) University of California Hearst Mining Building Berkeley, California 94720	7b. ADDRESS (City, State, and ZIP Code) Bldg. 410, Bolling AFB Washington, D.C. 20322 ATTN: Dr. A. H. Rosenstein, AFOSR/NE
8a. NAME OF FUNDING/SPONSORING ORGANIZATION Same as 7a	8b. OFFICE SYMBOL (If applicable) NE
9. PROCUREMENT INSTRUMENT IDENTIFICATION NUMBER AFOSR-82-0181	
8c. ADDRESS (City, State, and ZIP Code) Same as 7b	10. SOURCE OF FUNDING NUMBERS PROGRAM ELEMENT NO. 61102F; PROJECT NO. 2306; TASK NO. A1; WORK UNIT ACCESSION NO.

11. TITLE (Include Security Classification)
FATIGUE BEHAVIOR OF LONG AND SHORT CRACKS IN ALUMINUM ALLOYS
(Unclassified)

12. PERSONAL AUTHOR(S)
RITCHIE, Robert O. and YU, Weikang

13a. TYPE OF REPORT	13b. TIME COVERED	14. DATE OF REPORT (Year, Month, Day)	15. PAGE COUNT
Annual Final	FROM 84/4/15 TO 87/4/14	1987 May 1	

16. SUPPLEMENTARY NOTATION

(Key words)

17. COSATI CODES			18. SUBJECT TERMS (Continue on reverse if necessary and identify by block number)
FIELD	GROUP	SUB-GROUP	Fatigue; Defect-tolerant fatigue design; Variable amplitude loading; Fatigue in aluminum alloys; Fatigue behavior of long and short cracks; Fatigue cracks: crack closure

19. ABSTRACT (Continue on reverse if necessary and identify by block number)

The fatigue behavior of short cracks, which are small compared to the scale of the microstructure, small compared to the scale of local plasticity or simply physically small (i.e., $\lesssim$1 mm), must be considered as one of the major factors limiting the application of defect-tolerant fatigue design for airframe and engine components. Accordingly, this program was aimed at identifying factors which govern the growth of such short cracks (in contrast to long cracks) in a series of commercial aluminum alloys, with specific reference to behavior at near-threshold levels (below $\sim 10^{-9}$ m/cycle).

Based on experiments in 2124, 7150 and 2090 alloys, it is shown that whereas the behavior of long ($\gtrsim$ 10 mm) cracks at near-threshold levels is largely controlled by the magnitude of the crack tip shielding from crack closure and deflection mechanisms, short crack growth rates are invariably faster because of their inability to develop shielding

20. DISTRIBUTION/AVAILABILITY OF ABSTRACT	21. ABSTRACT SECURITY CLASSIFICATION
☒ UNCLASSIFIED/UNLIMITED ☐ SAME AS RPT. ☐ DTIC USERS	Unclassified
22a. NAME OF RESPONSIBLE INDIVIDUAL ~~Robert O. Ritchie~~ Dr Witmer 202-767 4984	22b. TELEPHONE (Include Area Code) ~~(415) 642-0417~~	22c. OFFICE SYMBOL NE

DD FORM 1473, 84 MAR 83 APR edition may be used until exhausted. All other editions are obsolete.

SECURITY CLASSIFICATION OF THIS PAGE
Unclassified

due to their limited wake. Experiments whereby the wake material is physically removed confirm such notions and indicate that the predominant closure forces are located close (within 500 μm) of the tip. Analogous experiments involving periodic compression overloads are similarly employed to reduce near-tip crack closure (by the crushing of asperities). Due to the reduction of shielding, crack growth at the threshold is then observed following the compression cycle. Materials, such as 2090-T8E41 aluminum-lithium alloy, are particularly prone to such compression-induced crack growth as their shielding mechanisms are largely derived through the wedging of asperities. Studies on through-thickness physically short (50 to 400 μm) and small (10 to 400 μm) surface cracks indicate growth at nominal stress intensities at, and below, the threshold ΔK_{TH}. Short crack growth rates are observed to decay progressively until arrest (or before merging with long crack data), concurrent with measured changes in crack closure and hence the near-tip "driving force" ΔK_{eff}. Numerical predictions of such closure (in both plane stress and plane strain) are shown to underpredict consistently measured values, as the actual sources of shielding involve closure from oxide and asperity wedging in addition to the plasticity-induced mechanism. It is concluded that the near-threshold behavior of small cracks is strongly influenced by considerations of crack tip shielding, specifically from crack deflection and crack closure mechanisms. Other factors responsible for "anomalous" small crack behavior, however, can be identified depending upon the "type" of small flaw involved, and are discussed in this report.

Final Report

to

U.S. Air Force Office of Scientific Research

on

FATIGUE BEHAVIOR OF LONG AND SHORT CRACKS IN ALUMINUM ALLOYS

Grant AFOSR-82-0181

for period 15 April 1984 to 14 April 1987

submitted to

U.S. Air Force Office of Scientific Research
Building 410, Bolling Air Force Base
Washington, D.C. 20322
Attention: Dr. Alan H. Rosenstein

submitted by

R. O. Ritchie and W. Yu
Department of Materials Science
and Mineral Engineering
University of California
Berkeley, California 94720

May 1987

TABLE OF CONTENTS

FATIGUE BEHAVIOR OF LONG AND SHORT CRACKS IN ALUMINUM ALLOYS

R. O. Ritchie

(Grant No. AFOSR-82-0181)

FORWARD

This manuscript constitutes the Final Report on Grant No. AFOSR-82-0181, administered by the U.S. Air Force Office of Scientific Research, with Dr. Alan H. Rosenstein as program manager. The work, covering the period April 15, 1984, through April 14, 1987, was performed under the direction of Dr. R. O. Ritchie, Professor of Materials Science, University of California in Berkeley, with Dr. W. Yu as Research Engineer, and E. Zaiken and J. Miwa as graduate students.

ABSTRACT

The fatigue behavior of short cracks, which are small compared to the scale of the microstructure, small compared to the scale of local plasticity or simply physically small (i.e., $\lesssim$ 1 mm), must be considered as one of the major factors limiting the application of defect-tolerant fatigue design for airframe and engine components. Accordingly, this program was aimed at identifying factors which govern the growth of such short cracks (in contrast to long cracks) in a series of commercial aluminum alloys, with specific reference to behavior at near-threshold levels (below $\sim 10^{-9}$ m/cycle).

Based on experiments in 2124, 7150 and 2090 alloys, it is shown that whereas the behavior of long ($\gtrsim$ 10 mm) cracks at near-threshold levels is largely controlled by the magnitude of the crack tip shielding from crack closure and deflection mechanisms, short crack growth rates are invariably faster because of their inability to develop shielding due to their limited wake. Experiments whereby the wake material is physically removed confirm such notions and indicate that the predominant closure forces are located close (within 500 μm) of the tip. Analogous experiments involving periodic compression overloads are similarly employed to reduce near-tip crack closure (by the crushing of asperities). Due to the reduction of shielding, crack growth at the threshold is then observed following the compression cycle. Materials, such as 2090-T8E41 aluminum-lithium alloy, are particularly prone to such compression-induced crack growth as their shielding mechanisms are largely derived through the wedging of asperities. Studies on through-thickness physically short (50 to 400 μm) and small (10 to 400 μm)

surface cracks indicate growth at nominal stress intensities at, and below, the threshold ΔK_{TH}. Short crack growth rates are observed to decay progressively until arrest (or before merging with long crack data), concurrent with measured changes in crack closure and hence the near-tip "driving force" ΔK_{eff}. Numerical predictions of such closure (in both plane stress and plane strain) are shown to underpredict consistently measured values, as the actual sources of shielding involve closure from oxide and asperity wedging in addition to the plasticity-induced mechanism. It is concluded that the near-threshold behavior of small cracks is strongly influenced by considerations of crack tip shielding, specifically from crack deflection and crack closure mechanisms. Other factors responsible for "anomalous" small crack behavior, however, can be identified depending upon the "type" of small flaw involved, and are discussed in this report.

1. INTRODUCTION

The objective of this program was to identify mechanical, microstructural and environmental factors governing the fatigue crack growth of long ($\gtrsim$ 10 mm) and short ($\lesssim$ 1 mm) cracks in commercial aluminum alloys with specific reference to behavior at ultralow, near-threshold growth rates below typically 10^{-9} m/cycle. This report describes several projects, specifically involving a review of the "small crack" problem, its origins and implications, the role of microstructure in influencing fatigue crack growth and closure behavior in 7150 alloy, the development of crack closure with crack size for long and short cracks in 2124 and 7150, the role of crack tip shielding on large and small (10 to 400 μm), through-thickness and surface cracks in 2124, and the influence of periodic compression overload cycles on such properties in 2124, 7150 and aluminum-lithium alloy 2090. Based on these results, an overall assessment of the small crack problem is presented, and suggestions are made for its potential solution, both with respect to defect-tolerant life prediction and alloy design.

2. REVIEW OF SMALL CRACK BEHAVIOR

2.1 Introduction

Despite an increasing interest, both academically and technologically, in conventional long crack fatigue crack propagation, particularly at near-threshold levels (e.g., ref. 1), a major limitation in the application of such information to defect-tolerant design must be regarded as the problem of short flaws. By short flaws, it is implied

that flaws are i) small compared with the scale of microstructure, ii) small compared with the scale of local plasticity, or iii) simply physically small (i.e., $\lesssim$ 0.5 to 1 mm). Design codes at present attempt to predict the growth rates of in-service flaws based on data collected in the laboratory with specimens containing crack sizes of the order of 25 mm. In service, however, initial defects sizes are often far smaller than this. This leads to a potential for non-conservative defect-tolerant lifetime predictions since the vast majority of experimental observations[2-20] on the behavior of short cracks has shown that their growth rates are in excess of long cracks at the same nominal driving force (e.g., at the same stress intensity range ΔK) and furthermore that such short cracks can initiate and propagate at ΔK levels **below** the "long crack" fatigue threshold ΔK_{TH} (Fig. 2.1).

During this study, extensive reviews of all aspects of the small crack problem have been performed,[19] including the environmental behavior of small fatigue cracks.[20] Papers published on these reviews are appended to this report. For completeness, summaries are presented below.

2.2 Propagation of Short Fatigue Cracks[19]

Fatigue crack propagation in engineering materials has been the subject of considerable research, and extensive review articles have appeared over the past several years. Most of these investigations focused on the behavior of 'long' fatigue cracks, even though the characteristics associated with the extension of small cracks in metals and alloys remain relatively unexplored, despite their unquestionable importance from an engineering standpoint. In the review, the mechanics

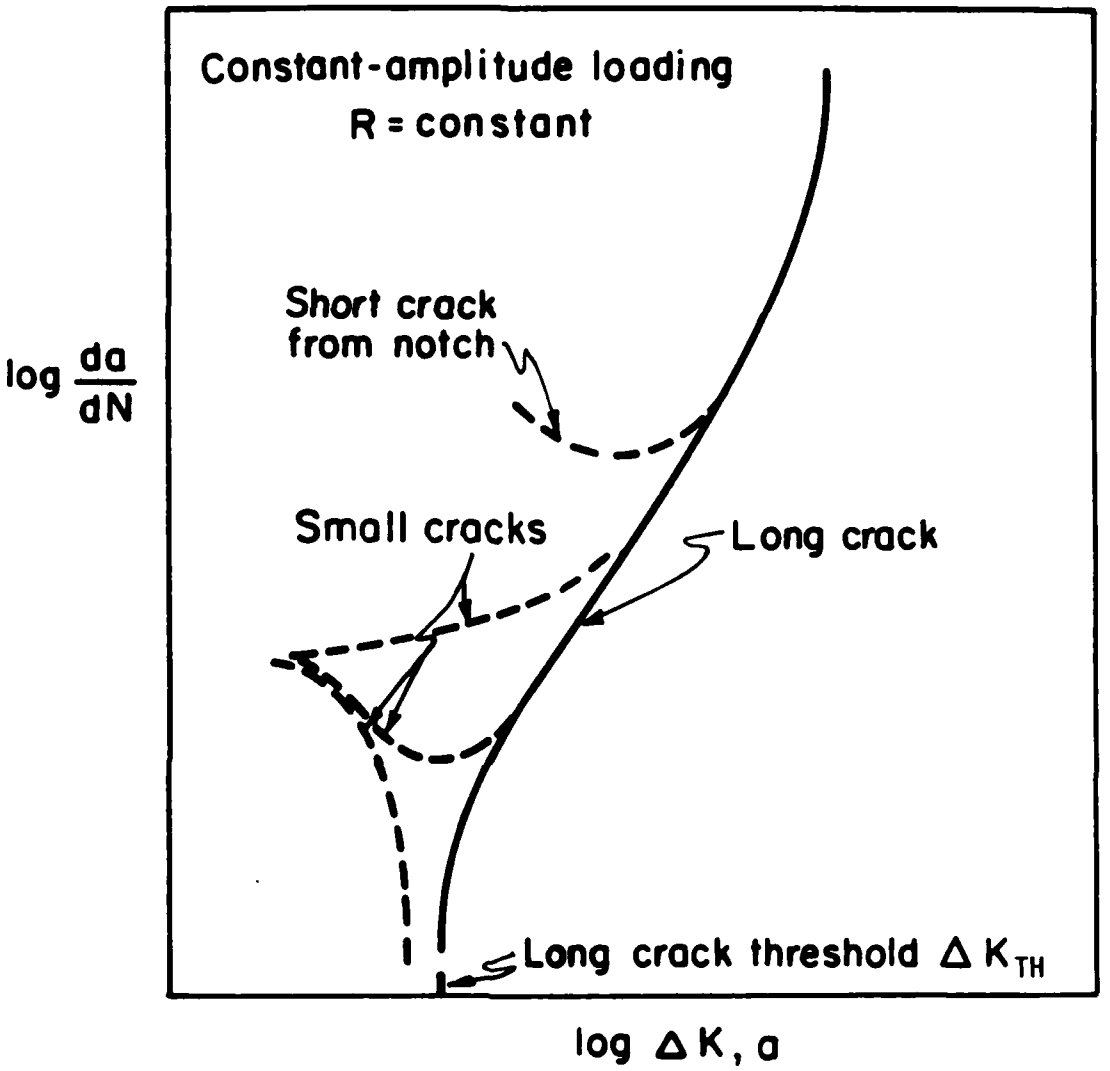

Fig. 2.1: Schematic representation of the typical variation in fatigue crack growth rates da/dN, with the nominal cyclic stress intensity factor ΔK, or crack length a, for "long" and "small" cracks. ΔK_{TH} is the nominal threshold stress intensity range below which long cracks remain dormant.

and micromechanisms of the subcritical growth of small fatigue cracks are examined, and aspects of their propagation behavior are contrasted with those of long cracks in terms of fracture mechanics, microstructure, and environment. Cracks are defined as being small i) when their size is small compared to relevant microstructural dimensions (a continuum mechanics limitation), ii) when their length is small compared to the scale of local plasticity (a linear elastic fracture mechanics limitation), or iii) when they are simply physically small (e.g., $\lesssim$ 0.5-1 mm). Since all three types of small flaw are known to propagate faster than (or at least at the same rate as) corresponding long fatigue cracks subjected to the same **nominal** driving force, current defect tolerant fatigue design procedures which utilize long crack data can, in certain applications, result in overestimates of lifetimes. The characteristics of the small crack problem are critically reviewed in the light of the influences of local plasticity, microstructure, crack tip environment, growth mechanisms, crack driving force, and the premature closure of the crack.

2.3 Environmental Effects Novel to the Propagation of Short Fatigue Cracks

Crack size and opening morphology dominate the mechanical and chemical driving forces for fatigue propagation in embrittling environments. Similitude based on a crack tip field parameter is compromised, particularly for small cracks ($\lesssim$ 5 mm) which grow up to several orders of magnitude faster than projected and below apparent threshold conditions. Environment sensitive mechanical and chemical mechanisms which govern the growth of small cracks are reviewed. For the

former the retarding effect of crack closure; originating from wake plasticity, surface roughness, deflection, corrosion debris or fluid pressure; increases with increasing crack size particularly within the near threshold regime. Data for high strength steel in H_2 demonstrate the importance of such mechanisms, however, precise models of crack size dependencies and systematic closure measurements are lacking. Considering the chemical driving force, the embrittling activity of the occluded crack differs from that of the bulk environment, and is geometry dependent. The deleterious influence of small crack size is demonstrated experimentally for steels in aqueous chloride solutions, and related quantitatively to crack opening shape and size effects on diffusion, convective mixing and electrochemical reaction. Small crack size promotes hydrogen embrittlement due to enhanced hydrolytic acidification and reduced oxygen inhibition. Chemical crack size effects are material and environment specific; criteria defining limiting crack sizes and opening shapes for K or J-based similitude do not exist.

3. EXPERIMENTAL PROCEDURES AND MATERIALS

3.1 Materials

The following commercial wrought aluminum alloys, namely 7150, 2024, 2124, and lithium-containing 2090, were obtained from ALCOA in the solution treated, quenched and stretched (2%) conditions. Nominal chemical compositions are shown below in Table 3.1. All alloys were received in the form of 25 mm thick plate, except the 2090 which was 13 mm plate.

Table 3.1: Nominal Chemical Compositions in wt% of Alloys

	Si	Fe	Cu	Li	Mn	Mg	Cr	Zn	Ti	Zr	Al
2024	0.50	0.50	4.50	--	0.50	1.50	0.10	0.25	0.15	--	balance
2124	0.20	0.30	4.50	--	0.50	1.50	0.10	0.25	0.15	--	balance
7150	0.07	0.11	2.10	--	--	2.16	--	6.16	0.02	0.13	balance
2090	0.12	0.10	2.70	2.20	0.05	0.25	--	--	0.15	0.12	balance

Fatigue tests were performed on 6.4 mm thick compact C(T) test-pieces, heat-treated in the 2124 and 7150 alloys to yield peak-aged (PA) microstructures and underaged (UA) and overaged (OA) microstructures at the same approximate yield strength. The rationale for this was to examine, at constant yield strength, the influence of different plastic flow mechanisms, i.e., underaged (i.e., T3) structures are associated primarily with deformation via planar slip due to the coherent nature of the hardening precipitates whereas overaged (i.e., T7) structures are associated with a more homogeneous wavy slip from incoherent particle hardening mechanisms.

Specific heat treatment schedules and room temperature mechanical properties are listed in Tables 3.2 and 3.3, respectively. The nature of these microstructures has been discussed elsewhere.[21] Briefly, in the 7150 alloy, underaged structures were characterized by coherent GP zones ($\sim$ 4-8 nm diameter), which were replaced in the T6 condition by semi-coherent η' precipitates (Fig. 3.1). T7 structures were hardened by coarsened η' in the matrix and by predominately incoherent η precipitates in both matrix and grain boundaries, the latter resulting in small precipitate-free-zones ($\sim$ 30 nm half width), as shown in Fig. 3.1c. Grains were pancake-shaped with an approximate size of 15 by 5 μm.

Table 3.2: Heat-Treatments Utilized

	7150 Alloy	2024 and 2124 Alloys
Underaged	ST* + 1½ hr at 121°C	ST* + naturally aged (ambient)
Peak Aged	ST* + 100 hr at 121°C	ST* + 12 hr at 190°C
Overaged	ST* + 24 hr at 121°C + 40 hr at 163°C	ST* + 48 hr at 190°C

*ST = solution treated, stretched 2%

Table 3.3: Room Temperature Mechanical Properties of Alloys Tested

	Yield Strength (MPa)	U.T.S. (MPa)	Elong.* (%)	Redn. Area (%)	Work Hardening Exponent
7150					
Underaged	371	485	6.8	12.1	0.055
Peak Aged (T6)	404	480	6.0	10.3	0.046
Overaged (T7)	372	478	7.1	12.5	0.058
2024					
Underaged (T351)	360	471	17.6	24.3	-
Peak Aged (T851)	432	473	8.4	22.6	-
Overaged	340	471	9.0	22.8	-
2124					
Underaged (T351)	360	488	17.8	26.7	-
Peak Aged (T851)	447	479	10.0	23.3	-
Overaged	370	440	10.2	21.9	-
2090					
Peak Aged (T851)	535	565	11.0	-	-

*On 25 mm gauge length

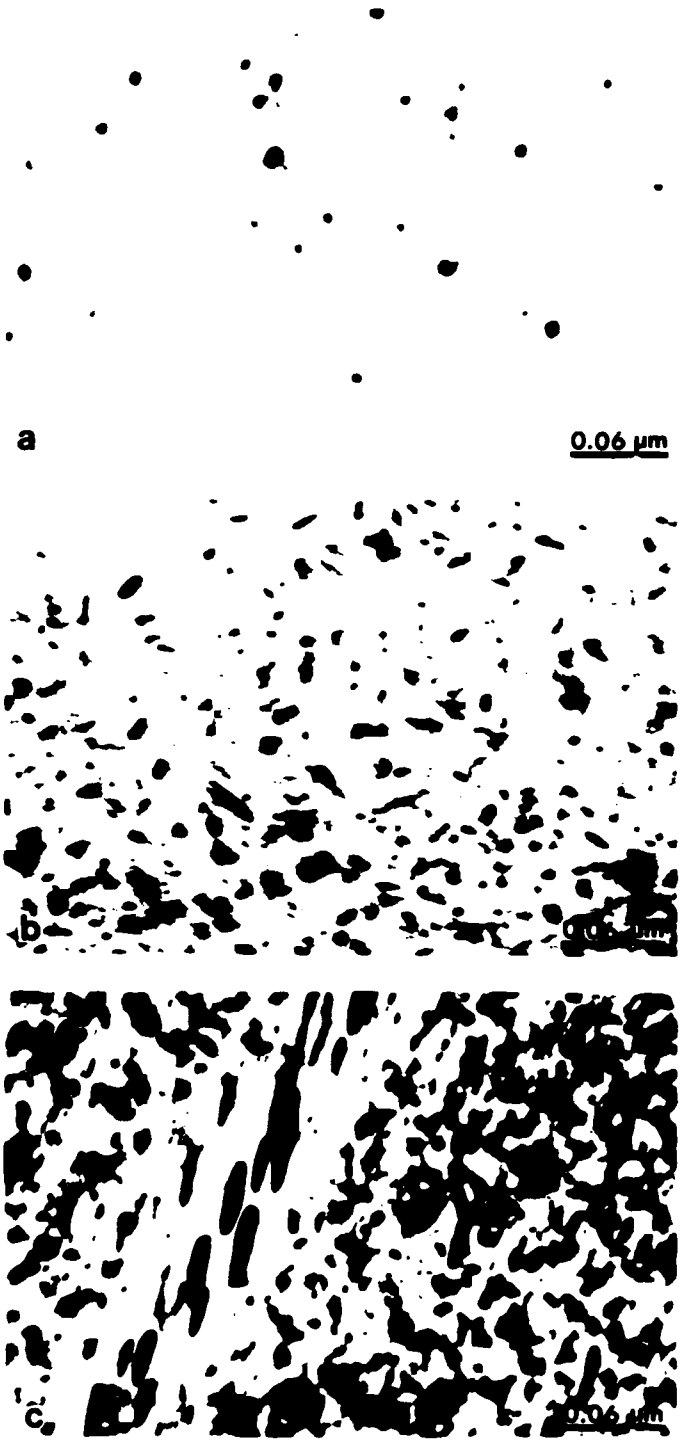

Fig. 3.1: Transmission electron micrographs of a) underaged, b) peak aged (T6) and c) overaged (T7) I/M 7150 aluminum alloy.

In the 2124 and 2024 alloys, in addition to the widely distributed second phase inclusions, the naturally aged (underaged) structures were also strengthened by G-P zones. At the peak aged condition, the major strengthening particles include the Al-Cu θ" and the magnesium-containing S' phase, both semi-coherent. The overaged structures were characterized by the formation of incoherent θ' and θ phases in the matrix and, most noticeably, along the grain boundaries. The precipitate-free zones were readily found. The grains were pancake shaped with an approximate diameter of 350 μm and thickness of 50 μm (Fig. 3.2). Corresponding heat-treatments and mechanical properties for 2024 and 2124 alloys also are listed in Tables 3.2 and 3.3.

In addition, specimens were taken from a plate of commercial lithium-containing aluminum alloy 2090. The material was furnished by ACLOA in the T8-E41 condition. The alloy was hot-rolled to a thickness of 13 mm, solution treated at 549°C, water quenched, and stretched $\sim$ 6% prior to aging 24 hr at 163°C. The chemical composition of 2090 is listed in Table 3.1; mechanical properties (longitudinal orientation) are listed in Table 3.3.

The microstructure of 2090 consisted of large, unrecrystallized grains with planar, elongated shape (Fig. 3.3). Grains were of approximate size 20 μm thick in the short direction, 500 μm wide in the transverse direction, and a few millimeters long in the rolling direction. The microstructure of 2090 has been characterized by Rioja and Ludwiczak.[22] They note that the alloy contains four metastable phases, δ', β', T_1', and T_2', which are thought to be percursors to the equilibrium β, T_1, and T_2 phases. The δ' phase (Al_3Li) normally exists

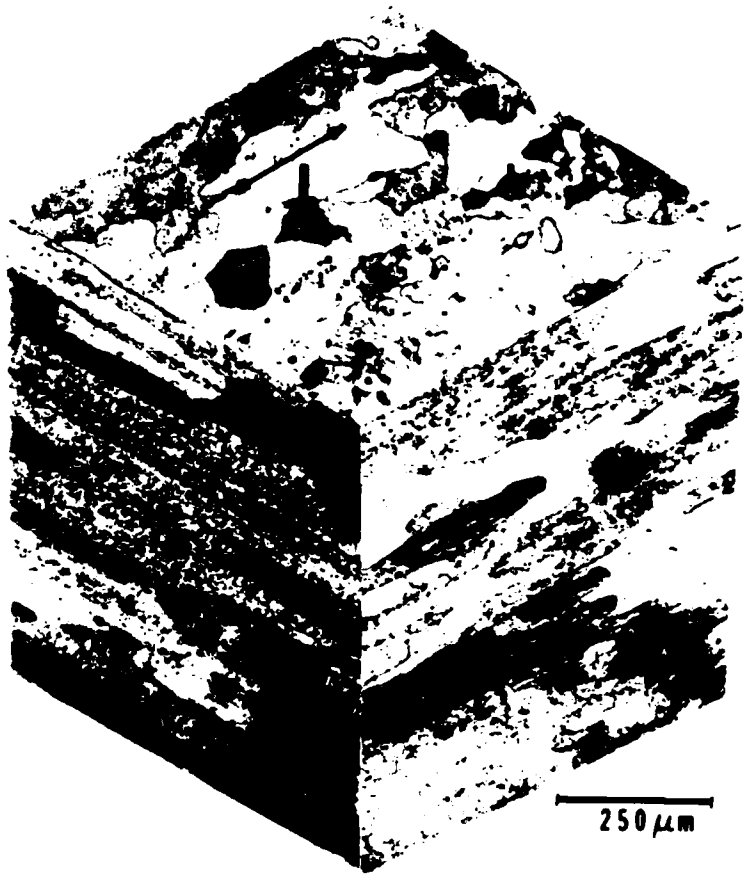

Fig. 3.2: Three-dimensional grain structure of aluminum alloy 2125-T351 (Keller's reagent etch).

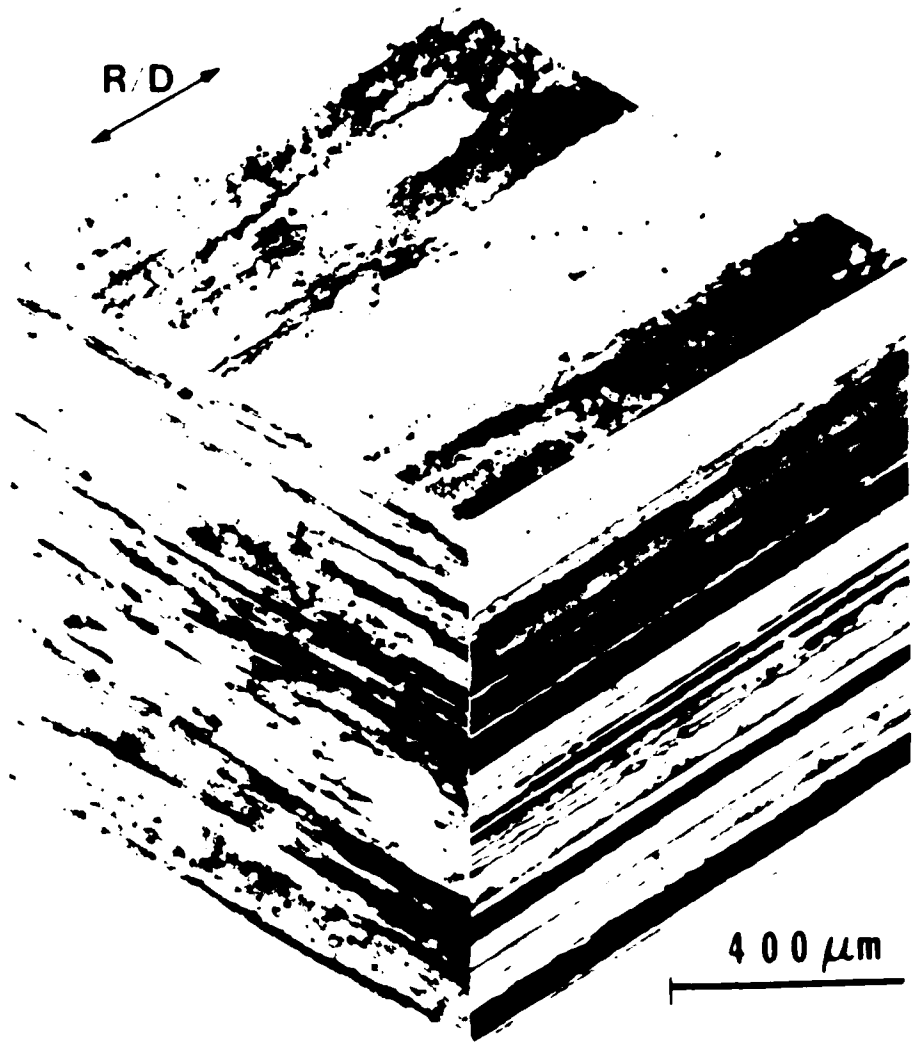

Fig. 3.3: Three-dimensional optical micrograph showing the grain structure of aluminum-lithium alloy 2090-T8E41 (Keller's reagent etch).

as spherical precipitates, but small precipitates can also wet the surfaces of the β' (Al_3Zr) and T_1' (Al_5CuLi_3) phases. It is thought that the δ' phase is responsible for the strongly-directional mechanical properties of this alloy.

3.2 Test Procedures

To obtain a comparison between long and short crack near-threshold behavior and to demonstrate experimentally that the anomalous behavior of through-thickness short cracks results from a lesser effect of closure in the wake of the crack tip, the "3-in-1" test specimen/procedure was utilized, shown schematically in Fig. 3.4.

Starting with a conventional 1-T compact C(T) test-piece, 6.4 mm thick, long crack threshold tests were performed at 50 Hz using standard load shedding procedures to determine the near-threshold crack growth behavior and the value of the fatigue threshold range ΔK_{TH} for long cracks[1] (A). To demonstrate the effect of closure in the wake of the crack tip, two procedures were then adopted for the long crack arrested at ΔK_{TH}. In certain specimens, material was machined away behind the crack tip to "remove" closure in the wake.[23,24] Conversely, closure was "removed" by applying a single compression overload.[25-27] In either case, following such procedures, the subsequent growth of the formerly arrested long crack was monitored, under nominally constant ΔK conditions, until closure re-developed with increase in crack length to approach crack arrest (B). The third stage of the test was then to carefully machine away the majority of the test-piece to leave a (two-dimensionally) small crack in a strip of metal (C), which was then tested

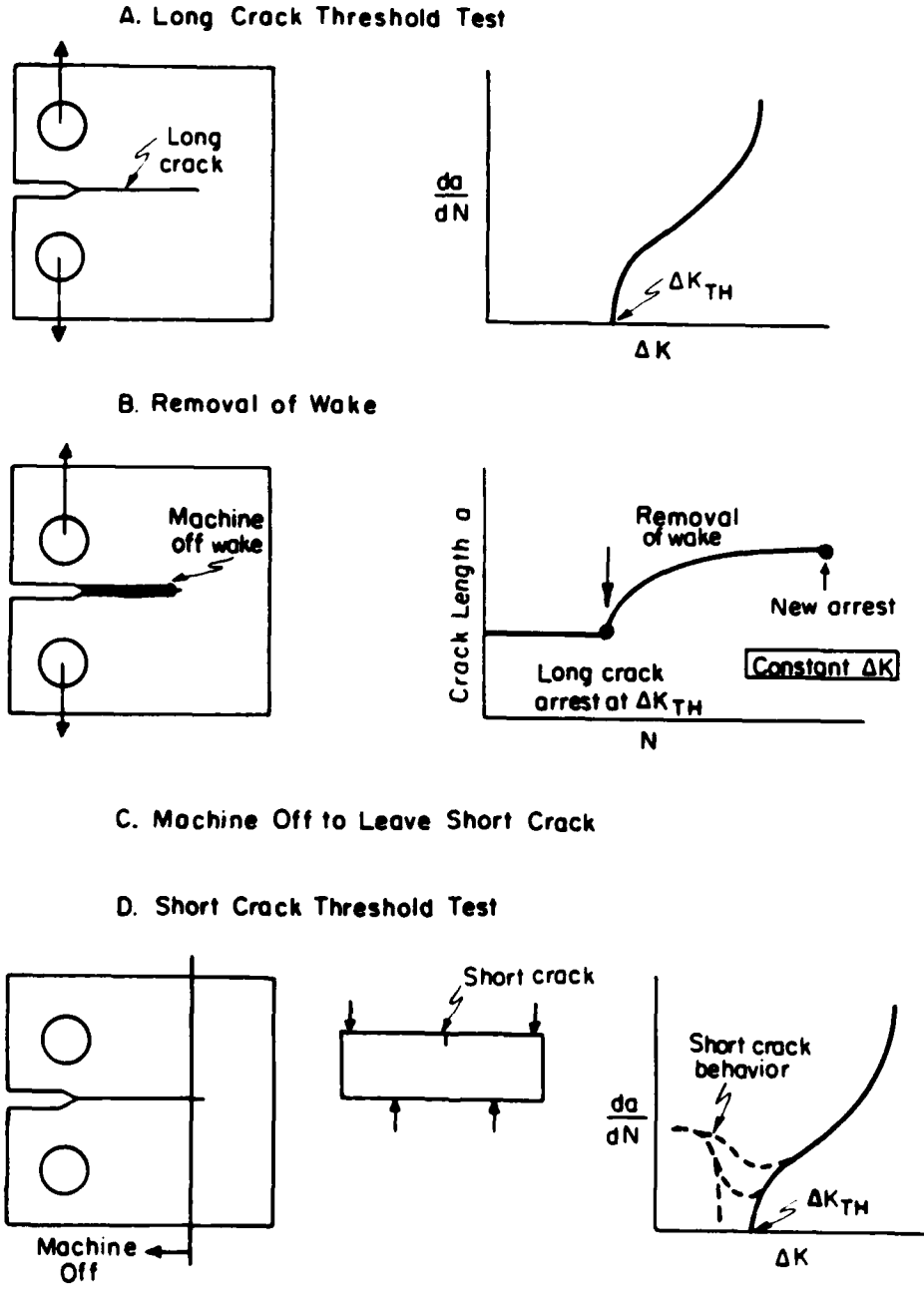

Fig. 3.4: Test geometries, procedures, and expected results for the "3-in-1" specimen developed to experimentally demonstrate the role of closure and the differences between long and short crack behavior.

in four-point bend to investigate near- (and sub-) threshold short crack behavior (D).[28]

In addition, tests were performed to examine the behavior of naturally-occurring (three-dimensional) small surface cracks, using replication techniques. The replication was performed with cellulose acetate tape and acetone on the top (tensile) surface of rectangular bend specimens (64 mm x 13 mm x 6.4 mm), tested in four-point bending. Tests were carried out at a load ratio of R = 0.1 such that the maximum stress due to bending was 0.9 times the yield stress of the material. Prior to testing, specimens were metallographically polished and etched to reveal the grain structure.

3.3 In-Situ Crack Closure Measurements

Despite the widespread adoption of the concept of fatigue crack closure, there remains much uncertainty as to the most reliable methods of measurement. The majority of procedures involve the use of gauges to obtain a compliance curve for the cracked specimen and determining the point of deviation from linearity during elastic unloading along this curve.[29-35] Other methods involve laser inferometry techniques,[35] electrical potential measurements,[36] ultrasonics[37] and surface replication.[10]

Although perhaps the most accurate of all procedures, at least for surface measurements, the laser inferometry technique for detecting crack closure requires special instrumentation.[35] Electrical potential techniques, although widely used for crack length measurement, suffer from the presence of crack surface oxide films which can result in uncertainty on the exact point of crack surface contact. Replica

techniques are accurate, but provide only a surface measurement and do not lend themselves to automation. For standard automated testing, compliance gauge measurements offer the most practical solution. The gauges can be mounted at the crack mouth (e.g., clip gauges), on the side surfaces (e.g., Elber gauges) or on the back-face. Location on the side surfaces is not preferred as measurements become strongly sensitive to the position of the crack in relation to the gauge. Of the remaining locations, the back-face strain approach was selected as it offered substantially greater resolution than the use of a crack mouth-mounted clip gauge.

The back-face strain method,[29,30] used to evaluate crack closure,[28,30-32] is based on compliance measurements from a strain gauge mounted on the back face of the specimen. The closure stress intensity, K_{cl}, which is defined at first contact between mating crack surfaces on unloading, is measured at the point of deviation from linearity of the elastic unloading compliance curve.

In order to monitor crack closure continuously in real time during a high frequency (e.g., 50 Hz) fatigue test, an algorithm was developed with the present system to automate the process of deriving the point of closure from compliance data. Load and back-face strain signals were first amplified with two identical amplifiers and digitized to feed into a PDP-11 computer. Although care was taken to keep the signals in-phase, due to the nature of the amplifiers some phase difference between the load and strain signals was found to exist. Since this can introduce false hysteresis and cause error in the closure measurement, a phase

shifting circuit was used for compensation. Active filter circuits are also used to remove the high frequency noise in the measurement system.

In order to automate detection of the closure point at first deviation in linearity from the unloading compliance curve, the straight line portion of the curve was defined as the correlation coefficient used as an indicator for linearity. First, starting from maximum load, points from 5 to 10% of the total curve were used to determine the baseline correlation coefficient. Points were then added one by one to the data set and correlation coefficients calculated. Since the correlation coefficient will decrease if the next point deviates from linearity, and increase if it falls on the straight line, the closure point was defined where the correlation coefficient had the highest value, i.e., at the end of the straight line portion of the curve.

This technique was relatively immune to signal noise because the correlation coefficient is itself an indicator of noise. Moreover, its use removes the ambiguities inherent in the manual determination of closure. Accuracy depends primarily on the accuracy of the digitizing process and the noise level. Sensitivity and the speed of the analog-to-digital converter are also crucial to the success of the method. In the present system, where the speed of the algorithm was a strong function of the computation speed, the unloading compliance curve was digitized into about 350 points within a half fatigue cycle, and involved a computation process of about 10 seconds. This readily permitted closure measurements to be made automatically during the test approximately once every 30 seconds.

4. MECHANISMS OF CRACK TIP CLOSURE IN 7150 ALLOY

4.1 Introduction

Recent studies into the mechanics and mechanisms of fatigue have identified a prominant role of crack closure in influencing crack propagation behavior (e.g., refs. 13,16,19-21,23-28,33-35,37-45). This is particularly apparent at low growth rates (i.e., below $\sim 10^{-9}$ m/cycle) near the fatigue threshold stress intensity range for no crack growth, ΔK_{TH}. In this regime, the origin of such closure has been associated with mechanisms such as crack surface corrosion deposits,[37-40] irregular fracture morphologies coupled with crack tip shear displacements,[41-43] and fluid-induced pressure[44] in addition to conventional mechanisms relying on cyclic plasticity[33] (Fig. 4.1). The effect of the closure, which induces contact between mating fracture surfaces at positive stress intensities (K_{cl}) during the loading cycle, is to reduce the local driving force for crack advance from nominally applied levels, e.g., $\Delta K = K_{max} - K_{min}$, to some near-tip effective level, $\Delta K_{eff} = K_{max} - K_{cl}$, where K_{max}, K_{min}, K_{cl} and ΔK are the maximum, minimum, closure and range of stress intensity, respectively.

Effects of variable amplitude loading, frequency, load ratio, microstructure, environment and temperature have all been associated with closure phenomena (for review, see ref. 45). Elber[33] first applied the concept of (plasticity-induced) closure to cyclic behavior in aluminum alloys in an attempt to explain variable amplitude loading and load ratio effects in these alloys. Subsequent studies in this system have focussed largely on effects of microstructure and environment. An important mechanism in aluminum alloys appears to be associated with roughness-

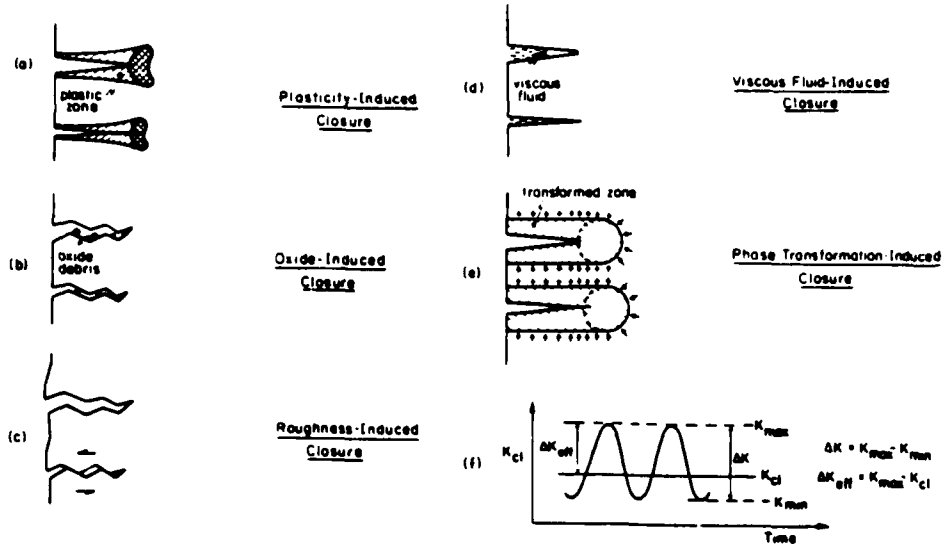

Fig. 4.1: Schematic illustration of primary mechanisms of fatigue crack closure and the nomenclature required in the definition of stress intensities representative of the fatigue cycle.

induced closure,[41-43] where it has been suggested that the strongly crystallographic nature of crack paths, particularly in underaged structures, promotes closure[41-43] and crack deflection[46] and thus reduces near-threshold growth rates.

In the present work, effects of microstructure during precipitation hardening are examined on fatigue crack propagation in a high purity 7150 alloy, for underaged, peak-aged and overaged conditions, in the light of quantitative measurements oxide film thickness, fracture surface roughness and closure stress intensity values. It is shown that near-threshold growth rates are slowest in underaged structures, consistent with the highest measured closure loads, and the most deflected crack paths. Little evidence of oxide-induced closure could be detected.

4.2 Results

Growth Rate Behavior:

The variation in fatigue crack propagation rates (da/dN) with stress intensity range (ΔK) for 7150 in the underaged (UA), peak-aged (PA) and overaged (OA) conditions is shown in Fig. 4.2 for load ratios of 0.10 and 0.75. Although growth rates above $\sim 10^{-9}$ m/cycle are similar at each load ratio for all three microstructures, at near-threshold levels it is evident that underaged structures show the highest fatigue resistance in terms of lowest growth rates and highest threshold ΔK_{TH} values. Compared to the underaged structure, threshold ΔK_{TH} values in these results are roughly 15% and 28% lower in the peak-aged and overaged structures, respectively, at R = 0.10 (Table 4.1). Thresholds are similarly reduced

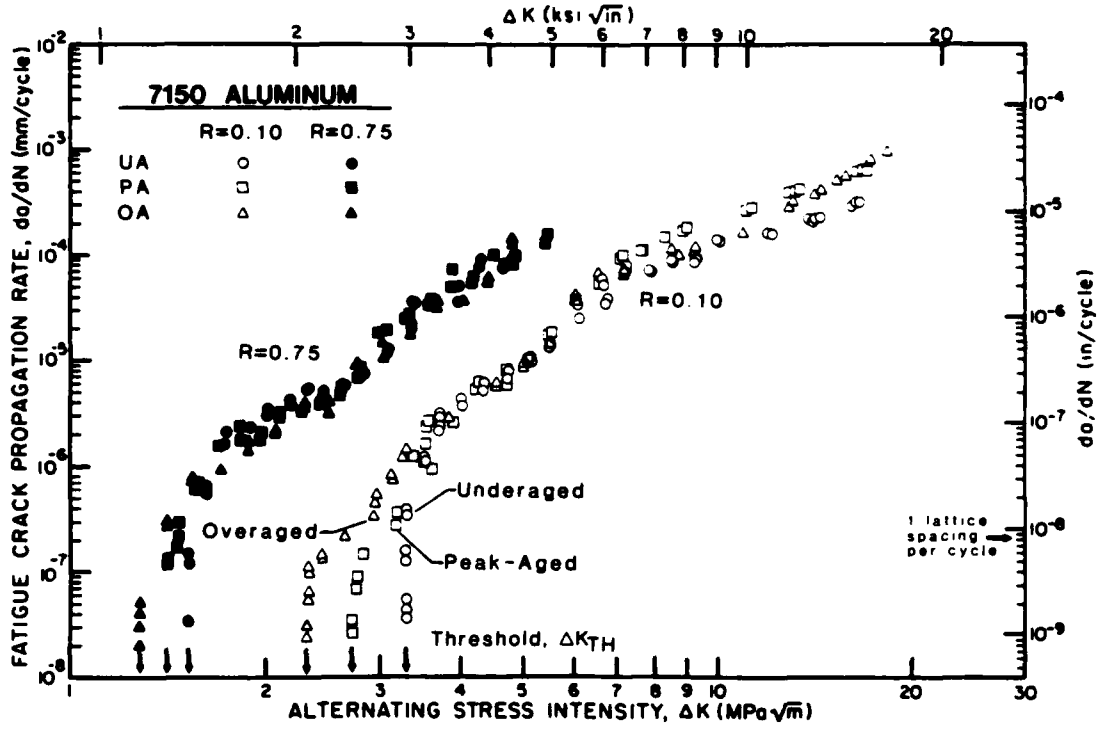

Fig. 4.2: Variation in fatigue crack growth rate (da/dN) as a function of stress intensity range (ΔK) for I/M 7150 aluminum alloy tested at R = 0.10 and 0.75 in controlled moist air. Data are shown for underaged, peak-aged (T6) and overaged (T7) microstructures.

Table 4.1: Threshold Data for 7150 Alloy at Load Ratios of 0.10 and 0.75

Code	Load Ratio	ΔK_{TH}	Plastic Zone Size*†		$\Delta CTOD$*†	Maximum K_{cl}/K_{max}*	Excess Oxide Thickness*	Lineal Roughness** Parameter
			Cyclic	Maximum				
	(K_{min}/K_{max})	($MPa\sqrt{m}$)	(μm)	(μm)	(nm)		(nm)	
UA	0.10	3.05-3.31	2.9	14.5	100	0.88	∿ 3	1.26
	0.75	1.51	0.4	24.5	22	0	∿ 3	
PA	0.10	2.44-2.94	1.8	8.8	65	0.85	∿ 3	1.21
	0.75	1.27	0.4	25.2	14	0	∿ 3	
OA	0.10	2.23-2.33	1.5	7.4	50	0.75	∿ 3	1.06
	0.75	1.16	0.4	24.8	13	0	∿ 3	

Underaged | Peak-Aged (T6) | Overaged (T7)

*At the threshold, ΔK_{TH}.

**Ratio of total crack length to projected length on plane of maximum tensile stress.

†Computed from $r_\Delta = 1/2\pi\,(\Delta K/2\sigma_y)^2$, $r_{max} = 1/2\pi(K_{max}/\sigma_y)^2$ and $\Delta CTOD = \frac{1}{2}(\Delta K^2/2\sigma_y E)$, where r_Δ and r_{max} are the cyclic and maximum plastic zone sizes, σ_y the yield strength and E Young's modulus.[49]

with increased aging at R = 0.75, although the absolute magnitude of the differences in ΔK_{TH} values is much smaller.

Crack Closure Data:

Corresponding crack closure data, in terms of back-face strain measurements of K_{cl}/K_{max} as a function of ΔK, are shown in Fig. 4.3 for the three microstructures at both R = 0.10 and 0.75. Similar to behavior reported for several ferrous and non-ferrous alloys at low load ratios (e.g., refs. 27,28,34), the degree of crack closure increases sharply with decreasing ΔK level, approaching a maximum of K_{cl}/K_{max} close to unity at ΔK_{TH}. Although no evidence of closure could be detected experimentally in any microstructure at R = 0.75, at low load ratios underaged structures showed the highest closure levels, consistent with their highest thresholds.

Fractography:

Scanning electron micrographs of the fatigue fracture surfaces close to ΔK_{TH} in the three aging conditions are shown in Fig. 4.4. The fractography is transgranular in all cases with evidence of slip steps, ledges and facets. Such facets are particularly pronounced in the underaged structure and have an appearance characteristic of crystallographic fatigue surfaces. The rougher or more tortuous nature of the crack path in the underaged structures can be seen more clearly in Fig. 4.5 where crack profiles are shown for the three conditions. In contrast to the zig-zag appearance of underaged fractures, crack paths in the overaged structures are predominately linear with far fewer crack deflections.

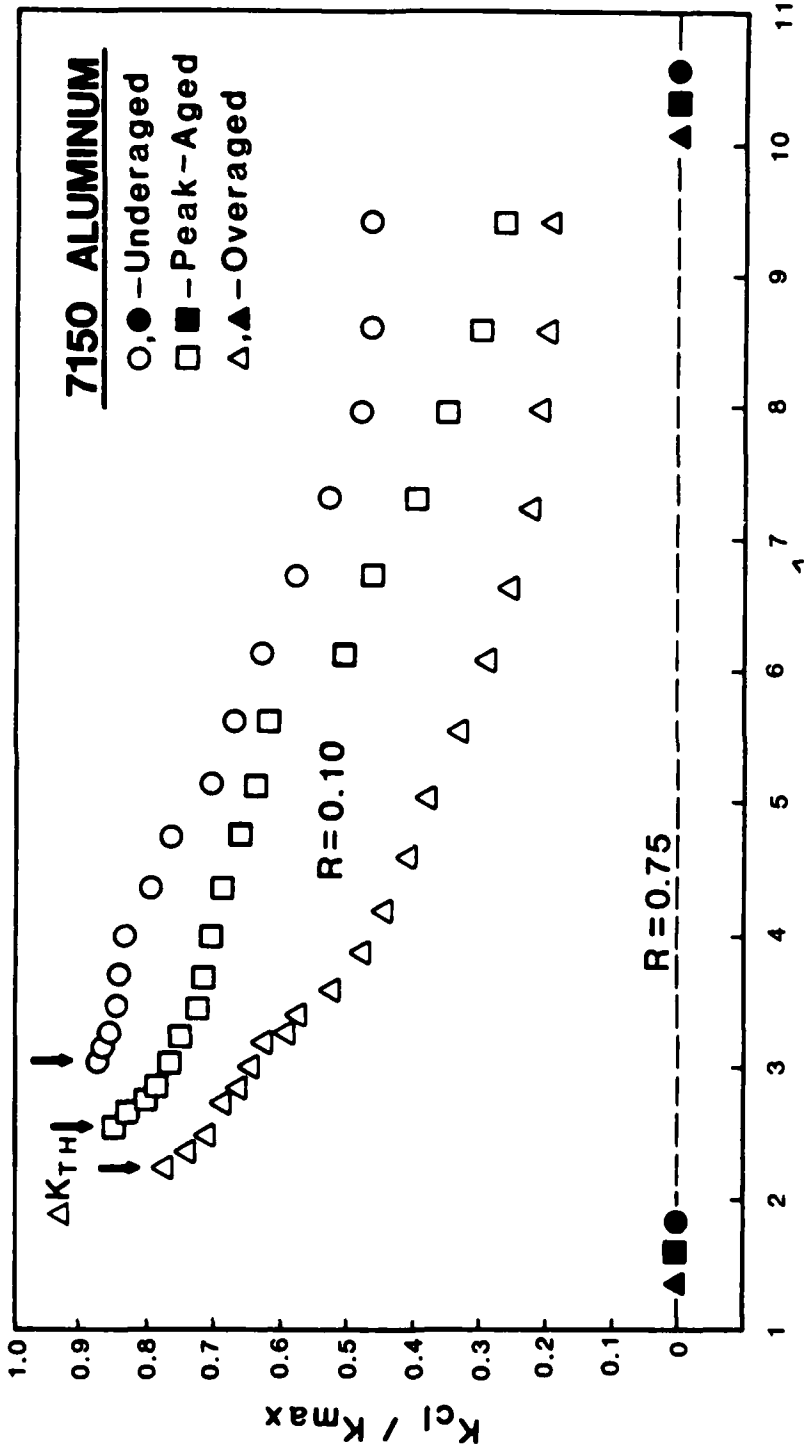

Fig. 4.3: Variation in crack closure, in terms of the ratio of closure to maximum stress intensity, K_{cl}/K_{max}, as a function of ΔK, for underaged, peak-aged (T6) and overaged (T7) 7150 alloy at R = 0.10 and 0.75.

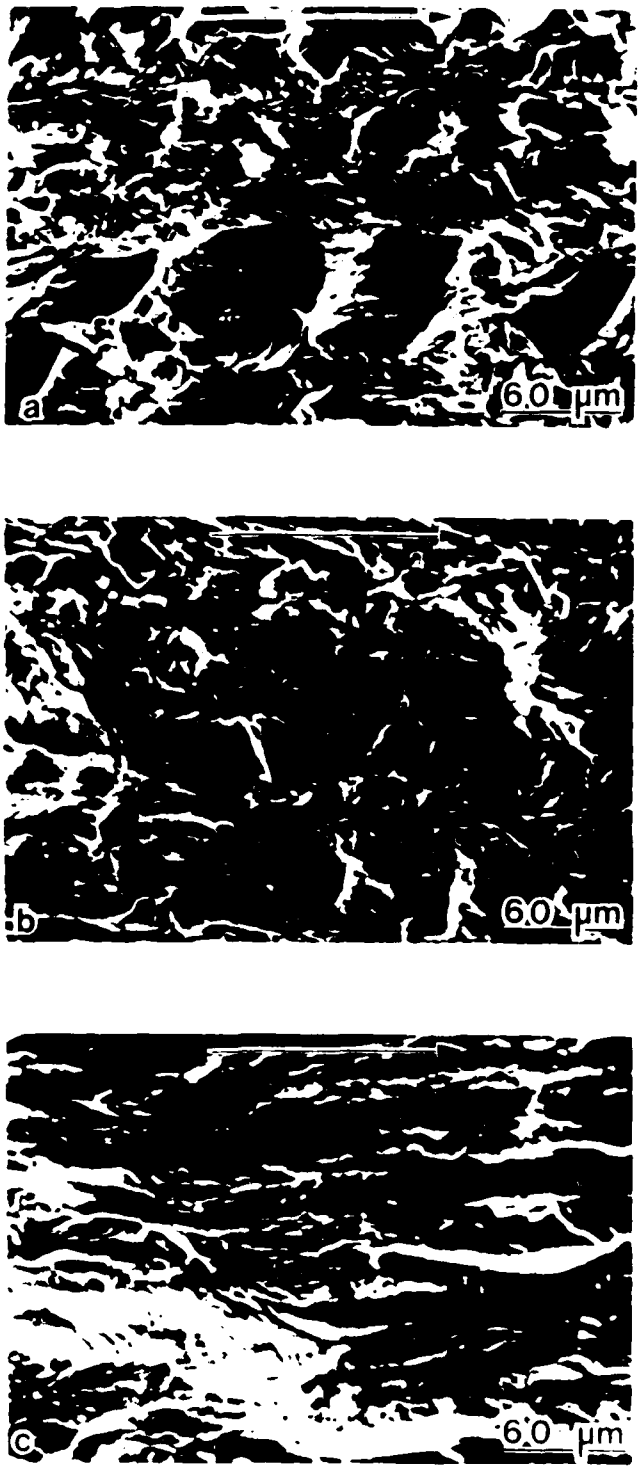

Fig. 4.4: Scanning electron micrographs of fatigue fracture surfaces close to ΔK_{TH} (R = 0.10) in I/M 7150 aluminum alloy, showing the morphology in a) underaged, b) peak-aged (T6) and c) overaged (T7) microstructures.

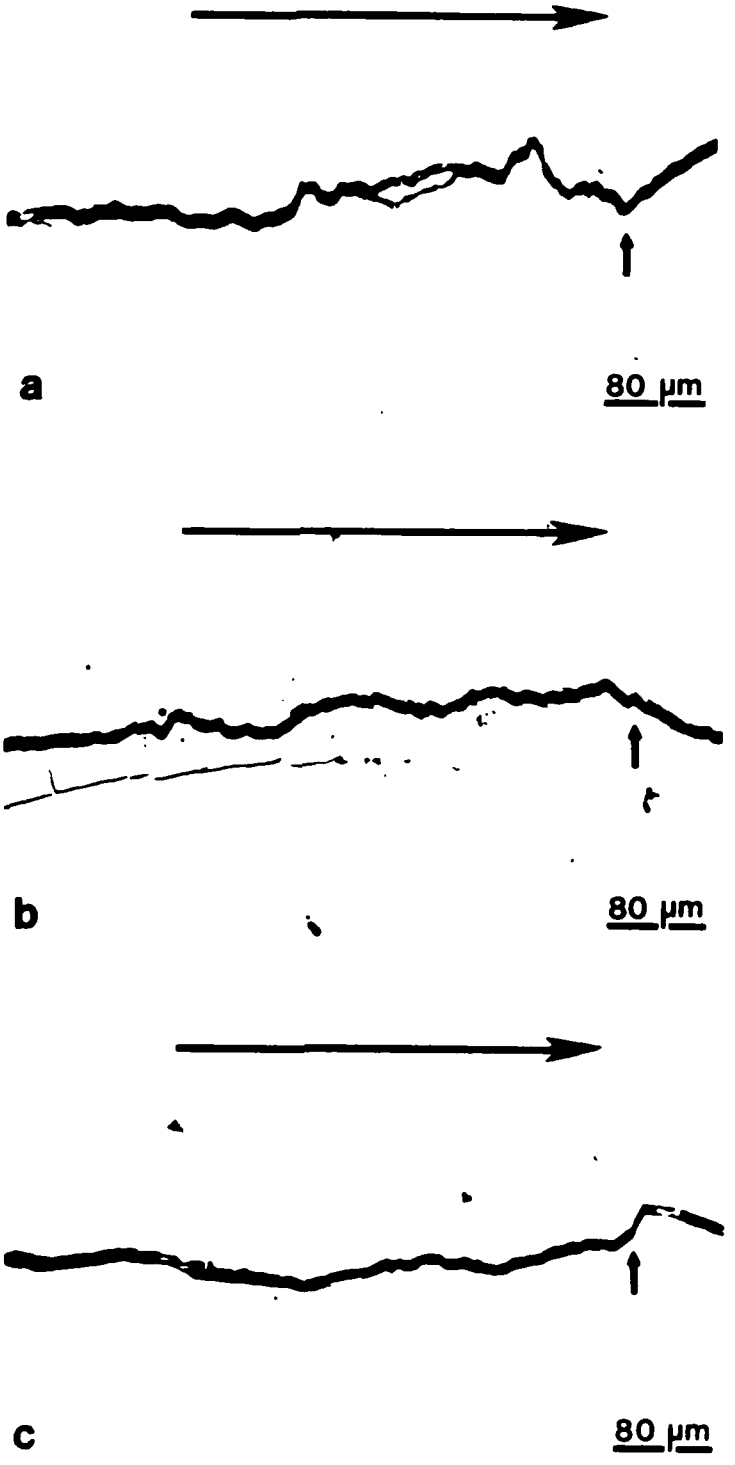

Fig. 4.5: Crack path morphology of near-threshold fatigue cracks in I/M 7150 aluminum alloy in the a) underaged, b) peak-aged (T6) and c) overaged (T7) conditions.

Associated Auger measurements of the extent of crack surface corrosion deposits are shown in Fig. 4.6. In marked contrast to behavior in lower strength steels,[37,40] there is no evidence in this present alloy of any pronounced oxide accumulation within the crack even at threshold levels. Oxide films were similar for all aging conditions at both load ratios with a measured thickness, of the order of 3 nm, comparable with the limiting thickness of naturally-occurring oxides in this alloy. As listed in Table 4.1, the excess oxide film thicknesses in 7150 are small compared to computed values of the cyclic crack tip opening displacements (ΔCTOD) indicating that, for this alloy tested in room air environments, the contribution from oxide-induced crack closure is likely to be minimal.

4.3 Discussion

Similar to other aluminum alloys (e.g., refs. 21,27,28,47), the present results on a high purity 7150 alloy indicate clearly that underaged microstructures have superior near-threshold fatigue crack propagation resistance to overaged and peak-aged microstructures. This is seen in terms of lower growth rates below $\sim 10^{-9}$ m/cycle and higher threshold ΔK_{TH} values at both low and high load ratios, although the magnitude of the effect is diminished at R = 0.75 (Fig. 4.2). The higher thresholds in the underaged structures are consistent with an increased magnitude in crack closure (Fig. 4.3), faceted and crystallographic fracture surfaces (Fig. 4.4) and more tortuous crack paths (Fig. 4.5), compared to the smoother, more linear (undeflected) crack morphology in overaged structures. Data indicating this trend of lower thresholds with

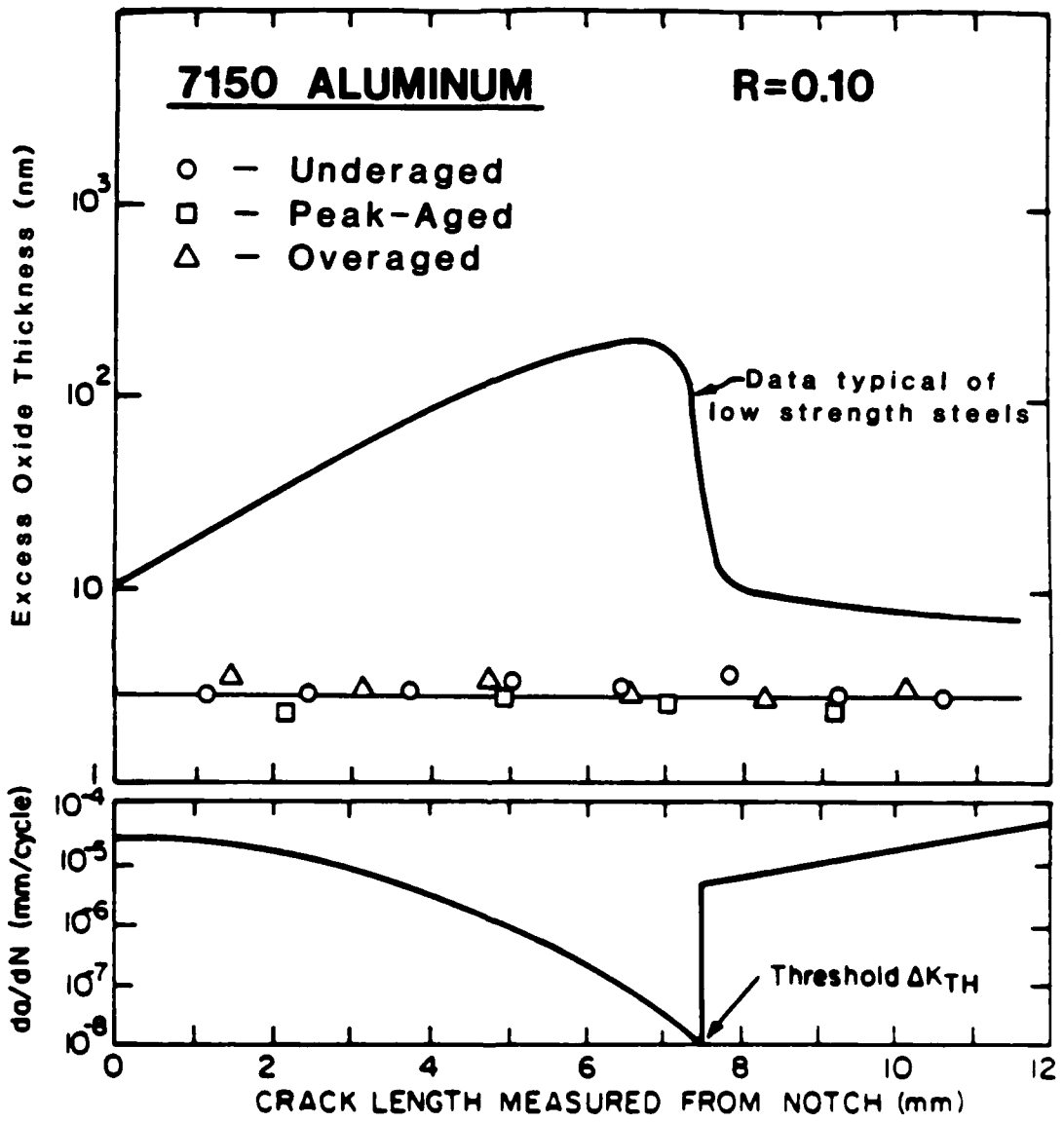

Fig. 4.6: Scanning Auger spectroscopic measurements of excess crack surface oxide deposits as a function of fatigue crack length and growth rate (da/dN). Data points, for I/M 7150 aluminum alloy in the underaged (UA), peak-aged (PA) and overaged (OA) microstructures are compared with prior data[40] on lower strength steels at low load ratios.

decreasing K_{cl}/K_{max} values and decreasing degrees of fracture surface roughness for increased aging are listed in Table 4.1.

In keeping with current notions on the role of crack closure,[45] this trend, is to be expected. Akin to behavior in dual phase steels,[31] beta-annealed titanium[35] and aluminum-lithium alloys,[27,47] the generation of a meandering crack path, either by crack deflection at harder phases or in the present case by crystallographic deflection at grain boundaries, can lead to slower fatigue crack growth rates through a reduction in local crack driving force. This results from three major factors: i) lower effective da/dN due to a longer path length of the crack, ii) lower effective stress intensities at the crack tip due to crack deflection from the plane of maximum tensile stress, and iii) lower effective ranges of stress intensity at the crack tip due to the resulting production of *increased crack closure due* to asperity contact behind the crack tip. Since the thicknesses of crack surface oxide films are so small compared to CTOD values, it would appear that the major contribution to this closure in the present alloy originates from the roughness-induced mechanism (Fig. 4.1), aided by the rough out-of-plane crack morphologies and the crack tip shear displacements which result. These effects are far less pronounced in the overaged structures where crack paths are more linear (Fig. 4.5) such that corresponding crack growth rates are higher. Furthermore, at the high load ratios, differences between underaged and overaged microstructures are reduced because the role of crack closure is diminished at the larger crack opening displacements (Fig. 4.3).

This argument is consistent with previous explanations based solely on microstructural factors.[48] In underaged precipitation hardening systems, where the mode of alloy hardening is primarily the shearing of small coherent precipitates, the resulting heterogeneous deformation (i.e., coarse planar slip) promotes a crystallographic crack path. Because slip is occurring on fewer slip systems, the degree of slip reversibility is greater and hence the crack tip damage per cycle is less. Conversely, in overaged systems where the mode of hardening is now Orowan bypassing of larger, semicoherent or incoherent, non-shearable precipitates, the resulting homogeneous deformation (i.e., wavy slip) generates a far more planar fracture surface due to the larger number of finer slip steps. This leads to greater slip irreversibility and more crack tip damage per cycle. Furthermore, the larger precipitate free zones in overaged 7000 series aluminum alloys, arising from the growth of incoherent grain boundary precipitates, must contribute somewhat to the lower fatigue resistance in these microstructures.

Finally, it is interesting to note that the microstructures which show superior fatigue crack growth resistance at near-threshold levels do not necessarily retain such resistance at higher growth rates. For example, although the effect is not apparent in 7150 (Fig. 4.2), underaged microstructures in many aluminum alloys show faster growth rates above $\sim 10^{-9}$ m/cycle, and slower growth rates close to ΔK_{TH}, compared to overaged structures. Such observations tend to support explanations based on crack closure since at higher growth rates, with associated larger crack tip opening displacements, the effect of closure mechanisms relying on asperity contact (i.e., roughness-induced) would be

reduced. Conversely, where crack closure and deflection mechanisms are important, e.g., for transient crack growth behavior under variable amplitude loading conditions, underaged structures clearly show the longest post-overload retardations and the highest general resistance to crack growth. However, these planar slip characteristics of coherent particle precipitation hardened systems, which are so important in generating **superior fatigue** crack growth resistance through inhomogeneous deformation, rough crystallographic crack paths and enhanced closure and deflection, can lead simultaneously to **inferior** crack initiation **toughness** from a greater tendency for strain localization. This is particularly evident in aluminum-lithium alloys where the increased coherency between lithium-containing intermetallics and the matrix can result in exceptionally good fatigue crack propagation resistance,[27,47] through enhanced crack path tortuosity, yet at the same time can produce extremely low fracture toughness values.

4.4 Conclusions

Based on a study of fatigue crack propagation behavior in high purity 7150 aluminum alloy tested at high and low load ratios in moist air with under, peak and overaged microstructures, the following conclusions can be made:

i) With increased aging, resistance to fatigue crack extension is decreased, in the form of faster near-threshold growth rates and lower fatigue threshold ΔK_{TH} values, consistent with reduced measured levels of crack closure and a decreasing tortuosity in crack path.

ii) The superior fatigue crack growth resistance of the underaged structures is attributed to greater slip reversibility and to enhanced roughness-induced crack closure and deflection from more tortuous crack paths, factors which result from the non-homogeneous, planar slip characteristics of deformation in microstructures hardened by coherent (shearable) precipitates.

iii) Crack flank corrosion deposits in all microstructures were small compared to near-threshold crack tip opening displacements at both load ratios, indicating that the contribution from oxide-induced crack closure in this alloy is minimal.

5. DEVELOPMENT OF CRACK CLOSURE FOR LONG AND SHORT CRACKS

5.1 Introduction

In recent years the existence of a fatigue threshold, representing a stress intensity range ΔK_{TH} below which long cracks appear dormant, has been shown to be intimately associated with the development of crack closure in the wake of the crack tip (e.g., refs. 34,45). Such closure, which results from interference between mating fracture surfaces, acts to reduce the local crack driving force from nominal levels, based on global measurements of applied loads and crack size, e.g., ΔK, to some lower effective near-tip level, e.g., ΔK_{eff}. There is also a growing body of evidence that suggests that the "anomalous" behavior of small cracks, which are small compared to microstructural size-scales or the extent of local plasticity or simply physically small ($\lesssim$ 1 mm), is linked similarly to the development of closure,[10,13,16,19,28,35] as such cracks can initiate and grow at progressively decreasing growth rates below the

threshold before arresting or merging with long crack behavior (Fig. 2.1). Specifically, small cracks by virtue of their limited wake are presumed initially to be only marginally influenced by closure (e.g., refs. 13,16,19) such that, compared to equivalent long cracks at the same nominal driving force, their effective driving force is higher, implying violation of K or J-based similitude. With increasing length, the corresponding development of closure can compensate initially for the increase in nominal ΔK, such that the effective driving force can pass through a minimum, with a corresponding minimum in growth rates. Crack closure, however, is only one of several mechanisms which may contribute to discrepancies between long and short crack behavior[19] although, in the absence of major electrochemical effects,[20] it appears to be the most significant.

Evidence to support such hypotheses is still comparatively limited, due possibly to theoretical difficulties with the mechanics of cracks of limiting continuum dimensions and experimental difficulties in monitoring their crack propagation and closure behavior. Studies in lower strength steels have claimed a direct correspondence between short crack and conventional long crack growth rate data when closure is accounted for through characterization with ΔK_{eff}, based on experimental K_{cl} measurements.[13,49] Mechanistically, this is difficult to rationalize as current models for crack closure, which rely on mechanisms involving cyclic wake plasticity,[33] crack surface corrosion product formation,[38-40] fracture surface roughness[41-43] fluid pressure within the crack,[44] and metallurgical phase transformations[45] (summarized in Fig. 4.1), in general do not define a crack size dependence of closure forces.

However, analytical modelling of fluid-induced closure[44] and experimental measurements of roughness-induced closure alloys[28,49] do show increasing closure with increasing crack length until "saturation" long crack levels are reached.

One promising experimental approach to describing this role of crack closure in influencing near-threshold long cracks and sub-threshold short cracks has been to monitor behavior following the physical removal of closure forces. This has been achieved principally through the micro-machining of material left in the wake of the crack tip,[24,28,34,49] although one study has employed single compression overloads.[25] These procedures have the added advantage of defining the most prominent location of closure along the crack length. Recent work employing mechanical or electro-discharge machined slots to remove wake material in P/M and I/M aluminum alloys and in low alloy steels[24,28,34,49] have shown i) that long cracks previously arrested at the threshold ΔK_{TH} behave as short cracks and recommence to propagate at threshold levels and ii) that closure well behind the crack tip is relatively less important compared to near-tip closure (i.e., within 1 mm or so from the tip).

The objective of the present investigation is to utilize this technique to examine the development, location and effect of crack closure on arrested threshold fatigue cracks in under, peak and overaged microstructures in a 7150 aluminum alloy, where the salient mechanisms of closure are a strong function of the degree of precipitation hardening.

5.2 Fatigue Testing

Constant amplitude crack growth data were obtained between $\sim 10^{-3}$ and 10^{-8} mm/cycle under both decreasing and increasing ΔK conditions.

Procedures involved in the wake removal experiments are shown schematically in Fig. 3.4. A threshold long crack, with total length (including notch) typically of $\sim$ 25 mm, was produced by manual load shedding until arrest at ΔK_{TH}. Material in the wake of the crack tip was then removed progressively in steps of roughly 1 mm, whilst the specimen was maintained at mean load, using a fine jeweler's saw with a width of cut of approximately 300 μm. The micro-machining was conducted extremely slowly to minimize heating effects. Closure measurements to determine K_{cl} values were performed after each machining step, with the remaining fatigue crack varying in length (a) between 7.5 and 0.5 mm. Following removal of material to within 500 μm of the tip, cyclic loads were reapplied to maintain a constant $\Delta K = \Delta K_{TH}$, and subsequent crack extension and closure behavior closely monitored. As the presence of the machined notch can affect the nominal stress intensity K at the tip of the fatigue crack, it is necessary to show that notch correction factors do not compromise the interpretation of the wake removal experiments. For a small flaw, of length $\tilde{a}$, emanating from a notch of length c, i.e., total length $a = c + \tilde{a}$, the limiting K solutions for the short and long crack, K_s and K_l, respectively, are given in terms of the nominal stress σ_{nom}, and the stress concentration of the notch k_t, as:[50]

$$K_s = 1.12\, k_t\, \sigma_{nom}\sqrt{\pi\tilde{a}} \quad , \tag{5.1}$$

and

$$K_l = Q\, \sigma_{nom}\sqrt{\pi a} \quad , \tag{5.2}$$

where Q is the geometrical factor tabulated in handbooks,[51] and the nominal stress for the compact specimen is given in terms of applied load P, specimen width W, and thickness B, as:

$$\sigma_{nom} = \frac{2P(2W + c)}{B(W - c)^2} \quad . \tag{5.3}$$

With increasing flaw size, $\tilde{a}$, the actual K solution initially follows Eq. 5.1 until a transition flaw size, $\tilde{a}^*$, is exceeded, whereupon the notch concentration is no longer felt and the K solution approximates to Eq. 5.2. The transition size, where $K_s = K_1$, can be considered as the extent of the elastic field of the notch[50] and is given by:

$$\tilde{a}^* = \frac{c}{(1.12\ k_t/Q)^2 - 1} \tag{5.4}$$

These K solutions are plotted in Fig. 5.1 as a function of $\tilde{a}$ for the present experimental conditions at ΔK_{TH} of P $\sim$ 0.55 kN and c $\sim$ 23 mm. With the compact geometry of W = 50 mm and B = 6.4 mm, k_t for the micro-machined notch, with root radius $\rho \sim 0.2$ mm, was taken to be of the order of 8 from the numerical calculations of Wilson.[52] It is apparent that the notch field is felt only for flaw sizes below $\tilde{a} \approx 50$ μm (i.e., $\tilde{a} \sim \rho/4$). As the minimum length of the remaining fatigue crack, $\tilde{a}$, in the current experiments was a factor of 10 larger than this, i.e., $\sim 2\frac{1}{2}$ times the root radius of the notch, Eq. 5.2 relevant to the C(T) geometry was utilized for all K computations with no notch correction factors incorporated. Furthermore, crack growth was assumed to be beyond any mechanically damaged zone due to the machining.

5.3 Results

The variations, with stress intensity range (ΔK), of crack growth rates (da/dN) and corresponding crack closure at R = 0.10 and 0.75 are shown respectively in Figs. 4.2 and 4.3 for 7150 alloy as a function of aging treatment. Although behavior is similar at high load ratios, at

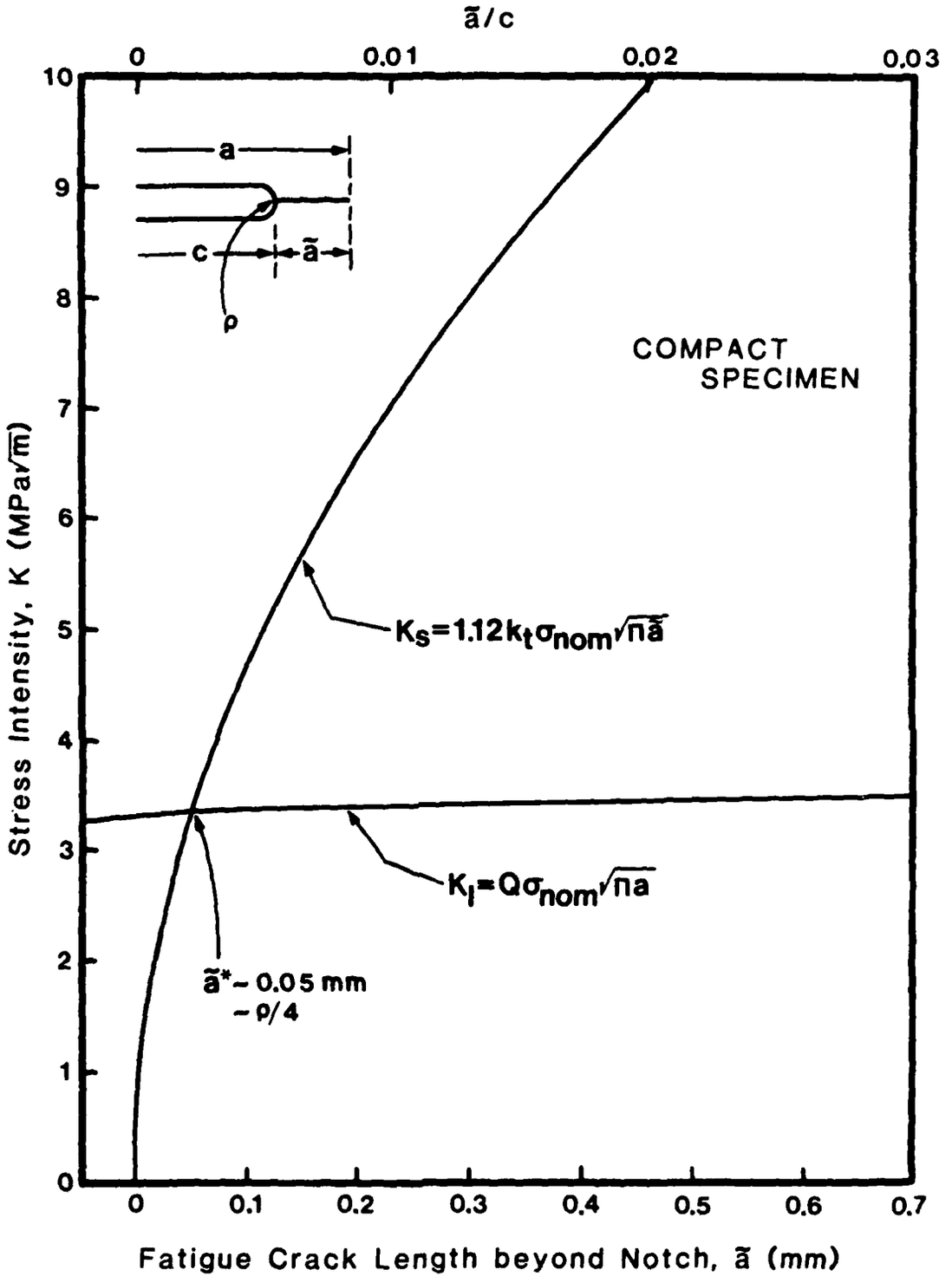

Fig. 5.1: Long and short crack limiting stress intensity solutions, K_I and K_S respectively, for a small flaw (length ã) emanating from a notch (length c, root radius ρ) in the compact C(T) geometry. K calculations are relevant to current experimental conditions at threshold levels with an applied load P of 0.55 kN and c = 23 mm.

R = 0.10 near-threshold growth rates are slowest, and threshold values highest, in the underaged microstructures, consistent with their highest measured levels of closure. As described in Section 4, the extent of closure at R = 0.10 in all three structures progressively increases with decreasing ΔK as the threshold is approached, with $K_{cl}/K_{max} \rightarrow 1$ as $\Delta K \rightarrow \Delta K_{TH}$. No closure could be detected experimentally at R = 0.75.

The specific location of such closure can be inferred from the wake machining experiments. Shown in Fig. 5.2 is the variation in closure plotted as a function of remaining fatigue crack length during removal of the wake of cracks arrested at ΔK_{TH}. Results for all three microstructures are plotted in the form of the ratio of K_{cl}/K_{max} as a function of the remaining fatigue crack length, $\tilde{a}$, normalized by the initial length of the threshold crack, $\tilde{a}_{TH}$. Similar to observations on T6 alloys,[21,34] although the extent of closure is fairly evenly distributed over the majority of the crack length, roughly 50% is confined to a region within $\sim$ 500 μm of the crack tip at R = 0.10. For example, at ΔK_{TH} in the peak aged alloy, the arrested fatigue crack, of length $\tilde{a} \approx 7.5$ mm, has a closure stress intensity $K_{cl} \approx 2.5$ MPa$\sqrt{m}$ ($\Delta K_{eff} \approx 0.4$ MPa$\sqrt{m}$) at the nominal threshold of $\Delta K_{TH} = 2.6$ MPa$\sqrt{m}$ (R = 0.10). After removal of $\sim$ 7.0 mm of wake, closure is reduced, i.e., $K_{cl} \approx 1.1$ MPa$\sqrt{m}$ ($\Delta K_{eff} \approx 1.8$ MPa$\sqrt{m}$), and must be confined to the very near-tip region. It is noticeable, however, that the overaged condition, which develops the least closure overall at near-threshold stress intensities, also has the least closure removed by micro-machining of the wake material. As expected, the absence of detectable closure at high

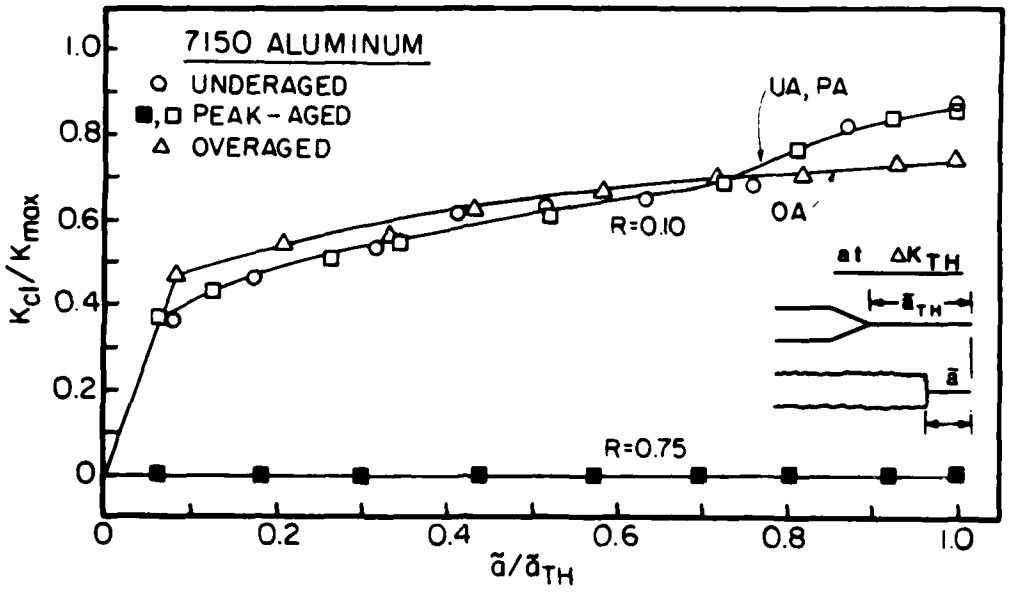

Fig. 5.2: Experimentally-measured variation in crack closure during progressive micro-machining of material left in the wake of long cracks arrested at the fatigue threshold at R = 0.10 and 0.75 in underaged, peak-aged and overaged 7150 alloy. Plotted is the ratio of closure to maximum stress intensity, K_{cl}/K_{max}, as a function of remaining length of fatigue crack $\tilde{a}$, normalized by its initial length at ΔK_{TH}, $\tilde{a}_{TH}$.

load ratios was not changed during subsequent removal of the wake of threshold cracks arrested at R = 0.75 (Fig. 5.2).

The effect of the reduction in closure from micro-machining is readily apparent by immediate re-cycling of previously arrested threshold cracks, following wake removal, at a constant stress intensity range of $\Delta K = \Delta K_{TH}$. As shown in Figs. 5.3 and 5.4, even though nominal ΔK levels do not exceed the threshold, crack growth re-commences in all three microstructures at R = 0.10 with the locally increased ΔK_{eff}. After an initial acceleration,* subsequent growth rates in the under and peak aged structures reach a plateau after $\sim$ 20 and $\sim$ 50 μm of crack extension (i.e., roughly 2 to 7 times the maximum plastic zone size) but do not re-arrest completely (Fig. 5.3). This presumably is due partly to experimental difficulties in maintaining constant ΔK control at the threshold value in a growth rate regime where the dependence of propagation rates on stress intensity range is very strong. Behavior in the overaged structure is somewhat different in that growth rates following re-initiation are high but progressively decelerate to an apparent plateau after approximately 100 μm of further crack extension (i.e., roughly 15 times the maximum plastic zone size). When plotted in terms of da/dN vs. ΔK in Fig. 5.4, such behavior clearly resembles that of short cracks. K_{cl} measurements carried out where the growth rates approach the plateau indicated that closure was being regenerated to

---

*Short delays of $\sim 5 \times 10^4$ and $\sim 3 \times 10^4$ cycles were observed in under and peak aged structures, respectively, at the start of cycling following micro-machining (Fig. 5.3). Such delayed re-initiation was conspicuously absent for overaged structures and is of unclear origin.

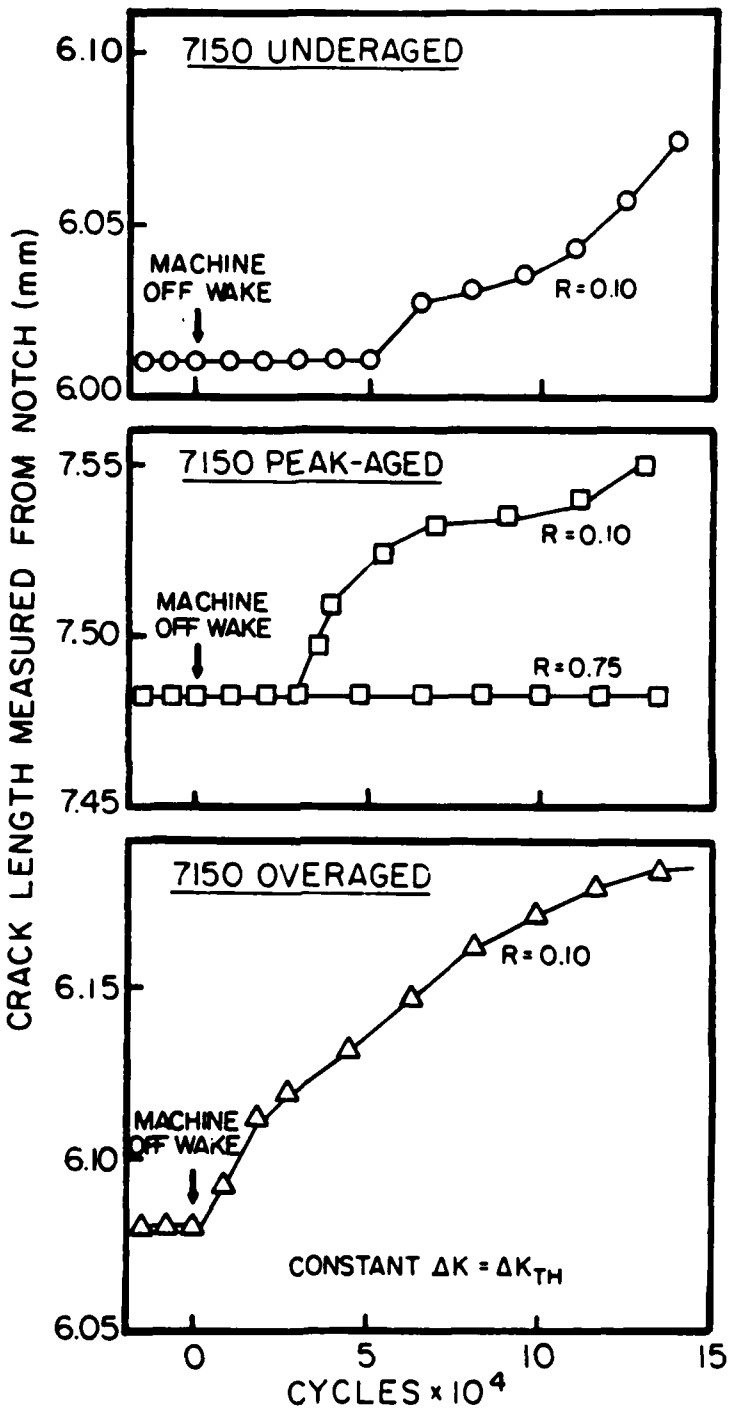

Fig. 5.3: Fatigue crack growth behavior, in terms of crack length versus number of cycles, in 7150 aluminum alloy cycled at a constant ΔK equal to the threshold ΔK_{TH}, before and after removal of material in the wake of the tip of arrested crack (remaining fatigue crack length $\tilde{a}$ = 500 μm). Data are shown for a) underaged structure at R = 0.10, b) peak-aged structure at R = 0.10 and 0.75, and c) overaged structure at R = 0.10.

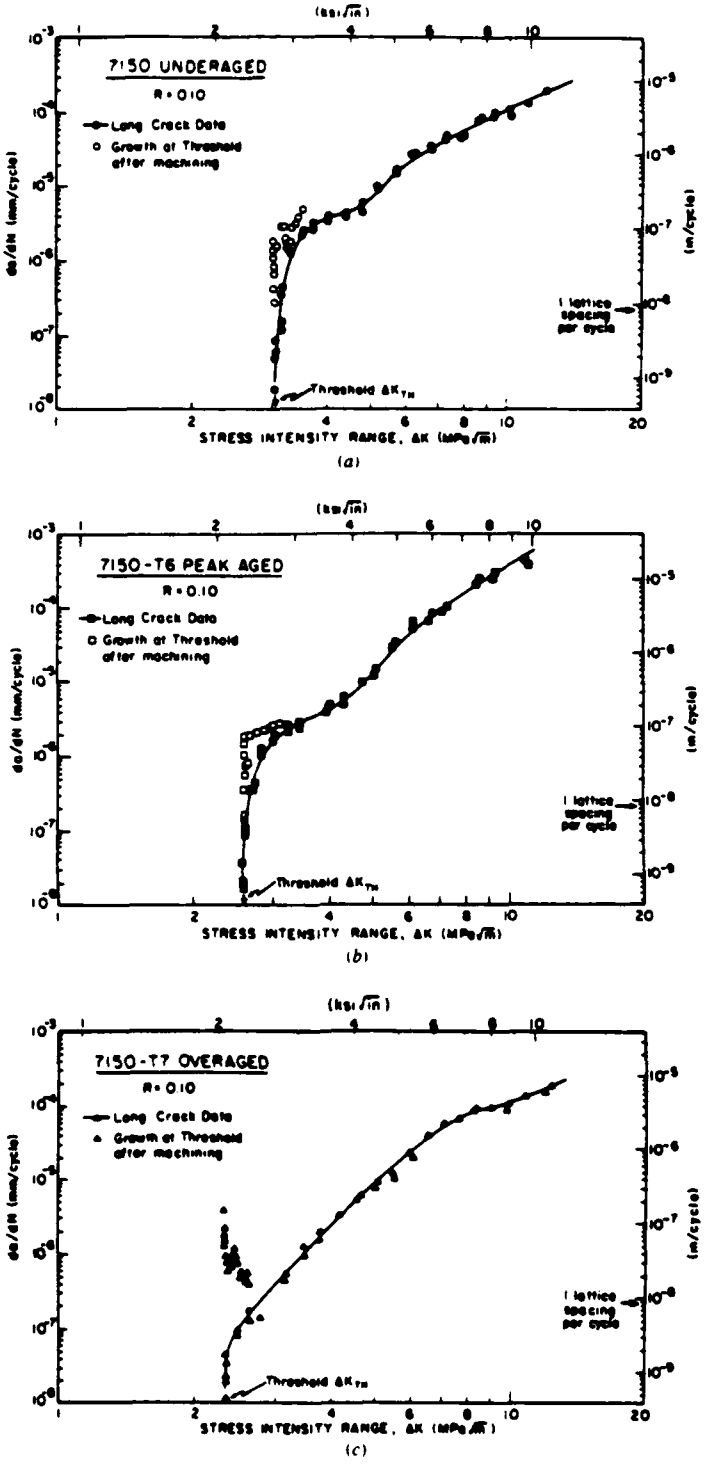

Fig. 5.4: Fatigue crack growth rate behavior of previously arrested threshold cracks immediately following removal of material left in the wake to within 500 μm of the crack tip (open symbols). Data for 7150 aluminum alloy at R = 0.10 in a) underaged, b) peak-aged, and c) overaged conditions.

levels approaching, but always less than, that for the constant amplitude data (Table 5.1). However, for the tests performed at high load ratios on the peak aged condition, where no closure could be measured, no development of closure or further extension of the arrested threshold cracks could be detected on re-cycling at ΔK_{TH} (Fig. 5.3b).

The near-threshold fractography associated with such behavior is summarized in Fig. 4.5 and is described in Section 4. Briefly, fracture surfaces in the underaged microstructures at low ΔK levels are comparatively rough and faceted with a crack path morphology showing many examples of deflection. With increased aging, fracture surfaces become progressively smoother with an essentially linear profile in crack path.

5.4 Discussion

The present study, whereby cracks arrested at ΔK_{TH} recommence to propagate due to a reduction in K_{cl} following wake removal, provides further confirmation that the existence of a fatigue threshold for the propagation of "long" cracks at low load ratios is controlled primarily by a decrease in local driving force due to the development of crack closure in the wake of the crack tip. The lack of a similar effect at high load ratios is consistent with this notion as the role of closure is minimized there from the larger crack opening displacements. Further, by monitoring the reduction in K_{cl} during the removal process, it is also clear that, although such closure is distributed fairly evenly over most of the crack length, as much as 50% is confined to the crack tip region within 500 μm or so from the tip. It should be noted at this point that the above interpretation of the wake removal experiments, which also represent the behavior of physically short cracks emanating from notches,

can be questioned in light of the stress concentration of the machined slot and the effect of any machining damage on subsequent crack extension. However, based on the stress intensity computations shown in Fig. 5.1, it is clear that such complications are inappropriate in the current study as the minimum length of the remaining fatigue crack was always large compared to the root radius of the machined slot and no effects were observed during identical experiments at R = 0.75.

Although values of K_{cl} are reduced by micro-machining of the wake causing crack propagation at ΔK_{TH}, closure re-develops on further crack extension to approach $\sim$ 70 to 80% of previous (pre-machining) levels (Table 5.1). This is manifest as a slowing down in post-machining growth rates to approach an apparent plateau (Fig. 5.3), where the da/dN data tend to merge with the long crack constant amplitude results (Fig. 5.4). The plateau is reached quite rapidly in the underaged structure after $\sim$ 20 μm of crack extension, compared to $\sim$ 50 and $\sim$ 100 μm in the peak and overaged structures, respectively. Although precise interpretation is difficult in view of uncertainties in data taken over size-scales not much larger than the resolution of the crack monitoring technique, the inference from this result is clear. Significant crack closure can develop over smaller amounts of crack extension in the underaged structure compared to the more heavily aged conditions. Furthermore, the distances involved are comparable with microstructural dimensions and are far larger than the size-scales representative of local crack tip plasticity (c.f., maximum and cyclic plastic zone sizes in Table 4.1).

Such results are consistent with the origin of crack closure mechanisms in precipitation hardened aluminum alloys, which tend to be

Table 5.1: Crack Closure Data for 7150 Alloy at $\Delta K = \Delta K_{TH}$ ($R = 0.10$)

	Experimental K_{cl}/K_{max} Values at Threshold		
	At Initial Arrest	Following Wake Removal	Following Subsequent Growth to "Plateau"
Underaged	0.88	0.37	0.61
Peak-Aged (T6)	0.85	0.36	0.59
Overaged (T7)	0.75	0.48	0.57

based largely on microstructural rather than continuum plasticity factors.[21] Near-threshold crack growth in underaged structures, by virtue of the inhomogeneous mode of deformation (i.e., coarse planar slip) resulting from coherent (shearable) particle hardening, is generally far more crystallographic in nature than in peak and overaged structures.[48] This gives rise to a rougher, more faceted fracture surface indicative of a meandering crack path with many deflections from the normal crack propagation plane. These fracture surface morphologies primarily enhance roughness-induced crack closure, such that closure levels in general are higher. Correspondingly, near-threshold growth rates are lower than in the more heavily aged microstructures, where the more homogeneous mode of deformation (i.e., wavy slip) from incoherent (non-shearable) particle hardening promotes a more linear crack path.

In the context of the present results, as fatigue crack closure clearly develops over microstructural dimensions in this alloy, it is promoted in the underaged structures where the roughness-induced mechanism is most potent due to the tortuous nature of the crack path (see Section 4). The formation of closure in the more heavily aged microstructures, where fracture surfaces are far smoother, is thus less

efficient and correspondingly must involve larger amounts of crack extension to re-develop. Since the yield strengths of the under and overaged structures are identical, their markedly different post-machining fatigue behavior strongly suggests that the above effects are microstructure and closure-related, rather than a sole function of notch or crack tip plasticity.[53]

Although the current experiments have not been performed on naturally-occurring short cracks, they do indicate that when fatigue cracks possess a limited wake, e.g., when they are short or emanating from a notch, they are subjected to a smaller influence from closure forces, which accounts for their ability to propagate at nominal stress intensities **below** the fatigue threshold. Moreover, their subsequent crack propagation will depend strongly on the generation of crack closure. As the effective crack driving force for this process, e.g., ΔK_{eff}, must reflect both an increase in crack length (which increases ΔK_{eff}) and an increase in closure (which decreases ΔK_{eff}), subsequent behavior will depend predominately on the efficiency of developing new closure and the specific mechanisms involved. This can be governed by mechanical factors, such as the creation of a wake of plastically-deformed material, environmental factors, such as the oxidation of the crack surface, or microstructural factors, such as the interaction and deflection of the crack at phase or grain boundaries. This implies that growth rates in this regime will be non-unique with stress intensity range, i.e., K-based similitude is violated.[20] In the present case, where the contribution from roughness-induced closure varies with aging treatment, it is the microstructural factors which appear prominant.

Thus, as illustrated in Fig. 5.4, depending upon the particular aging condition, growth rates may increase or decrease with increasing crack length, before merging with the long crack constant amplitude data, similar to naturally-occurring short crack behavior.

5.5 Conclusions

Based on a study of the development, location, and effect of crack closure on near-threshold fatigue growth rate behavior in 7150 aluminum alloy heat treated in the under, peak and overaged conditions, the following conclusions can be made:

1. The existence of a threshold stress intensity range for the extension of long fatigue cracks appears to be controlled primarily by the level of crack closure.

2. Based on the measurement of closure stress intensities during the in situ removal of material left in the wake of threshold cracks arrested at ΔK_{TH}, approximately 50% of the closure was found to be confined to the immediate vicinity of the crack tip (i.e., within 500 μm).

3. On removal of wake material to within 500 μm of the tip, previously-arrested cracks (at R = 0.10) recommenced to propagate even though nominal stress intensity ranges did **not** exceed threshold levels, representing the behavior of physically short cracks emanating from notches. In similar experiments performed at high load ratios (R = 0.75), threshold cracks remained dormant.

4. At threshold levels, crack closure re-developed on subsequent extension of the physically short cracks over distances comparable with

microstructural dimensions, leading to a deceleration in growth rates. The development of closure was most efficient in the underaged microstructures where the inhomogeneous nature of deformation promoted faceted crack growth and hence roughness-induced crack closure.

6. ROLE OF CRACK TIP SHIELDING IN LONG AND SHORT CRACK GROWTH IN 2124 ALLOY

6.1 Introduction

There are many factors which contribute to differences in behavior between long and short cracks.[1-20,28,35,49] The problem of microstructurally-small flaws, for example, may simply result from the inappropriate use of continuum mechanics involving the preferential initiation and growth of flaws in "soft spots" in the microstructure. Conversely, where crack sizes are comparable with the extent of crack tip plasticity, or where cracks are embedded within the plastic zone of a notch, differences may result simply from the inappropriate use of LEFM in characterizing crack tip fields.[53] Other major differences have been related to the three-dimensional nature of crack growth,[49] anomalously higher plastic strains at the tips of microstructurally-small cracks,[54] and environmental effects.[18,20] However, in essence, the problem is one of a breakdown in similitude[20] and thus in defining the appropriate "crack driving force" for small crack growth. Such a driving force must account for excessive plasticity ahead of the crack tip and more importantly crack tip shielding[28] behind it.

Whereas crack tip plasticity, non-uniform growth, and environmental effects all represent important factors which distinguish the behavior of

small flaws, explanations based on shielding, principally relying on a reduced effect of crack closure at small crack sizes, appear to be the most critical (e.g., refs. 16,19,24,34,49). Theoretical models, however, showing a variation in closure with crack length are rare. In fact, apart from the finite element models of plasticity-induced closure (e.g., ref. 55), only the analytical model of fluid pressure-induced closure[44] predicts a reduction in closure at short crack sizes. Furthermore, owing to difficulties in experimental measurement, there are few experimental results which provide confirmation.

6.2 Crack Tip Shielding

In fracture mechanics terms, the extension of a crack can be considered to be driven by the presence of a **"crack driving force"** and opposed by the **resistance of the microstructure.** Here the driving force is generally defined by a field characterizing parameter, such as the stress intensity K_I or path-independent integral J, which describes the dominant stress and deformation fields in the vicinity of the crack tip from a knowledge of crack size, applied load and geometry. By similitude, cracks are then assumed to extend at equal rates when subjected to equal "driving forces". Crack advance is thus restrained by lowering the applied load or by "toughening" the material, e.g., impeding crack growth through compositional or microstructural modification.

In alloy design, it is generally the perception that toughening, or more generally resistance to crack growth, is achieved by increasing the inherent microstructural resistance, e.g., by coarsening particle spacings, increasing ductility, etc.; a process termed **intrinsic toughening.** However, in many material systems, e.g., during fatigue

crack growth in metals, and cracking in ceramics, rocks and fiber composites, the actual source of toughness may be distinctly different, arising from mechanisms of **crack tip shielding.**[28] Here crack extension is impeded, by mechanical, microstructural and environmental factors which locally reduce the crack driving force; a process termed **extrinsic toughening.**

The various micro-mechanisms of crack tip shielding, categorized into several distinct classes, are illustrated in Fig. 6.1. These classes involve shielding from a) crack deflection and meandering, b) inelastic or dilated zones surrounding the wake of the crack, termed "zone shielding", c) wedging, bridging and/or sliding between crack surfaces, termed "contact shielding", and d) combined zone and contact shielding.[28]

Under monotonic loading, shielding results in a reduction in the local driving force, whereas under cyclic loading the effect may take different forms (Fig. 6.2). Since the principal driving force for fatigue crack advance (under small-scale yielding) is the **range** of stress intensity, ΔK may be reduced locally by a decrease in K_{max} and a smaller decrease in K_{min}, as with crack deflection; a decrease in K_{max} and an increase in K_{min}, as with briding or sliding; or simply an increase in K_{min}, as in wedging. The nature of the mechanism or combination of mechanisms involved will thus dictate the specific behavior observed. For example, crack deflection produces a multiplicative reduction in the local Mode I stress intensity,[46] and thus may be expected to have an equal effect throughout the range of growth rates (unless the crack path morphology changes). Zone shielding from enclaves of plastic zones or

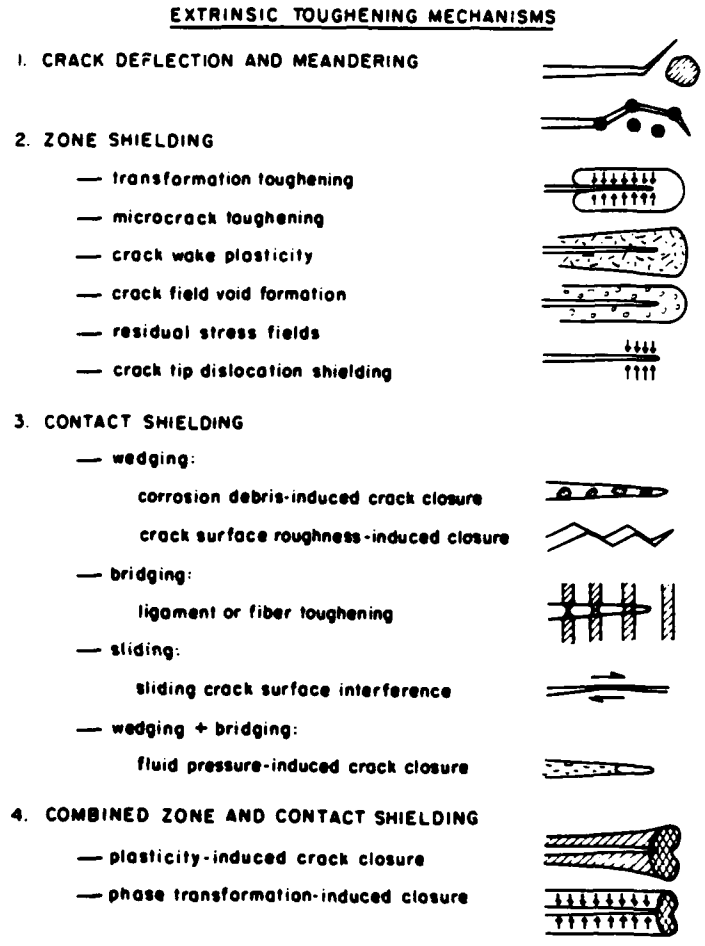

Fig. 6.1: Schematic representation of the classes and mechanisms of crack tip shielding.

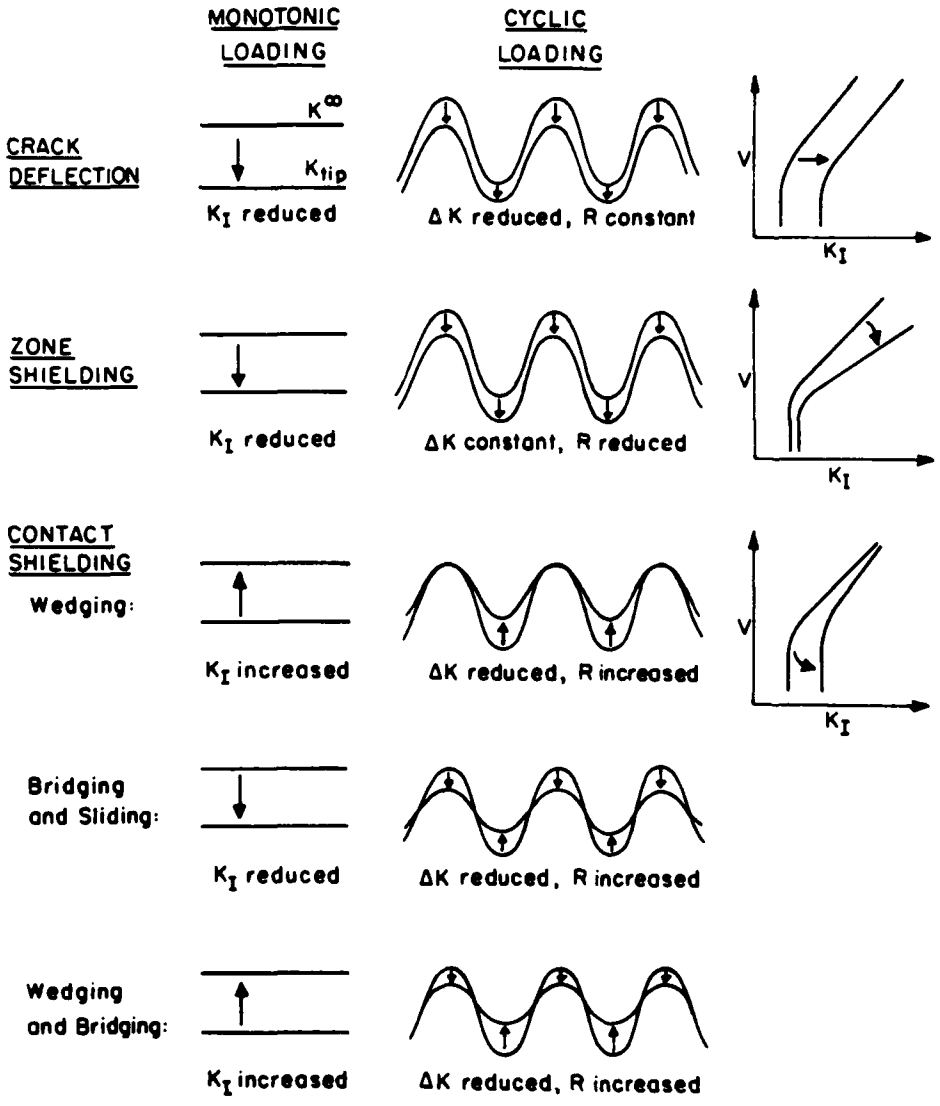

Fig. 6.2: Effect of specific crack tip shielding mechanisms on the driving force, e.g., the stress intensity K_I, and crack velocity, v, under monotonic and cyclic loading.

dilated zones of material undergoing phase transformation, microcracking or void formation, on the other hand, produces a fixed reduction in local stress intensity, at least for a constant equilibrium zone size.[56] These mechanisms are thus less potent in fatigue as the range of stress intensity remains unchanged, although the mean K_I or load ratio ($R = K_{min}/K_{max}$) is reduced. Contact shielding through wedging, conversely, raises the local stress intensity under monotonic loading, yet reduces the driving force for fatigue by opposing the closing of the crack. This latter process is the essence of the well-known phenomenon of fatigue crack closure, whereby the nominal ΔK range is reduced by effectively raising K_{min}. Contact shielding through bridging (e.g., ligament or fiber toughening[57]), or sliding (e.g., sliding crack surface interference[58]), results in a reduced driving force for both monotonic and cyclic crack extension as these mechanisms oppose both the opening and closing of the crack.

The direct implications of crack propagation dominated by shielding are a reduced cracking rate, from the lower local driving force, and crack-size dependent behavior, as the shielding mechanisms act on the wake of the crack. Three important scenarios follow.

First, the material will show resistance-curve fracture toughness behavior where the driving force to sustain cracking will increase with increasing crack length (until steady-state). Such R-cruves are common in ductile metals, where zone shielding from prior plastic zones left in the wake of the crack induces a lower strain singularity ahead of the tip (c.f., the 1/r strain singularity for a fully plastic stationary crack with the ln(1/r) singularity for a non-stationary crack[59,60]). Marked R-

curve toughness behavior is also evident in ceramics,[56] where shielding can occur from transformation and microcrack toughening, and in rocks, where shallower curves have been reported due to microcracking phenomena.

Second, microstructural factors known to be beneficial for resistance to crack initiation and the growth of small cracks may have a very different effect on the growth of long cracks.[19] This follows because the role of extrinsic mechanisms becomes negligible where the crack wake is small or non-existant. There are numerous examples of this in the fatigue literature; for example in steels, increasing yield strength or decreasing grain size results in lower thresholds for (long) crack growth, yet higher thresholds for crack initiation, i.e., higher fatigue limits.[1] In addition, grain size, texture, slip character and precipitate/phase distribution appear to have a relatively minor influence on small crack growth,[61] yet these factors have a significant influence on long crack growth rates primarily through their effect on crack closure and deflection.[45]

Third, "small crack" effects are to be expected, since, at the same nominal driving force, the small crack may experience a higher local driving force, due to diminished shielding, which causes it to propagate at a rate in excess of the long crack.

During Mode I fatigue crack propagation, the predominant shielding mechanisms are crack closure, induced primarily by cyclic plasticity[33] (combined zone and contact), corrosion debris,[38-40] fracture surface roughness (contact by wedging) and fluid pressure[44] (contact by combined wedging and bridging), and to a lesser extent crack deflection[46]

(although deflection promotes roughness-induced closure). With the exception of the plasticity-induced mechanism, all are enhanced at near-threshold stress intensities due to the smaller crack tip opening displacements and a greater tendency of fatigue cracks to follow a microstructurally-sensitive or crystallographic crack path. It is in this regime, pertinent to the present study, where the most important small crack effects are found and moreover where the microstructural features favoring (long) crack growth are most at variance with those favoring initiation.[45] Accordingly, experiments were designed to demonstrate the size-dependence of short crack growth rates and to verify the dominant role played by crack tip shielding in promoting such behavior.

6.3 Results

Long Crack Behavior:

Fatigue crack growth rate data at R = 0.1 for underaged and overaged microstructures in 2124 alloy are shown in Fig. 6.3 for 17.5 to 38 mm long cracks over the range 5×10^{-11} to 10^{-7} m/cycle. Corresponding results at higher load ratios are shown in Fig. 6.4. Growth rates (da/dN) are plotted as a function of both the nominal stress intensity range, ΔK, and, after allowing for crack closure (Fig. 6.5), the effective stress intensity range, ΔK_{eff}, defined as $K_{max} - K_{cl}$.

Similar to long crack results in 7000 series alloys (Fig. 4.1), underaged structures show lower near-threshold fatigue crack propagation rates and higher threshold ΔK_{TH} values compared to overaged structures. Such superior crack growth properties have been associated with the planar slip characteristics of coherent particle hardened

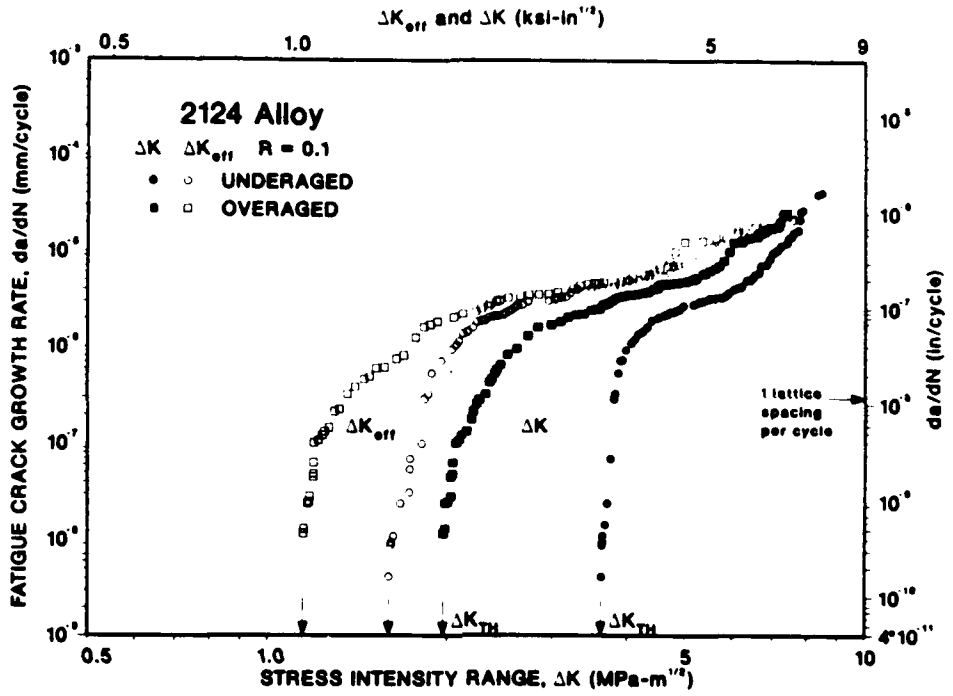

Fig. 6.3: Fatigue crack propagation behavior of long cracks in underaged (T351) and overaged 2124 alloy at R = 0.10. Growth rates are plotted as a function of the nominal stress intensity range, ΔK, and ΔK_{eff} after correcting for crack closure.

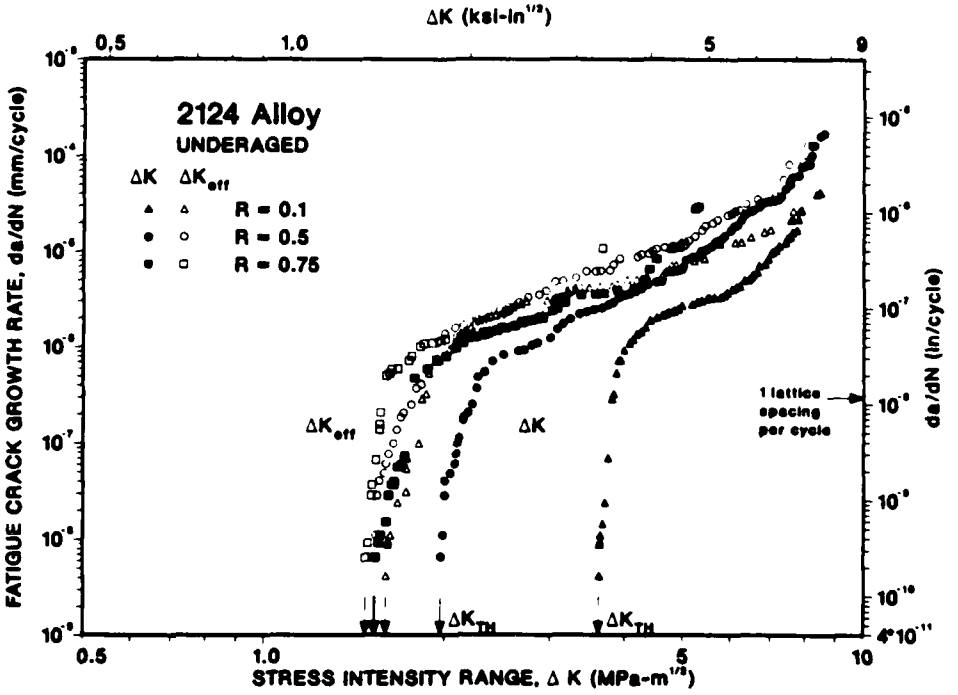

Fig. 6.4: Fatigue crack propagation behavior of long cracks in underaged (T351) 2125 alloy at load ratios of R = 0.10, 0.50, and 0.75. Note how the variation in da/dN and threshold values with R is significantly reduced when growth rates are characterized in terms of ΔK_{eff} rather than ΔK.

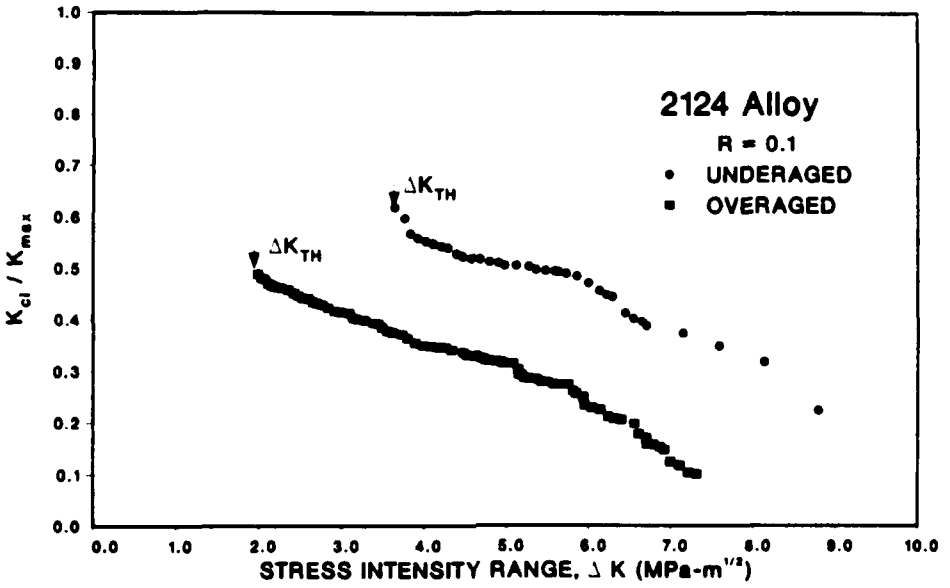

Fig. 6.5: Variation in fatigue crack closure with nominal stress intensity range for long cracks in underaged (T351) and overaged 2124 alloy at R = 0.10. Results, plotted as the ratio of closure to maximum stress intensity, K_{Cl}/K_{max}, are based on back-face strain measurements and correspond to the growth rate behavior presented in Fig. 6.3.

microstructures, as described in Section 4. The roughness-induced mechanism appears to be the most prominant mode of closure for air environments in this alloy as the extent of fracture surface corrosion deposits remain small compared to crack opening displacements and higher closure levels are detected in the underaged condition. However, it is clear from Fig. 6.3 that considerations of crack closure alone do not account for the full effect of microstructure on near-threshold growth rates.

Conversely, the effect of load ratio in lowering ΔK_{TH} values and in accelerating near-threshold growth rates appears to be attributable solely to a reduced influence of closure. As shown in Fig. 6.4, growth rate data are threshold values for load ratios of 0.1, 0.5 and 0.75, become virtually identical when ΔK_{eff} is used in place of ΔK as the crack driving force.

From Fig. 6.5, it is clear that the magnitude of closure for long cracks increases as the stress intensity range is decreased towards the threshold. To define the distribution of such closure along the crack length, measurements of K_{cl} were made on arrested threshold cracks (at $R = 0.1$) during the progressive removal of their wake. Results, in the form of the reduction in K_{cl} as a function of the length of the remaining (unmachined) fatigue crack (Fig. 6.6), indicate significant closure in the immediate vicinity of the crack tip, consistent with previous studies (described in Section 5). In the present underaged microstructure, over 60% of the closure is located within 900 μm of the tip.

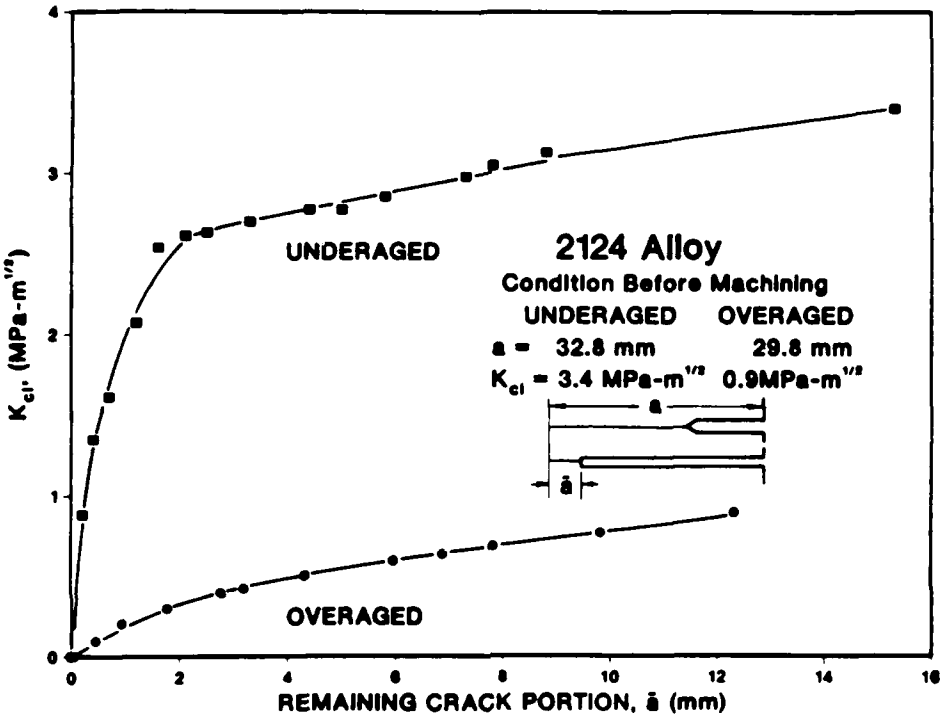

Fig. 6.6: Measurements in K_{cl}, performed during wake removal, showing the distribution of crack closure along the length of an arrested threshold long crack in a) underaged (T351) and b) overaged 2124 alloy.

Following removal of their wake, threshold cracks arrested at R = 0.1 were observed to propagate when cycling resumed at the threshold ΔK_{TH}, similar to behavior reported for 7090, 7150 aluminum alloys and A508 steel.[23,24,34,49] Such observations of crack growth at the threshold provide confirmation that experimentally measured values of K_{TH} are associated primarily with the build-up of closure, and do not necessarily represent an intrinsic material threshold. Consequently, where shielding mechanisms are inhibited, such as with small flaws or cracks at notches, or in the presence of compressive overload cycles,[25,26,27] the consequent increase in near-tip driving force may result in crack growth at or below ΔK_{TH}, and in general to growth rates which exceed those of long cracks at the same stress intensity level.

Short Crack Behavior at Notches:

The experiment described above, where crack extension at ΔK_{TH} was observed following removal of the wake of an arrested threshold crack, additionally provides an example of the accelerated growth of short cracks at notches, i.e., a fatigue crack (of length 250 μm) growing from a notch (of root radius $\sim$ 300 μm) in a region well beyond the notch field. Under constant load conditions with ΔK initially at ΔK_{TH}, cracks at R = 0.75 remain stationary, whereas at R = 0.1 they commence to propagate in both structures. Even though the nominal ΔK levels are marginally increasing, such growth occurs at a progressively decreasing growth rate over the first 300 μm, displaying the "trough-like" behavior characteristic of small cracks at near-threshold levels (Fig. 6.7).

Such behavior can be readily accounted for by considerations of crack tip shielding, specifically through characterization in terms of a

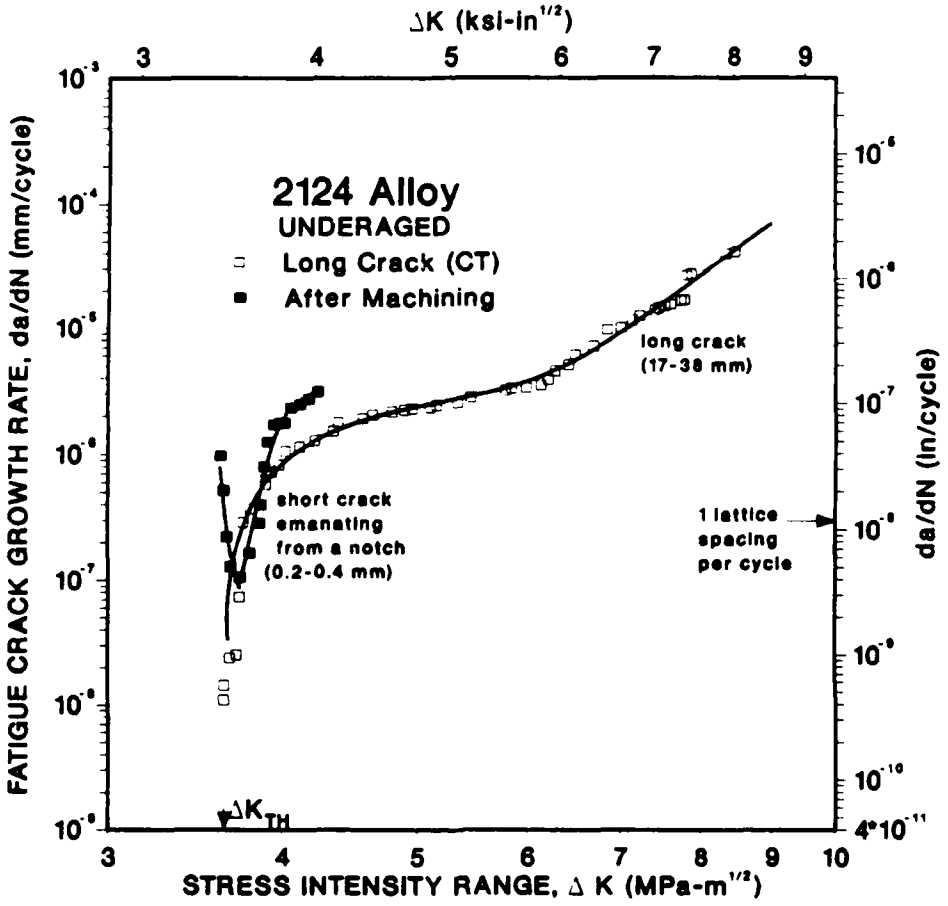

Fig. 6.7: Comparison of fatigue crack propagation data in underaged (T351) 2124 aluminum alloy at R = 0.10, showing results for long cracks (a = 17-38 mm) and physically-short cracks (a = 200-400 μm) emanating from a machined notch.

local driving force (see Section 5). Concurrent back-face strain measurements of K_{cl}, over the 1 mm of growth following wake removal, show a steady increase in closure with initial short crack extension (Fig. 6.8). The value of K_{cl} approaches an apparent saturation value, after roughly 400 μm of crack extension, comparable with the long crack K_{cl} value at threshold. As indicated in the figure, when such K_{cl} data are incorporated into the calculation of an effective stress intensity range, it can be seen that the initial progressive reduction in growth rates shown by the short crack is directly consistent with a corresponding progressive decrease in ΔK_{eff}.

It should be noted that the "small crack effect" observed in this experiment was achieved with a short crack of length 200 to 400 μm; length dimensions which are large compared to the scale of local plasticity (maximum plastic zone sizes do not exceed 20 μm). Thus, so-call.. "anomalous" behavior of small flaws does not necessarily result simply from a breakdown of linear elastic fracture mechanics, but rather from differences in the **local** crack driving force due to the varying influence of crack tip shielding with crack length.

Physically-Short Crack Behavior:

Results for the behavior of physically-short cracks growing from a free surface are shown in Figs. 6.9-6.10 for the underaged (T351) microstructure. Specimens were cycled at a series of stepwise increasing ΔK levels starting well below the threshold ΔK_{TH}. As shown in Fig. 6.9, for an initial crack length of approximately 50 μm, short crack growth commences with a rate initially exceeding 10^{-8} m/cycle at a ΔK level as low as 0.58 MPa$\sqrt{m}$, only to decelerate progressively until arrest at 0.67

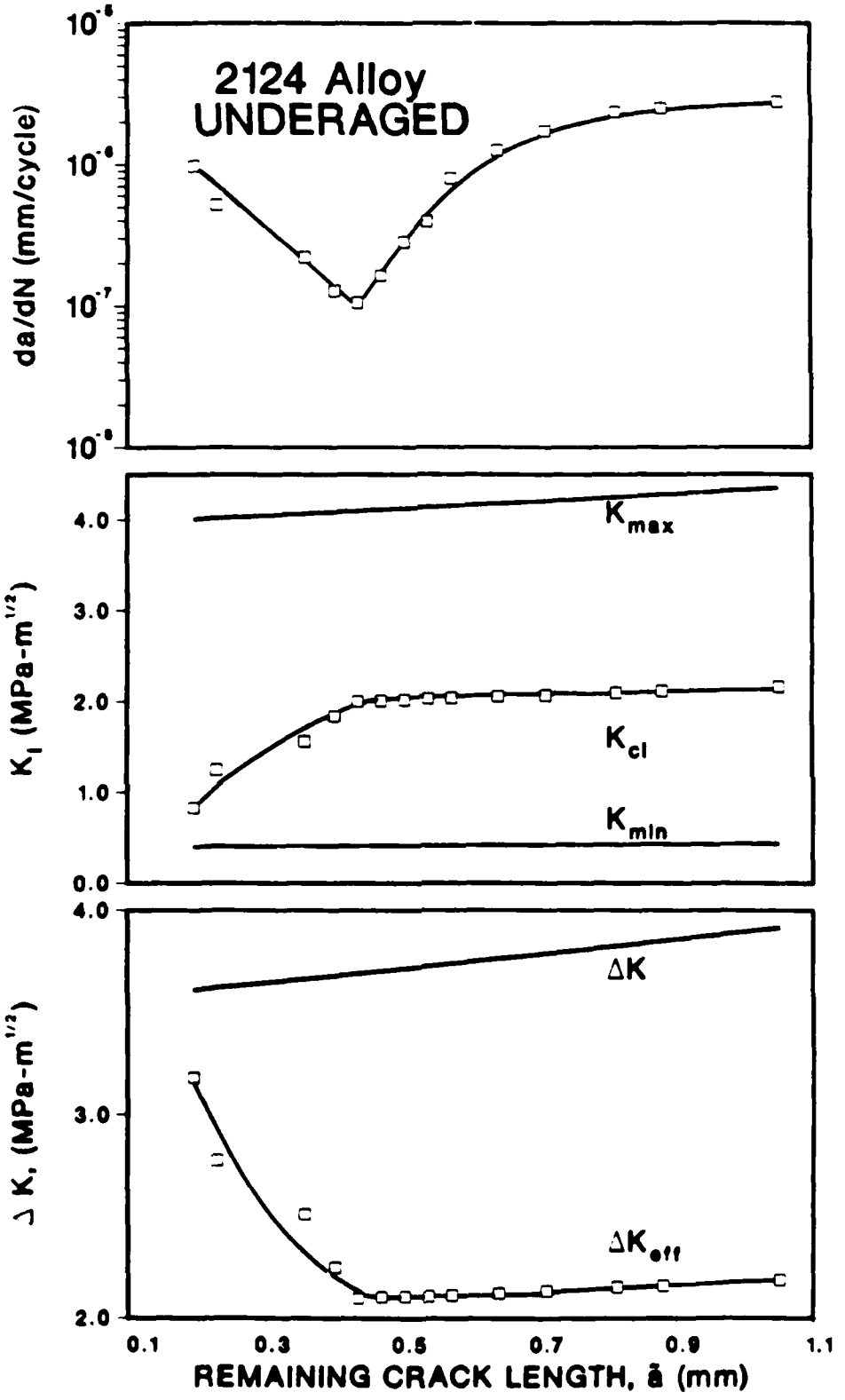

Fig. 6.8: Variation in growth rate, K_{cl}, and nominal and local crack driving forces, ΔK and ΔK_{eff}, respectively, with initial crack extension at $\Delta K = \Delta K_{TH}$ for physically-short cracks (a = 100-400 μm) emanating from a machined notch in 2124-T351 alloy at R = 0.10.

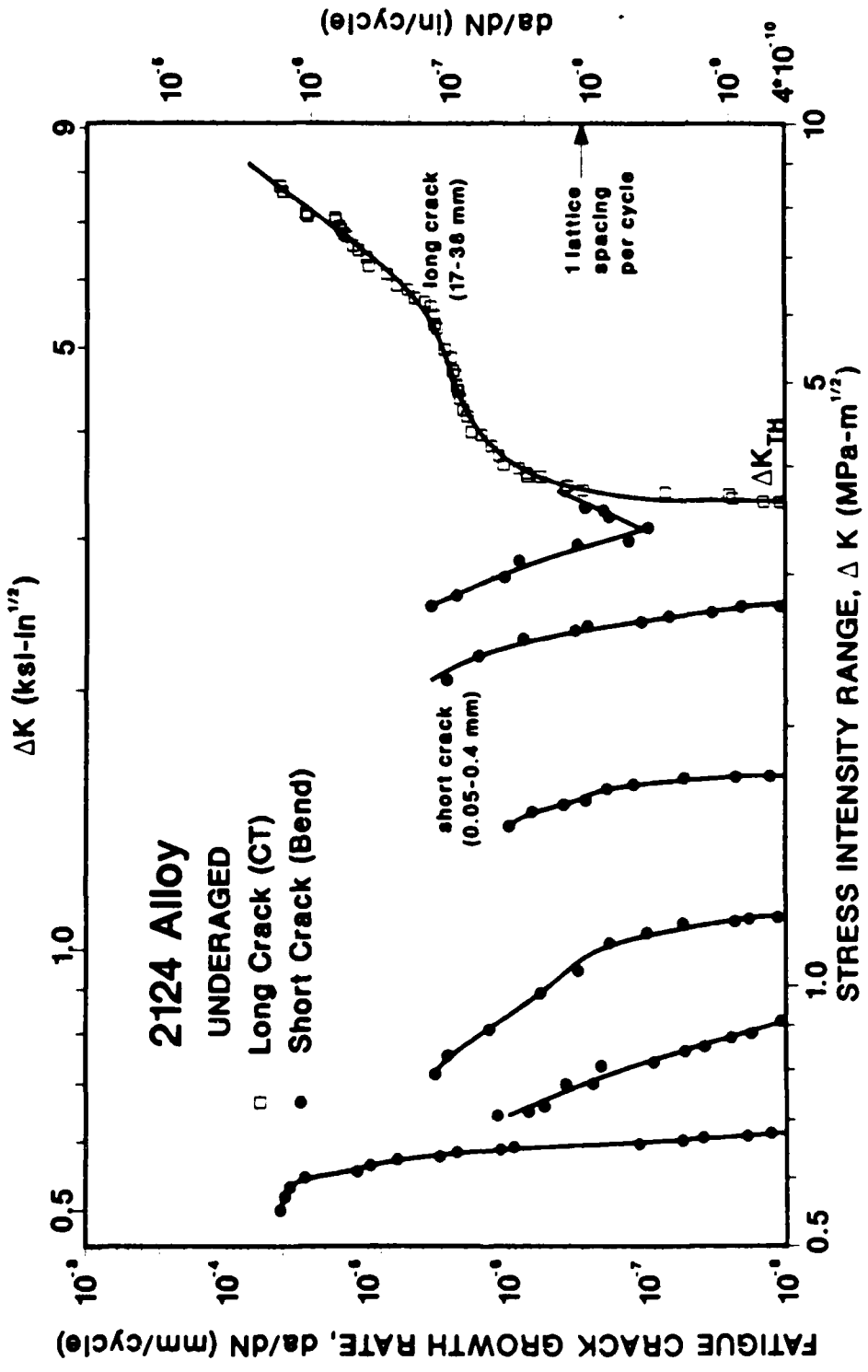

Fig. 6.9: Variation in fatigue crack growth rates in 2124-T351 alloy at R = 0.10, showing a comparison of results for long cracks (a = 17-38 mm) and physically-short cracks (a = 50-400 μm) emanating from a free surface. Note how the short crack grows at sub-threshold stress intensities at progressively decreasing growth rates, arresting after each decay sequence until finally merging with long crack data.

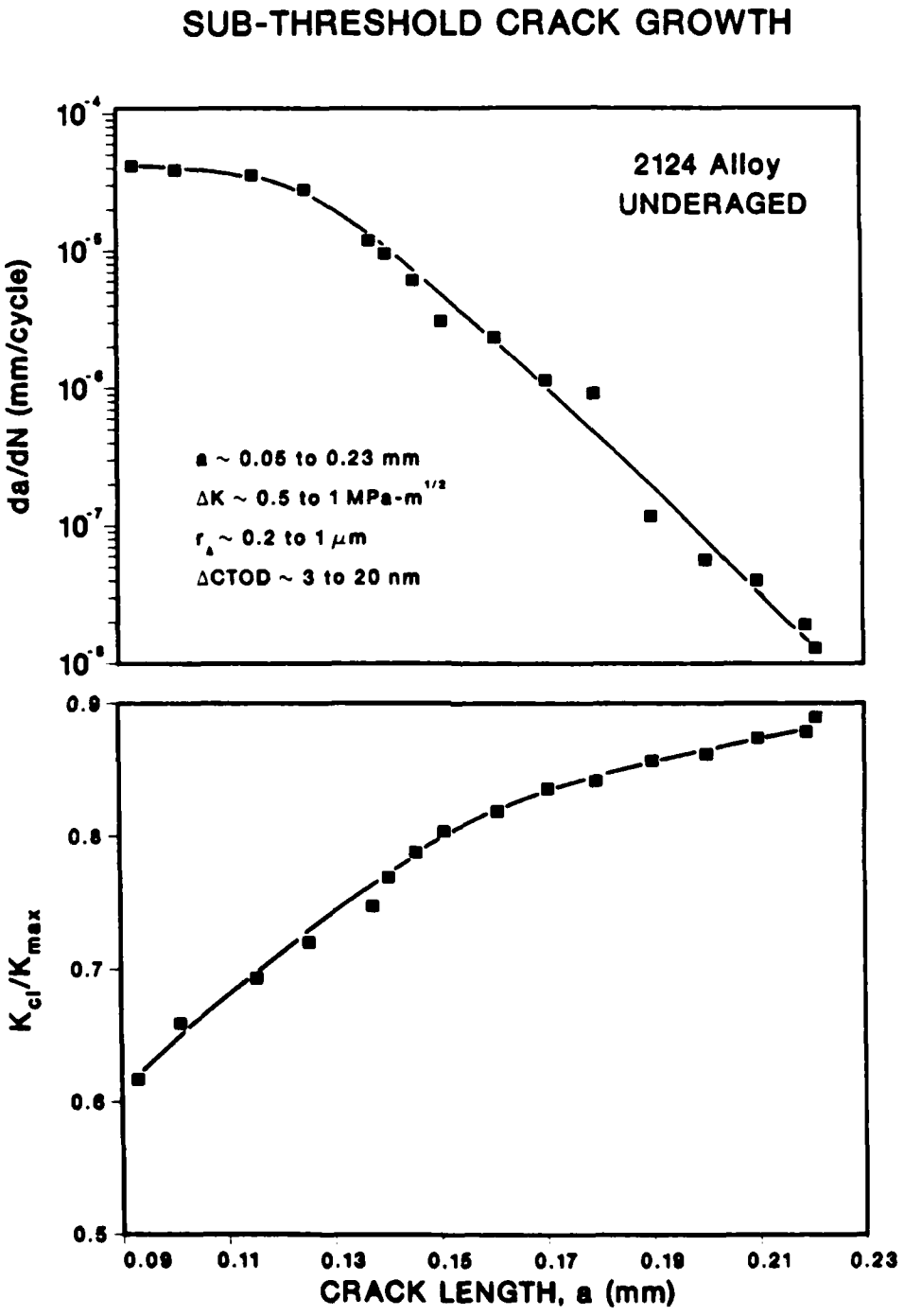

Fig. 6.10: Variation in da/dN and K_{cl}/K_{max} with crack extension during sub-threshold propagation of physically-short cracks in 2124-T351 alloy, corresponding to data in Fig. 6.9. Note how crack closure is generated during initial crack extension (a = 90 to 230 μm), concurrent with the progressive decay in growth rates to crack arrest.

$MPa\sqrt{m}$ after an extension of roughly 140 μm. After an increase in applied load, cracking abruptly re-starts, again followed by progressive deceleration to arrest. This sequence of events is repeated several times until the crack length reaches 450 μm, whereupon the short crack data merges with long crack results following a characteristic minimum in growth rates.

During each deceleration and arrest event for the short crack, the development of crack closure with crack extension was closely monitored. Results for one such event, involving the extension of a 90 μm long crack to 230 μm, are shown in Fig. 6.10. **The progressive reduction in growth rates leading to arrest can be seen to be associated directly with a concurrent increase in crack closure,** which results in a corresponding reduction in ΔK_{eff}. The magnitude of this increase is associated with very high levels of K_{cl}/K_{max} approaching 0.9, far in excess of those for long cracks. Although closure data were not measured during every arrest event in Fig. 6.9, it was apparent that, since the crack retained closure generated from previous load steps, there was a cumulative increase in K_{cl} throughout the entire sequence.

6.4 Discussion

The current experimental results provide quantitative evidence of the dominant role of crack tip shielding, specifically from fatigue crack closure, in influencing the near-threshold behavior of both long and physically-short fatigue cracks. First, with respect to long cracks, wake machining experiments clearly show that i) the existence of a threshold stress intensity range for no crack growth, ΔK_{TH}, and ii) the effect of load ratio in influencing ΔK_{TH}, can be attributed to variations

in the magnitude of the closure stress intensity, K_{cl}. The commonality of threshold values for each structure, when computed in terms of ΔK_{eff}, would appear to suggest that some intrinsic threshold does exist for long cracks.

Second, for (two-dimensional) physically-short cracks, both emanating from a sharp notch or at a free surface, observations of crack growth at stress intensities below ΔK_{TH}, at rates which progressively decay to arrest or merge with long crack data, have been shown to be associated quantitatively with an initial lack of shielding and its subsequent development with crack extension. Specifically, the sub-threshold decay in short crack growth rates has been related to a concurrent increase in K_{cl}, such that the local driving force, ΔK_{eff}, sees a minimum.

6.5 Conclusions

Based on an investigation into the role of crack tip shielding in influencing the behavior of long and small fatigue cracks, involving an experimental study of long ($\gtrsim$ 25 mm) and physically-short ($\sim$ 50-400 μm) near-threshold cracks in 2124 aluminum alloy, the following conclusions can be made:

1. The existence of a threshold stress intensity range ΔK_{TH} for the dormancy of long cracks was found to be associated with high levels of crack closure, with values of K_{cl}/K_{max} approaching 0.7. By accounting for such closure through the use of the ΔK_{eff} parameter, the influence of load ratio, but not microstructure, in affecting long crack growth rates and threshold values became minimal.

2. Through removal of material from the wake of long cracks, arrested at the threshold, to discern the distribution of shielding, over 60% of the closure was found to be located within 900 μm of the crack tip.

3. Through-thickness physically-short cracks, both emanating from a sharp notch or from a free surface, were observed to propagate at nominal stress intensity ranges at, or below, ΔK_{TH}. Short crack growth rates were observed to decay progressively until arrest (or before merging with long crack data), concurrent with a measured increase in K_{cl} and consequent reduction in ΔK_{eff}.

4. Differences in behavior between long and physically-short cracks appear to be rationalized largely by the variation in crack closure with the extent of crack wake. However, as short cracks were still observed to propagate **below** the effective threshold stress intensity range (after accounting for closure), other factors, such as enhanced crack tip plastic strains, must be involved.

7. ROLE OF COMPRESSION OVERLOADS IN INFLUENCING FATIGUE CRACK PROPAGATION IN 7150, 2124 AND 2090 ALLOYS

7.1 Introduction

Whereas compression cycles are often a common occurrence in service, particularly for aerospace applications, and are known to be of importance in the process of crack initiation in smooth specimens, their effect on the propagation of (long) fatigue cracks, at least at intermediate to high ΔK levels, has long been considered to be minimal (e.g., ref. 62). This is in keeping with standard fracture mechanics

concepts which imply that the crack will be closed during the compressive portion of the cycle, necessitating a stress intensity of zero at the tip, and the fact that tests invariably have been performed on long cracks where the magnitude of both tensile and compressive stresses are small. Although data are limited, several authors have found growth rates to be slightly faster at negative load ratios compared to R = 0 in both steels and aluminum alloys,[62-68] although the effect is negligible in certain alloys such as 7075-T6.[62] Under variable amplitude fatigue loading, however, cyclic compressive stresses immediately following tensile overloads are known to lessen the post overload retardation in growth rates which usually accompanies single tensile overloads.[69-71] Moreover, under certain conditions of cracks initiating from notches, fatigue crack growth has been demonstrated under purely cyclic compressive loading.[72] In fact, the technique has been used as a reliable means of producing small flaws for short crack experiments.[16,65]

Unlike behavior at higher growth rates where effects are small, recent studies at near-threshold levels have highlighted a significant role of compressive cycling on crack extension behavior.[25,26,65-68,78] Not only are threshold ΔK_{TH} values lower at R = -1 compared to R = 0, but large periodic compressive cycles (of the order of one half the yield stress) applied during positive R cycling have been shown to dramatically reduce the threshold and to accelerate crack growth rates in both mild steel[68] and 2024-T3 aluminum.[67,68] Physical explanations for these effects remain unproven, although several suggestions have been proffered including redistribution of residual stresses ahead of the crack tip and reduced closure forces due to a diminished deformation zone left behind

the crack tip.[67] In addition, periods of compression during the fatigue cycle are likely to result in a flattening of fracture surface asperities and a compacting of corrosion debris on crack faces, both processes leading to a reduction in closure via the roughness-induced and oxide-induced mechanisms, respectively.

The objectives of the current study were to investigate the role of single compression overload cycles on the propagation behavior of cracks arrested at the threshold, and specifically to monitor the variation in crack closure, both macroscopically in terms of K_{cl} measurements and microscopically in terms of changes in fracture surface morphology. Precipitation hardened aluminum alloys 7150, 2124 and 2090 were chosen for the study because in such systems the operative mechanisms of closure can be readily varied by heat treatment.

7.2 Experimental Procedures

Compression overload experiments were performed by first determining the long crack threshold using manual load shedding cycling, as described elsewhere.[1] In this manner, constant amplitude (steady-state) crack growth data between $\sim 10^{-6}$ and 10^{-11} m/cycle were obtained under decreasing ΔK conditions, with the threshold ΔK_{TH} operationally defined as the highest stress intensity range giving growth rates less than 10^{-11} m/cycle. Single (spike) compressive overloads were then applied to cracks arrested at ΔK_{TH}. The length of such arrested cracks was of the order 5 to 7 mm beyond the 17.5 mm initial notch in the compact specimen, i.e., a $\approx$ 23 to 25 mm. With the applied loading conditions then maintained at a constant $\Delta K = \Delta K_{TH}$, subsequent growth rate and crack closure behavior were monitored closely. The magnitudes of the

compression overload cycles were varied between 1 and 5 times the maximum tensile load in the fatigue cycle, i.e., up to a maximum compressive load between 1.8 and 2.8 kN corresponding to a fictitious "negative" stress intensity of 12 to 17 MPa$\sqrt{m}$. The application of the single compression overloads at $\Delta K = \Delta K_{TH}$ was repeated two or three times on each specimen with at least 200 μm of crack extension between each event.

7.3 Results

Steady-State Fatigue Behavior: 7150

The variation in fatigue crack propagation rate (da/dN) and corresponding crack closure data as a function of the nominal stress intensity range (ΔK), at R = 0.10 and 0.75, are shown in Figs. 4.2 and 4.3 for the under-, peak and overaged microstructures in 7150 alloy under steady-state (non variable amplitude conditions). Results indicate that the progressively lower threshold values (and higher near-threshold growth rates), which are seen with increased aging, are consistent with less measured closure at R = 0.10. Relevant threshold data for these microstructures, including the extent of crack surface oxidation and degree of fracture surface roughness, are listed in Table 4.1.

Steady-State Fatigue Behavior: 2090-T8E41, 2124

Fatigue crack propagation rate data for 2090-T8E41 are plotted in Fig. 7.1 as a function of ΔK and ΔK_{eff}. Data are compared with 2124 alloy. Corresponding closure K_{cl} values are given by the data points in Fig. 7.2. At R = 0.1, the alloy shows a nominal fatigue threshold of ΔK_{TH} = 3.4 MPa$\sqrt{m}$, which is comparable with other high strength aluminum alloys, such as 2124 and 7150, in their commercial tempered conditions

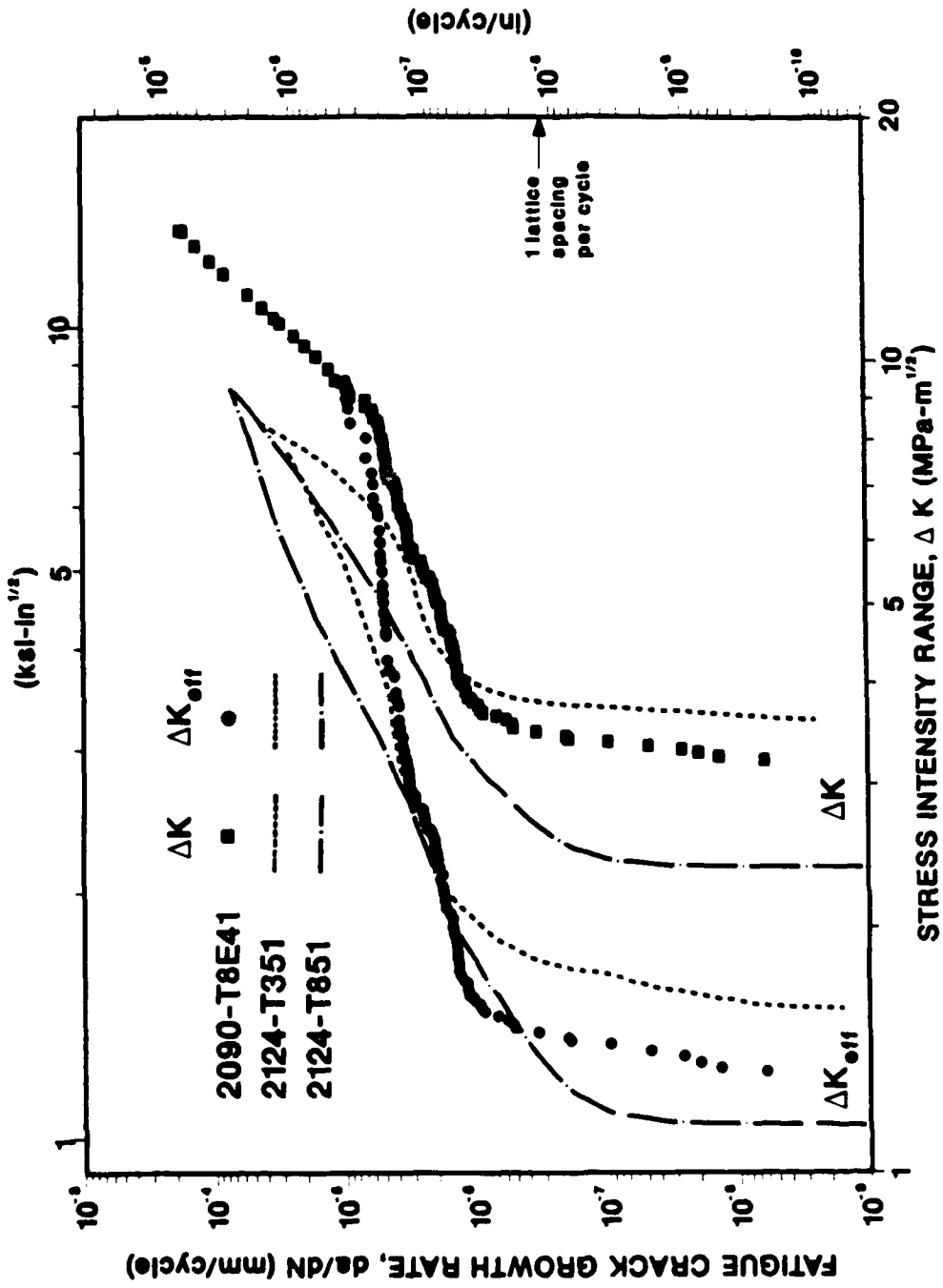

Fig. 7.1: Fatigue crack propagation behavior of 2090-T8E41, compared to 2124, at R = 0.10 in moist air, plotted as a function of the nominal and effective stress intensity range, ΔK and ΔK_{eff}, respectively. ΔK_{eff} values are based on crack closure measurements shown in Fig. 7.2.

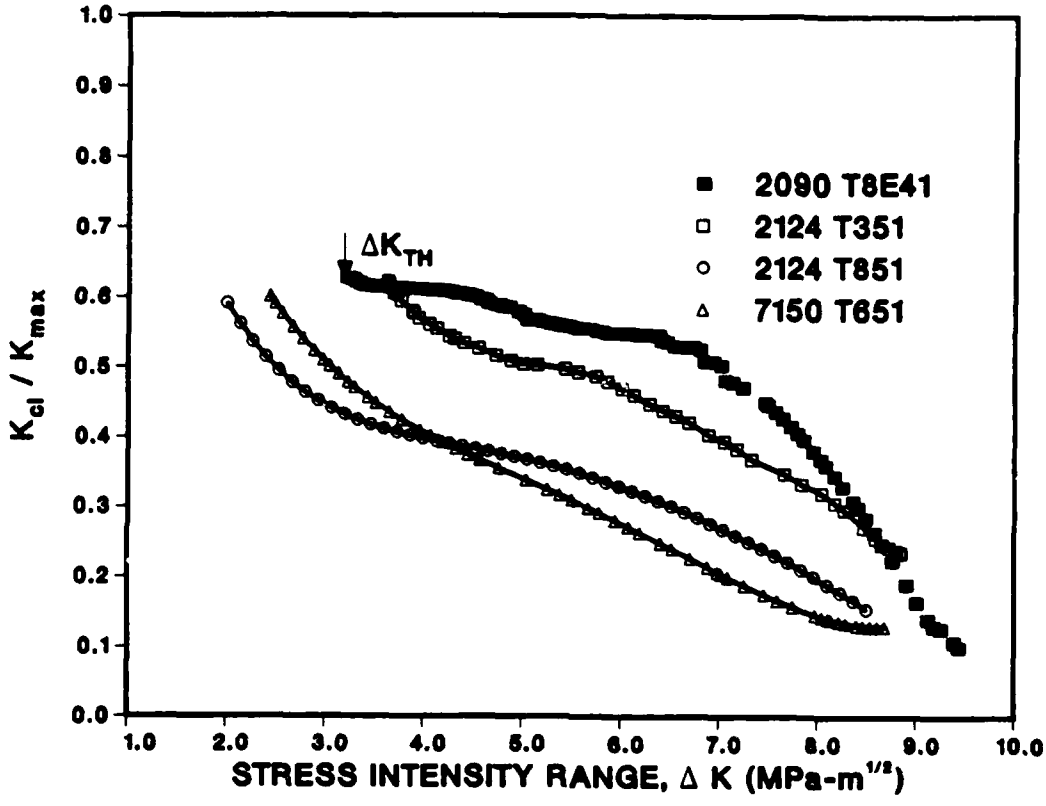

Fig. 7.2: Variation in closure stress intensity, K_{cl}, normalized with respect to K_{max}, with nominal stress intensity range, ΔK, for 2090-T8E41 alloy at R = 0.10. For comparison, crack closure data are also shown for 2124 and 7150 alloys.

(Fig. 7.3). Despite having at least 30% higher strength than the other alloys, crack advance in 2090 can be seen to be consistently slower over the entire range of growth rates (except for near-threshold growth in 2124-T351), and to show a particular superiority above 10^{-9} m/cycle. The latter observations are not associated solely with an increased elastic modulus, as 2090 still shows lower growth rates compared to 2124 and 7150 when the data are replotted in terms of ΔK, normalized with respect to Young's modulus (Fig. 7.3b). Conversely, the improved crack growth properties appear to be consistent with the fact that, unlike 2124, crack closure levels in 2090 do not decay rapidly with increasing stress intensity range above the threshold; rather K_{cl} values remain above 50% K_{max} out to ΔK levels above 7 MPa$\sqrt{m}$ (Fig. 7.2).

The higher levels of crack closure, which give rise to a lower ΔK_{eff} and hence to slower growth rates, are consistent with the highly crystallographic nature of the crack path in 2090, compared to traditional aluminum alloys, such as 2124, as illustrated in Fig. 7.4. Similar to that reported for other aluminum-lithium alloys,[47] the crack path shows frequent deflections at both near-threshold and particularly higher ΔK levels, giving it a marked "zig-zag" appearance from propagation along slip bands. Resulting fracture surfaces are thus characterized by numerous "cleavage-like" facets, with additional evidence of secondary cracking.

Although such crystallographic crack path morphologies are not uncommon in precipitation-hardened aluminum alloys, particularly at near-threshold levels in coherent particle-hardened (planar slip) microstructures (see Section 4), behavior in Al-Li alloys is striking in

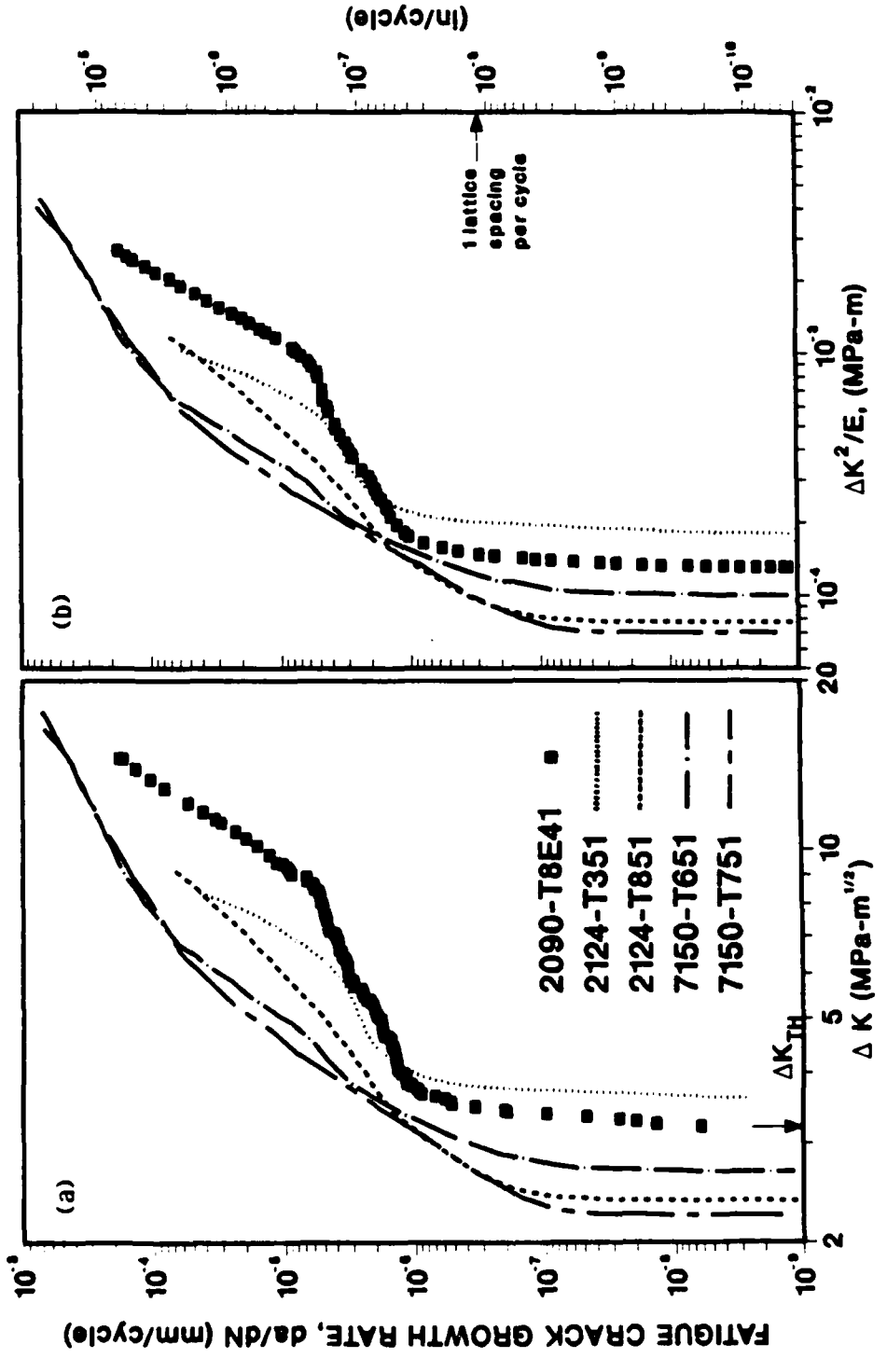

Fig. 7.3: Comparison of fatigue crack propagation behavior at R = 0.10 in 2090-T8E41 alloy with behavior 2124 and 7150 alloys. Growth rates are compared on the basis of a) the nominal stress intensity range, ΔK, and b) ΔK^2, normalized with respect to Young's modulus, E.

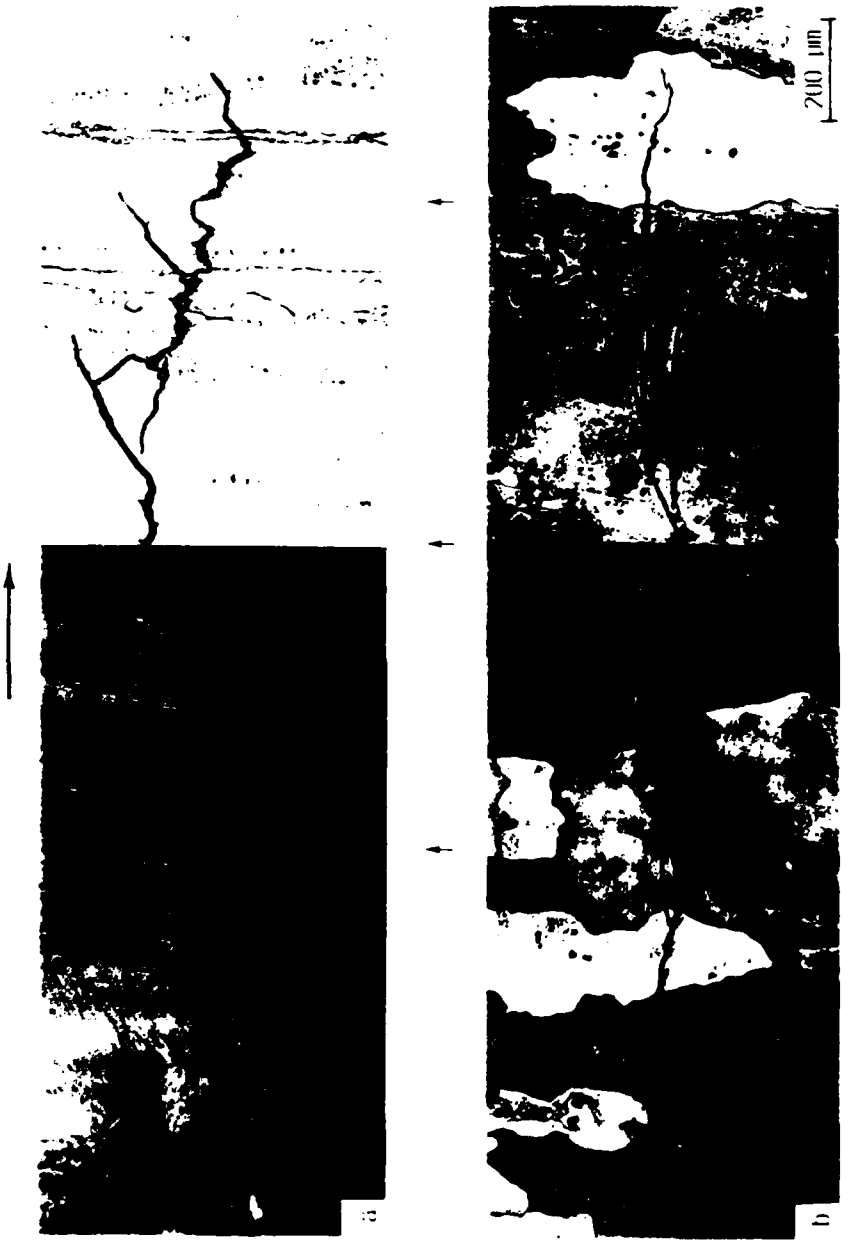

Fig. 7.4: Morphology of the fatigue crack path in a) 2090-T8E41 alloy, compared to b) 2124-T351 alloy tested under similar conditions. Note the strongly crystallographic and deflected crack path in the aluminum-lithium alloy. Crack path profiles are derived from metallographic sections, taken perpendicular to the crack surface at the center of the specimen.

that this mode persists to much higher growth rates, accounting for the higher levels of closure and much slower growth rates above 10^{-9} m/cycle. In this regard, aluminum-lithium resembles other alloy systems with strongly planar slip characteristics, such as the nickel-based superalloys, where a marked crystallographic crack growth is observed up to high ΔK levels.[74] It is in contrast to conventional alloys where the crystallographic mode predominates only at low stress intensities, approximately where the cyclic plastic zone size is of the order of, or less than, the grain size.[45]

Compression Overload Experiments: 7150

Application of 100 to 300% single (spike) compression overloads (corresponding to 1 to 3 times the peak tensile loads) was observed to have no effect on crack closure or crack growth of arrested cracks at the threshold in 7150 alloy. Crack growth behavior following the application of 500% compression overloads, however, is shown in Fig. 7.5 for the underaged, peak aged and overaged microstructures. Here the compressive cycle has been applied and the subsequent closure and growth rates monitored under constant $\Delta K = \Delta K_{TH}$ cycling conditions. It is clearly apparent that the application of the compressive overload causes immediate propagation of the arrested cracks, even though the stress intensity range does not exceed ΔK_{TH}. Moreover, under such constant ΔK conditions, the initial acceleration, to as high as $\sim 10^{-8}$ m/cycle, is followed by a progressive deceleration in growth rates until re-arrest. The extent of crack growth before re-arrest occurs is of the order of 60 μm in the underaged structure, far smaller than in the peak and overaged structures where the crack extends a further 130 and 170 μm,

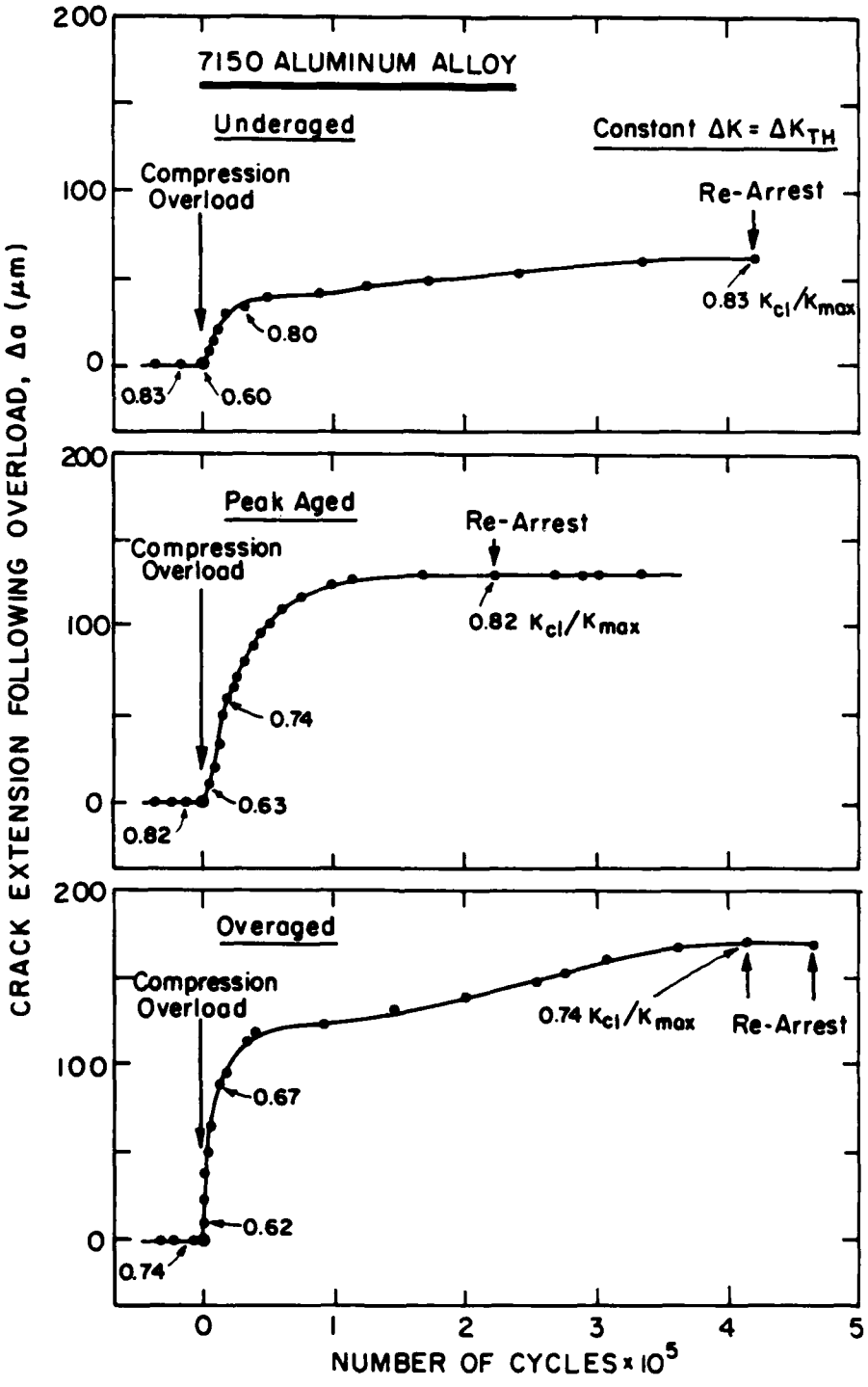

Fig. 7.5: Fatigue crack extension as a function of the number of cycles following application of 500% compression overloads on arrested threshold cracks in underaged, peak-aged and overaged 7150 aluminum alloy. Data obtained under constant $\Delta K = \Delta K_{TH}$ cycling conditions at R = 0.10. K_{cl}/K_{max} closure data are listed at the bottom of each figure.

respectively, before arrest. Application of a second single compression overload on the re-arrested crack at this stage produced identical results.

Such behavior was accompanied by significant changes in the magnitude of the crack closure. The initially high closure values which are associated with the original arrest at the threshold, i.e., K_{cl}/K_{max} values of the order of 0.75-0.85, were reduced immediately by 16 to 28% to approximately 0.60 by the compressive overload. With further crack extension, however, the closure was re-generated until arrest again occurred at a K_{cl}/K_{max} level similar to that of the original (pre-overload) threshold. Such closure measurements, together with the corresponding effective ΔK_{eff} values, are listed in Table 7.1. Plots of the pre- and post-overload growth rates as a function of both ΔK and ΔK_{eff}, computed from these data for individual tests, are shown in Figs. 7.6 and 7.7, respectively. It can be seen that the "anomalously" high growth rates at ΔK_{TH}, resulting from the application of the compression cycles, fall within the scatter-band for steady-state growth rates when characterized in terms of ΔK_{eff} rather than ΔK. This clearly implies a dominant role of closure. Following compression overload cycles, the well-defined features of the fatigue fracture surfaces (e.g., Fig. 4.4) become obscured somewhat. As shown in Fig. 7.8, there are clear indications of abrasion, compacted fretting oxide debris and the cracking and flattening of fracture surface asperities close behind the crack tip. These features, which always predominated in the immediate vicinity of the crack tip, were profuse in underaged structures where the asperities were most pronounced due to the faceted nature of the crack path.

Table 7.1: ΔK_{eff} and Crack Extension Data at $\Delta K = \Delta K_{TH}$ Before and After Compression Overloads on Arrested Cracks

Microstructure	ΔK_{TH}	At Initial Arrest		Following Overload		At Re-Arrest		Crack Ext. to Re-Arrest
		K_{cl}/K_{max}	ΔK_{eff}	K_{cl}/K_{max}	ΔK_{eff}	K_{cl}/K_{max}	ΔK_{eff}	
	(MPa$\sqrt{m}$)		(MPa$\sqrt{m}$)		(MPa$\sqrt{m}$)		(MPa$\sqrt{m}$)	(μm)
Underaged	3.14	0.83	0.59	0.60	1.40	0.83	0.59	60
Peak-Aged (T6)	2.81	0.82	0.56	0.63	1.15	0.82	0.56	130
Overaged (T7)	2.17	0.74	0.63	0.62	0.92	0.74	0.63	170

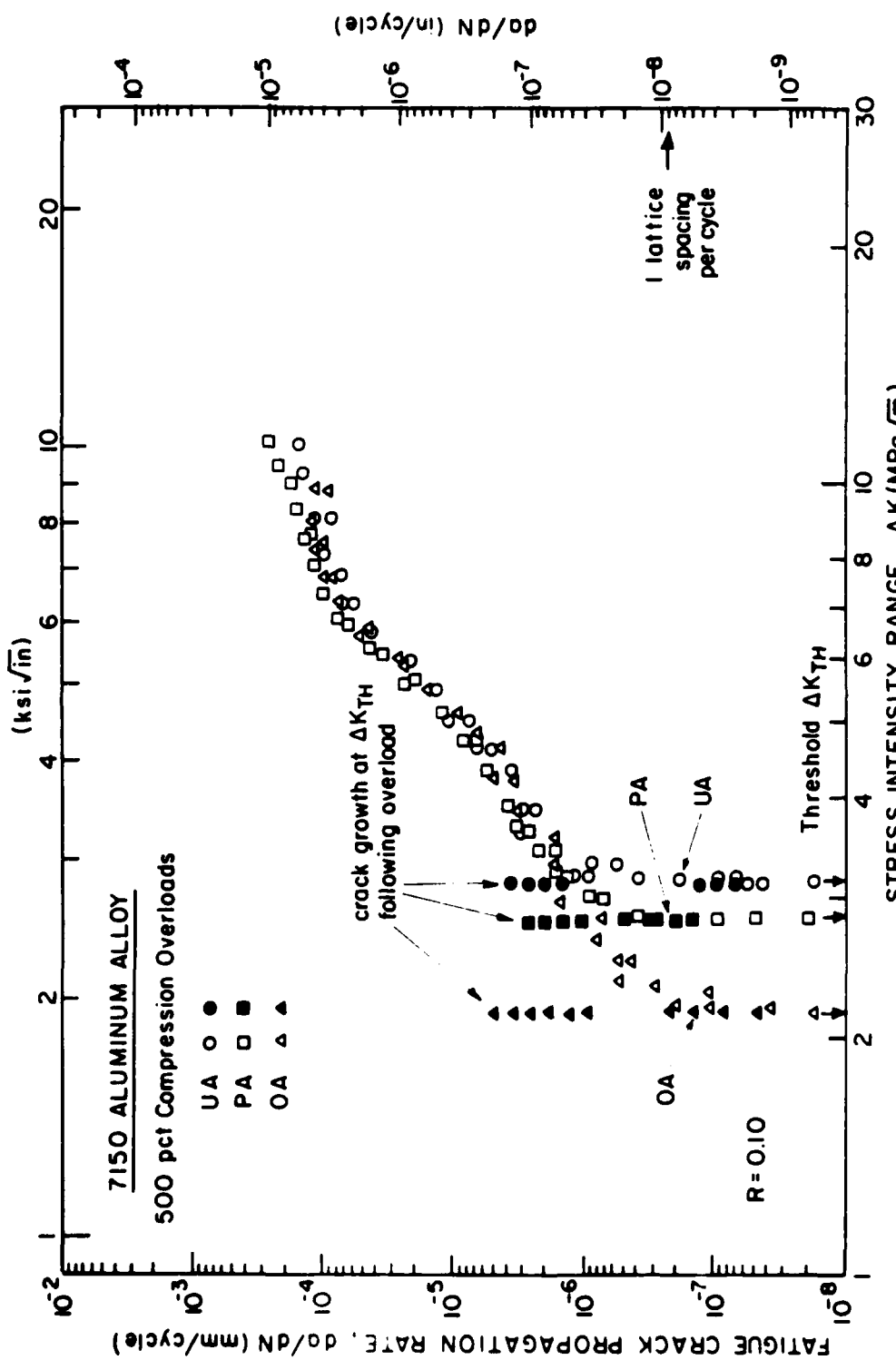

Fig. 7.6: Fatigue crack growth rate behavior, as a function of nominal stress intensity range (ΔK), for cracks previously arrested at the threshold (ΔK_{TH}) following the application of single 500% compression overloads (solid symbols). Data for underaged (UA), peak-aged (PA) and overaged (OA) microstructures in 7150 aluminum alloy are compared with steady-state results from individual tests at R = 0.10 (open symbols).

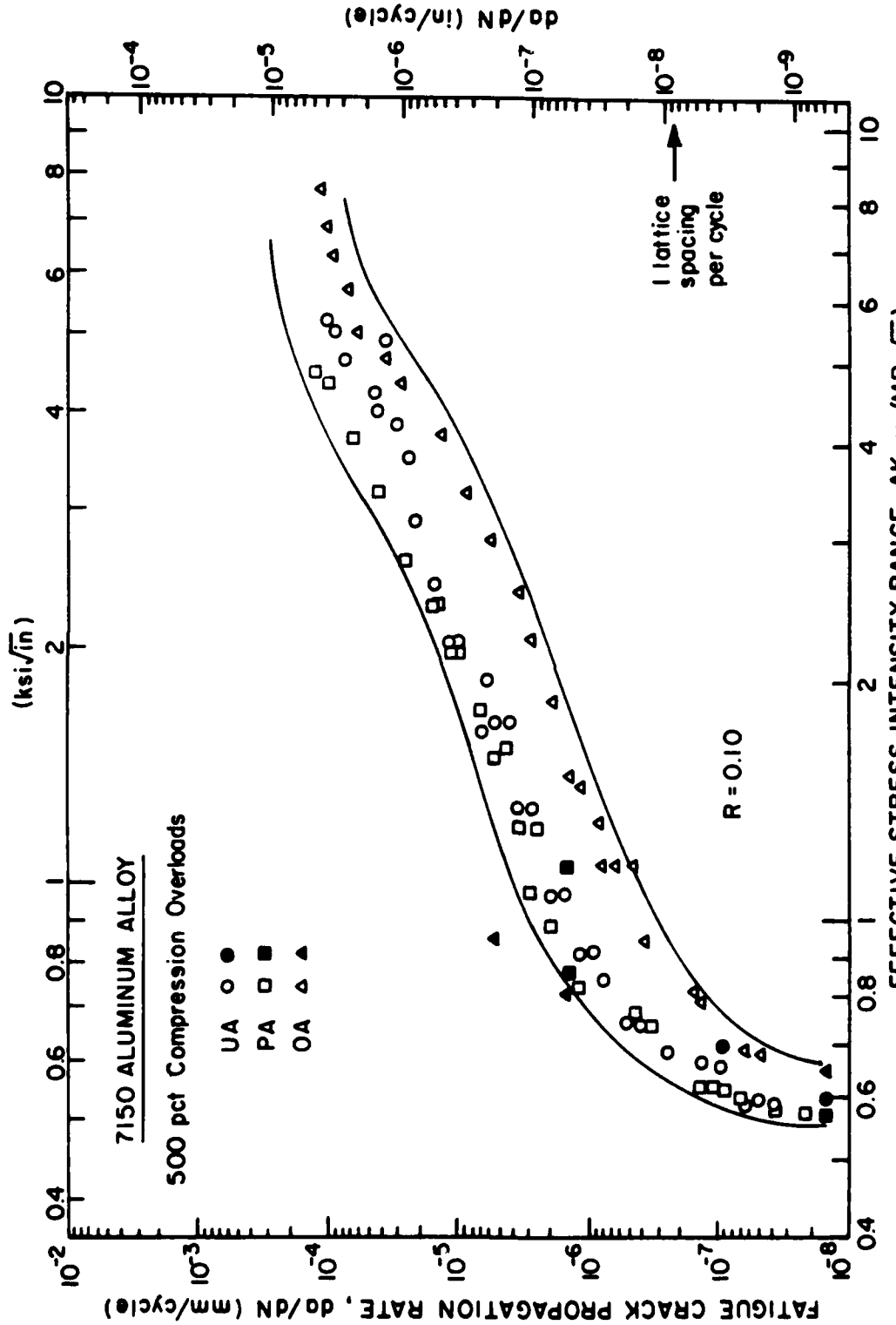

Fig. 7.7: Fatigue crack growth rates, as a function of the effective stress intensity range (ΔK_{eff}), for both steady-state behavior (open symbols) and following application of 500% compression overloads (solid symbols). Data from Fig. 7.5 for underaged (UA), peak-aged (PA) and overaged (OA) microstructures in 7150 aluminum alloy. ΔK_{eff} calculations based on measured closure stress intensity data.

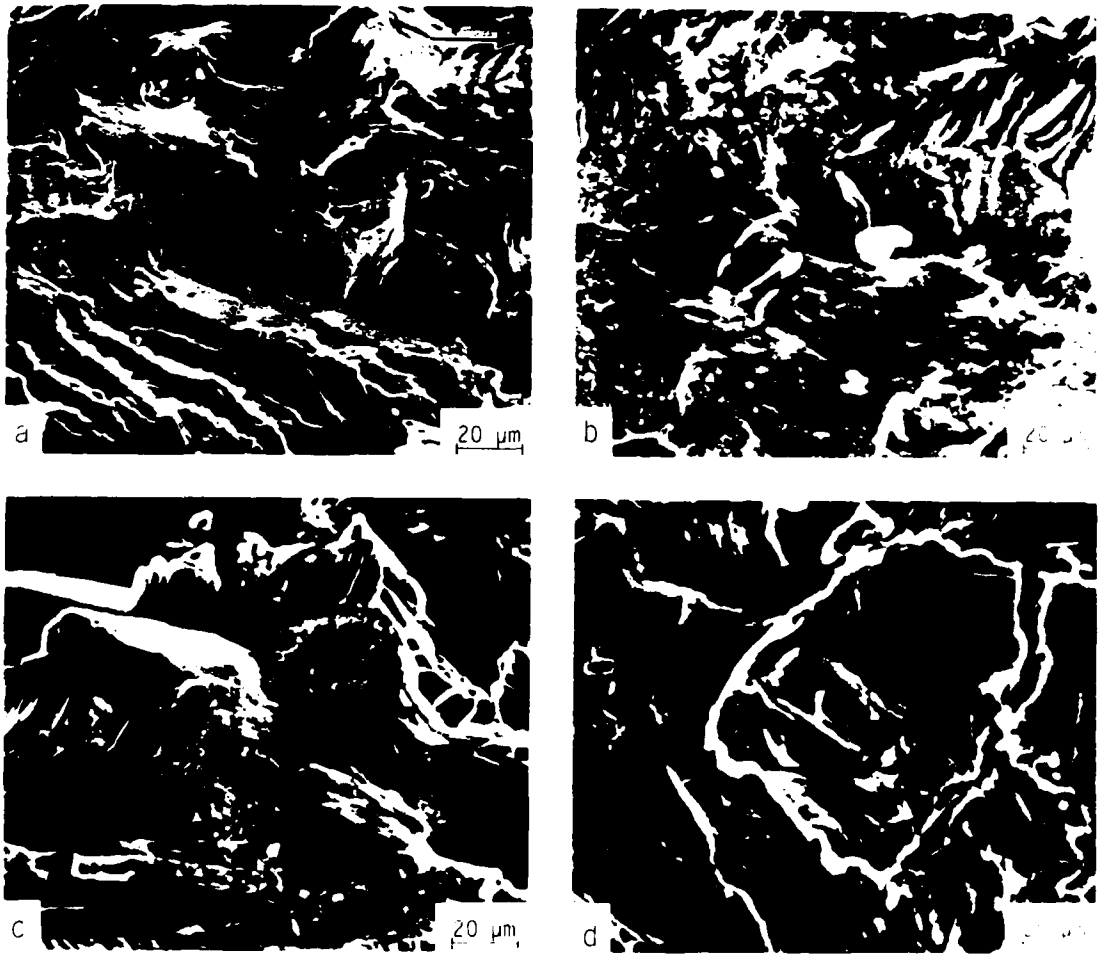

Fig. 7.8: Scanning electron micrographs of fatigue fracture morphology in underaged 7150 aluminum alloy directly behind the crack tip at the threshold ($\Delta K \approx 3.2$ MPa$\sqrt{m}$), showing a) well-defined facets before the application of the compression overload, and b) fretting oxide debris, c) asperity flattening and d) asperity cracking after the application of the overload. Arrow indicates general direction of crack growth.

Compression Overload Experiments: 2090-T8E41

The effect of single (spike) compressive overloads on cracks in 2090 arrested at ΔK_{TH} is shown in Fig. 7.9, in terms of post-overload crack extension as a function of number of cycles. The application of a 100% compression cycle (corresponding to a compressive load of equal magnitude to the peak tensile load at threshold) showed no detectable effect on either crack closure or crack growth. Compression cycles of 200% and above, however, resulted in rapid crack extension, following short dormant periods, even though conditions were maintained at a constant ΔK equal to the threshold. Above 400% compression, cracking commenced immediately following the overload, without any dormant period.

The initial acceleration at ΔK_{TH}, which is shown in Fig. 7.10 as function of compressive load amplitude, was followed by a progressive deceleration in growth rates until re-arrest. Post-overload crack extensions to re-arrest ranged from 110 μm, following 200% compression, to 410 μm, following 400% compression. Similar to 7150 alloy, such behavior was found to be concurrent with a measured reduction in K_{cl} at the overload, and the subsequent re-generation in closure with further crack extension. Quantitative estimates of the consequent increase in local "crack driving force", ΔK_{eff}, at the overload, and its decay with crack extension until re-arrest, are plotted in Fig. 7.11. Fractographically, the reduction in closure following compression overload cycles could be attributed to signs of fretting debris and specifically to compaction of asperities and abrasion on fracture surfaces, similar to behavior in 7150.

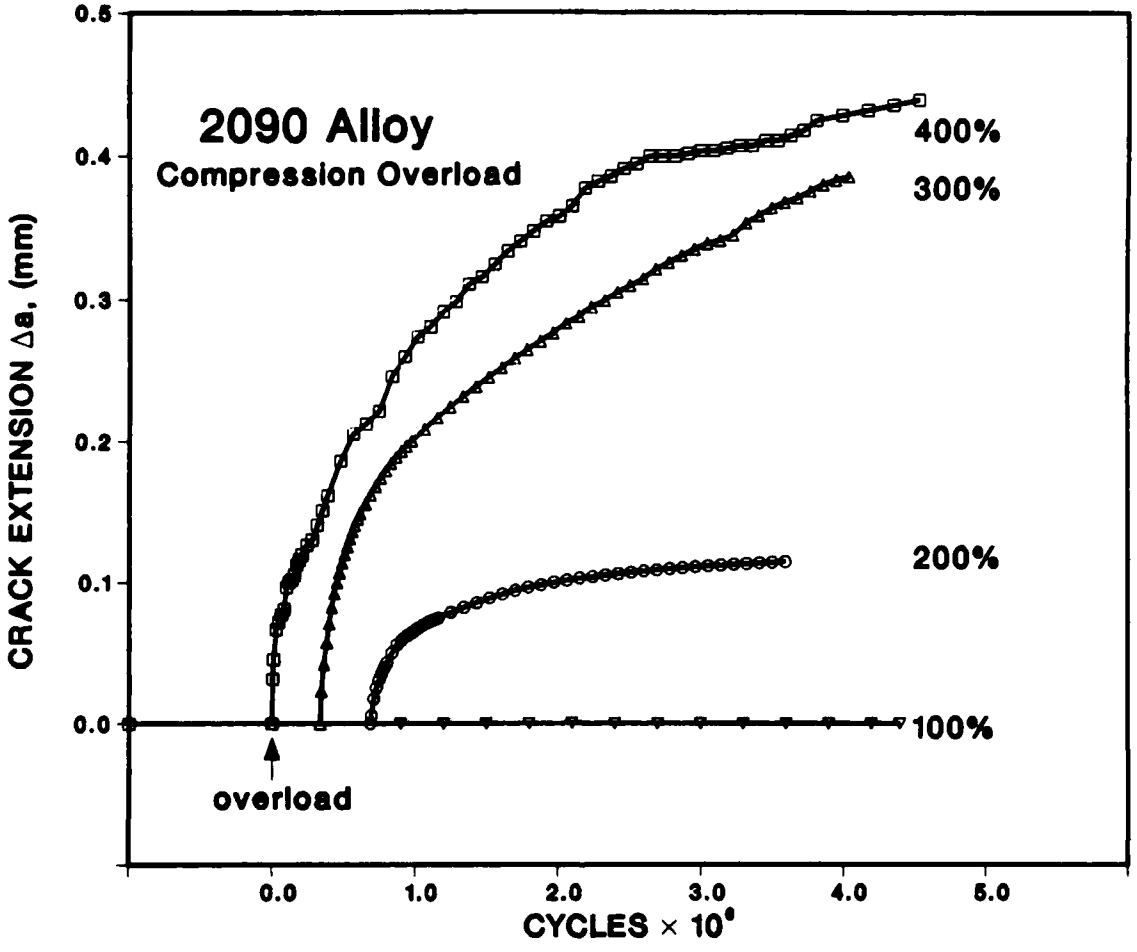

Fig. 7.9: Fatigue crack extension at constant $\Delta K = \Delta K_{TH}$ in 2090-T8E41 alloy, as a function of the number of cycles following the application of 100, 200, 300 and 400% single compression overload cycles. Compression overloads are applied to cracks arrested at the threshold ΔK_{TH} at R = 0.10.

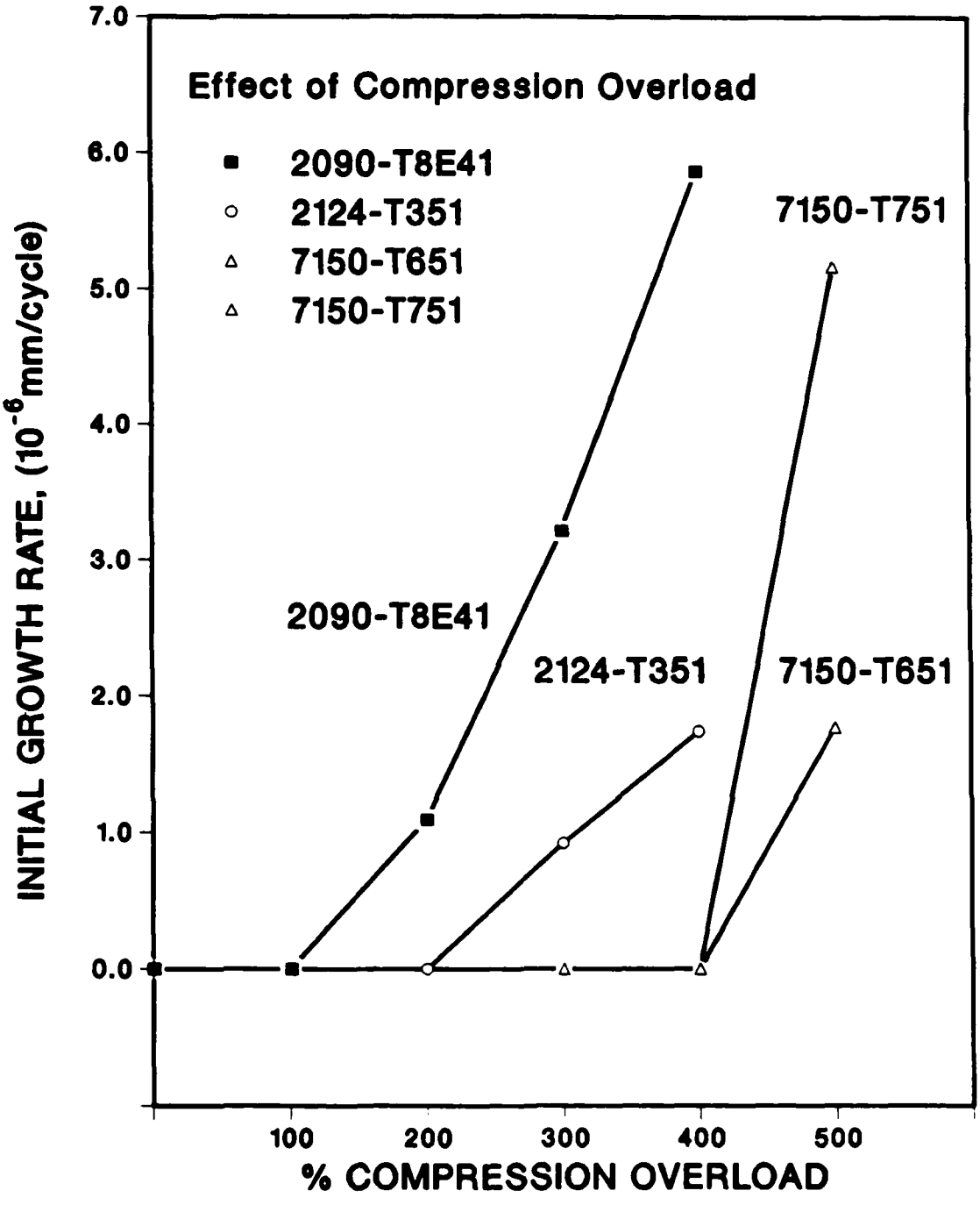

Fig. 7.10: Comparison of compression overload results for 2090-T8E41 with results for 2124 and 7150, showing initial crack growth rate, following the compression cycle, as a function of the magnitude of the overload. Note the increased sensitivity of the aluminum-lithium alloy to the compression cycles.

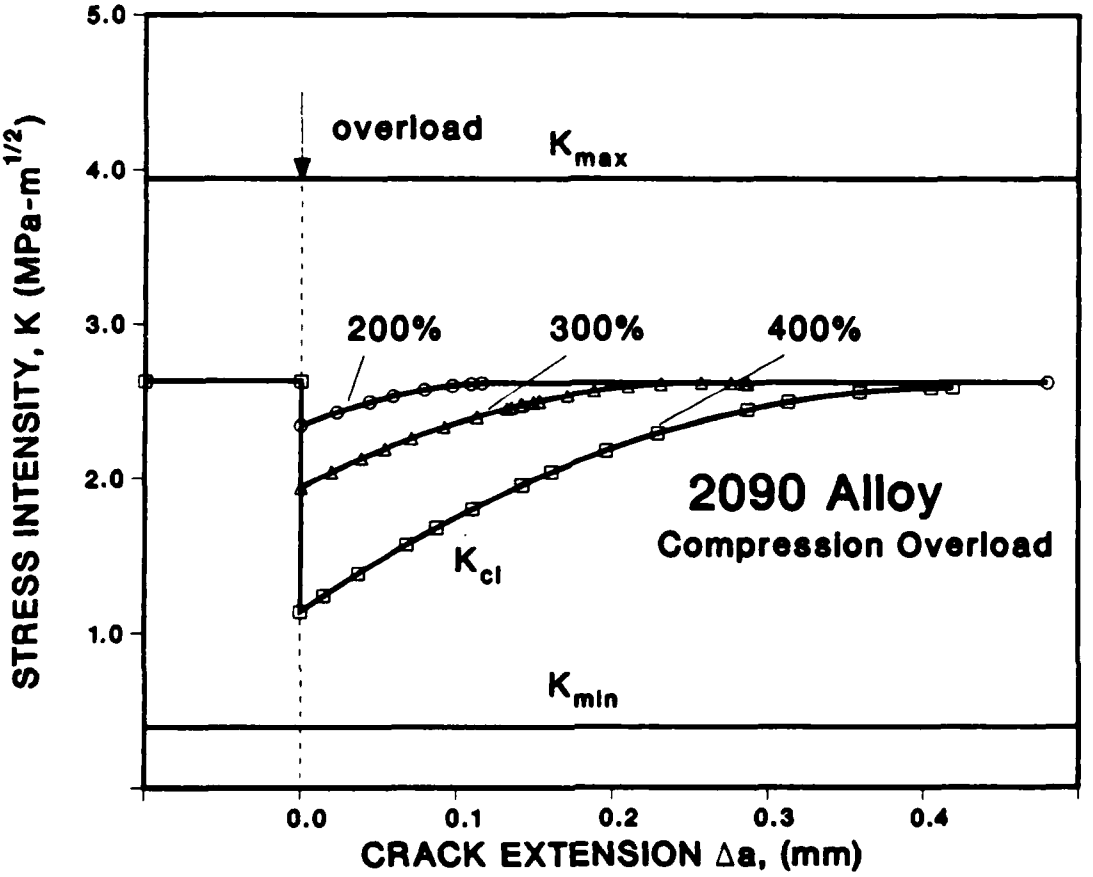

Fig. 7.11: Variation in ΔK (= K_{max} - K_{min}) and ΔK_{eff} (= K_{max} - K_{cl}) with crack extension at ΔK_{TH} for fatigue crack growth following compressive overloads on arrested threshold cracks in 2090-T8E41 alloy. ΔK_{eff} values are computed from K_{cl} data, measured using the back-face strain compliance technique.

7.4 Discussion

For comparison, data for 2124-T351, 7150-T651 and 7150-T751, measured under identical test conditions, are included in Fig. 7.10. Whereas 200% compression overloads are required to re-initiate cracking at ΔK_{TH} in 2090, at least 300% overloads are required in 2124 and 500% overloads in 7150. It is apparent that, although the aluminum-lithium alloy shows much improved crack growth properties under constant amplitude conditions, in the presence of periodic compression loading, the growth of arrested threshold cracks can occur far more readily. Paradoxically, both features are a consequence of the same phenomenon, i.e., the tortuous crack paths and resultant crack closure from asperity wedging, which are characteristic of coherent particle-hardened microstructures and particularly of aluminum-lithium alloys. The crack deflection and roughness-induced closure certainly provide enhanced crack tip shielding to impede crack extension, yet, by the same token, the increased dependence on crack closure due to any wedging mechanism inside the crack will necessarily make the alloy prone to "damage" (i.e., reduced shielding and a higher ΔK_{eff}) in the presence of compressive loads from the potential break-up of the wedge.

The present experiments are analogous to prior studies (Sections 5 and 5) in 7150 and 2124 on the effect of the mechanical removal of material left in the wake of threshold cracks. Here, the micro-machining away of wake material causes a similar reduction in closure, leading to a recommencement of growth of previously arrested cracks. Subsequent crack extension again is associated with progressively decreasing growth rates (but not in this case complete arrest) as closure is re-developed over

AD-A182 949 FATIGUE BEHAVIOR OF LONG AND SHORT CRACKS IN ALUMINUM ALLOYS..(U) CALIFORNIA UNIV BERKELEY DEPT OF MATERIALS SCIENCE AND MINERA.. R O RITCHIE ET AL. 01 MAY 87 2/3

UNCLASSIFIED UCB/RP/87/A1047 AFOSR-TR-87-0872 F/G 11/6.1 NL

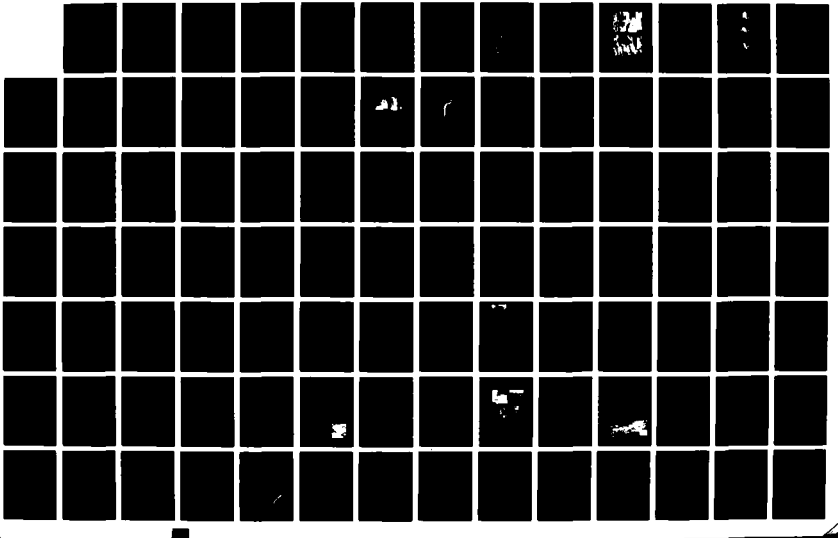

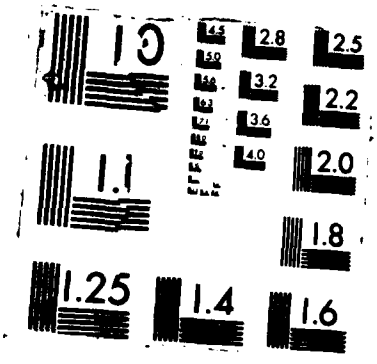
1.0
1.1
1.25
1.4
1.6
1.8
2.0
2.2
2.5
2.8
3.2
3.6
4.0
4.5
5.0
5.6

roughly 2 to 10 grain sizes. The difference in the two types of experiment appears to be in the location of the closure which is removed. Whereas micro-machining can only remove closure away from the crack tip vicinity (i.e., reliably no closer than 500 μm),[24] the nature of the fracture surface damage in Fig. 7.8 suggests that compression overloads may primarily limit the more important near-tip closure.

This study, as with prior studies[23,24,34,49] on the role of wake removal, clearly identifies the existence of a fatigue threshold with the phenomenon of crack closure. Furthermore, the results show that wherever closure is restricted, such as in the present case with the application of large compression cycles, steady-state propagation rate data characterized in terms of ΔK can no longer be relied upon to predict crack growth behavior in a given material.

7.5 Concluding Remarks

Despite early claims to the contrary,[62,69] compressive loading in the form of single (spike) overloads clearly can lead to dramatic increases in fatigue crack growth rates at low stress intensity ranges and most notably to crack propagation at the threshold. These results are consistent with the recent work of Topper and his co-workers[67,68] who found a linear decrease in threshold values with increasing compressive peak stress, and an accentuation of the effect when the compressive overloads were applied more frequently. Such observations serve to highlight the inherent danger of utilizing low load ratio threshold ΔK_{TH} values in engineering design to predict the absence of fatigue cracking. The existence of the threshold is linked intimately to the degree of closure which controls the effective near-tip driving force, yet such

considerations are not incorporated into nominal stress intensity calculations used in defect-tolerant life prediction analyses. Thus, wherever the extent of crack closure is restricted, such as at high load ratios, with small flaws or cracks at notches, or in the presence of large compressive stresses, the consequent increase in near-tip crack driving force can lead to accelerated and non-unique growth rate behavior and, more importantly, to **crack extension at ΔK levels at or below the ΔK_{TH} threshold.**

7.6 Conclusions

Based on a study on the effect on single (spike) compression overloads on near-threshold fatigue crack propagation at R = 0.10 in 7150, 2090 and 2124 aluminum alloys, the following conclusions can be made:

1. A single compression overload, of magnitude 5 times the tensile peak load, resulted in immediate re-initiation of growth of cracks arrested at the fatigue threshold in 7150 alloy, even though the applied ΔK was maintained constant at ΔK_{TH}, consistent with a measured 16 to 28% reduction in crack closure.

2. The application of single compression overloads, of magnitude two and three times the tensile peak load at ΔK_{TH}, was sufficient to cause the extension of cracks arrested at the threshold ΔK_{TH} in 2090-T8E41 and 2124-T351, respectively, again consistent with a reduction in closure.

3. The reduction in closure stress intensity (K_{cl}) following the compressive cycle was related primarily to a reduced contribution from

roughness-induced crack closure arising from abrasion between mating crack surfaces, i.e., fractographically to the flattening and cracking of fracture surface asperities in the vicinity of the crack tip.

4. Crack growth at $\Delta K = \Delta K_{TH}$ following the application of the overload was characterized by a progressive deceleration until re-arrest occurred within 1 to 4 grain diameters. Such behavior was accompanied by a measured increase in crack closure back to original pre-overload threshold levels.

5. Due to an increase dependence on crack tip shielding, 2090-T8E41 shows the highest sensitivity to periodic compressive load cycles, compared to traditional high strength aluminum alloys. Specifically, the compressive loads required to cause crack growth at ΔK_{TH} were over a factor of two smaller in 2090, than in 2124 or 7150.

8. EXPERIMENTAL AND NUMERICAL ANALYSIS OF LARGE, SMALL, THROUGH-THICKNESS AND SURFACE CRACKS

8.1 Introduction

The widespread adoption of the damage tolerance approach to the fatigue analysis and design of both military and civil aircraft has resulted in far greater research emphasis on **crack propagation** in aerospace materials, rather than on traditional stress-strain/life (S/N) approaches which rely largely on **crack initiation**. This follows because the damage tolerant concept assumes that flaws pre-exist from the first loading cycle, such that total life is comprised solely of crack propagation. While specific design requirements for this approach may vary from country to country, most resemble the U.S. Air Force mandatory

specification MIL-A-83444, which for example prescribes an initial flaw size for the airframe of 1.27 mm. However, durability requirements may additionally require consideration of initial defects as small as 0.127 mm.

A potential problem with this approach can arise from the anomalous behavior of fatigue cracks, which is observed for physically small ($\lesssim$ 1 mm) cracks or for flaws of dimensions approaching the size scales of microstructure or local plasticity. Most data show such small cracks to extend at rates exceeding those of long cracks at the same nominal "driving force", and to grow at stress intensity ranges below the fatigue threshold ΔK_{TH}, where long cracks become dormant.

Results showing enhanced crack extension rates for small cracks are not uncommon (e.g., refs. 3-20), both for the extrinsic toughness behavior of ceramics and composites and for fatigue crack growth in metals, yet there is a paucity of experimental data showing the buildup of shielding with crack extension.[24,28,34,49] Similarly, few analytical models exist for the crack-size dependence of shielding under cyclic loading.[44] Several numerical models, however, for both plane stress[75,76] and plane strain[77] do predict a progressive increase in shielding with initial crack extension to a saturation (long crack) level, but are specific to crack closure induced solely by cyclic plasticity.

The primary objective of this study is thus to examine, both experimentally and numerically, the role of crack tip shielding in influencing the growth behavior of long (typically exceeding 10 mm) and small (typically 2 to 400 μm) fatigue cracks in underaged and overaged microstructures in a 2124 aluminum alloy, where the principal mechanisms

of shielding, namely crack deflection and more importantly roughness-induced crack closure, are well documented (see Section 6). Specifically, measured and numerically predicted values of crack closure are compared, as a function of crack length, for through-thickness long and physically-short cracks, and the resulting growth rate behavior compared with that for microstructurally-small surface cracks.

8.2 Numerical Analysis

Crack closure induced by cyclic plasticity[33] has been modelled both analytically (e.g, ref. 78) and numerically (e.g., ref. 79). The analytical models, however, are exclusively derived from the Dugdale model and therefore are strictly only applicable to plane stress, although some workers introduce a plastic constraint factor to simulate plane strain behavior.[75] Elastic-plastic finite element computations,[79] conversely, have verified the existence of plasticity-induced closure in plane strain, and found its magnitude to be far less than in plane stress.

In the present study, the latter approach was followed with numerical modelling performed using elastic-plastic finite element calculations on growing cracks in both compact C(T) and SEN(B) bend specimens, under the same test conditions (load ratio, crack size, etc.) as were used experimentally. Although plane strain conditions existed experimentally, for comparison numerical solutions for both plane stress and plane strain were obtained.

In the numerical procedures,[79] crack propagation is simulated by releasing the crack tip node at maximum load in the cycle (although any type of strain or displacement criteria may be used), and changing the

boundary conditions. On unloading, the contact problem in the wake of the crack tip is solved by decreasing the loads in steps (avoiding interpenetrating crack surfaces). The closure load, P_{cl}, and hence K_{cl}, are defined at the load which causes first contact of the fracture surfaces. Thereafter, the unloading sequence is continued stepwise to minimum load, and a further search made for contact points behind the crack tip. If any error occurs in the equilibrium solution, the prior load step is modified using the stored stress, strain and displacement field, but with a new load decrement. Two convergence criteria are applied during this procedure; namely all closed node displacements at the crack surfaces are defined at less than 10^{-8} mm, and the difference in modified (transfer) loads at less than 0.05 N. Opening loads are determined in an analogous manner during increasing stepwise increments.

In the present analysis, material behavior was modelled as an isotropic strain hardening solid, with the exact shape of the stress-strain curve utilized. The finite elements were two-dimensional triangles with cubic base functions. In order to avoid prescribing a specific type of singularity at the crack tip (as the nature of the stress and deformation fields near the tip of a small, cyclically loaded crack is unknown), the crack tip singularity was deduced using a very fine mesh in the vicinity of the crack tip. Fig. 8.1 shows the finite element discretization of the bend specimen. In order to obtain convergent results of mesh-size independent closure loads, approximately 15 to 20 elements had to be used in the plastic zone, a requirement which determined the minimum element length.

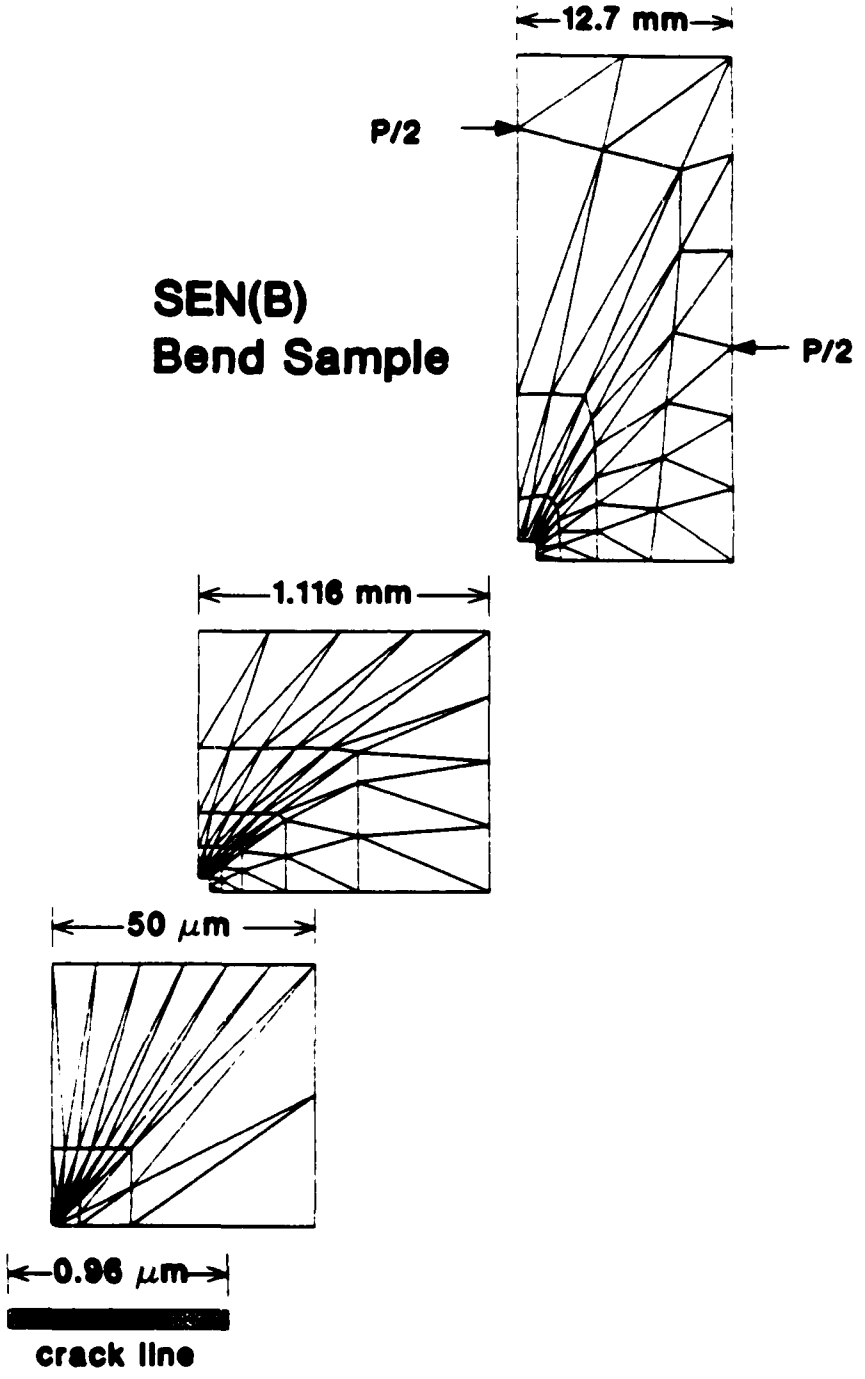

Fig. 8.1: Finite element discretization of the single edge notched SEN(B) bend specimen used in the numerical calculations, showing increasingly magnified views of the crack tip region.

8.3 Long Crack Behavior

Experimental results. Long crack fatigue crack growth rate data, in the underaged T351 structure at a load ratio of 0.1, are plotted in Figs. 6.3 and 6.4 as a function of both ΔK and ΔK_{eff}. Corresponding crack closure data are shown in Fig. 6.5, and indicate increasing closure with decreasing ΔK, characteristic of behavior dominated by wedge shielding mechanisms.

The measured levels of closure, especially in the underaged (T351) condition, are consistent with the highly branched and meandering nature of the crack path (Fig. 8.2). Such crack path morphologies promote significant contributions to shielding from crack deflection and asperity wedging (roughness-induced crack closure.

Numerical results. Finite element plane strain and plane stress predictions of the crack closure, in the form of normalized closure levels, K_{cl}/K_{max}, as a function of crack length, a, are plotted in Fig. 8.3 for crack extension in 2124-T351 at R = 0.1. The build-up of closure in the wake of the growing crack can also be appreciated by examining the distribution of normal stresses in the vicinity of the tip of a long crack (a = 32.8 mm) in the C(T) geometry under plane stress conditions. Stress distributions are plotted during unloading at the maximum, closure and minimum loads in Figs. 8.4a,b & c, respectively. Crack closure becomes evident from the compressive stresses (drawn below the plane) in the wake of the growing crack at tensile loads.

The continuum predictions in Figs. 8.3 and 8.4 naturally pertain to the contribution to shielding from plasticity-induced closure only. Correspondingly, similar to previous numerical studies,[79,80]

Fig. 8.2: Morphology of the fatigue crack path in a) underaged T351 and b) overaged 2124 aluminum alloy at ΔK values between 3.5 and 5 MPa$\sqrt{m}$. Crack path profiles were obtained from metallographic sections, taken perpendicular to the crack surface at center thickness (Keller's reagent etch). Arrow indicates direction of crack propagation.

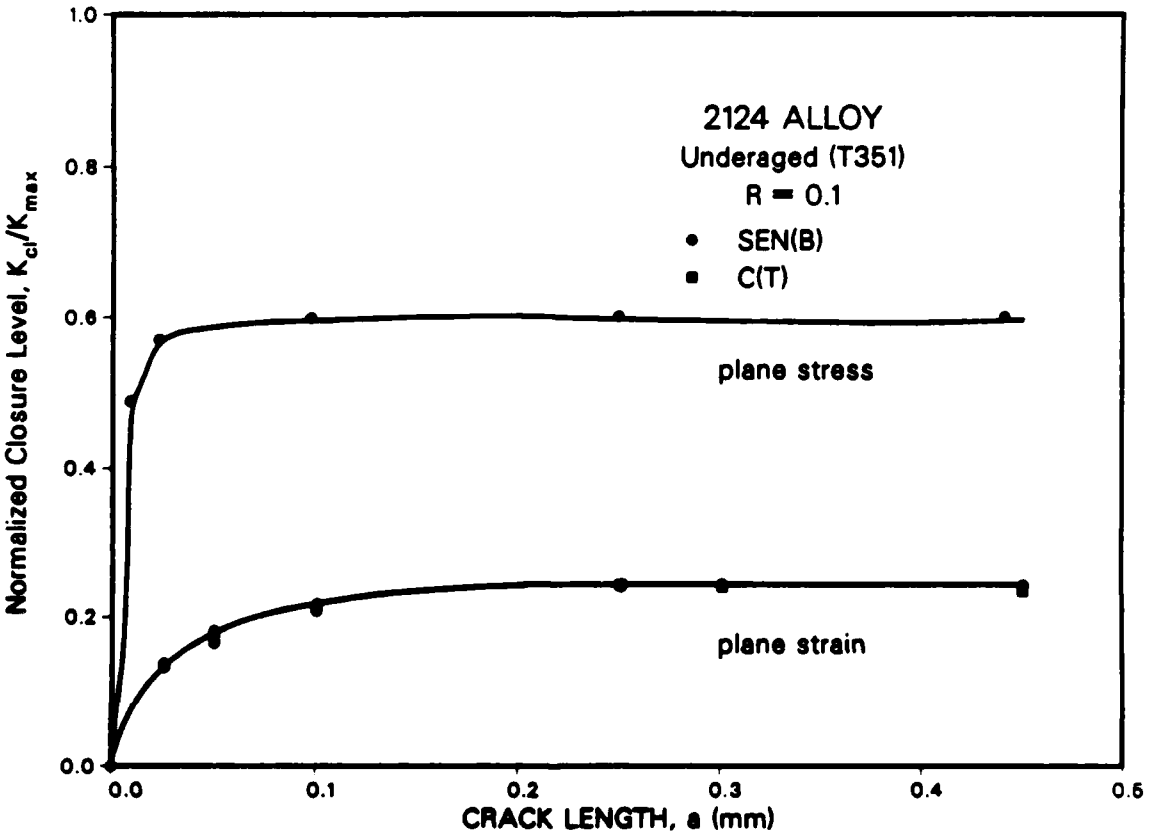

Fig. 8.3: Finite element predictions of the normalized crack closure, K_{Cl}/K_{max}, as a function of crack length, a, for long and short cracks in C(T) and SEN(B) specimens of 2124-T351 at R = 0.10. Numerical predictions pertain to elastic-plastic conditions in either plane stress or plane strain.

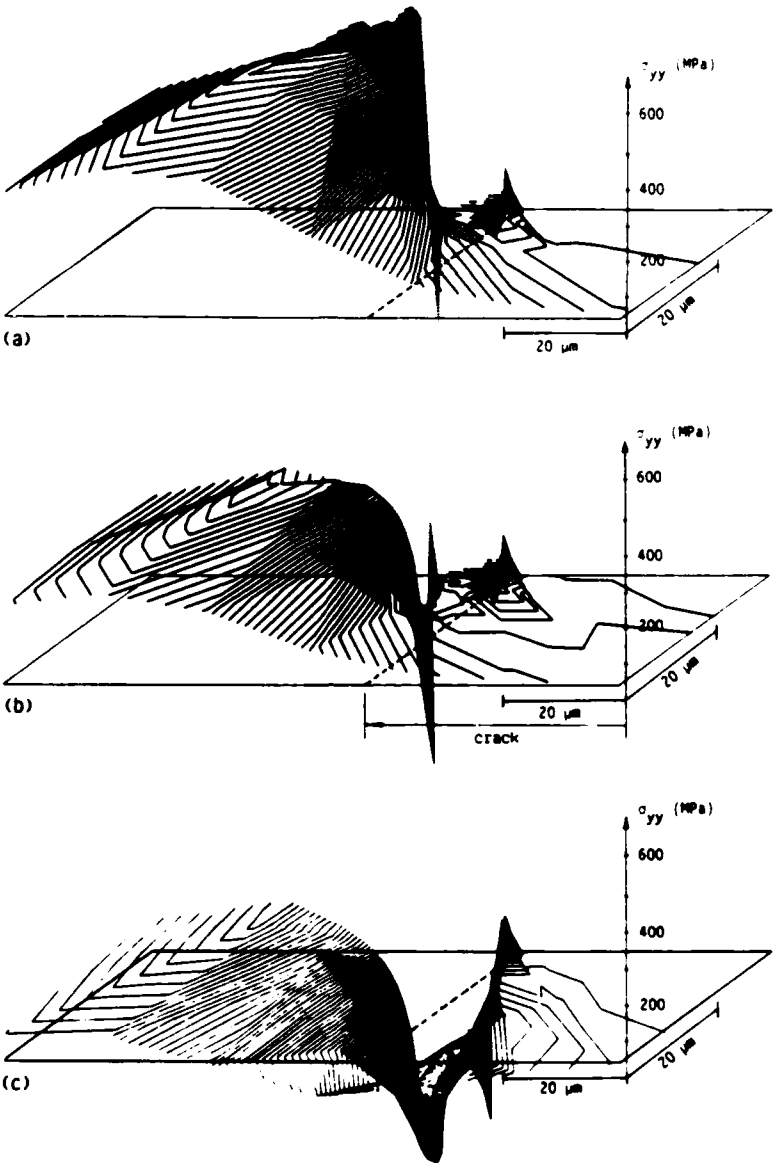

Fig. 8.4: Finite element predictions of the distribution of normal stresses **during unloading** in the vicinity of a long (a = 32.8 mm) fatigue crack in the C(T) geometry under plane stress conditions (R = 0.10) at a) the maximum load (326 N), b) the closure load (195 N), and c) the minimum load (33 N). Stresses above the plane are tensile, below are compressive. The crack tip is located at the point of maximum compressive stress; the tensile peak to the right is due to the first compressive contact during the initial load cycle and has no effect on subsequent results.

significantly higher levels of closure are predicted for plane stress conditions. Results for the C(T) geometry, pertinent to long crack behavior, are shown for crack lengths in excess of 0.1 mm and indicate no change in closure above the crack size. It should be noted that similar sized cracks in the SEN(B) bend specimens gave identical closure levels.

In Fig. 8.5, these results are used to compute ΔK_{eff} values, and are compared with the experimentally derived values for the growth rate data in the underaged and overaged microstructures at R = 0.1. It is apparent that the numerical results for plane strain indicate significantly higher ΔK_{eff} values, particularly below 10^{-9} m/cycle, because of predictions of far lower closure levels. Numerical predictions of ΔK_{eff} values based on the plane stress assumption, on the other hand, are closer to the experimentally measured results, especially for near-threshold behavior in the underaged microstructure, although in reality it is clear that such plane stress conditions did not apply experimentally.

8.4 Through-Thickness Short Crack Behavior

Experimental results. Growth rate data for the through-thickness physically-short (50 to 400 μm) cracks in the underaged (T351) microstructure are shown in Fig. 6.9, and indicate that short cracks can grow at ΔK levels well below the long crack threshold ΔK_{TH}.

As discussed in Section 6, during each deceleration and arrest event for the short crack, the development of crack closure with crack extension was experimentally monitored. Results for each such event, involving the extension of a 90 μm long crack to 230 μm, are shown in Fig. 8.6. **The progressive reduction in growth rates leading to arrest can be seen to be associated directly with a concurrent increase in crack**

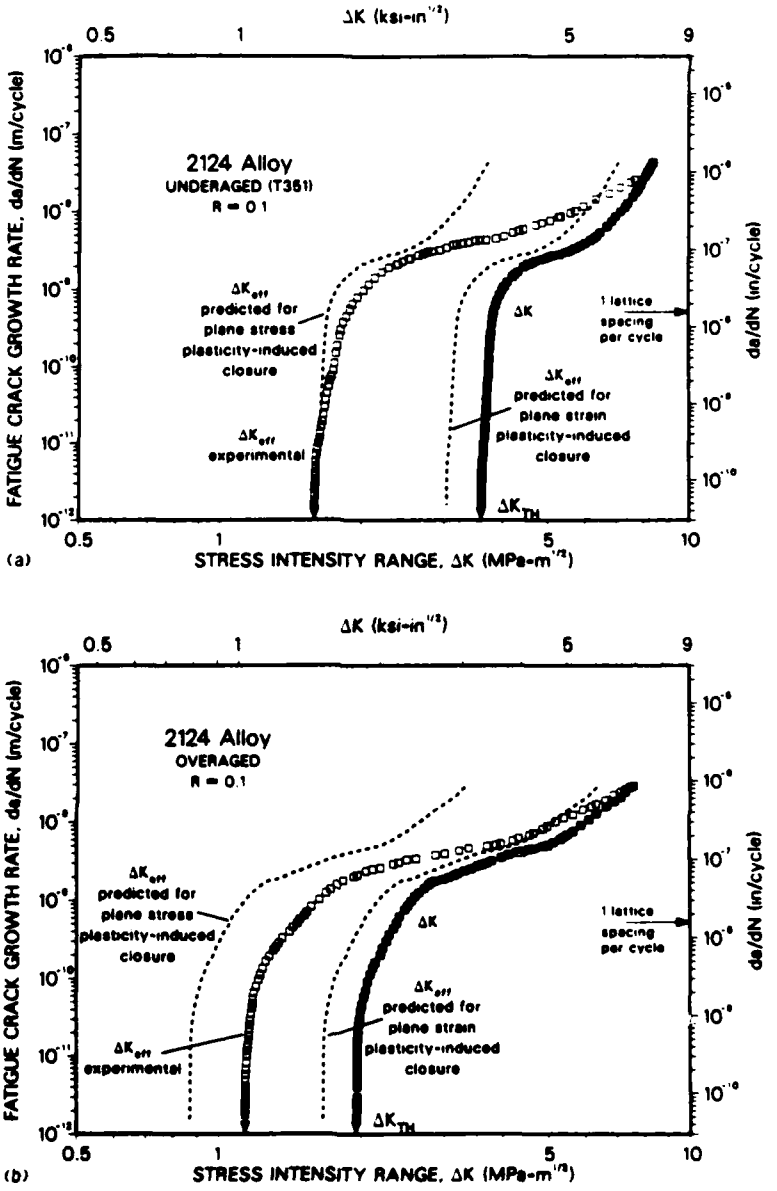

Fig. 8.5: Fatigue crack propagation behavior of long cracks at R = 0.10 in a) underaged T351 and b) overaged 2124 aluminum alloy, as a function of ΔK and ΔK_{eff}, showing difference in ΔK_{eff} values derived from numerical predictions and experimentally measured K_{cl} data.

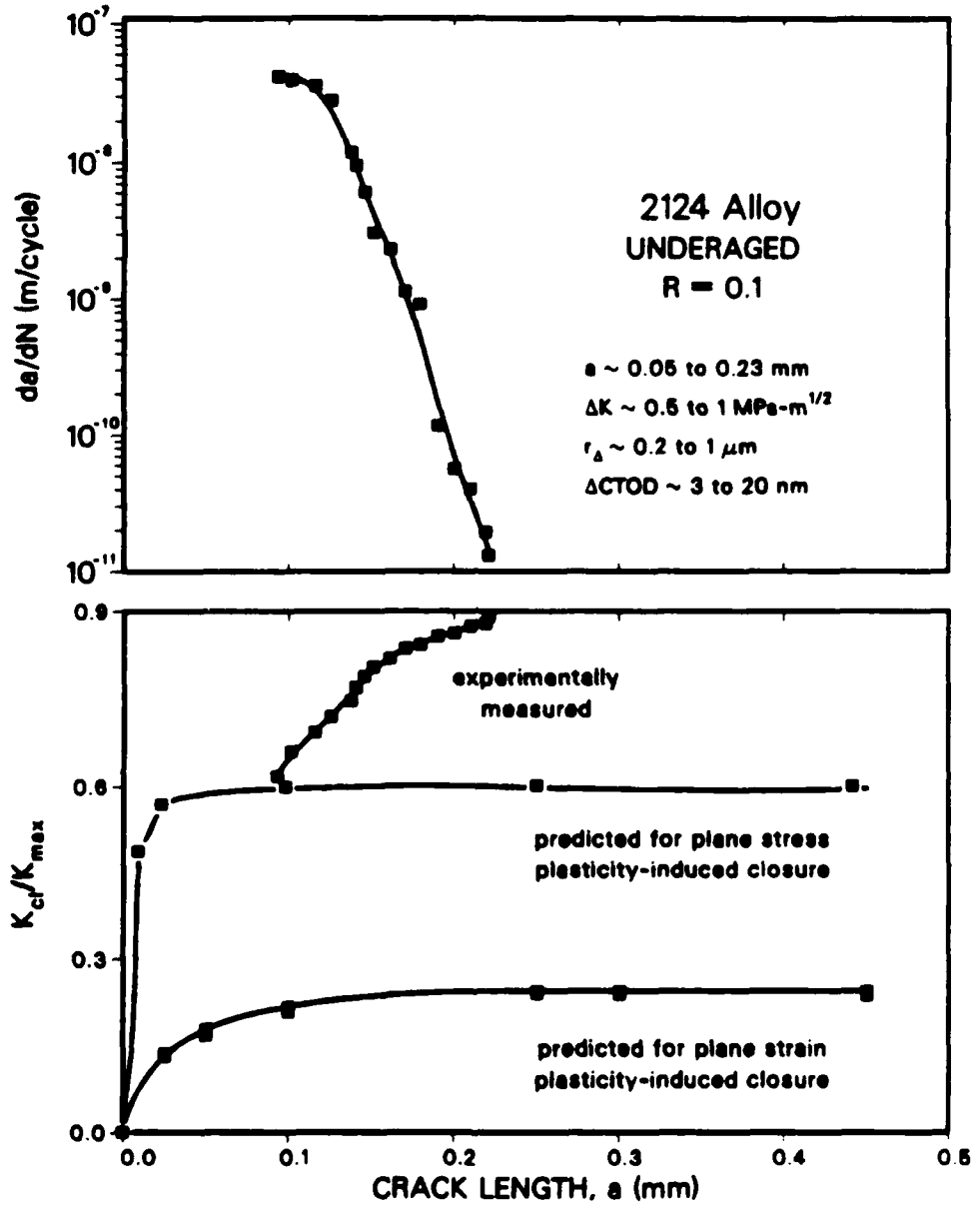

Fig. 8.6: Variation in growth rate and crack closure with crack extension during sub-threshold propagation of physically-short cracks in 2124-T351 aluminum alloy, showing how closure is generated during initial crack extension (a = 90 to 230 μm) concurrent with the progressive decay in growth rates to arrest. Crack closure is represented as the normalized closure ratio, K_{Cl}/K_{max}, and shows a comparison of experimentally measured values with those predicted numerically for both plane stress and plane strain conditions.

closure resulting in a corresponding reduction in ΔK_{eff}. The magnitude of this increase is associated with very high levels of K_{cl}/K_{max} approaching 0.9, far in excess of those for long cracks. Using such closure data, short crack growth rates are plotted as a function of ΔK_{eff} in Fig. 8.7.

Numerical results. Numerical plane stress and plane strain predictions of crack closure for short cracks in the SEN(B) bend specimens are shown in Fig. 8.3, and are compared with experimentally determined values in Fig. 8.6. Clearly, at small crack lengths below $\sim$ 100 to 200 μm, both theoretical and experimentally measured closure levels decay markedly with progressive decrease in crack length, indicating that the local ΔK_{eff} experienced by the short crack will be in excess of that ahead of long cracks at the same nominal ΔK. However, as before, plane strain predictions from the finite element model yield far lower closure levels (by a factor of 4 to 5) compared to those measured experimentally. Plane stress predictions are much closer to the measured values, but are still up to 50% lower.

8.5 Naturally-Occurring Small Surface Crack Behavior

Corresponding experimental results for the naturally-occurring small (2 to 400 μm) semi-elliptical surface cracks are shown in Fig. 8.8 for the underaged (T351) and overaged conditions. Data are plotted as a function of nominal ΔK values and are compared with equivalent results on long through-thickness cracks. Considerable scatter is apparent in the small crack growth rates. This is to be expected as measurements of growth rates are made at the microstructural level and thus include the frequent impedance to crack advance from local interactions with

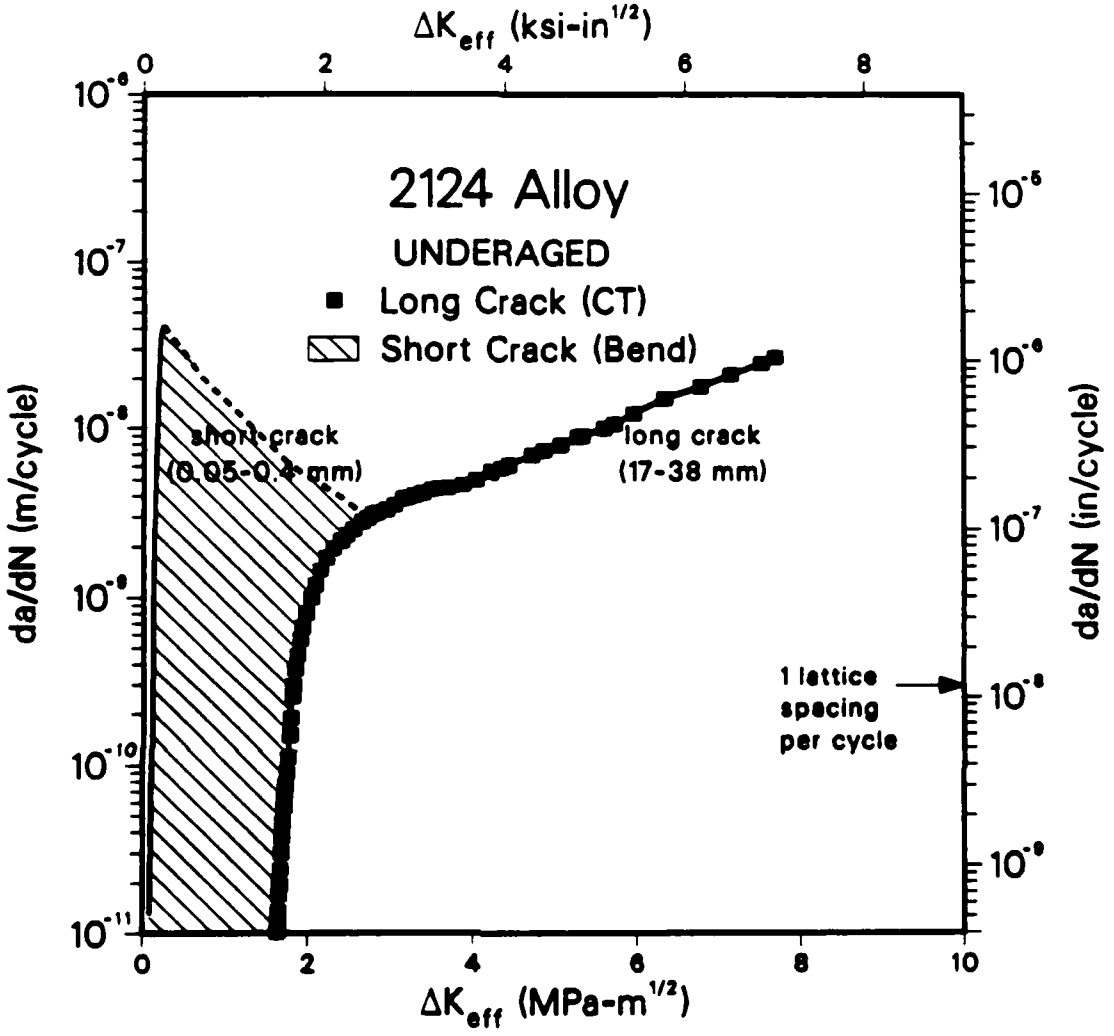

Fig. 8.7: Variation in fatigue crack growth rates in 2124-T351 alloy at R = 0.10 for long (17-38 mm) cracks and physically-short (90-400 μm) cracks, plotted as a function of ΔK_{eff} (derived from experimental closure data). Note that physically-short cracks propagate below the effective threshold, indicating that differences in behavior between long and short cracks may not be solely attributable to closure effects.

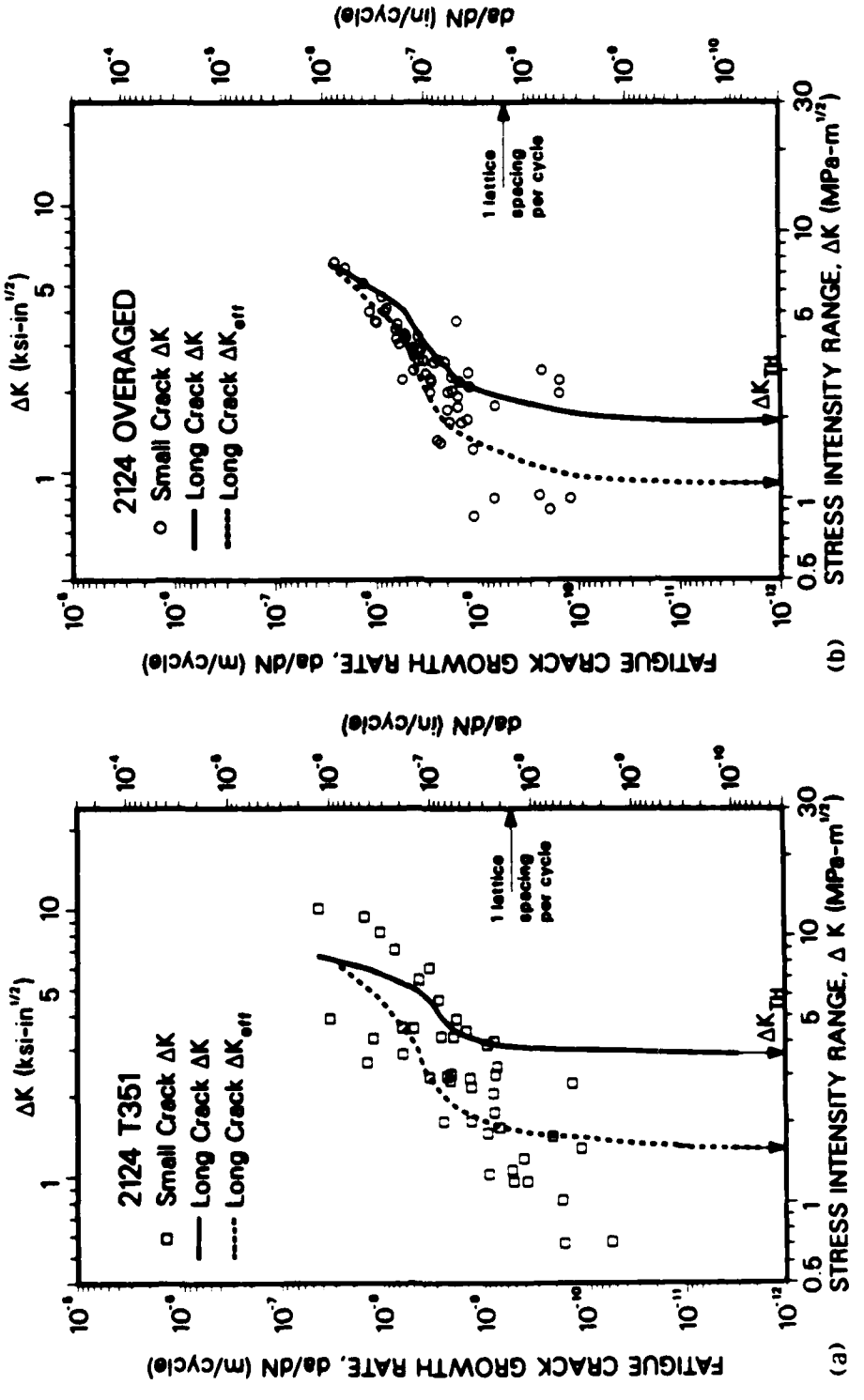

Fig. 8.8: Comparison of growth rates of long (17-38 mm) and naturally-occurring small (2-400 μm) surface cracks in a) underaged T351 and b) overaged 2124 aluminum alloy, as a function of ΔK and ΔK_{eff}.

microstructural features, as shown by the crack path profiles in Fig. 8.9. However, it is clear that microstructurally-small cracks propagate, without evidence of a threshold, at rates generally in excess (by up to 3 orders of magnitude) of equivalent long through-thickness cracks at the same nominal ΔK. Moreover, they grow at stress intensity ranges as low as 0.9 MPa$\sqrt{m}$, well below the long crack threshold.

A primary reason for the accelerated growth of such small flaws can be appreciated by comparing the small crack data with long crack growth rates plotted as a function of ΔK_{eff}. It is apparent that once crack closure has been subtracted out, reasonable correspondence is achieved between long and small crack results.

8.6 Discussion

Role of Crack Tip Shielding

This work has attempted to provide quantitative evidence of the dominant role of crack tip shielding,[28] specifically from crack closure, in distinguishing the near-threshold fatigue behavior of through-thickness long cracks, through-thickness physically-short cracks, and naturally-occurring microstructurally-small surface cracks. Both numerical computations and experimental measurements have confirmed that closure levels stay reasonably constant for long cracks (at fixed R), yet progressively decay to zero for crack sizes in the present alloy below roughly 100 μm. The latter variation in shielding with crack length clearly can result in some degree of non-uniqueness in growth rate behavior at small crack sizes, particularly in the near-threshold regime where closure effects are enhanced. This is illustrated in Fig. 8.10, where a comparison of measured growth rates for long, through-thickness

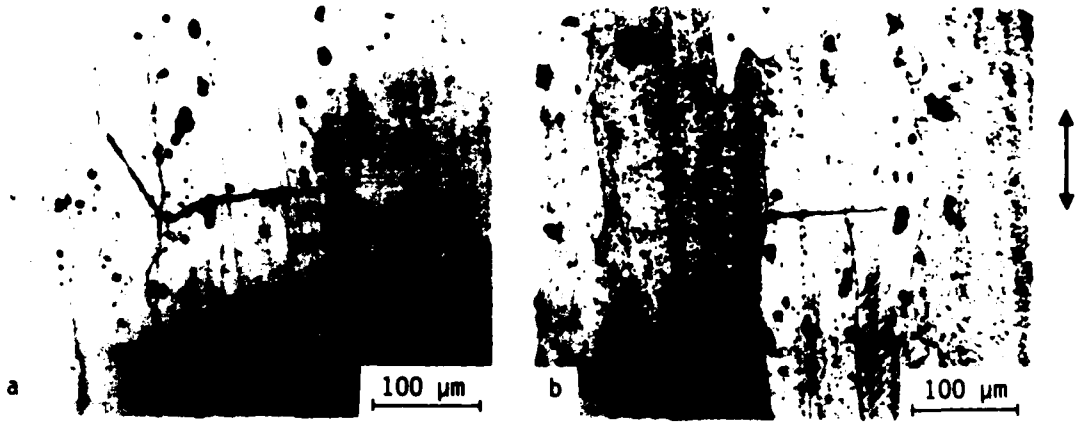

Fig. 8.9: Naturally-occurring microstructurally-small (2-400 μm) surface cracks in a) underaged T351 and b) overaged 2124-T351 aluminum alloy. Replicas of small cracks were obtained by surface replication. Arrow indicates direction of tensile stress axis.

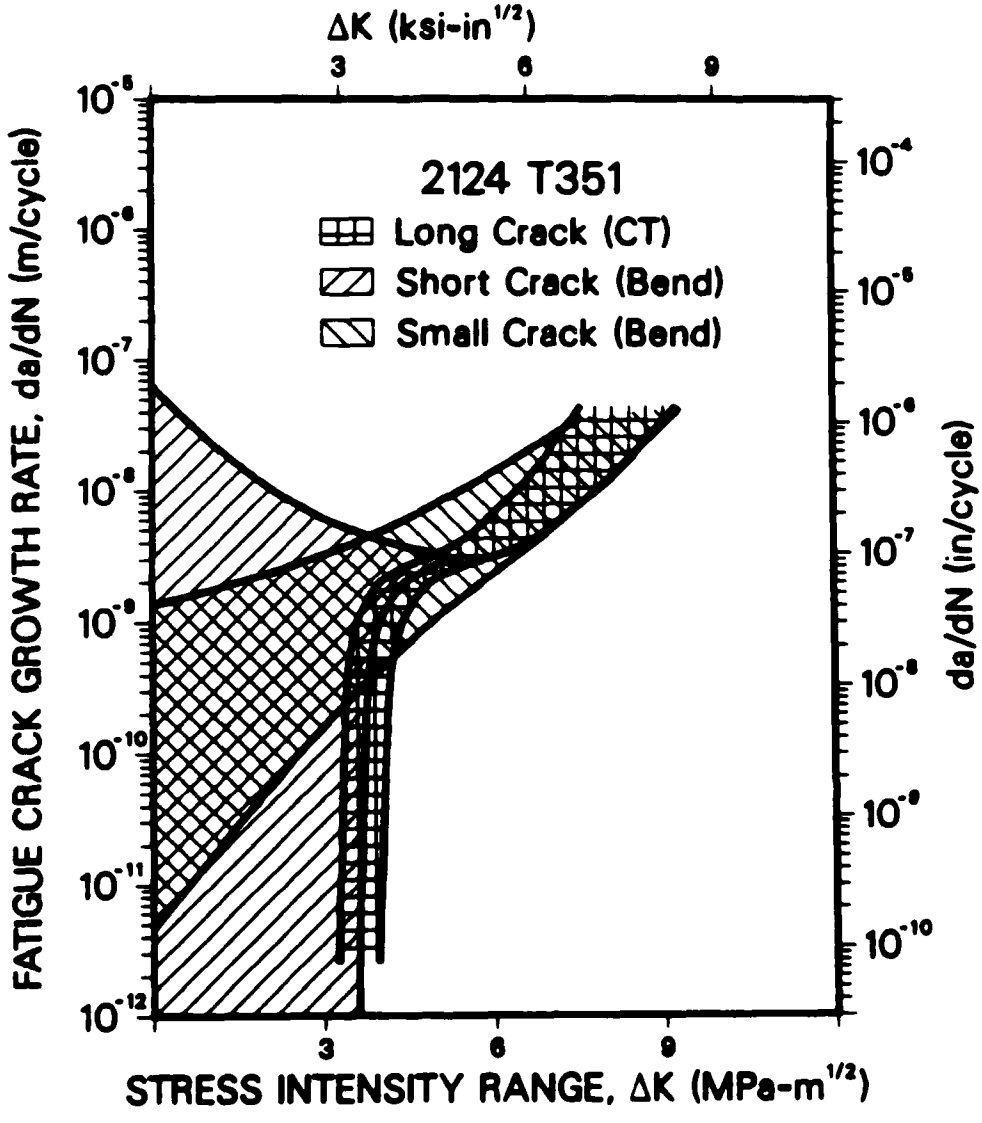

Fig. 8.10: Fatigue crack growth rate behavior in 2124-T351 aluminum alloy, as a function of nominal ΔK, for through-thickness long (17-38 mm) cracks, through-thickness short (50-400 μm) cracks, and naturally-occurring small (2-400 μm) surface cracks.

short and small surface cracks in 2124-T351 shows increasingly more scatter as the threshold is approached.

The role of such closure is illustrated, for example, by the observation that the load ratio dependence of thresholds for **long cracks** can be attributed primarily to *variations in* K_{cl} levels. Moreover, the commonality of threshold values in each microstructure, when computed in terms of ΔK_{eff}, would suggest that some intrinsic threshold does exist for long cracks, provided closure is fully accounted for.

With through-thickness **physically-short cracks**, observations of crack growth at stress intensities below ΔK_{TH}, at rates which progressively decay to arrest or merge with long crack data, have also been shown to be associated quantitatively with an initial lack of shielding and its subsequent development with crack extension. *Specifically, the sub-threshold decay in* short crack growth rates has been related to a concurrent increase in K_{cl}, such that the local driving force, ΔK_{eff}, sees a minimum. Similarly, the accelerated and sub-threshold behavior of **naturally-occurring small cracks** appears to be consistent with a lack of shielding generated during the extension of semi-elliptical surface flaws with limited wake. In addition, naturally-occurring small flaws are likely to show somewhat enhanced growth rates even at higher ΔK levels, as compared to pre-existing through-thickness flaws, they tend to initiate preferentially in the most favorably oriented grains and are less likely to have their growth averaged over many disadvantageously oriented grains.

Of particular significance in this work is the comparison of numerically computed closure levels with those measured experimentally on

both long and short flaws. Progressively, as growth rates are reduced towards the threshold, the predicted magnitude of closure for plane strain conditions can be seen to fall far short of experimental measurements (Figs. 8.5 and 8.6). Several authors previously (e.g., refs. 75,76) have used plane stress numerical models in order to predict higher levels of closure at near-threshold levels in, for example, spectrum loading fatigue lifetime prediction analyses. As shown in the present study, such models do predict levels of closure closer to that measured experimentally, although such predictions are artificial as near-threshold conditions are invariably plane strain.

The logical reason for the discrepancy between theory and experiment is that at lower stress intensities, where crack tip opening displacements (CTOD) are restricted, the major sources of crack closure (in addition to that induced by cyclic plasticity) originate from the wedging of fracture surface asperities[41-43] and corrosion debris,[38-40] whereas numerical models predict merely the plasticity-induced contribution. This discrepancy is particularly striking in 2124-T351 as the alloy develops strong contributions from roughness-induced closure, due to the branched and deflected nature of the crack path near ΔK_{TH} (Fig. 8.2).

Although care must be exercised in interpreting growth rate data plotted as a function of ΔK_{eff}, due to uncertainties in evaluating the magnitude of K_{cl}, it is apparent from the present results that, whether closure is assessed in terms of the cyclic plasticity mechanism alone in numerical calculations or in terms of the combined effects of all possible closure mechanisms in experimental measurements, through-

thickness short and semi-elliptical small surface cracks are still seen to propagate below the long crack (ΔK_{eff}) threshold (Fig. 8.7). Thus, despite its major significance, shielding via crack closure alone apparently does not provide a complete rationalization for the accelerated growth rates of small flaws, at least where the crack driving force is defined in terms of modifications to the **elastic** stress intensity range, ΔK.

8.7 Role of Crack Tip Singularity and Plastic Zone Size

Several factors in addition to crack closure have been postulated to explain the "anomalous" behavior of small cracks (reviewed in refs. 19 and 20). Discussed below are those factors which pertain to the choice of a crack tip characterizing parameter based on K_I, specifically involving the neglect of higher order terms in the series expansion of the crack tip stress field and the variation in the morphology of the plastic zone with crack length. In this regard, it should be noted that, although nonlinear elastic, small-scale yielding parameters, such as the cyclic J-integral, the strain energy density range (ΔS) or the cyclic strain energy release rate,[7,8,81] have been proposed as "driving forces" for small cracks, none constitutes a viable alternative due to the violation in the fracture mechanics similitude concept from the crack tip shielding effects discussed above.

Elastic crack tip field considerations. Talug and Reifsnider[82] have suggested that the inclusion of nonsingular stresses in the description of the linear elastic crack tip stress field will become increasingly more significant as the length of the crack decreases. Thus, to characterize the "driving force" for a small flaw, it is necessary to

derive the full stress field expansion, by finding a stress function which satisfies the biharmonic equation $\nabla^4\Phi = 0$ ($\nabla^2\Phi$ is the Laplace operator and Φ is the Airy stress function), while simultaneously satisfying the boundary conditions for the chosen geometry and mode of loading. This can be achieved by employing the Williams' stress function[83] or the numerically convenient Muskhelishvili's complex function approach,[84] and by recognizing that the crack surfaces must be free from traction, such that the stress field, as a function of radial distance r and polar angle θ, can be expressed as an infinite series, e.g., for the normal stress:

$$\sigma_{yy} = \sum_{n=1}^{\infty} \frac{n}{2} r^{(\frac{n}{2} - 1)} \left\{ A_n \left[(2 - \frac{n}{2} - (-1)^n) \cos(\frac{n}{2} - 1)\theta + (\frac{n}{2} - 1) \cos(\frac{n}{2} - 3)\theta \right] - B_n \left[(2 - \frac{n}{2} + (-1)^n) \sin(\frac{n}{2} - 1)\theta + (\frac{n}{2} - 1) \sin(\frac{n}{2} - 3) \right] \theta \right\} \quad (8.1)$$

where n is the number of terms. From Eq. 8.1, σ_{yy} can be solved for any number of terms. For example, at $n = 1$ and $\theta = 0$, the stress field can be written:

$$\sigma_{yy} = A_1 r^{-\frac{1}{2}} \quad (8.2)$$

such that A_1 must equal $K_I/\sqrt{2\pi}$. In the present study, higher order terms were solved by comparing with the fully elastic finite element calculations for σ_{yy}, using the mesh depicted in Fig. 8.1. By employing an increasing number of terms in the series expansion, the resulting

stress intensity factors, expressed as a dimensionless parameter $K_I B\sqrt{W}/P$ (B is the specimen thickness, W the width), are shown in Fig. 8.11 as a function of crack length for the SEN(B) specimen, and are compared with the standard long crack K_I solution.[51] From these results, it is readily apparent that the effect of the higher order, nonsingular terms is not insignificant in deriving K_I solutions to characterize the crack advance of very small falws, although the number of terms which should be used is uncertain.

A second complication for small surface cracks is that although depthwise extension is in plane strain, the intersection of the semi-elliptical crack with the free surface is in plane stress. At this point, the elastic stress field singularity is also very different from the inverse square root K_I-field singularity, commonly employed in LEFM.[85]

Plasticity consideration. A further factor to be considered in the description of a characterizing parameter for the stress and deformation fields associated with very small cracks is the size and the shape of the plastic zone. From the present numerical calculations in the SEN(B) specimen, finite element predictions of the extent of local plasticity ahead of a 0.16 μm long crack were determined for both plane strain and plane stress conditions. These are illustrated in Fig. 8.12 and indicate marked departures with the usual shape of the long crack plastic zone, owing to the close proximity to a free surface. Similar to previous analyses for plane strain only,[86] even under monotonically increasing loads, elastic enclaves are predicted immediately ahead of the crack tip (on the $\theta = 0$ plane) and behind the tip at the free surface. Such

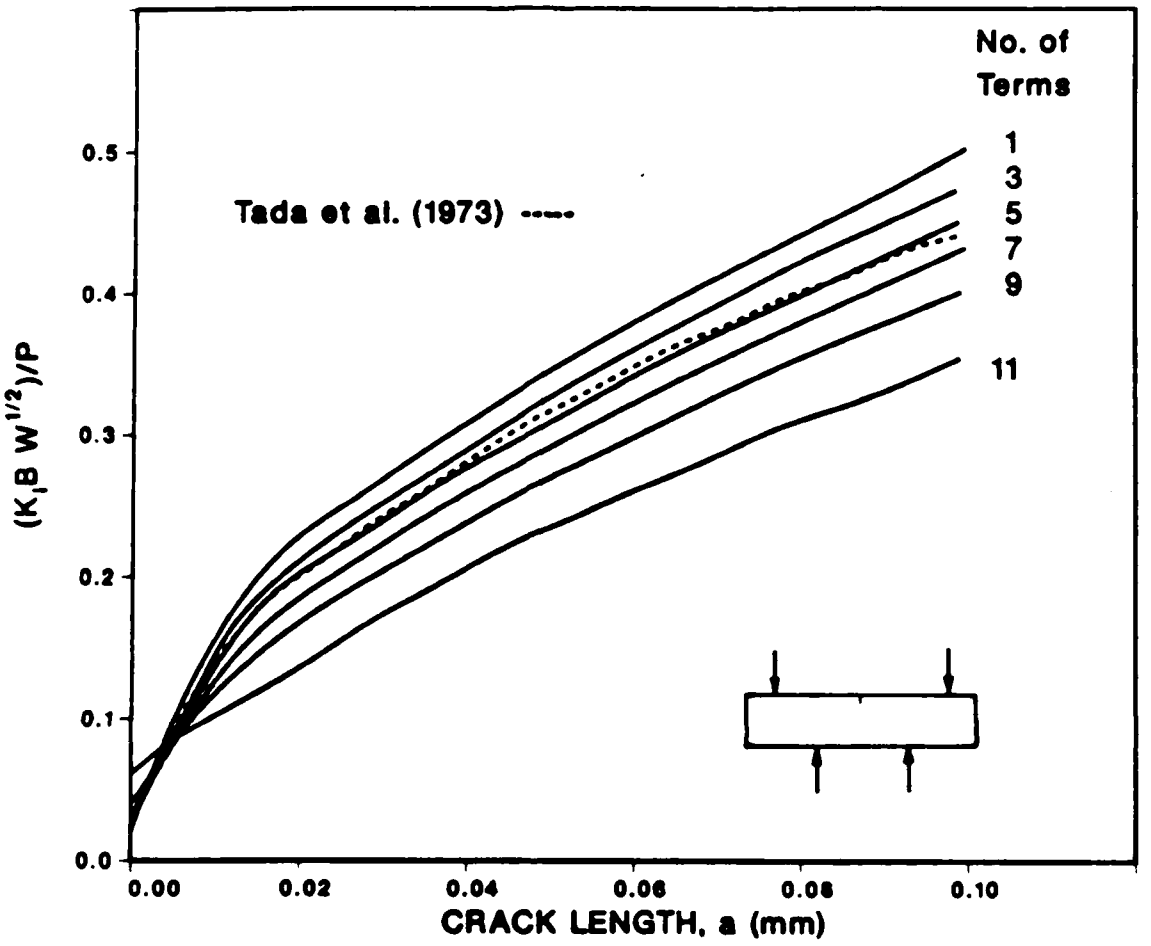

Fig. 8.11: Variation in dimensionless stress intensity factor, $K_I B\sqrt{W}/P$, with short crack length, a, in SEN(B) specimen, showing effect of including higher order terms in the series expansion for the crack tip field. Numerical results are compared with the standard linear elastic K_I solution for a long crack from Tada et al.[51]

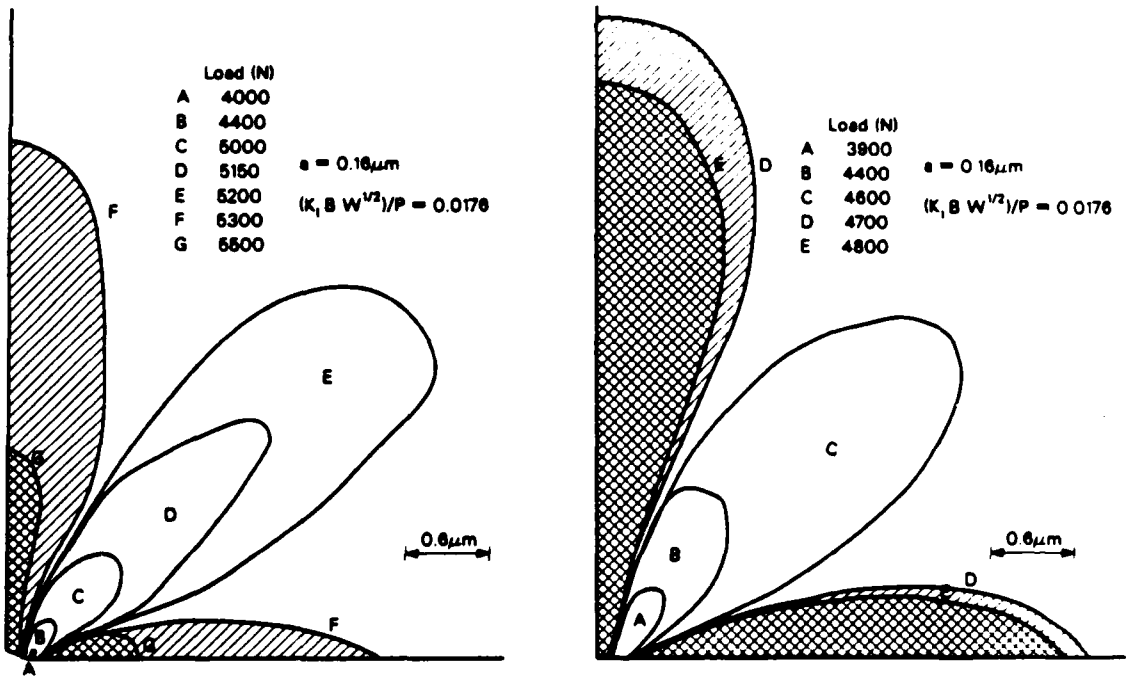

(a) (b)

Fig. 8.12: Elastic-plastic finite element predictions of the plastic zone shapes in a) plane strain and b) plane stress for a very short (0.16 μm) crack (at location A) in an SEN(B) specimen of 2124-T351, as a function of increasing loads. Elastic enclaves are represented by hatched areas immediately ahead of the crack tip and behind the tip at the free surface.

results are also consistent with earlier numerical studies[79] on three-point bend specimens of a 2024 aluminum alloy, where it was found that the maximum extent of the plastic zone was 8 times larger for a small (10 μm) crack, compared to an equivalent long crack (a = W/2) at a ΔK of ~ 2 MPa$\sqrt{m}$. Moreover, it was found that, with increasing crack length, the shape of the zone was developed more in the wake of the growing crack, consistent with the higher levels of plasticity-induced crack closure generated by long flaws.

8.8 Conclusions

Based on an investigation into the role of crack tip shielding in influencing the behavior of large and small fatigue cracks, involving an experimental and finite element study of through-thickness long (17-38 mm) cracks, through-thickness physically-short (50-400 μm) cracks, and naturally-occurring small (2-400 μm) surface cracks in underaged (T351) and overaged microstructures of a 2124 aluminum alloy, the following conclusions can be made:

1. The existence of a threshold stress intensity range ΔK_{TH} for the dormancy of long cracks was found to be associated with high levels of crack closure, with values of K_{cl}/K_{max} approaching 0.7.

2. Through-thickness physically-short cracks were observed to propagate at nominal stress intensity ranges at, and below, ΔK_{TH}. Such short crack growth rates were found to decay progressively until arrest (or before merging with long crack data), concurrent with a measured and numerically predicted increase in the closure stress intensity, and a consequent reduction in the local "driving force" ΔK_{eff}.

3. Naturally-occurring microstructurally-small surface cracks were observed to propagate at rates up to 3 orders of magnitude faster than corresponding long cracks subjected to the same nominal ΔK level. Moreover, such small cracks were found to advance at rates in the range 10^{-10} to 10^{-8} m/cycle at ΔK levels below ΔK_{TH}. However, when compared with long crack data analyzed in terms of ΔK_{eff} (after correcting for closure), reasonable correspondence was found between long and small surface crack growth rates (above the ΔK_{eff} threshold).

4. Elastic-plastic finite element analyses of plasticity-induced crack closure, under both plane stress and plane strain conditions, confirmed the development of closure with increasing crack length, up to a transition length ($\sim$ 100 to 200 μm) where the extent of closure saturates at the long crack value, in qualitative agreement with experimental observations. Predicted normalized closure levels, K_{cl}/K_{max}, were approximately 3 times larger for plane stress conditions.

5. Measured closure levels (in plane strain) were found to be significantly higher than numerical plane strain predictions for both long and short cracks, particularly at low stress intensity ranges. Plane stress predictions were closer to, but still less than, measured (plane strain) values. Such discrepancies were attributed to the fact that the primary contributions to closure at near-threshold levels originate from wedge shielding mechanisms, specifically in 2124 from the wedging of fracture surface asperities (roughness-induced closure), resulting from the deflected crack path.

6. Differences in behavior between long, physically-short and small surface cracks appear to be rationalized largely by the variation in

crack tip shielding with the extent of crack wake. However, as cracks of small size were still observed to propagate **below** the effective threshold stress intensity range, other factors, such as the computation of K_I for small cracks in terms of varying plastic zone morphology and the inclusion of higher order terms in the stress field expansion, should be considered.

9. ASSESSMENT OF THE SMALL CRACK PROBLEM

9.1 Introduction

The total fatigue life of engineering structures and components is often dominated by the time (or number of cycles) during which incipient cracks are small (typically less than 1 mm) and propagating at low growth rates. However, it is in this regime that the behavior of such cracks may become non-unique, and exhibit growth rates far in excess of those of long cracks (typically larger than 10 mm) subjected to the same nominal "driving force", e.g., the same stress intensity range.[3-20, 28,49,54,55,61,76,77,81]

In this section, the salient features of the problem are summarized with respect to the various classes of small flaws. In addition, some thoughts are offered on the incorporation of small crack methodology into current design and fatigue life prediction analyses and on the development of new materials with superior resistance to the growth of microcracks by fatigue.

9.2 The Small Crack Problem

The small crack problem is in essence one created by fracture mechanics through a breakdown in the similitude concept at small crack sizes.[28] For example, it has been shown[54] that crack tip strain fields for large and microstructurally-small fatigue cracks, *driven by nominally* equivalent cyclic stress intensities, are qualitatively and quantitatively dissimilar. It is thus a problem of defining a flaw size-independent "crack driving force" to account for observations that small cracks can propagate at rates different from those of corresponding long cracks at the same nominal driving force. In the large majority of cases, small crack growth rates exceed those of long cracks, although there is evidence in steels of a mild reverse effect.[87,88] Following initiation, small cracks are observed to grow at stress intensities below the long crack threshold; some extend *with decaying growth rates until* arrest, while others propagate quite rapidly to merge with long crack behavior (Fig. 2.1). The problem therefore has practical significance, because damage-tolerant fatigue lifetime computations are invariably based on long crack data. As overall life is most influenced by low growth rate behavior, the accelerated and sub-threshold extension of small flaws can lead to potentially dangerous over-predictions of life.

9.3 Definition of a Small Crack

Adjectives describing various types of small crack currently abound, although some consensus is emerging. For example, the distinction between (three-dimensional) small flaws and (two-dimensional) short flaws, the latter being small in all but one dimension, clearly is of importance.[49,54] Short flaws are generally through-thickness cracks,

often no smaller than 50 μm, which are created artificially by removing the wake material from long through cracks. Their behavior appears to be dominated, like that of large cracks, by the cyclic stress intensity factor ΔK (for small-scale yielding), corrected by considerations of crack closure.[28,49] Naturally-occurring small flaws, conversely, often approach microstructural dimensions, and although their behavior is still largely affected by closure, several other factors, including crack shape,[49] enhanced crack tip plastic strains,[54] and local arrest at grain boundaries,[89] are of comparable significance.

Useful qualifiers remain microstructurally-, mechanically- and physically-small (or short), which pertain respectively to cracks small compared to microstructural dimensions, to the scale of local plasticity, and simply to cracks of a size less than 0.5 to 1 mm.[19] In addition, fatigue cracks have also been described, with reference to environmental effects, as chemically-small,[18,20,90] as described below. Each of these classes of small flaw is associated with particular phenomena which primarily distinguish it from long crack behavior (Table 9.1). For example, for mechanically-small flaws, characterization in terms of elastic-plastic fracture mechanics (e.g., through the use of ΔCTOD of ΔJ[7,8]), or even in terms of the strain energy density ΔS,[81] may help resolve differences in growth rates behavior between long and small cracks. On the other hand, for physically-small flaws, allowance for differences in the magnitude of crack closure (e.g., through the use of ΔK_{eff}) appears to be the predominant correlating factor.[13,16,19,20, 24,28,49,55] In the case of microstructurally-small flaws, all these factors may be important, plus others associated with local

Table 9.1: Classes of Small Fatigue Cracks

Type of Small Crack	Dimension	Responsible Mechanism	Potential Solution
Mechanically-small	$a \lesssim r_y$[a]	excessive (active plasticity	use of ΔJ, ΔS $\Delta CTOD$
Microstructurally-small	$a \lesssim d_g$[b]	crack tip shielding enhanced $\Delta\varepsilon_p$	probabilistic approach
	$2c \lesssim 5\text{-}10\ d_g$	crack shape	
Physically-small	$a \lesssim 1$ mm	crack tip shielding (crack closure)	use of ΔK_{eff}
Chemically-Small	up to ~ 10 mm[c]	local crack tip environment	

[a] r_y is plastic zone size or plastic field of notch.

[b] d_g is critical microstructural dimension, e.g., grain size, a is the crack depth and 2c the surface length.

[c] Critical size is a function of frequency and reaction kinetics.

inhomogeneities in the microstructure, non-uniform growth retardation at grain boundaries, and so forth.[54,89]

In particular, the microstructurally-small, rapidly growing crack corresponds to a three-dimensional crack whose plastic zone is less than the key microstructural dimension, which in most cases is the grain size. Thus, the crack tip tends to operate as it would in a single crystal preferentially oriented for operation of the relevant crack extension mechanism. In addition, the crack front encompasses relatively few grains, so that growth is not averaged over many disadvantageously oriented grains. The latter is probably a major factor in distinguishing small cracks from short through-thickness cracks, whose fronts must necessarily sample many grains. It further provides an explanation why

crack tip shielding alone is generally sufficient to rationalize behavior of the short through-thickness crack.

9.4 Origins of Differences Between Long and Small Crack Behavior

Several major factors have been identified which are primarily responsible for differences in long and small crack behavior (Table 9.1). Of particular significance is the varying contribution of crack tip shielding, with size of the crack wake, in locally reducing the effective driving force experienced at the tip.[28] Such shielding arises in fatigue from crack closure (e.g., ref. 45), and to lesser extent from crack deflection,[46] and has been shown to be diminished at small crack sizes.[19,20] However, for microstructurally-small cracks, it is now apparent that closure does not provide the entire solution (although uncertainties in experimental measurement make this question difficult to resolve). There is now considerable evidence that, additionally, such flaws are impeded locally by grain boundaries,[89] influenced by non-uniform growth,[49] and may experience higher cyclic plastic strains at their tips.[54] Finally, differences in local crack tip environment with crack size provide the source of the chemically-short effect,[15,20,90] as described in Section 9.5.

9.5 Environmental Effects

One of the most complex issues involved in the small crack problem is associated with (liquid) environmental effects.[15,20,90] The chemically-short crack may propagate 1.5 to several hundred times faster than long cracks subjected to the same mechanical driving force. Moreover, it may be somewhat larger than the microstructurally- or

mechanically-short flaw, as short crack behavior has been reported for crack sizes upwards of $\sim$ 10 mm. (Precise statement of the size range for chemically-short cracks cannot be defined; it depends upon several factors and is principally controlled by frequency and reaction kinetics.) The discrepancy in behavior is attributed to differences in local crack tip chemical environment and conditions.[15,20,90] The critical issues thus pertain to the determination of crack tip conditions, as a function of crack length, in terms of the coupled processes of fluid transport and chemical/electrochemical reactions within the crack, and the determination of the origin of the environmentally-enhanced cracking rates in relation to the hydrogen embrittlement and film rupture/dissolution mechanisms.

9.6 "Driving Force" for Small Crack Propagation

Several authors (e.g., refs. 7,19,28,49,90) have sought improved field characterizing parameters to describe the driving force for small crack advance (Table 9.1). Although parameters such as $\Delta\sigma$ and $\Delta\varepsilon_p$ have been suggested,[91] only those parameters that can be measured globally, yet define (at least nominally) local conditions, are reviewed here. For mechanically-small cracks, where the extent of local plasticity is comparable with crack size, elastic-plastic fracture mechanics solutions have been proposed through the use of ΔJ[7] and ΔS.[81] While certainly appropriate for taking account of excessive plasticity ahead of the tip, it should be noted that J is a nonlinear elastic parameter, and thus cannot account for the vital influence of wake plasticity (prior plastic) zones behind the tip. Similarly, the use of ΔS cannot account for the varying contribution from wake-related crack tip shielding. To allow for

such wake effects, which principally cause crack closure, the adoption of a closure-corrected ΔK_{eff} appears to be a suitable approach for physically-small cracks[28,49] and cracks emanating from notches.[13] For microstructurally-small flaws, however, such deterministic treatments may simply not apply, as initial cracking may center on local preferential growth sites ("soft spots") in the microstructure.[54] Here a probabilistic approach may be the optimum treatment to describe the behavior of such tiny flaws.

9.7 Intrinsic Thresholds

There is now good evidence that intrinsic threshold cyclic stress intensities may exist for long fatigue cracks. By subtracting out the contribution from crack closure through the use of the ΔK_{eff} parameter, threshold values at low load ratios approach those at high load ratios where closure effects are minimal (e.g., refs. 16,28). Similarly, intrinsic thresholds may exist for physically- and mechanically-short cracks, of magnitude comparable with the effective long crack value.[28,49,61] For microstructurally-small cracks, however, the question of an intrinsic threshold may not be meaningful. Here the "fatal" flaws are the ones that initiate first at local weak areas in the microstructure. As their dimensions are well below any continuum approximation, characterization in terms of a material parameter clearly would be inappropriate. Further, in light of evidence[54] suggesting the invalidity of ΔK within this flaw size regime, it may be more appropriate to consider a threshold stress, rather than a stress intensity, for microstructurally-small flaws (i.e., akin to the fatigue limit).

9.8 Small Crack Methodology in Life Prediction and Design

For physically- or mechanically-small cracks, the adoption of small crack methodology in life prediction analyses would appear to be feasible by mere extension of the current damage-tolerant procedures to smaller crack sizes through the use of ΔK_{eff}, or an equivalent elastic-plastic characterizing parameter. Such an approach would greatly enhance projected lifetimes, as computations are dominated by the regimes where the crack is small and advancing slowly. Conversely, for the reasons outlined above, descriptions of the extension of microstructurally-small flaws will not be generally amenable to deterministic analyses which rely on (continuum) material parameters, and should be treated with probabilistic approaches.

9.9 Small Crack Considerations in Alloy Design

From an alloy design perspective, the study of small cracks and associated long crack thresholds has resulted in a far clearer understanding of the various contributions to fatigue resistance. Moreover, it has led to the realization that microstructural features which benefit resistance to the growth of (long) cracks may have an entirely different influence on crack initiation and small crack growth. To impede long crack growth, the primary mechanisms are extrinsic, whereby mechanical, microstructural, and even environmental mechanisms are utilized to reduce locally the crack driving force.[28] Here, promotion of crack tip shielding, principally through crack closure and deflection, provides the most potent effect under cyclic loading. Conversely, to impede crack initiation and the early growth of microstructurally-small cracks, where shielding effects are minimized,

the primary mechanisms are **intrinsic**. For example, fine grain sizes offer best resistance to crack initiation and small crack growth in many alloys (e.g., ref. 61), yet in these same materials it is the coarse grain structures which promote the roughest crack paths and hence provide greatest resistance to long crack growth (through crack deflection and roughness-induced closure) (e.g., ref. 45).

In essence, the ideal alloy design approach is to clean-up the material for optimum resistance to crack initiation, incorporate small, randomly oriented grains to inhibit small crack growth, and then to add microstructural "crack stoppers" through shielding mechanisms to impede long crack growth. It may also be possible to minimize the small crack problem by incorporating texture, so that as few grains as possible are oriented for easy crack extension relative to a known uniaxial loading axis.

9.10 Conclusions

1. Small fatigue cracks can be characterized as mechanically-small (comparable with the extent of local plasticity), microstructurally-small (comparable with the scale of microstructure), physically-small (typically less than 1 mm in size), or chemically-small. Their common property is that they can propagate at rates which differ from, and generally exceed, those of long cracks at the same nominal stress intensity factor, leading to potentially non-conservative damage-tolerant lifetime predictions.

2. The primary factors responsible for differences in behavior between long and mechanically- and physically-small flaws are, respectively, extensive plasticity ahead of the tip, and crack tip

shielding from crack closure behind the tip. Such differences may be in part normalized through characterization in terms of ΔK_{eff}, or an equivalent elastic-plastic field parameter.

3. The behavior of microstructurally-small flaws differs from long cracks because of several factors, including excess crack tip plasticity, crack closure, crack shape and deflection, retardation at grain boundaries, and enhanced crack tip plastic strains. Such flaws may not be amenable to characterization in terms of a global field parameter, as their dimensions lie below continuum size-scales.

4. Approaches to apply small crack methodology to fatigue life prediction are suggested in terms of i) the use of ΔK_{eff}, or equivalent elastic-plastic parameter, to extend damage-tolerant procedures into the physically-small crack regime, and ii) probabilistic analyses of the initiation and early growth of microstructurally-small flaws.

5. In life prediction, the concern is with predicting the growth of the most rapidly growing, ultimately fatal, small crack. To design alloys which are resistant to such behavior, the approach must be to eliminate such maverick flaws, by creating microstructures to arrest the microstructurally-small cracks which are able to nucleate. Thus, for optimum fatigue resistance, the approach may involve using clean materials to inhibit crack initiation, small randomly oriented grains to inhibit small crack growth, and employing crack tip shielding (i.e., microstructural "crack stoppers") to impede the growth of long cracks.

10. ACKNOWLEDGEMENTS

The work was funded by the U.S. Air Force Office of Scientific Research under Grant No. AFOSR-82-0181, with Dr. Alan H. Rosenstein as program manager. Thanks are due to Dr. Rosenstein for his continued support, to Drs. A. F. Blom, R. J. Bucci, J. Lankford, R. P. Gangloff and S. Suresh for helpful discussions and collaborative ventures, and to the Aluminum Company of America, specifically Drs. Bucci and P. E. Bretz, for provision of materials. Assistance from Ms. Madeleine Penton for her efforts in preparing this report also is greatly appreciated.

11. REFERENCES

1. R. O. Ritchie: International Metals Reviews, 1979, vol. 20, p. 205.

2. M. E. Fine and R. O. Ritchie: in Fatigue and Microstructure, p. 245, American Society for Metals, Metals Park, OH, 1979.

3. S. J. Hudak: J. Eng. Matls. Tech., Trans. ASME Series H, 1981, vol. 103, p. 26.

4. S. Pearson: Eng. Fract. Mech., 1975, vol. 7, p. 235.

5. H. Kitagawa and S. Takahashi: Proc. 2nd Intl. Conf. on Mech. Beh. of Materials, p. 627, American Society for Metals, Metals Park, OH, 1976.

6. Y. H. Kim, T. Mura and M. E. Fine: Eng. Fract. Mech., 1978, vol. 11, p. 1697.

7. N. E. Dowling: ASTM Spec. Tech. Publ. 637, American Society for Testing and Materials, Philadelphia, PA, 1978, p. 97.

8. M. H. El Haddad, N. E. Dowling, T. H. Topper and K. N. Smith: Int. J. Fract., 1980, vol. 16, p. 15.

9. R. A. Smith and K. J. Miller: Int. J. Mech. Sci., 1977, vol. 19, p. 11.

10. W. L. Morris: Metall. Trans. A, 1980, vol. 11A, p. 1117.

11. B. N. Leis and T. N. Forte: ASTM Spec. Tech. Publ. 743, American Society for Testing and Materials, Philadelphia, PA, 1982, p. 100.

12. S. Usami and S. Shida: Fat. Eng. Matls. Struct., 1979, vol. 1, p. 471.

13. K. Tanaka and Y. Nakai: Fat. Eng. Matls. Struct., 1983, vol. 5, p. 315.

14. G. P. Sheldon, T. S. Cook, T. W. Jones and J. Lankford: Fat. Eng. Matls. Struct., 1981, vol. 3, p. 219.

15. R. P. Gangloff: Res. Mech. Letters, 1981, vol. 1, p. 299.

16. J. F. McCarver and R. O. Ritchie: Mater. Sci. Eng., 1982, vol. 55, p. 63.

17. J. Lankford: Fat. Eng. Matls. Struct., 1982, vol. 5, p. 223.

18. R. P. Gangloff: Metall. Trans. A, 1985, vol. 16A, p. 953.

19. S. Suresh and R. O. Ritchie: International Metals Reviews, 1984, vol. 29, p. 445.

20. R. P. Gangloff and R. O. Ritchie: in Fundamentals of Deformation and Fracture, Eshelby Memorial Symp., B. A. Bilby, K. J. Miller and J. R. Willis, eds., Cambridge University Press, U.K., p. 529, 1985.

21. E. Zaiken and R. O. Ritchie: Mater. Sci. Eng., 1985, vol. 70, p. 151.

22. R. J. Rioja and E. A. Ludwiczak: in Aluminium-Lithium Alloys III, C. Baker et al., eds., Inst. Metals, London, U.K., p. 471, 1986.

23. E. Zaiken and R. O. Ritchie: Scripta Met., 1984, vol. 8, p. 847.

24. E. Zaiken and R. O. Ritchie: Metall. Trans. A, 1985, vol. 16A, p. 1467.

25. E. Zaiken and R. O. Ritchie: Eng. Fract. Mech., 1985, vol. 22, p. 35.

26. P. Donehoo, W. Yu and R. O. Ritchie: Mater. Sci. Eng., 1985, vol. 74, p. 11.

27. W. Yu and R. O. Ritchie: J. Eng. Mater. Technol., Trans ASME 1987, vol. 109, p. 81.

28. R. O. Ritchie and W. Yu: in Small Fatigue Cracks, R. O. Ritchie and J. Lankford, eds., TMS-AIME, Warrendale, PA, p. 167, 1986.

29. C. E. Richards and W. F. Deans: in The Measurement of Crack Length and Shape during Fracture and Fatigue, C. J. Beevers, ed., EMAS Ltd., Warley, U.K., p. 28, 1980.

30. M. Kikukawa, M. Jono and K. Tanaka: in Proc. 2nd Intl. Conf. on Mechanical Behavior of Materials, ASM, Metals Park, OH, p. 254, 1976.

31. V. B. Dutta, S. Suresh and R. O. Ritchie: Metall. Trans. A, 1984, vol. 15A, p. 1193.

32. M. N. James and J. F. Knott: Mater. Sci. Eng., 1985, vol. 72, p. L1.

33. W. Elber: Eng. Fract. Mech., 1970, vol. 2, p. 37.

34. K. Minakawa, J. C. Newman and A. J. McEvily: Fat. Eng. Matl. Struct., 1983, vol. 6, p. 359.

35. J. M. Larsen, T. Nicholas, A. W. Thompson and J. C. Williams: in Small Fatigue Cracks, R. O. Ritchie and J. Lankford, eds., TMS-AIME, Warrendale, PA, p. 499, 1986.

36. K. D. Unangst, T. T. Shih and R. P. Wei: Eng. Fract. Mech., 1977, vol. 9, p. 725.

37. S. Suresh, D. M. Parks and R. O. Ritchie: in Fatigue Thresholds, J. Bäcklund, A. Blom and C. J. Beevers, eds., EMAS Ltd., Warley, U.K., vol. 1, p. 391, 1982.

38. R. O. Ritchie, S. Suresh and C. M. Moss: J. Eng. Mater. Technol., Trans. ASME (H), 1980, vol. 102, p. 293.

39. A. T. Stewart: Eng. Fract. Mech., 1980, vol. 13, p. 463.

40. S. Suresh, G. F. Zamiski and R. O. Ritchie: Metall. Trans. A, 1981, vol. 12, p. 1435.

41. N. Walker and C. J. Beevers: Fat. Eng. Mat. Struct., 1979, vol. 1, p. 135.

42. K. Minakawa and A. J. McEvily: Scripta Met., 1981, vol. 15, p. 937.

43. S. Suresh and R. O. Ritchie: Metall. Trans. A, 1982, vol. 13A, p. 1627.

44. J.-L. Tzou, C. H. Hsueh, A. G. Evans and R. O. Ritchie: Acta Met., 1985, vol. 33, p. 117.

45. S. Suresh and R. O. Ritchie: in Fatigue Crack Growth Threshold Concepts, D. L. Davidson and S. Suresh, eds., TMS-AIME, Warrendale, PA, p. 227, 1984.

46. S. Suresh: Metall. Trans. A, 1983, vol. 14, p. 2375.

47. A. K. Vasudévan, P. E. Bretz, A. C. Miller and S. Suresh: Mater. Sci. Eng., 1984, vol. 64, p. 113.

48. E. Hornbogen and K. H. Zum Gahr: Acta Met., 1976, vol. 24, p. 581.

49. A. Pineau: in Small Fatigue Cracks, R. O. Ritchie and J. Lankford, eds., TMS-AIME, Warrendale, PA, p. 191, 1986.

50. N. E. Dowling: Eng. Fract. Mat. Struct., 1979, vol. 2, p. 129.

51. H. Tada, P. C. Paris and G. R. Irwin: in The Stress Analysis of Cracks Handbook, Del Research Corp., St. Louis, MO, 1973.

52. W. K. Wilson: J. Press. Ves. Tech., Trans. ASME, 1974, vol. 96, p. 293.

53. M. M. Hammouda and K. J. Miller: in Elastic-Plastic Fracture, ASTM STP 668, American Society for Testing and Materials, Philadelphia, PA, p. 703, 1979.

54. J. Lankford and D. L. Davidson: in Small Fatigue Cracks, R. O. Ritchie and J. Lankford, eds., TMS-AIME, Warrendale, PA, p. 51, 1986.

55. J. C. Newman, Jr.: in Behaviour of Short Cracks in Airframe Components, AGARD Conf. Proc. No. 328, Advisory Group for Aerospace Research and Development, Neuilly sur Seine, p. 6-1, 1983.

56. R. M. McMeeking and A. G. Evans: J. Amer. Cer. Soc., 1982, vol. 64, p. 242.

57. A. G. Evans et al.: in 5th Intl. Conf. on Composite Matls., W. C. Harrigan et al., eds., TMS-AIME, Warrendale, PA, p. 543, 1985.

58. R. O. Ritchie, F. A. McClintock, E. K. Tschegg and H. Nayeb-Hashemi: in Multiaxial Fatigue, ASTM STP 853, K. J. Miller and M. W. Brown, eds., American Society for Testing and Materials, Philadelphia, PA, p. 203, 1985.

59. W. J. Drugan, J. R. Rice and T.-L. Sham: J. Mech. Phys. Solids, 1982, vol. 30, p. 447.

60. R. O. Ritchie and A. W. Thompson: Metall. Trans. A, 1985, vol. 16A, p. 233.

61. C. W. Brown and J. E. King: in Small Fatigue Cracks, R. O. Ritchie and J. Lankford, eds., TMS-AIME, Warrendale, PA, p. 73, 1986.

62. C. M. Hudson and J. T. Scardina: Eng. Fract. Mech., 1969, vol. 1, p. 429.

63. T. R. Gurney: Metal Constr., 1969, vol. 1, p. 91.

64. R. P. Skelton and J. R. Haigh: Mater. Sci. Eng., 1978, vol. 36, p. 17.

65. S. Usami: in Fatigue Thresholds, J. Bäcklund, A. Blom and C. J. Beevers, eds., EMAS Ltd., Warley, U.K., vol. 1, p. 205, 1982.

66. A. F. Blom, A. Hadrboletz and B. Weiss: in Mechanical Behavior of Materials IV, Proc. 4th Intl. Conf., J. Carlsson and N. G. Olhsen, eds., Pergamon Press, Oxford, U.K., vol. 2, p. 755, 1984.

67. P. Au, T. H. Topper and M. L. El Haddad: in Behavior of Short Cracks in Airframe Components, AGARD Conf. Proc. No. 328, AGARD, France, p. 11.1, 1983.

68. M. T. Yu, T. H. Topper and P. Au: in Fatigue '84, C. J. Beevers, ed., EMAS Ltd., Warley, U.K., vol. 1, p. 179, 1984.

69. T. M. Hsu and W. M. McGee: in Effect of Load Spectrum Variables in Fatigue Crack Initiation and Propagation, ASTM STP 714, American Society for Testing and Materials, p. 79, 1980.

70. D. Gan and J. Weertman: Eng. Fract. Mech., 1981, vol. 15, p. 87.

71. J. Schijve and D. Broek: Aircraft Engineering, 1962, vol. 34, p. 314.

72. S. Suresh, T. Christman and M. Bull: in Small Fatigue Cracks, R. O. Ritchie and J. Lankford, eds., TMS-AIME, Warrendale, PA, p. 513, 1986.

73. R. Marissen, K. H. Trautmann and H. Nowack: Eng. Fract. Mech., 1984, vol. 19, p. 863.

74. M. Gell and G. R. Leverant: Acta Met., 1968, vol. 16, p. 553.

75. J. C. Newman, Jr.: in Methods for Predicting Fatigue Crack Growth under Random Loading, ASTM STP 748, American Society for Testing and Materials, p. 53, 1981.

76. J. C. Newman, Jr., M. H. Swain and E. P. Phillips: in Small Fatigue Cracks, R. O. Ritchie and J. Lankford, eds., TMS-AIME, Warrendale, PA, p. 427, 1986.

77. D. K. Holm and A. F. Blom: in Proc. of the 14th Congress of the Intl. Council of Aeronautical Sciences, Toulouse, France, p. 783, 1984.

78. B. Budiansky and J. W. Hutchinson: J. Appl. Mech., 1978, vol. 45, p. 267.

79. A. F. Blom and D. K. Holm: Eng. Fract. Mech., 1985, vol. 22, p. 997.

80. J. C. Newman, Jr. and I. Raju: Eng. Fract. Mech., 1981, vol. 15, p. 185.

81. R. S. Vecchio and R. H. Hertzberg: Eng. Fract. Mech., 1985, vol. 22, p. 1049.

82. A. Talug and K. Reifsnider: in Cyclic Stress-Strain and Plastic Deformation Aspects of Fatigue Crack Growth, ASTM STP 637, American Society for Testing and Materials, Philadelphia, PA, p. 81, 1977.

83. M. L. Williams: J. Appl. Mech., 1957, vol. 24, p. 109.

84. N. I. Muskhelishvili: Some Basic Problems of the Mathematical Theory of Elasticity, Noordhoff, Groningen, Holland, 1963.

85. J. P. Benthem: Intl. J. Solids Structures, 1977, vol. 13, p. 479.

86. Wang Tzu Chiang and K. J. Miller: Fatigue Eng. Mater. Struct., 1982, vol. 5, p. 249.

87. J. Lankford: Eng. Fract. Mech., 1977, vol. 9, p. 617.

88. M. A. Daeubler and A. W. Thompson: in Small Fatigue Cracks, R. O. Ritchie and J. Lankford, eds., TMS-AIME, Warrendale, PA, p. 157, 1986.

89. M. R. James and W. L. Morris: in Small Fatigue Cracks, R. O. Ritchie and J. Lankford, eds., TMS-AIME, Warrendale, PA, p. 145, 1986.

90. R. P. Gangloff and R. P. Wei: in Small Fatigue Cracks, R. O. Ritchie and J. Lankford, eds., TMS-AIME, Warrendale, PA, p. 239, 1986.

91. K. J. Miller: Fatigue Eng. Mater. Struct., 1982, vol. 5, p. 223.

12. PROGRAM ORGANIZATION AND PERSONNEL

The work described was performed in the Department of Materials Science and Mineral Engineering, University of California in Berkeley, under the supervision of Dr. R. O. Ritchie, Professor of Materials Science, aided by research engineer, Dr. W. Yu, graduate student research assistants, E. Zaiken and J. Miwa, and undergraduate research helpers. The individual personnel are listed below:

i) Professor R. O. Ritchie, Principal Investigator
(Department of Materials Science and Mineral Engineering)

ii) Dr. W. Yu, Research Engineer
(Department of Materials Science and Mineral Engineering)

iii) E. Zaiken, Graduate Student Research Assistant
(Department of Mechanical Engineering)

iv) J. Miwa, Graduate Student Research Assistant
(Department of Materials Science and Mineral Engineering)

v) P. Donehoo, Undergraduate Engineering Aide
(Department of Materials Science and Mineral Engineering)

vi) H. Hayashigatani, Undergraduate Engineering Aide
(Department of Materials Science and Mineral Engineering)

13. PUBLICATIONS

1983

1. R. O. Ritchie and S. Suresh: "The Fracture Mechanics Similitude Concept: Questions Concerning its Application to the Behavior of Short Fatigue Cracks," Materials Science and Engineering, 1983, vol. 57, pp. L27-L30.

2. R. O. Ritchie and S. Suresh: "Mechanics and Physics of the Growth of Small Cracks," in Behavior of Short Cracks in Airframe Components, AGARD, vol. CP328, pp. 1.1-1.14, North Atlantic Treaty Organization, AGARD, France, 1983.

3. S. Suresh: "Crack Deflection: Implications for the Growth of Long and Short Cracks," Metallurgical Transactions A, 1983, vol. 14A, pp. 2375-2385.

1984

4. S. Suresh and R. O. Ritchie: "Propagation of Short Fatigue Cracks," International Metals Reviews, 1984, vol. 29, pp. 445-476.

5. E. Zaiken and R. O. Ritchie: "On the Location of Crack Closure and the Threshold Condition for Fatigue Crack Growth," Scripta Metallurgica, 1984, vol. 8, pp. 847-850.

1985

6. E. Zaiken and R. O. Ritchie: "Effects of Microstructure on Fatigue Crack Propagation and Crack Closure Behavior in Aluminum Alloy 7150," Materials Science and Engineering, 1985, vol. 70, pp. 151-160.

7. R. P. Gangloff and R. O. Ritchie: "Environmental Effects Novel to the Propagation of Short Fatigue Cracks," in Fundamentals of Deformation and Fracture, Proc. Eshelby Memorial Symp., B. A. Bilby, K. J. Miller and J. R. Willis, eds., Cambridge University Press, 1985, pp. 529-558.

8. E. Zaiken and R. O. Ritchie: "On the Development of Crack Closure at the Threshold Condition for Long and Short Cracks in 7150 Aluminum Alloys," Metallurgical Transactions A, 1985, vol. 16A, pp. 1467-1477.

9. E. Zaiken and R. O. Ritchie: "On the Role of Compression Overloads in Influencing Crack Closure and the Threshold Condition for Fatigue Crack Growth in 7150 Aluminum Alloy," Engineering Fracture Mechanics, 1985, vol. 22, pp. 35-48.

10. P. Donehoo, W. Yu and R. O. Ritchie: "On the Growth of Cracks at the Fatigue Threshold Following Compression Overloads: Role of Load Ratio," Materials Science and Engineering, 1985, vol. 75, pp. 11-17.

1986

11. R. O. Ritchie and W. Yu: "Short Crack Effects in Fatigue: A Consequence of Crack Tip Shielding," in Small Fatigue Cracks, R. O. Ritchie and J. Lankford, eds., TMS-AIME, Warrendale, PA, 1986, pp. 167-189.

12. R. O. Ritchie and J. Lankford: "Small Fatigue Cracks: A Statement of the Problem and Potential Solutions," Materials Science and Engineering, 1986, vol. 84, pp. 11-16.

1987

13. W. Yu and R. O. Ritchie: "Fatigue Crack Propagation in 2090 Aluminum-Lithium Alloy: Effect of Compression Overload Cycles," Journal of Engineering Materials and Technology, Transactions of ASME, Series H, 1987, vol. 109, pp. 81-85.

14. R. O. Ritchie, E. Zaiken and A. F. Blom: "Is the Concept of a Fatigue Threshold Meaningful in the Presence of Compression Cycles?," in Basic Questions in Fatigue, Volume I, ASTM STP 924, J. T. Fong and R. J. Fields, eds., American Society for Testing and Materials, Philadelphia, PA, 1987, in press.

15. R. O. Ritchie, W. Yu, D. K. Holm and A. F. Blom: "Development of Fatigue Crack Closure with the Extension of Long and Short Flaws in Aluminum Alloy 2124: A Comparison of Experimental and Numerical Results," in Fatigue Crack Closure, ASTM STP, J. C. Newman, Jr., and W. Elber, eds., American Society for Testing and Materials, Philadelphia, PA, 1987, in press.

16. R. O. Ritchie, W. Yu, A. F. Blom and D. K. Holm: "An Analysis of Crack Tip Shielding in Aluminum Alloy 2124: A Comparison of Large, Small, Through-Thickness and Surface Fatigue Cracks," Fatigue and Fracture of Engineering Materials and Structures, 1987, vol. 10, in press.

14. DISTRIBUTION LIST

AFOSR/NE
ATTN: Dr. A. H. Rosenstein
Bldg. #410
Bolling Air Force Base
Washington, D.C. 20332

AFWAL/MLLM
ATTN: Branch Chief
Wright-Patterson Air Force Base
Dayton, OH 45433

AFWAL/MLLS
ATTN: Branch Chief
Wright-Patterson Air Force Base
Dayton, OH 45433

AFWAL/MLLN
ATTN: Branch Chief
Wright-Patterson Air Force Base
Dayton, OH 45433

Dr. Hugh R. Gray
NASA Lewis Research Center
Materials and Structures Division
21000 Brookpark Rd.
Cleveland, OH 44135

Drs. R. J. Bucci, P. E. Bretz, and J. T. Staley
Alcoa Technical Center
Alcoa Laboratories
Alcoa Center, PA 15069

APPENDICES

Propagation of short fatigue cracks

S. Suresh and R. O. Ritchie

Fatigue crack propagation in engineering materials has been the subject of considerable research, and extensive review articles have appeared over the past several years. Most of these investigations focused on the behaviour of 'long' fatigue cracks, even though the characteristics associated with the extension of small cracks in metals and alloys remain relatively unexplored, despite their unquestionable importance from an engineering standpoint. In this review, the mechanics and micromechanisms of the subcritical growth of short fatigue cracks are examined, and aspects of their propagation behaviour are contrasted with those of long cracks in terms of fracture mechanics, microstructure, and environment. Cracks are defined as being short (i) when their length is small compared to relevant microstructural dimensions (a continuum mechanics limitation), (ii) when their length is small compared to the scale of local plasticity (a linear elastic fracture mechanics limitation), or (iii) when they are simply physically small (e.g. ≤ 0.5–1 mm). Since all three types of short flaw are known to propagate faster than (or at least at the same rate as) corresponding long fatigue cracks subjected to the same *nominal* driving force, current defect tolerant fatigue design procedures which utilize long crack data can, in certain applications, result in overestimates of lifetimes. The characteristics of the short crack problem are critically reviewed in the light of the influences of local plasticity, microstructure, crack tip environment, growth mechanisms, crack driving force, and the premature closure of the crack. IMR/137

Professor S. Suresh, BTech, MS, ScD, is in the Division of Engineering, Brown University, Providence, RI, USA. Professor R. O. Ritchie, MA, PhD, FIM, CEng, is in the Department of Materials Science and Mineral Engineering and the Lawrence Berkeley Laboratory, University of California at Berkeley, Cal., USA. Professor Suresh was formerly with the University of California at Berkeley.

LIST OF SYMBOLS

a = crack length

a_0 = intrinsic crack length, i.e. constant characteristic of material or material condition in expression for ΔK (equation (24))

Δa = increment of crack extension

da/dN = fatigue crack propagation rate

A = constant in cyclic constitutive law (Fig. 5)

b = sum of crack length a and blocked slip band zone ρ_0 (equations (18) and (19))

B = thickness of testpiece (Fig. 11)

c = depth of edge notch or half length of internal notch

$\bar{c}$ = half width of surface microcrack

C = experimentally determined scaling constant (equation (2))

d = proportionality factor dependent on yield strain ϵ_0 and work hardening exponent n (equation (13))

d_g = grain size

d_0 = maximum thickness of excess oxide layer

e = nominal difference in crack length between fatigue crack of length a in unnotched specimen and equivalent fatigue crack of length l growing from notch

E = elastic (Young's) modulus

E' = effective value of Young's modulus under different loading conditions

f = function of stress intensity factor range ΔK and load ratio R (equation (15))

f_{ij} = dimensionless function of polar angle θ measured from crack plane (equation (3))

f'_{ij}, f''_{ij} = universal functions of both polar angle θ measured from crack plane and work hardening exponent n (equation (10))

G = strain-energy release rate

J = scalar amplitude of crack tip stress and strain field under nonlinear elastic conditions

ΔJ = cyclic component of J

k_f = fatigue strength reduction factor

k_t = theoretical elastic stress concentration factor

K_ϵ, K_σ = strain and stress concentration factors

K_{cl} = closure stress intensity factor

K_c^m = critical value of microscopic stress intensity at tip of slip band

K_I = stress intensity factor in mode I loading

K_{Ic} = critical stress intensity at failure (plane strain fracture toughness)

K_{II}^m = mode II value of microscopic stress intensity at tip of slip band (Fig. 17)

K_l = limiting stress intensity for long crack emanating from notch

K_{max}, K_{min} = maximum and minimum stresss intensities during cycle

K_s = limiting stress intensity for short crack emanating from notch

K_{th} = threshold stress intensity factor

K_0 = long crack threshold stress intensity factor

K_1, K_2 = local mode I and mode II stress intensity factors for non-linear crack

ΔK = nominal stress intensity factor range ($K_{max} - K_{min}$)

ΔK_{eff} = effective stress intensity factor range ($K_{max} - K_{cl}$)

ΔK_{eq} = equivalent stress intensity range for short crack

ΔK_i = initial stress intensity range

ΔK_{th} = threshold stress intensity factor range

ΔK_ϵ = pseudo-elastic–plastic strain intensity range

ΔK_0 = long crack threshold stress intensity factor range

l = length of crack growing from notch

l_0 = transition size of crack growing from notch

m = exponent in Paris power law (equation (2))

m' = exponent in power law for elastic–plastic fatigue crack growth (equation (12))

n, n' = monotonic and cyclic work hardening exponents, respectively

N = number of cycles

N_i = number of cycles necessary to initiate macrocrack

N_p = number of cycles necessary to propagate macrocrack subcritically until failure

P_{cl} = closure load during fatigue cycle

P_{max}, P_{min} = maximum and minimum loads during fatigue cycle

q = fraction of elastic strain with values between 0.5 and 1 (equation (22))

Q = dimensionless function of geometry (equation (8))

r = radial distance from crack tip

r_{max}, r_Δ = maximum and cyclic sizes of plastic zone

r_y = size of plastic zone

r_Δ^F = cyclic size of plastic zone at fatigue limit

R = load or stress ratio (K_{min} K_{max}

R_ϵ = ratio of minimum to maximum strain (Fig. 24)

s = half distance between location of thickest oxide layer and crack tip

S = compliance of microcrack in completely opened state

s_0 = length of blocked slip band zone

$\Delta W_e, \Delta W_p$ = elastic and plastic components of strain-energy density range

ν = ratio of mode II to mode I crack tip displacements

α = empirical constant in Peterson's (equation (32))

β = constant in equation (36)

γ = non-dimensional fracture surface roughness factor

δ, δ_t = crack tip opening displacement

$\delta_{max}, \Delta\delta$ = maximum and range of crack tip opening displacement

$\delta(\sigma_{max})$ = crack tip opening displacement at maximum stress

$\delta(0)$ = crack tip opening displacement at zero load

$\Delta\delta_t$ = crack tip opening displacement range

ϵ = local strain

ϵ_p = plastic strain

ϵ_0 = yield strain

$\Delta\epsilon$ = local strain range

$\Delta\epsilon_e, \Delta\epsilon_p$ = elastic and plastic strain ranges

θ = polar angle measured from crack plane

θ_0, θ_1 = angles associated with crack deflection (Fig. 31)

ν = Poisson ratio

ρ = notch root radius

σ = local stress

σ^∞ = nominal stress

$\sigma_{cl}, \sigma_{max}$ = closure and maximum stresses

σ_e = tensile stress corresponding to fatigue limit

σ^{*}_{fr} = normal frictional stress for dislocation motion

σ_{ij} = local crack tip stresses dependent on distance from crack tip and inclination to crack plane

σ_{th} = threshold stress for no crack growth

σ_{y} = yield or flow stress

$\Delta\sigma$ = local stress range

$\Delta\sigma^{\infty}$ = nominal stress range

$\Delta\sigma_{e}$ = fatigue limit or endurance strength

$\Delta\sigma_{th}$ = threshold stress range for no crack growth

τ^{*}_{fr} = shear frictional stress for dislocation motion (Fig. 17)

Fatigue fractures account for the vast majority of in-service failures in most engineering structures and components, either as a result of pure mechanical loading or in conjunction with sliding and friction between surfaces (fretting fatigue), rolling contact between surfaces (rolling contact fatigue), aggressive environments (environmentally assisted or corrosion fatigue) or elevated temperatures (creep fatigue). Such progressive fracture of materials by incipient growth of flaws under cyclically varying stresses, termed fatigue, can be categorized into the following discrete yet related phenomena:

(i) initial cyclic damage in the form of cyclic hardening or softening
(ii) creation of initial microscopic flaws (microcrack initiation)
(iii) coalescence of these microcracks to form an initial 'fatal' flaw (microcrack growth)
(iv) subsequent macroscopic propagation of this flaw (macrocrack growth)
(v) final catastrophic failure or instability.

In engineering terms the first three stages, involving cyclic deformation and microcrack initiation and growth, are generally classified together as (macro-) crack initiation, implying the formation of an 'engineering sized' detectable crack (e.g. of the order of several grain diameters in length). Thus, in such terms, the total fatigue life N can be defined as the number of cycles necessary both to initiate a (macro-) crack, N_i, and to propagate it subcritically until final failure, N_p, i.e.

$$N = N_i + N_p \quad . \quad . \quad . \quad . \quad . \quad . \quad . \quad (1)$$

In fatigue design, where data from laboratory sized specimens are used to predict the lifetime of more complex components in service (*see* Fig. 1 after Ref. 1), this distinction between initiation and propagation lives can be critical. Conventional approaches to fatigue design involve the use of S–N curves (stress S, number of cycles), representing the *total* life resulting from a given stress (or strain) amplitude, suitably adjusted to take into account effects of mean stress (using, for example, Goodman diagrams); effective stress concentrations at notches (using fatigue strength reduction factors or local strain analysis); variable amplitude loading (using the Palmgren–Miner cumulative damage law or rainflow counting methods); multiaxial stresses; environmental effects; and so forth (for a summary, *see* Ref. 2). Although based on total life, this approach – which is in widespread use, particularly in the automotive industry – essentially represents design against crack *initiation*, since near the fatigue limit, especially in smooth specimens, most of the lifetime is spent in the formation of an engineering sized crack. In procedures for predicting lifetimes, such S–N or low cycle fatigue (LCF) testing might simulate the initiation and early growth of the fatigue crack within the fully plastic region of the strain field at some stress concentrator (*see* Fig. 1).

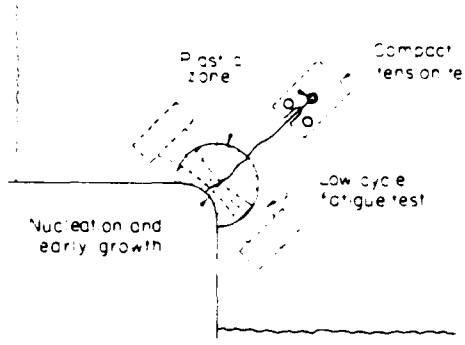

1 Schematic diagram showing various stages of fatigue in engineering components and typical laboratory tests to evaluate fatigue life[1]

For safety-critical structures, especially those with welded and riveted components, the approach is different. There has been a growing awareness that the presence in a material of defects below a certain size must be assumed and taken into account at the design stage. Under such circumstances the integrity of a structure will depend on the lifetime spent in crack propagation, and since the crack initiation stage will be short, the use of conventional S–N total life analyses may lead to dangerous overestimates of life. Such considerations have led to the adoption of the so-called 'defect tolerant' approach in which the fatigue lifetime is assessed in terms of the time, or number of cycles, necessary to propagate the largest undetected crack to failure.[3] Here the initial size of the crack is estimated using non-destructive evaluation or proof tests, whereas the final size is defined in terms of the fracture toughness K_{Ic}, the limit load, or some allowable strain criterion. This approach, the only one used for certain applications in the nuclear and aerospace industries, for example, relies on the integration of an expression for crack growth, representing a fracture mechanics characterization of relevant fatigue crack propagation data suitably modified to account for mean stress effects (e.g. using the Forman equation), variable amplitude loading (e.g. using the Wheeler or the Willenborg model), environmental effects, and so forth, as required (for a summary, *see* Ref. 4). Such expressions are generally based on the original Paris power law relationship, i.e. are of the form

$$da/dN = C\Delta K^{m} \quad . \quad . \quad . \quad . \quad . \quad . \quad (2)$$

where C and m are experimentally determined scaling constants, da/dN is the crack growth

increment per cycle, and ΔK is the alternating stress intensity factor given by the difference between the maximum and minimum stress intensities in the fatigue cycle ($\Delta K = K_{max} - K_{min}$).[5] In its simplest form equation (2) provides a reasonable description of growth rate in the so-called intermediate range of growth rates, typically between 10^{-6} and 10^{-3} mm/cycle. However, it underestimates propagation rates of higher values of ΔK, as final instability is approached (e.g. as $K_{max} \to K_{Ic}$), but overestimates propagation rates at lower values of ΔK approaching the so-called long crack fatigue threshold stress intensity range ΔK_0, below which long cracks remain dormant or grow at experimentally undetectable rates.[6] Since the time for crack initiation is generally taken to be zero, such defect-tolerant lifetime predictions are assumed to be inherently conservative and to simulate the macroscopic growth of the fatigue crack (*see* Fig. 1). In its most widely used form, that based on linear elastic fracture mechanics (LEFM), the latter approach would imply crack growth outside the notch strain field where the crack tip plastic zone is small compared to the crack length, i.e. that a long crack propagates under nominally elastic conditions.[5,6]

Current practice in the determination of the relevant crack growth 'law'* for a particular material under a particular set of conditions for a given application is to use data from laboratory tests on fatigue crack propagation, characterized in terms of the linear elastic stress intensity range ΔK. However, most of these data have been obtained from testpieces containing cracks of 25 mm or so, whereas many defects encountered in service are far smaller than this, particularly in turbine discs and blades, for example. In the relatively few cases where the fatigue behaviour of such short cracks has been studied experimentally (for earlier reviews, *see* Refs. 7–12), it has been found – almost without exception – that, under the same nominal driving force, the growth rates of short cracks are greater than (or at least equal to) the corresponding growth rates of long cracks (*see* Fig. 2). This implies a breakdown in the similitude concept generally assumed in fracture mechanics, as described in the section 'Similitude concept' below. Furthermore, it suggests that the use of data for long cracks in defect tolerant lifetime calculations for components where the growth of short flaws represents a large proportion of the lifetime, can lead to considerable overestimates.

There are several ways of defining 'short'† cracks:

(i) cracks which are of a length comparable to the scale of the microstructure (e.g. of the order of the grain size)

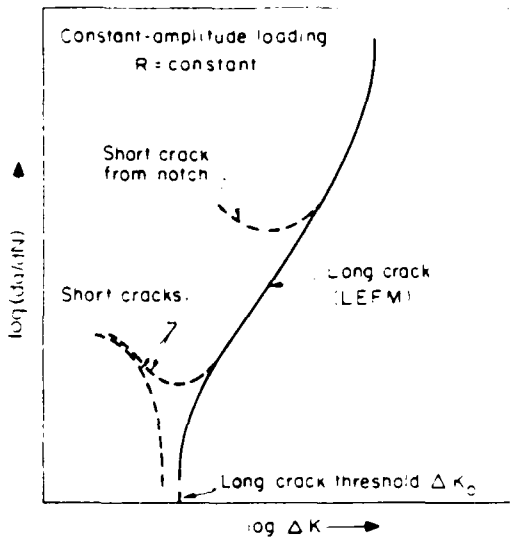

2 Typical fatigue crack propagation rates (da/dN) for long and short cracks as function of stress intensity factor range ΔK

(ii) cracks which are of a length comparable to the scale of local plasticity (e.g. small cracks embedded in the plastic zone of a notch or of a length comparable with their own crack tip plastic zones, typically $< 10^{-2}$ mm in ultrahigh strength materials and ≤ 0.1–1 mm in low strength materials)

(iii) cracks which are simply physically small (e.g. ≤ 0.5–1 mm).‡

Most investigations to date have focused on the first two factors, which represent, respectively, a continuum mechanics limitation and an LEFM limitation to current analyses. Here, presumably with an appropriate micro- or macro-mechanics characterization of crack advance, it should be possible to establish a correspondence between data for the growth rates of long and short cracks. However, physically short flaws, which are 'long' in terms of continuum mechanics and LEFM analyses, have also been shown to propagate more quickly than corresponding long cracks under the same nominal driving force (*see* e.g. Refs. 11 and 12). This may reflect basic differences in the physical micro-mechanisms associated with the extension of long and short cracks. Thus, physically short cracks represent a limitation in the similitude concept of fracture mechanics.

In this article is presented a review of the experimental results that have been obtained and of the ways in which the growth of short fatigue cracks in engineering materials has been interpreted. The literature on 'conventional' crack initiation and 'long' crack growth is examined only briefly since these are topics which have been given ample coverage in Refs. 4–7. However, a concerted effort has been made to review *all* the currently available information on short cracks. Since this is a rapidly expanding field some references may have inadvertantly been missed, and the authors regret any such omissions.

*Although often termed 'laws', such crack growth relationships are invariably totally empirical and are derived simply by fitting mathematical equations, of the form of equation (2), to sets of experimental data.

†A distinction is sometimes made between small cracks, which are small in all dimensions, and short cracks, which are small in all but one dimension (presumably the width), although such definitions are not considered in the present review.

‡Such physically small flaws are sometimes referred to as 'chemically small' where environmental effects are dominant.[11]

Situations in which short and long cracks may grow differently are discussed, from both an engineering and a mechanistic viewpoint, in terms of (i) appropriate fracture mechanics characterization and (ii) the physics and mechanisms involved in crack advance. In the former case the short crack problem is treated principally in terms of elastic–plastic fracture mechanics (EPFM) analyses in which the effects of local crack tip plasticity and the strain fields at notches are taken into account, whereas in the latter case differences in crack growth behaviour are examined in terms of the role of crack size and shape, microstructure, environment, and mechanisms for crack closure and extension. First, though, a brief summary is given of the fracture mechanics procedures used to characterize fatigue crack propagation for both long and short cracks.

FRACTURE MECHANICS CHARACTERIZATION OF FATIGUE CRACK GROWTH

Linear elastic fracture mechanics

The fracture mechanics approach to correlating cyclic crack advance begins with characterizing the local stress and deformation fields at the crack tip. This is achieved principally through asymptotic continuum mechanics analyses where the functional form of the local singular field is determined to within a scalar amplitude factor whose magnitude is calculated from a complete analysis of the applied loading and geometry. For the linear elastic behaviour of a nominally stationary crack subjected to tensile (mode I) opening, the local crack tip stresses σ_{ij} can be characterized in terms of the K_I singular field:[13,14]

$$\sigma_{ij}(r,\theta) = \frac{1}{(2\pi r)^{1/2}} K_I f_{ij}(\theta) + O(r^{1/2}) + \ldots$$

$$\lim_{r \to 0} \sigma_{ij}(r,\theta) = \frac{1}{(2\pi r)^{1/2}} K_I f_{ij}(\theta) \quad \ldots \quad (3)$$

where K_I is the mode I stress intensity factor, r the distance ahead of the tip, θ the polar angle measured from the crack plane, and f_{ij} a dimensionless function of θ. Similar expressions exist for cracks subjected to pure shear (mode II) and anti-plane strain (mode III). Provided this asymptotic field can be considered to 'dominate' the vicinity of the crack tip, over a region which is large compared to the scale of microstructural deformation and fracture events involved, the scalar amplitude factor K_I can be considered as a single, configuration independent parameter which uniquely and autonomously characterizes the local stress field ahead of a linear elastic crack and can be used as a correlator of crack extension.

For cracks subjected to cyclically varying loads, K_I must be defined at the extremes of the cycle, such that a maximum and a minimum stress intensity (K_{max} and K_{min}, respectively) for a particular crack length can be computed. According to the original analysis by Paris and Erdogan,[15] the crack growth increment per cycle in fatigue, da/dN, can be described in terms of a power law function (equation (2)) of the range of K_I, given by the stress intensity range ΔK. It is important to note here that such an asymptotic continuum mechanics characterization does not require a detailed quantitative knowledge of the microscopic behaviour of individual fracture events, and thus the analysis is independent of the specific micro-mechanism of crack advance.

One of the principal limitations of this approach, specifically of the adoption of K_I as a valid description of the crack tip field, is that a state of small scale yielding must exist. From equation (3) it is apparent that as $r \to 0$, stresses become infinite at the tip. However, in reality such stresses are limited by local crack tip yielding, which occurs over a region ahead of the crack tip known as the plastic zone. Calculations of the extent of this region vary according to the mode of applied loading and the geometry of the body,[16] but a rough estimate of the size r_y of the plastic zone ahead of a monotonically loaded crack is given by

$$r_y \approx \frac{1}{2\pi} \left(\frac{K_I}{\sigma_0} \right)^2 \quad \ldots \quad (4)$$

where σ_0 is the yield strength of the material. Provided this extent of local plasticity is small compared to the extent of the K_I-field, which is itself small compared to the overall dimensions of the body (including the crack length), the plastic zone can be considered as merely a small perturbation in the linear elastic field, and the K_I-field can be assumed to dominate the region around the crack tip. This situation, known as small scale yielding, occurs only when the size of the plastic zone is at most one-fifteenth of the in-plane dimensions of the crack length and the depth of remaining ligament.

The local yielding ahead of fatigue cracks is made somewhat more complex by reversed plasticity. However, following the analysis by Rice[17] of a cyclically stressed, elastic–perfectly plastic solid, plastic superposition of loading and unloading stress distributions can be used to compute the extent of the plastic zone ahead of a fatigue crack. On loading to K_{max}, a monotonic or maximum plastic zone is formed at the crack tip of dimension (from equation (4))

$$r_{max} \approx \frac{1}{2\pi} \left(\frac{K_{max}}{\sigma_0} \right)^2 \quad \ldots \quad (5)$$

However, on unloading from K_{max} to K_{min}, superposing an elastic unloading distribution of maximum extent $2\sigma_0$ gives rise to residual compressive stresses of magnitude σ_0 in a region ahead of the crack tip. This region is known as the cyclic plastic zone, and its size r_Δ is approximately a quarter of the size of the monotonic zone:

$$r_\Delta \approx \frac{1}{2\pi} \left(\frac{\Delta K}{2\sigma_0} \right)^2 \quad \ldots \quad (6)$$

where, strictly speaking, σ_0 is now the cyclic yield strength. Once again, the correlation of K_I with crack extension by fatigue will be a valid approach provided small scale yielding conditions apply, namely that r_{max} be small compared to the in-plane dimensions.

The numerical values of the stress intensity factors at the crack tip, K_I, ΔK, and so on, are

be determined from the asymptotic analyses, yet can be computed from the overall geometry and applied loading conditions; in fact, solutions for K_I applicable to a wide range of conditions are now tabulated in handbooks.[18–20] A useful example of such K_I solutions which is particularly relevant to the short crack problem is that of a crack (of length l) growing from a notch (of length $2c$) – *see* Fig. 3. Modelling the notch as a circular hole in an infinite plate under a remotely applied tensile stress σ^∞, the limiting analytical K_I solution for a short crack emanating from the notch is obtained as

$$K_S = 1.12 k_t \sigma^\infty (\pi l)^{1/2} \quad . \quad . \quad . \quad . \quad . \quad (7)$$

where k_t is the theoretical elastic stress concentration factor (equal to 3 here) and 1.12 is the free surface correction factor. However, when the crack becomes long the limiting stress intensity is obtained by idealizing the geometry so that the notch becomes part of a long crack of length $a = c + l$, such that

$$K_I = Q\sigma^\infty (\pi a)^{1/2} \quad . \quad . \quad . \quad . \quad . \quad (8)$$

where Q is a dimensionless function of geometry, such as a correction factor to allow for finite width. The numerically determined K_I solution for any crack emanating from a notch, shown by the dashed line in Fig. 3, can be seen to be given by the limiting cases of short and long cracks. As shown by Dowling,[21] the transitional crack size l_0, which can be interpreted as the extent of the local notch field, can then be obtained by combining equations (7) and (8) to give

$$l_0 = c/[(1.12 k_t/Q)^2 + 1] \quad . \quad . \quad . \quad (9)$$

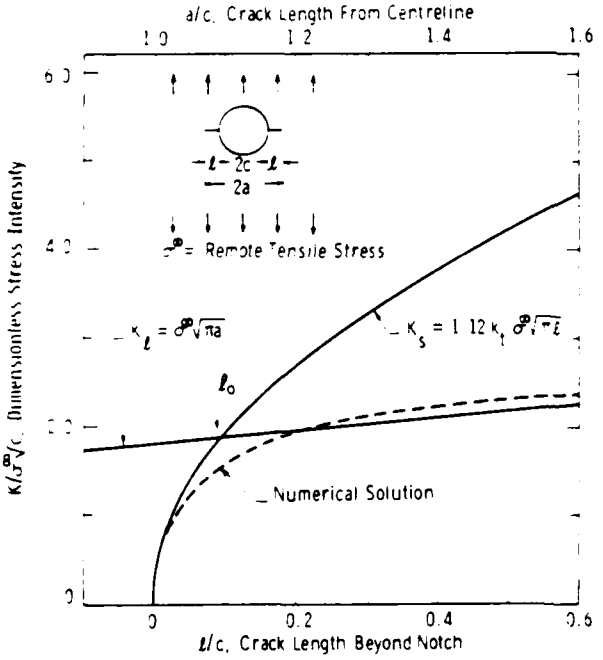

3 Linear elastic K_I solutions for crack of length l emanating from circular notch of radius c in an infinite plate subjected to remotely applied uniaxial tensile stress σ^∞; short crack (K_S) and long crack (K_I) limiting solutions and numerical solutions are shown[21]

Values of l_0 are generally a small fraction of the notch root radius ρ, and for moderate to sharp notches they generally fall in the range ρ 20 to ρ/4. Dowling[21] has further noted that $k_t\sigma^\infty$ values only 20–30% above σ_0 are sufficient to generate a notch tip plastic zone which engulfs the small crack region l_0 and thus, for small cracks at notches, LEFM analysis will often be suspect.

Elastic–plastic fracture mechanics

The above example serves to illustrate one aspect of the short crack problem, where the crack length is comparable with the size of the plastic zone around the notch tip. A similar situation, where small scale yielding conditions may not apply, is when the plastic zone at the tip of the fatigue crack itself is comparable with the crack length, i.e. when $a \sim r_y$. Since the use of K_I singular fields is no longer appropriate in such instances, alternative asymptotic analyses have been developed to define the crack tip stress and strain fields in the presence of more extensive local plasticity (for a recent review, *see* Ref. 22). Based on the deformation theory of plasticity (i.e. non-linear elasticity), the asymptotic form of these local fields for non-linear elastic power hardening solids obeying the constitutive law $\sigma \propto \epsilon_p^n$, is given by the Hutchinson Rice–Rosengren (HRR) singularity as[23,24]

$$\lim_{r\to 0} \sigma_{ij}(r, \theta) = (E' J/\sigma_0^2 r)^{n/(n+1)} \sigma_0 \tilde{f}_{ij}(\theta, n)$$
$$\lim_{r\to 0} \epsilon_{ij}(r, \theta) = (E' J/\sigma_0^2 r)^{1/(n+1)} \tilde{f}_{ij}(\theta, n) \quad (10)$$

where n is the work hardening exponent, E' the appropriate elastic modulus ($= E$ for plane stress or $E/(1-\nu^2)$ for plane strain), and $\tilde{f}_{ij}$ and $\tilde{f}_{ij}$ are universal functions of their arguments for plane stress and plane strain, respectively. The amplitude of this field is the so-called J-integral[25] and, analogous to K_I, J uniquely and autonomously characterizes the crack tip field under elastic plastic conditions, provided there is some degree of strain hardening. Furthermore, for small scale yielding J can be directly related to the strain energy release rate G, and hence to K_I, i.e.

$$J = G = K_I^2/E' \quad \text{(linear elastic)} \quad (11)$$

Despite difficulties in establishing the precise meaning of J as applied to a description of the growth of cyclically stressed (non-stationary) cracks, Dowling[26] and Dowling and Begley[27] proposed a power law correlation of fatigue crack growth rates under elastic–plastic conditions to the range of J, i.e.

$$da/dN \propto \Delta J^{m'} \quad . \quad . \quad . \quad . \quad . \quad . \quad (12)$$

Provided such analysis is fundamentally justified, the use of ΔJ does present a first approach to characterizing the growth of short cracks which are comparable in size to the extent of local yielding. However, as mentioned above, the validity of the ΔJ approach is often questioned since it appears to contradict a basic assumption in the definition of J – that stress is proportional to the current plastic strain.[25] This follows because J is defined from the deformation theory of plasticity, which does not allow for the elastic unloading and non-proportional loading effects which accompany

crack advance.[28] However, by recognizing that constitutive laws for cyclic plasticity (i.e. the cyclic stress–strain curve) can be considered in terms of stable hysteresis loops and that such loops can be mathematically shifted to a common origin after each reversal, the criterion of stress being proportional to current plastic strain can effectively be satisfied for cyclic loading.[22,29]

An alternative treatment of elastic–plastic fatigue crack growth, which is not subject to the restrictions required by non-linear elasticity, is to use the concept of crack tip opening displacement (CTOD). From equation (10) it is apparent that the opening of the crack faces as $r \to 0$ varies as $r^{n/(n+1)}$ such that this separation can be used to define the CTOD (δ_t) as the opening where 45° lines emanating back from the crack tip intercept the crack faces. Thus, for proportional loading

$$\left.\begin{aligned} \delta_t &= d(\epsilon_0, n)\, J\, \sigma_0^2 && \text{(elastic–plastic)} \\ \delta_t &= K_I^2 / \sigma_0 E' && \text{(linear elastic)} \end{aligned}\right\} \quad (13)$$

where d is a proportionality factor having a value of ~ 0.3–1 depending on the yield strain ϵ_0, the work-hardening exponent n, and whether plane stress or plane strain is assumed.[30] Since δ_t, like J, can be taken as a measure of the intensity of the elastic–plastic crack tip fields, it is feasible to correlate rates of fatigue crack growth to the range of δ_t, i.e. the cyclic CTOD $\Delta\delta_t$:

$$\left.\begin{aligned} da/dN &= \Delta\delta_t && \text{(elastic–plastic)} \\ da/dN &= \Delta K_I^2 / 2\sigma_0 E' && \text{(linear elastic)} \end{aligned}\right\} \quad (14)$$

Approaches based on J and δ_t are basically equivalent for proportional loading, and are of course valid under both elastic–plastic and linear elastic conditions. Therefore, they are generally applicable to a continuum description of the growth rate behaviour of cracks that are considered small because their size is comparable with the scale of local plasticity. For such short cracks the use of EPFM rather than LEFM may thus be expected, at least in part, to normalize differences in behaviour between long and short cracks. However, the short crack problem is not simply a breakdown in the application of LEFM since the use of elastic–plastic analyses cannot totally normalize differences between short and long cracks. Although elastic–plastic analysis is certainly important, differences in the behaviour of long and short cracks can also be attributed to microstructural, environmental, and closure effects. Thus the short crack problem relates to a breakdown, not simply in LEFM, but in the fracture mechanics similitude concept.

Similitude concept

The application of fracture mechanics to the propagation of fatigue cracks is based on the premise that the governing parameter, such as the stress intensity factor K_I or the J-integral, used to correlate growth rates fully describes the stress and deformation fields in the vicinity of the crack tip. In addition, it is implicitly assumed that the concept of similitude (*see* Fig. 4) is valid. This concept implies that, for two cracks of different sizes subjected to the same stress intensity (under small scale yielding) in a given material–microstructure–environment system, crack tip plastic zones are equal in size and the stress and strain distributions along the borders of these zones (ahead of the crack) are identical. Accordingly, equal amounts of crack extension Δa are to be expected. For a cyclic load denoted by K_{max} and K_{min}, this dictates that

$$\Delta a = da\ dN = f(K_{max}, K_{min}) = f(\Delta K, R) \quad (15)$$

for each cycle, where the stress intensity range $\Delta K = K_{max} - K_{min}$ and the load ratio $R = K_{min}/K_{max}$. However, this concept of similitude cannot be applied when

(i) crack sizes approach the local microstructural dimensions
(ii) crack sizes are comparable with the extent of local plasticity for non-stationary flaws
(iii) through thickness, out of plane stresses (which are independent of K_I) are different
(iv) crack extension mechanisms are different
(v) extensive fatigue crack closure is observed
(vi) external environments significantly influence crack growth,

to name but a few instances.[10,12,31,32] Most of these mechanisms are specific to the short crack problem and thus contribute to differences in the growth rate behaviour of long and short cracks at nominally identical driving forces. They are discussed below in terms of local plasticity, and microstructural and environmental factors. In general, however, their effect on the breakdown of the similitude concept for short cracks is that they influence (to varying degrees according to the crack length, for example) the local driving force (i.e. the characterizing parameter K_I or J effectively experienced in the region near the tip). It is this 'near tip' parameter that governs crack advance, not the 'nominal' global value of this parameter computed by conventional analyses of externally applied loads and measurements of macroscopic crack lengths. In only a few instances have the relationships between the 'near tip' and the 'nominal' driving forces been quantified, indicating that the methodology for a global fracture mechanics analysis of short crack growth has yet to be developed.

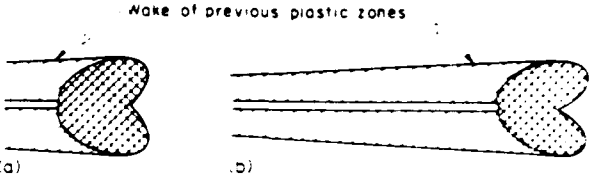

a short crack, $a \sim r_y$; *b* long crack, $a \gg r_y$

4 Schematic representation of similitude concept, which implies that cracks of differing length *a* subjected to same nominal driving force, e.g. ΔK, have equal plastic zone sizes r_y ahead of crack and will therefore advance by equal increments Δa per cycle

EXPERIMENTAL TECHNIQUES

In the experimental measurement of the propagation and threshold behaviour of small fatigue cracks, many complex problems associated with

reproducibility and scatter can be encountered. This is particularly true since most of the approaches used so far have involved adapting procedures originally designed for measuring long cracks.

Several experimental techniques are available for monitoring the growth rates of long fatigue cracks (*see* e.g. Refs. 33–35), including

(i) optical techniques (i.e. with the naked eye or travelling microscopes, or using high speed cameras)
(ii) methods based on measuring electrical resistance or potential using either dc or ac currents
(iii) compliance techniques using mouth opening (clip) or back-face strain gauges
(iv) acoustic emission
(v) ultrasonics
(vi) eddy current methods,

the first three being the most widely used. For long cracks, growth rates above 10^{-6} mm/cycle are generally measured by utilizing using such techniques at constant cyclic load levels (i.e. increasing ΔK with increasing crack length).[34] At levels near the threshold, on the other hand, crack growth rates ($da/dN \lesssim 10^{-6}$ mm cycle) and threshold ΔK_0 values for long cracks are normally measured using the so-called 'load shedding' (decreasing ΔK) method (*see* e.g. Ref. 6). This procedure involves making continual reductions in ΔK (starting from an intermediate value) of not more than 10%. At each ΔK level, the crack is then allowed to propagate over a distance at least four times the size of the maximum plastic zone generated at the previous higher ΔK level. This load reduction scheme is repeated until the threshold ΔK_0 for no detectable (long) crack advance is reached. Such procedures,[6] typically used to monitor the growth and arrest of long fatigue cracks, pose extreme difficulties when adopted for measuring short cracks. Firstly, one faces the problem of estimating the depth of a short crack, emanating from a surface, from its width. This requires an empirical calibration and/or an educated guess. Also, with load shedding procedures used near the threshold, the crack is continually growing and so may cease to be 'short' by the time the threshold is reached. Moreover, the initiation stage of a 'major' short crack may involve the linking up of several flaws (e.g. from cracked inclusions) at different locations. While low magnification optical techniques are not particularly suited to detecting the presence and monitoring the growth of short cracks during a fatigue test, other methods such as the potential, resistance, or compliance teachniques may not have the required resolution and reproducbility to enable the growth of (part through) short cracks of complex geometry to be characterized. In addition to the difficulties associated with the limitations of the crack monitoring device, the growth of a short crack can be a strong function of local microstructural characteristics and environment (*see* e.g. Refs. 7–12). This aspect of short crack advance can also lead to poor reproducibility.

Since load shedding procedures are often difficult to apply, there is always the question of whether short crack behaviour should be studied using an artificial or a natural crack. It is particularly difficult to create an artificial notch without damaging the material immediately ahead of it, yet this is essential since it is this region in which short crack growth must be studied. The areas around machined notches contain residual stresses, whereas notches or starter cracks introduced by electro-discharge machining have a locally melted zone at their tip. Subsequent annealing cannot be guaranteed to remove such damage without drastically changing the microstructure under test. As discussed below, there are procedures in which a long crack is grown and material in its wake is then machined off to leave a short crack. Reproducibility is a major problem here, as is crack shape, since any amount of non-uniformity or 'bowing' in the original long crack will introduce irregular short cracks. However, one very successful method for rapidly initiating short cracks without causing significant damage, but only for aluminium alloys, has been to embrittle the sample surface before fatigue using small drops of ink at well separated locations.[36] Although the precise mechanism (involving some environmentally influenced fatigue process) is unknown, short cracks have been found to initiate extremely rapidly.

Initiation and growth measurements of short cracks

Optical techniques

Crack monitoring techniques using visual methods have probably been the most widely used procedures to date. For example, using procedures first adopted by Barsom and McNicol[37] for studying crack initiation, Fine and co-workers[38,39] have used a metallurgical microscope with a long working distance for visual and photographic observations of crack initiation and microcrack growth in wide, single edge notch (SEN) samples of steels and aluminium alloys. The microscope was mounted on an x–y micrometer base for positioning and measuring crack length. A camera attachment was available for photographically recording the progressive changes in the surface of specimens subjected to cyclic loading.

Morris and co-workers[40–49] used tapered flexural and hourglass shaped fatigue samples to monitor microcracks in aluminium and titanium alloys. Cracks were initiated on the surface of the specimen using various techniques, including making starter notches and marking with felt-tip pens. Crack propagation rates were estimated by monitoring crack size at regular intervals by transferring the specimen to a scanning electron microscope (SEM). The specimens were loaded in the SEM to estimate the microcrack tip opening displacement at the maximum load. For example, an empirical calibration equation was obtained for 2219 T851 aluminium alloy from several measurements of surface microcracks to estimate their depth a from a knowledge of their width $2c$. The expression

$$a/2c = 0.362 + 25.01(\delta(\sigma_{max})/2c - 0.015) \quad (6)$$

was obtained,[47] where $\delta(\sigma_{max})$ is the CTOD at the maximum stress, σ_{max}.

Optical techniques have also been used to study short cracks at elevated temperatures. For example, Sheldon *et al.*[50] designed a microscope with a long working distance to monitor *in situ* the growth of short and long cracks in nickel-base superalloys at temperatures as high as 650°C. Cracks were initiated at high stress intensities at ambient temperature, whereupon the load was successively reduced until the approximate room temperature long crack threshold values were reached. Once load shedding was complete, the specimen was machined and polished to a configuration such that a crack only 0.06–0.16 mm long was left in the test panel. The cross-section of the specimen was a parallelogram containing the crack at one acute corner. Sheldon *et al.* claimed that the taper allows the location of the crack front to be defined more accurately, and that the crack in the taper interacted with only a small amount of material along its front. This was considered to be representative of a naturally occurring small crack.

Replication techniques

One of the most widely used techniques for monitoring the initiation and growth of small flaws has been the replication method. For example, Dowling[51,52] used cellulose acetate surface replicas for measuring the growth of short cracks during low cycle fatigue tests on smooth axial specimens of A533B steel. Tests were interrupted periodically for replicating with ~0.1 mm tape, softened with acetone to gain an impression of the specimen surface. The propagation rates of such surface flaws (of length 0.25–1.75 mm) were characterized in terms of EPFM, specifically involving ΔJ. Procedures for calculating J from the loading portion of the fatigue cycle, summarized in Fig. 5, involve the following approximations:[51]

(i) surface cracks were assumed to have depth a equal to half their surface length $2c$

(ii) ranges of stress and plastic strain, obtained from stable cyclic hysteresis loops, were used to quantify ΔJ

(iii) the value of ΔJ for such semicircular surface crack geometries was given by:

$$\Delta J \simeq 3.2\Delta W'_e a + 5.0\Delta W'_p a \quad . \quad . \quad 17$$

where ΔW_e and ΔW_p are the elastic and plastic components of the remote strain energy density ranges (*see* Fig. 5)

(iv) the scaling constants in equation (17), which incorporate correction factors for specimen geometry and flaw shape, were derived from equivalent linear elastic solutions.

In the general sense, there are problems with using either optical or replication techniques in that they are difficult to apply in hostile environments, such as in corrosive solutions or at elevated temperatures. More importantly, they give information only on the surface length of the crack, and therefore assumptions must be made if the internal profile is to be estimated.

Electrical potential techniques

Electrical potential techniques have also been developed for studying short cracks. Gangloff, for example, quantified the formation and subcritical propagation of small cracks emanating from artificial surface defects.[11,53,54] Flaws were introduced along a chord of an hourglass type (low cycle fatigue) specimen (at the minimum diameter) by either conventional grinding or electrospark discharge machining. The crack depth was continuously monitored via dc electrical potential measurements and an analytical calibration model,[53] and was found to agree reasonably well with the corresponding values measured optically. The calibration model used was claimed to account for crack shape as well as variations in depth for the elliptical surface flaws utilized in the experiments. This technique is particularly suitable

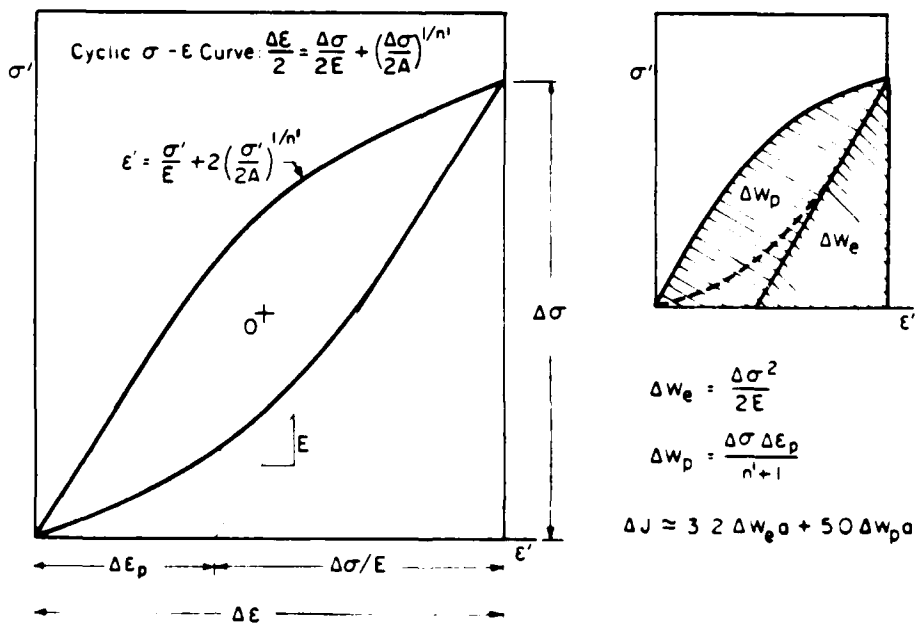

5 Procedure for estimating ΔJ from stress–strain hysteresis loops for growth of small cracks during low cycle fatigue of smooth axial specimens[51]

for physically short cracks, i.e. those 0.5–1 mm long, and so has been effective in gaining information on the growth of short fatigue cracks in higher strength materials. Furthermore, since it is a remote monitoring technique it can be applied even in aggressive environments.

Other techniques

Several other techniques have been proposed for the detection and monitoring of small flaws, and many, although still in the development stage, show excellent promise for obtaining measurements in the micrometre–millimetre range. For example, Nelson and co-workers[55] have utilized a method of monitoring surface acoustic waves to quantify the depth and crack closure characteristics of microscopic surface fatigue cracks. Using acoustic measurements of the reflection coefficient of Rayleigh waves incident on the crack, coupled with optical measurements of surface crack length, these authors were able to claim good accuracy over a range of crack aspect ratios for depths between 50 and 150 μm (Ref. 55). Several electrochemical methods have also been proposed for the early detection of microscopic fatigue damage, notably by Baxter.[56] Accuracies of ±10 μm have been reported for the detection of small fatigue cracks in both steels and aluminium alloys through the identification of locations where such cracks rupture the surface oxide film. Such rupture sites are imaged using photoelectron microscopy and, more recently, by measuring the re-anodization current or with the aid of a gel containing iodine.[56]

Measurements of short crack thresholds

The load shedding procedure commonly used to obtain the threshold ΔK_0 for no detectable propagation of long cracks is not readily applicable to short cracks (those of a size smaller than the local plastic zone or the characteristic microstructural dimension) because of the need to reduce the load to threshold levels over a considerable distance of crack growth. However, the procedure can be used for physically short (0.1–0.8 mm) cracks in ultrahigh strength materials where both the scale of local plasticity and the grain size are smaller than the crack depth, and load shedding procedures can be sufficiently rapid to enable the near-threshold region to be approached over small increments of crack advance (*see* e.g. Ref. 57).

Wiltshire and Knott[58] used two different methods to obtain short 'through-thickness' and 'thumbnail' cracks in a study of the effect of crack length on fracture toughness. Such procedures seem suitable for use in evaluating growth and thresholds for short cracks. For through-thickness cracks in maraging steels a long crack was first produced by fatiguing SEN specimens in bending, as shown in Fig. 6*a*, with the sample in the solution annealed condition. Short through-thickness cracks were then obtained by grinding away the upper surface, and the samples were subsequently aged to develop full strength. Similar procedures were used to produce short 'thumbnail' cracks, as shown in Fig. 6*b*. The two top edges of a bend specimen were machined away to leave a ridge along the centre, a slot was introduced in the ridge, and the specimen was fatigue precracked in bending. The

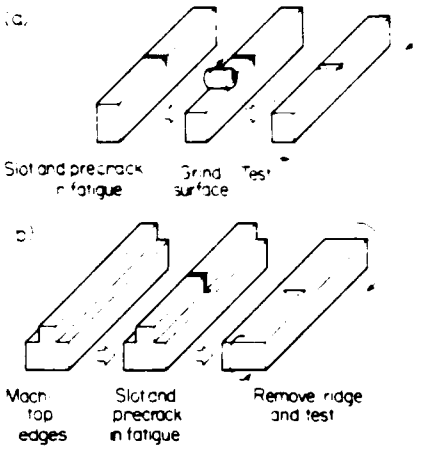

a through thickness crack; *b* thumbnail crack

6 Ways of preparing short cracks[58]

fatigue crack was found to propagate down the ridge as a straight fronted crack, and then into the bulk of the specimen with a semi-elliptical crack front. Its depth was controlled by stopping the bending after it had spread a certain distance across the prepolished shoulders. Finally, the ridge was removed to leave a semi-elliptical surface crack in the remaining rectangular section.

Such procedures have been used to produce through-thickness and part-through-thickness short cracks to measure the thresholds for the arrest of short cracks.[59–62] Usami and Shida,[59] for example, used this technique to measure fatigue thresholds in a range of steels for crack sizes between 0.1 and 0.3 mm. McCarver and Ritchie[60] used similar procedures to monitor the thresholds for physically short cracks in a wrought nickel-base superalloy, René 95. In both these investigations fatigue precracking was performed under a far-field cyclic compressive load on bend specimens. This results in growth and arrest of the precrack to a predictable depth which is a function of the size of the plastic zone as computed from the compressive loads. Such compression gives rise to residual tensile stresses which apparently act as the driving force for crack growth.* Following precracking and machining away of most of the crack, the samples were annealed in an attempt to minimize possible damage in the vicinity of the short crack tip. McCarver and Ritchie[60] subsequently measured short crack thresholds in such specimens, using a procedure analogous to defining a fatigue limit in unnotched specimens. Samples were cycled at different initial stress intensity ranges ΔK_i, and the short crack threshold defined in terms of the largest value of ΔK_i which did not cause failure for any

*Recent studies by Suresh[63] on crack initiation under compression in a wide range of alloys have revealed that cracks arrest at a length approximately equal to the cyclic plastic zone size in compression. However, at high cyclic compressive loads it was found that crack arrest can occur at critical lengths independent of applied load, apparently as a result of the development of closure behind the crack tip.

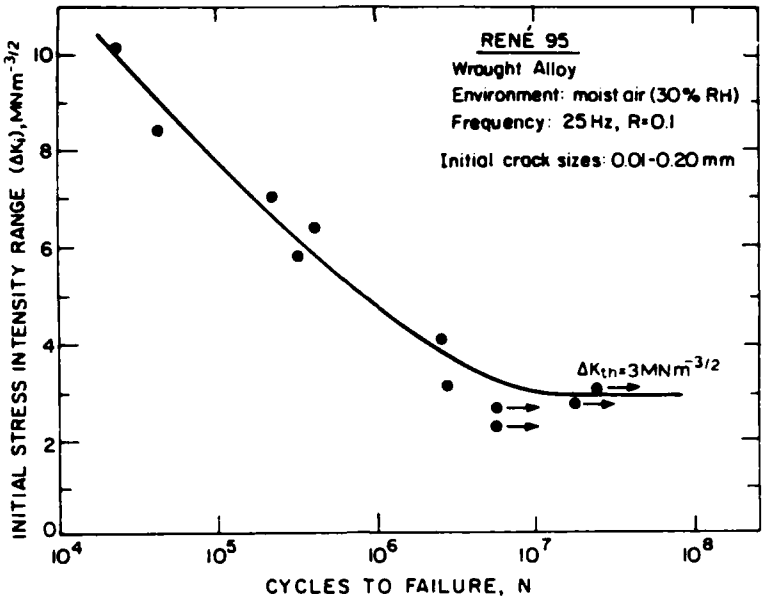

7 **Variation of initial stress intensity ΔK_i with number N of cycles to failure for physically short cracks in wrought René 95 (σ_0 = 1400 MNm^{-2}), showing definition of threshold ΔK_{th} for 0.01–0.2 mm cracks, fatigue tested in moist air at 25 Hz and R = 0.1 (Ref. 60)**

evidence of crack growth) in 10^8 cycles (*see* Fig. 7).

Measurement of closure of short cracks

The techniques available for routine monitoring of the premature closure of long fatigue cracks generally cannot be used for short cracks (whose growth involves considerable geometrical changes, and whose measurement suffers from irreproducibility and scatter) which demand far superior resolution in measurements. Closure in long fatigue cracks has been measured using optical techniques, compliance techniques, methods involving electrical resistance or potential, acoustic emission, and ultrasonics (*see* e.g. Refs. 33 and 34). Most of these techniques do not seem suitable for use with short cracks because of their insufficient resolution, insensitivity to short crack shape and geometry, and irreproducibility.

Early studies of crack closure for short cracks were carried out by Morris and Buck,[41] who used a compliance technique to determine the closure load for surface microcracks of up to one grain size produced in triangular specimens of aluminium alloys subjected to fully reversed loading. Scanning electron microscopy was then used to measure the compliance of surface microcracks. A 'home-made' fixture incorporated in the electron microscope was utilized to apply known loads to the samples *in situ*. High resolution micrographs of the crack were obtained at different load (stress) levels, from which the crack opening δ was estimated. Figure 8 shows a typical compliance curve for a microcrack obtained for 2219 T851 aluminium alloy. Morris and Buck defined the following parameters to characterize crack closure: $\delta(0)$, the crack opening displacement at zero load, σ_{cl}/σ_{max}, the closure stress ratio (taken to be the value of σ/σ_{max} at the inflection point in the stress–displacement curve), and $S = \Delta\delta/\Delta(\sigma/\sigma_{max})$ measured for $\sigma > \sigma_{cl}$, where S is a measure of the compliance of the microcrack in the completely opened state.

Compliance techniques were also used by Tanaka and Nakai[61,64] for measuring crack closure levels to examine the growth of short cracks emanating from notched centre-cracked specimens of a structural low carbon steel. Here, the hysteresis loop of load v. CTOD at the centre of the crack was recorded intermittently during the test, and the point of crack opening was determined as the inflection point of compliance,

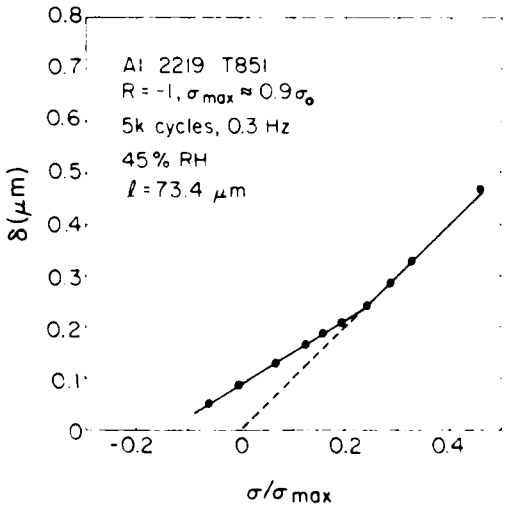

8 **Typical microcrack compliance curve for 2219 T851 aluminium alloy; δ is opening across microcrack, and σ/σ_{max} fraction of maximum load applied during fatigue[41]**

9 Appearance of typical surface microcrack initiated at β-phase (Cu_2FeAl_7) intermetallic in 2219 T851 aluminium alloy fatigue tested in humid air[45]

magnified by a circuit subtracting the elastic compliance from the loading curve.

Recently, procedures have been developed to monitor the behaviour of short fatigue cracks, using stereo-imaging techniques and *in situ* analyses in the SEM.[65,66] Such methods enable the crack opening (mode I) and sliding (mode II) displacements to be measured directly as functions of load for both short and long cracks subjected to cyclic loads within the electron microscope.

RESULTS ON GROWTH OF SHORT FATIGUE CRACKS

Microstructural effects

The first definition of a short fatigue crack (*see* the introductory section) refers to cracks which are of a size comparable to the scale of characteristic microstructural features. Figure 9 shows a micrograph of such a typical surface microcrack initiated at a β-phase (Cu_2FeAl_7) intermetallic in 2219 T851 aluminium alloy, taken from work by Morris.[15] A number of recent experimental studies[7–12,37–49,67–76] on the initiation and growth of cracks in a wide range of materials have revealed that such short cracks, initiated near regions of surface roughening caused by the to and fro motion of dislocations or at inclusions and grain boundaries, propagate at rates which are different from those of equivalent long cracks when characterized in terms of conventional fracture mechanics concepts. For example, it was first shown by Pearson[68] that in precipitation hardened aluminium alloys, cracks of a size comparable to the average grain diameter grew several times as quickly as long cracks at nominally identical alternating stress intensities (Fig. 10). Other studies of mild steels[69] (Fig. 11), silicon iron[70] (Fig. 12) and peak aged 7075 aluminium alloy[71] (Fig. 13), for example, clearly reveal this lack of correspondence between data for long and for microscopically short cracks. However, the results obtained by Lankford[71,72] and

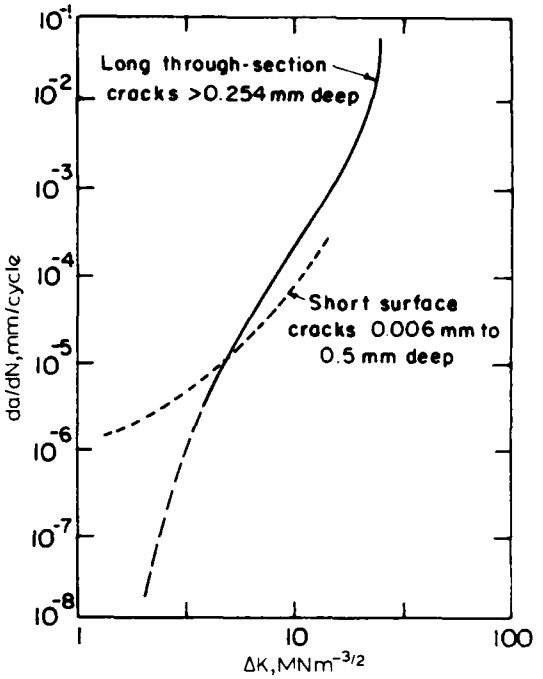

10 Difference in propagation rates da/dN of fatigue cracks as function of stress intensity factor range ΔK for precipitation hardened aluminium alloys[68]

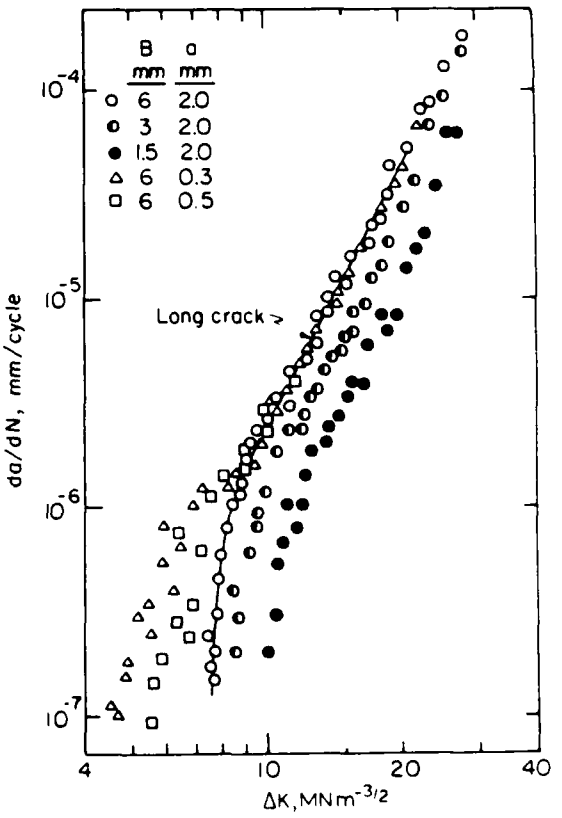

11 Difference in propagation rates da/dN of short and long fatigue cracks as function of stress intensity factor range ΔK for 0.035%C mild steel of yield strength σ_0 = 242 MNm^{-2}

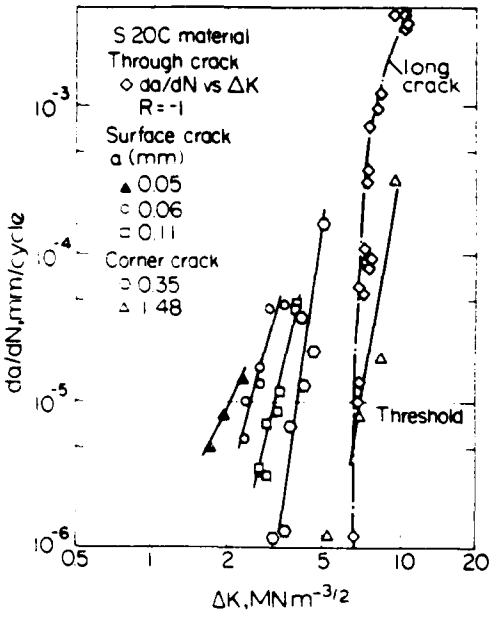

12 Difference in propagation rates da/dN of short and long fatigue cracks as function of stress intensity factor range ΔK for 3%Si iron of yield strength σ_0 = 431 MNm^{-2} (Ref. 70)

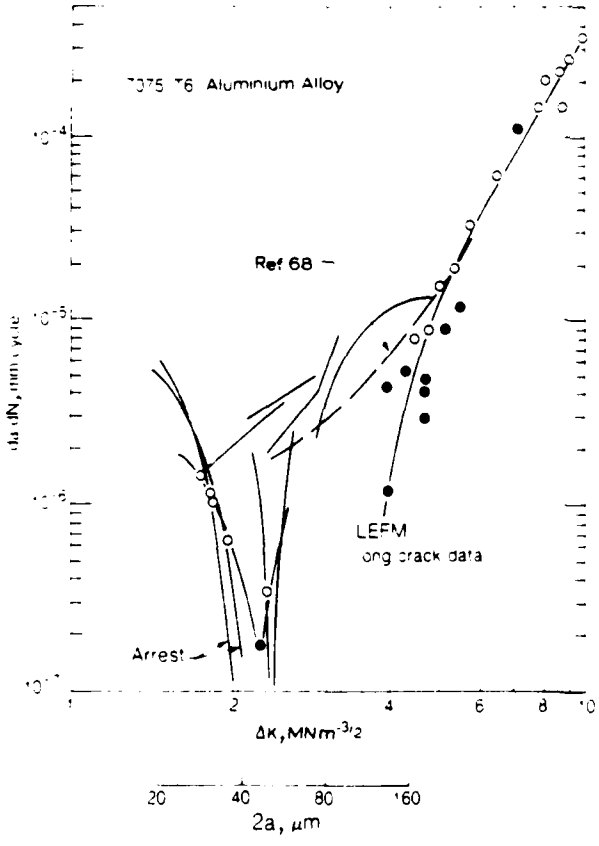

13 Difference in propagation rates da/dN of short and long fatigue cracks as function of stress intensity factor range ΔK for peak aged Al–Zn–Mg alloy (7075 T6) of yield strength σ_0 = 515 MNm^{-2} (Ref. 71)

others[39,49,69,70,73,74] have shown that there is generally a consistent trend to this variation between growth rates for long and short cracks. This trend is depicted clearly in Fig. 14 for 7075 T6 aluminium alloy, in which growth rates for long and for microscopically short (i.e. of a size comparable with the grain diameter) cracks are plotted as a function of the linear elastic stress intensity range.[71] It is apparent from this figure that the growth rates associated with the short cracks are up to two orders of magnitude faster than those of the long cracks, and further that such accelerated short crack advance occurs at stress intensity ranges well below the long crack fatigue threshold stress intensity range (ΔK_0).[71] The initially higher growth rates of the short cracks can be seen to decelerate progressively (and even arrest in certain cases) before merging with the long crack data at stress intensities close to ΔK_0, similar to observations reported elsewhere by Morris and co-workers,[42–46] Kung and Fine,[39] Tanaka and co-workers,[70,75,76] Taylor and Knott,[73] and others. The progressively decreasing growth rates of the short cracks below the long crack threshold is intriguing since in terms of conventional analyses one would imagine the nominal driving force for crack advance (e.g. ΔK) to increase with increasing crack length (e.g. as given by equations (7) and (8)), thereby leading to progressively increasing growth rates. However, the behaviour of microscopically short cracks has been rationalized in terms of a deceleration of growth as a result of crack closure and through interactions with microstructural features – particularly grain boundaries.[12,42–47,69–76] For example, specific observations of grain boundaries impeding the growth of short cracks have been reported for aluminium alloys,[42–46,71,72] nickel-base superalloys,[50] tempered martensitic high strength steels,[77,78] and lower strength mild steels.[75,76] Using arguments based on microplasticity and crack closure effects, Morris and

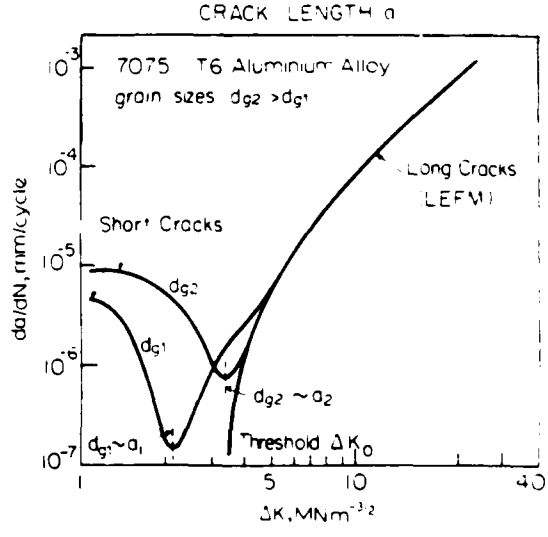

14 Effect of grain size d_g on growth of microstructurally short and long cracks in 7075 T6 aluminium alloy σ_0 = 515 MNm^{-2}; microcracks grow below long crack threshold ΔK_0 and show growth rate minima approximately where crack length $a \sim d_g$ (Ref. 71)

co-workers[44-49] have modelled the process in terms of two factors: the cessation of propagation into a neighbouring grain until a sizeable plastic zone is established, and a retardation in growth rates caused by an elevated crack closure stress. Tanaka and co-workers[76,79,80] similarly considered the impeded growth of microstructurally short cracks in terms of the pinning of slip bands, emanating from the crack tip, by the next grain boundary. The results obtained by Lankford[71] and shown in Fig. 14 indicate that the minimum crack growth rate appears to correspond to a crack length roughly equal to the smallest grain dimension (i.e. $a \sim d_g$). Furthermore, the depth of the deceleration 'well' appears to be determined by the degree of microplasticity involved in the crack traversing the boundary. For example, when the orientation between the grain containing the crack and the neighbouring grain was similar, there was little deceleration in growth rates at the boundary. Thus a consensus from these studies is that, despite their propagating faster than long cracks,

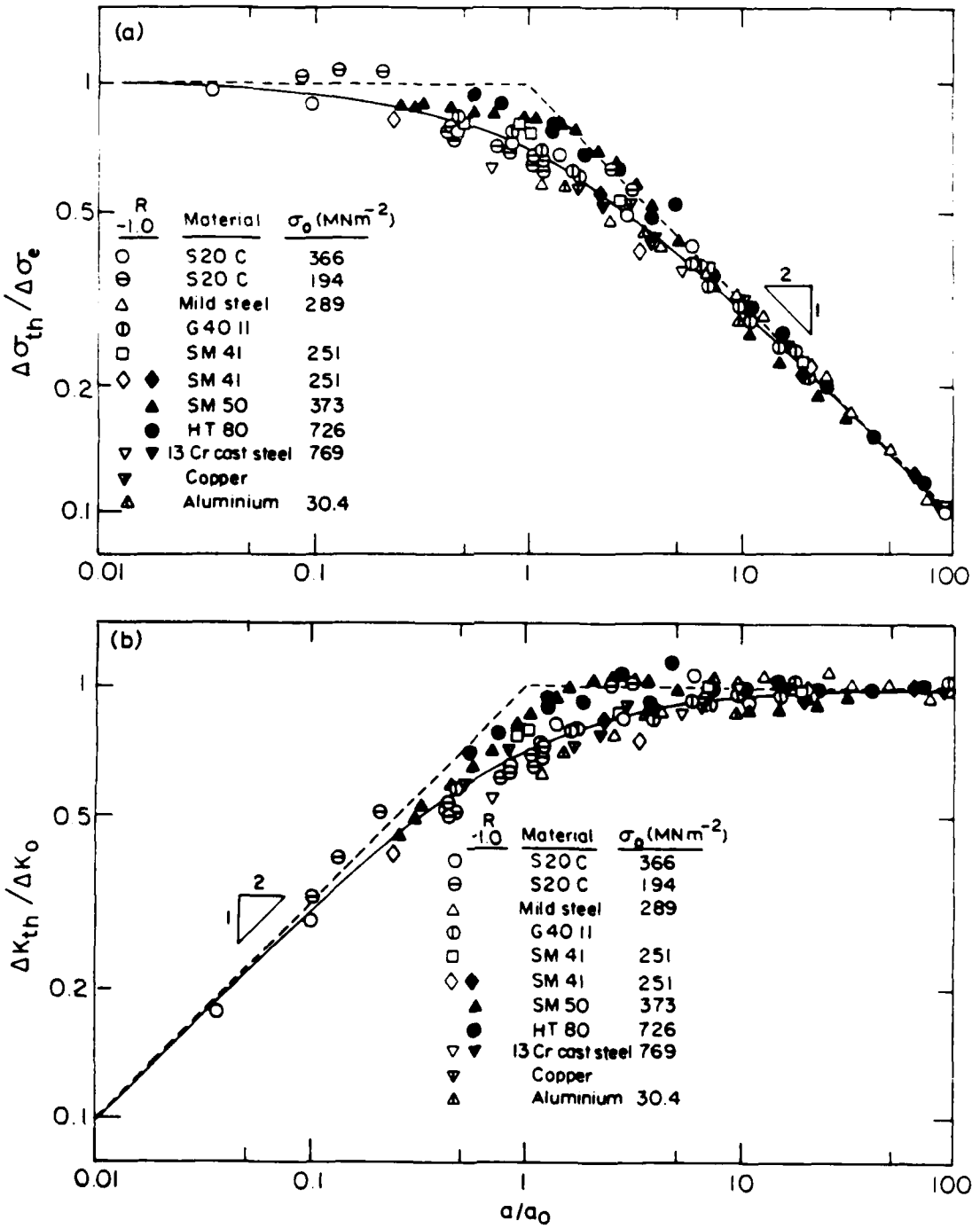

a threshold stress $\Delta\sigma_{th}$, normalized with respect to smooth bar fatigue limit $\Delta\sigma_e$; *b* threshold stress intensity range ΔK_{th}, normalized with respect to long crack threshold ΔK_0

15 **Variation of threshold stress and stress intensity with crack length *a*, normalized with respect to intrinsic crack length $a_0 = (1/\pi)(\Delta K_0/\Delta\sigma_e)^2$ (Ref. 76)**

short cracks are apparently impeded by the presence of grain boundaries, which in general would be unlikely to affect significantly the local propagation rates of long cracks. The extent of reductions in the effective driving force for various degrees of such short crack deflections at grain boundaries has recently been calculated by Suresh.[81] It is the present authors' opinion that the interaction of short cracks with microstructural features, which leads to the apparent progressive deceleration of short cracks below the value of ΔK_0 for long cracks, results principally from crack deflection[81] and associated crack closure[12,61] mechanisms. The specific evidence for this is examined in the 'Discussion' section below.

From such experimental studies, it is readily apparent that threshold stresses (or stress intensities) associated with long and short cracks are likely to be very different. Conventional fracture mechanics arguments imply that the threshold stress intensity range (ΔK_{th}) for a particular material should be independent of crack length (i.e. $\Delta K_{th} = \Delta K_0$, the long crack threshold, is constant). Kitagawa and Takahashi,[82] however, first showed that below a critical crack size the threshold ΔK_{th} for short cracks actually decreased with decreasing crack length, where the threshold stress $\Delta\sigma_{th}$ approached that of the smooth bar fatigue limit $\Delta\sigma_e$ at very short crack lengths (*see* e.g. Fig. 15). Typical experimental data showing this decay in the threshold stress intensity range ΔK_{th} at short crack lengths are shown in Fig. 16, taken from the results obtained by Romaniv *et al.*[69] for annealed mild steel, 0.45%C austenitic steel, and an Al–Zn–Mg alloy. Several workers have claimed that the critical crack size (below which ΔK_{th} is no longer constant with crack size depends on microstructural and mechanical factors.[8–10,12,47,64,69–76,80–83] It has even been suggested, for example, that this critical crack length above which LEFM is applicable is simply ten times the characteristic microstructural dimension.[83] However, from continuum mechanics arguments, an estimate of this crack size can be obtained in terms of $(1/\pi)(\Delta K_0/\Delta\sigma_e)^2$, with both ΔK_0 and $\Delta\sigma_e$ corrected for a common load ratio. Typical values of this dimension, which effectively represent the limiting crack size for valid LEFM analysis (*see* the section 'Fracture mechanics characterization of fatigue crack growth' above), vary from 1–10 μm in ultrahigh strength materials (i.e. $\sigma_0 \sim 2000$ MNm^{-2}) to 0.1–1 mm in low strength materials (i.e. $\sigma_0 \sim 200$ MNm^{-2}).[1–5]

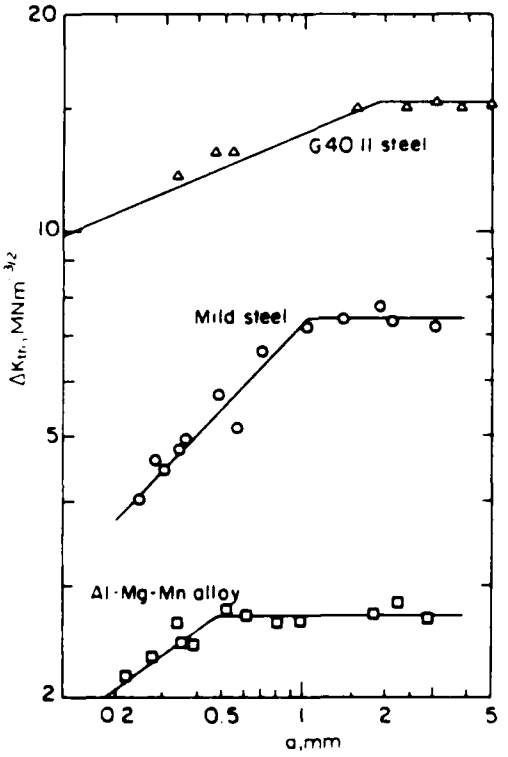

16 Variation of threshold stress intensity range ΔK_{th} with short crack length a in G40.11 austenitic 0.45%C steel, σ_0 = 550 MNm^{-2}, 0.035%C mild steel, σ_0 = 242 MNm^{-2}, and Al–Zn–Mg alloy, σ_0 = 180 MNm^{-2} (Ref. 69)

From such experimental results it is generally concluded that the threshold condition for no growth for long cracks is one of a constant stress intensity, i.e. ΔK_0, whereas the threshold condition for short cracks is one of a constant stress, i.e. the fatigue limit $\Delta\sigma_e$ or the endurance strength. Such a premise has been shown to be consistent with the models derived by Tanaka *et al.*[76] in which the threshold for short crack propagation is governed by whether the crack tip slip bands are blocked, or can traverse the grain boundary to an adjacent grain. This condition governing whether the slip band is blocked, shown in Fig. 17 in terms of a critical value of the microscopic stress intensity K_c^m at the tip of the band, yields expressions for the fatigue threshold stress σ_{th} and stress intensity K_{th}:

$$\sigma_{th} = \frac{K_c^m}{(\pi b)^{1/2}} + \frac{2}{\pi}\sigma_{fr}^* \cos^{-1}(a/b) \quad . \quad . \quad (18)$$

$$K_{th} = \sigma_{th}(\pi a)^{1/2} = K_c^m(a/b)^{1/2} + 2(a/\pi)^{1/2}\sigma_{fr}^* \cos^{-1}(a/b) \quad . \quad . \quad (19)$$

Here, for a slip band coplanar to the crack plane in the two dimensional model shown in Fig. 17, b is the crack length a plus the width a_0 of the blocked slip band zone, and σ_{fr}^* is the frictional

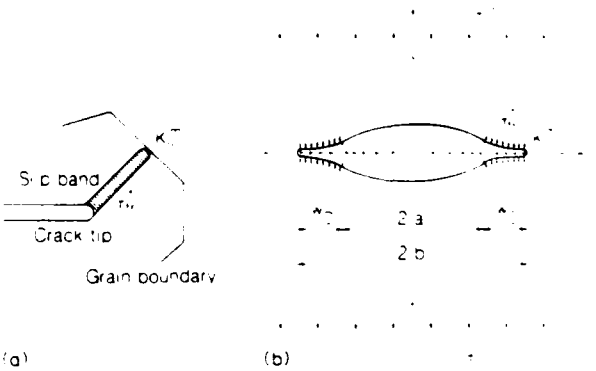

17 Schematic illustration of a crack tip slip band blocked by grain boundary and b coplanar slip band emanating from tip of isolated crack[76]

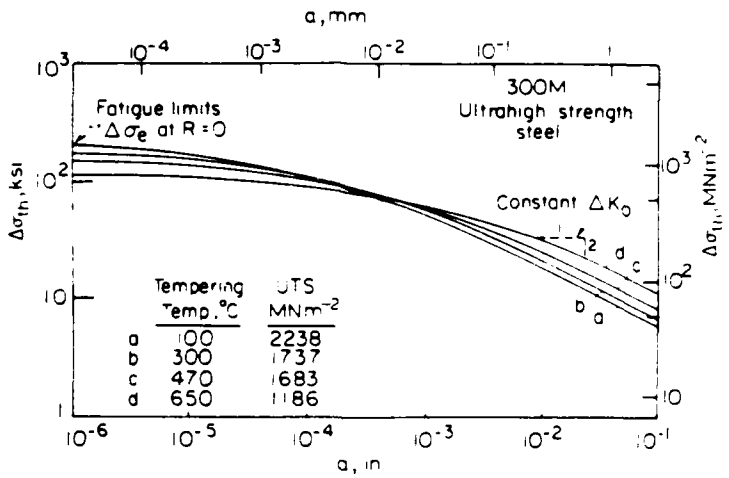

18 Predicted variation of threshold stress $\Delta\sigma_{th}$ at $R = 0$ with crack length a based on data for 300M ultrahigh strength steel (silicon modified AISI 4340), oil quenched and tempered between 100 and 650°C to vary tensile strength (1186 to 2338 MNm^{-2}) (Ref. 6)

stress for dislocation motion in the band. The long crack threshold stress intensity K_0 thus follows from equation (19) by taking the limit of K_{th} when $a_0' \ll a$, i.e.

$$K_0 = K_c^m + 2(2\tau)^{1/2}\sigma_{fr}^* a_0^{1/2} \quad . \quad . \quad . \quad (20)$$

whereas the short crack threshold stress, i.e. the fatigue limit σ_e, follows from equation (18) at $a = 0$, i.e.

$$\sigma_e = \sigma_{fr}^* + K_c^m/(\pi a_0)^{1/2} \quad . \quad . \quad . \quad . \quad (21)$$

Since, at the fatigue limit, the slip band can be considered to be constrained within a single grain, a_0 can be assumed to be approximately half the grain size d_g. The interesting aspect of the blocked slip band model is the prediction (from equations (20) and (21)) that the long crack threshold K_0 increases with grain size, whereas the short crack threshold, or fatigue limit σ_e, decreases.[76] Such predictions are borne out by experiment and highlight the fact that metallurgical factors which may improve resistance to the growth of long cracks (i.e. raise ΔK_0) may simultaneously lower resistance to the initiation and growth of small cracks (i.e. lower $\Delta\sigma_e$).[77] This effect is particularly pronounced in ferrous alloys: as shown in Fig. 18, increasing the tempering temperature to decrease strength level in an ultrahigh strength, silicon modified 4340 steel (300M) lowers the long crack threshold ΔK_0, yet raises the fatigue limit $\Delta\sigma_e$ (Ref. 6). A second example, shown in Fig. 19, is from the work of Usami and Shida,[59] who compared the threshold behaviour as a function of surface roughness (to simulate crack size) of a cast iron (σ_0 = 113 MNm^{-2}) and a maraging steel (σ_0 = 1906 MNm^{-2}). It is quite clear from this work[59] that the maraging steel, while of substantially higher strength and having a far superior fatigue resistance at short crack sizes (below 0.1–1 mm), is actually inferior to cast iron from the viewpoint of long crack threshold behaviour.

Local plasticity effects

The second definition of a short crack (see the introductory section) refers to cracks which are of a size comparable to the scale of local plasticity, such as the crack tip plastic zone

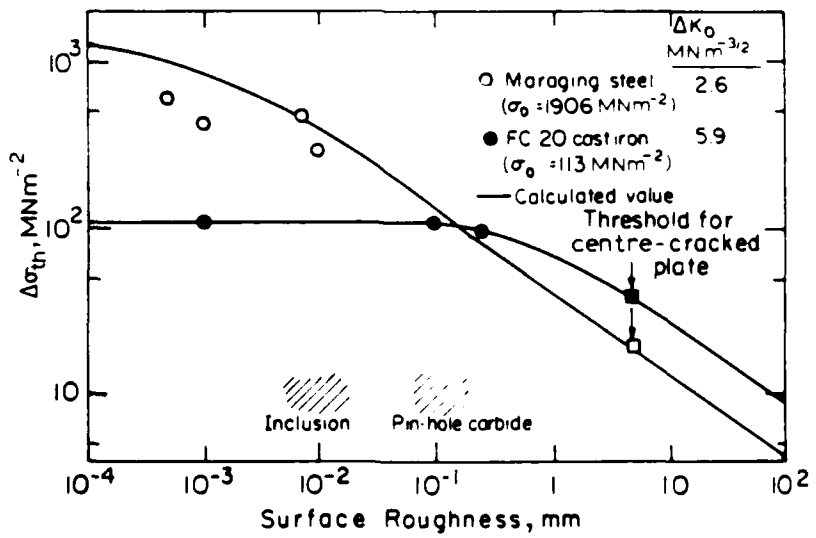

19 Comparison of threshold behaviour of cast iron, σ_0 = 113 MNm^{-2}, and maraging steel, σ_0 = 1906 MNm^{-2}, as function of surface roughness (to simulate crack size)[59]

generated by the crack itself (near-tip plasticity), or the strain field of a notch or a larger stress concentration which may encompass the crack in the vicinity of the notch (notch field plasticity). Each of these two local plasticity effects is examined below.

Near-tip plasticity effects

While elastic–plastic fracture mechanics analyses seem more suited to the characterization of short cracks comparable in size to the extent of self-induced near-tip plasticity, a comparison of their behaviour with equivalent long cracks using LEFM analyses (i.e. at the same nominal value of ΔK) shows that the short cracks grow much more quickly.[8–10,12,17,84] Part of the reason for such apparently anomalous results lies not in any physical difference between the behaviour of long and short cracks, but with the inappropriate use of LEFM analyses. This was shown particularly clearly by Dowling,[51] who monitored the growth of small surface cracks in smooth bar specimens of A533B nuclear pressure vessel steel subjected to fully reversed strain cycling. By analysing the growth rates da/dN in terms of ΔJ, using values of J computed from the stress–strain hysteresis loops (described by equation (17) and shown in Fig. 5), there was found a closer correspondence between the behaviour of long and short cracks (Fig. 20). Analogous approaches to the short crack problem have been suggested in terms of ΔK_ϵ, the pseudo-elastic–plastic strain intensity range,[85–87] or ΔK_{eq}, the equivalent stress intensity range.[87]

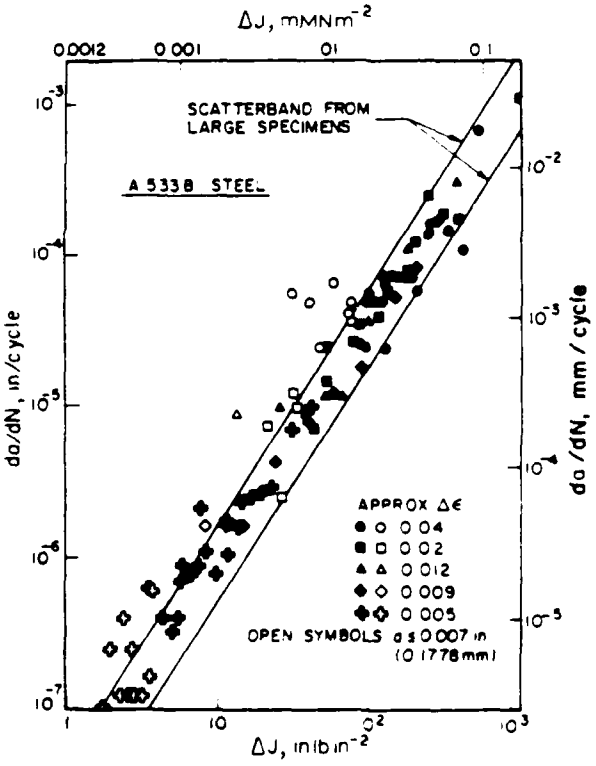

20 Variation of fatigue crack growth rates da/dN for long ($a \gtrsim 25$ mm) and short ($a \lesssim 0.18$ mm) cracks in A533B steel, $\sigma_0 = 480$ MNm^{-2}, under plastic loading; data analysed in terms of ΔJ (Ref. 51)

given in terms of a crack length a, elastic modulus E, and representative strain range $\Delta\epsilon$ as

$$\Delta K_\epsilon = \Delta\epsilon(\pi a)^{1/2} = (a\Delta\epsilon_e + \Delta\epsilon_p)(\pi a)^{1/2} \quad 22$$

$$\Delta K_{eq} = QE\Delta\epsilon(\pi a)^{1/2} \quad 23$$

where $\Delta\epsilon$ is the sum of the plastic strain range $\Delta\epsilon_p$ plus part of the elastic strain $a\Delta\epsilon_e$, where $0.5 \leq a \leq 1$, and Q is the compliance function based on the equivalent linear elastic K_I solution for the loading geometry in question. Recently, Starkey and Skelton[88] have shown that the ΔJ and ΔK_{eq} approaches are essentially the same up to high plastic strains, and good correlations have been found between data for long and short cracks at both room and elevated temperatures by expressing the crack growth data in terms of $(E\Delta J)^{1/2}$ or ΔK_{eq}.

Although analyses of the behaviour of short cracks in terms of elastic–plastic constitutive laws often seem necessary, even with the more appropriate characterization afforded by such fracture mechanics, it is still often apparent that short cracks propagate at somewhat faster rates (Fig. 20). In order to account for this further 'breakdown' in continuum mechanics characterization, El Haddad and co-workers[9,84,89,90] have proposed an empirical approach based on the notion of an intrinsic crack length parameter, a_0. These authors redefined the stress intensity factor in terms of the physical crack length plus a_0, such that the stress intensity range which characterizes the growth of fatigue cracks, independent of crack length, is given by the equation

$$\Delta K = Q\Delta\sigma^\infty[\pi(a + a_0)]^{1/2} \quad 24$$

where Q is the usual geometry factor.[84] The 'material-dependent constant' a_0 was estimated from the limiting conditions of crack length where the nominal stress $\Delta\sigma^\infty$ approaches the fatigue limit $\Delta\sigma_e$ when $a \to 0$ and where $\Delta K = \Delta K_0$, i.e.

$$a_0 \approx \frac{1}{\pi}\left(\frac{\Delta K_0}{\Delta\sigma_e}\right)^2 \quad 25$$

The value of the intrinsic crack size a_0 can be seen to be equivalent to the critical crack size above which ΔK_{th} becomes constant at the long crack threshold stress intensity ΔK_0 in Figs. 15 and 18. In other words, a_0 is an indication of the smallest crack size that can be characterized at the threshold in terms of LEFM. This intrinsic crack size approach has been claimed to be a special case of Tanaka and co-workers' blocked slip band model[76] discussed above, where the friction stress σ^*_{fr} in equation (20) is taken to be zero. Although somewhat physically unrealistic, setting $\sigma^*_{fr} = 0$, $K_0 = K^m_c$, and $a_0 = a_0$ in equations (18) and (19) gives[76]

$$\sigma_{th} = \frac{K_0}{[\pi(a + a_0)]^{1/2}} \quad 26$$

$$K_{th} = \frac{K_0\, a^{1/2}}{(a + a_0)^{1/2}} \quad 27$$

which are identical to the expressions derived by El Haddad *et al.*[84] In equations 26 and 27, a_0 is essentially a fitting parameter that reproduces the variation of $\Delta\sigma_{th}$ with crack length such that

Fig. 18. Furthermore, by recomputing both ΔJ and ΔK to include a_0, El Haddad *et al.*[91] have reanalysed the short crack data obtained by Dowling[51] (*see* Fig. 20) and claimed a closer correspondence between results for long and short cracks. This intrinsic or 'fictitious' crack size approach has also been used to characterize a short crack emanating from a notch,[64,91] as discussed in the next section.

Although such an approach is successful in explaining differences in the growth rate kinetics of long and short cracks obtained from conventional LEFM analyses, it is totally empirical, as the physical significance of the parameter a_0 is not understood; neither is there any convincing correlation between a_0 and any characteristic microstructural dimension.

A somewhat different approach to rationalizing the behaviour of long and short cracks, specifically with respect to the threshold condition, was adopted by Usami and co-workers.[59,92–94] To replace the notion that the threshold condition is one of constant stress for short cracks, but one of a constant stress intensity range for long cracks, these authors proposed a single criterion that the cyclic plastic zone dimension (r_Δ) at the fatigue limit is a material constant.[59,92–94] They used the Dugdale solution to approximate the size of this plastic zone at the fatigue limit (r_Δ^F) for $R \geq 0$, in terms of the yield stress σ_0 and crack size a, i.e.

$$r_\Delta^F = a\left[\sec(\pi\Delta\sigma_{th}/4\sigma_0) - 1\right] \quad . \quad . \quad (28)$$

which was shown to reproduce the form of the curve of $\Delta\sigma_{th}$ versus crack size shown in Figs. 15, 18, and 19. Similar to the model based on an intrinsic crack size, this model can again be considered a special case of the blocked slip band model (equations (18)–(21)) by setting $K_c^m = 0$ (Ref. 76). By developing similar expressions for negative R ratios, Usami and Shida[59] have also claimed to have explained the effects of stress ratio and yield strength on the behaviour of short cracks. However, experimental confirmation of the constancy of r_Δ^F at the threshold for long and short cracks and the validity of the Dugdale solutions for the size of the plastic zone in this instance has yet to be obtained.

Notch field plasticity effects

Local plasticity also has an important influence on the initiation and growth of cracks emanating from notches. Such cracks are defined as being short because their size is comparable to the extent of the strain field of the notch tip plastic zone (*see* Fig. 21).

Stress analyses and failure predictions for notched components have traditionally involved the use of theoretical elastic stress concentration factors k_t or, where plasticity is considered, procedures such as those developed by Neuber.[95] For example, the well-known Neuber rule suggests that the elastic stress concentration factor k_t, under conditions of plastic deformation, is given approximately by the geometric mean of the stress and strain concentration factors, k_σ and k_ϵ, respectively:[95]

$$k_t = (k_\sigma k_\epsilon)^{1/2} \quad . \quad . \quad . \quad . \quad . \quad . \quad (29)$$

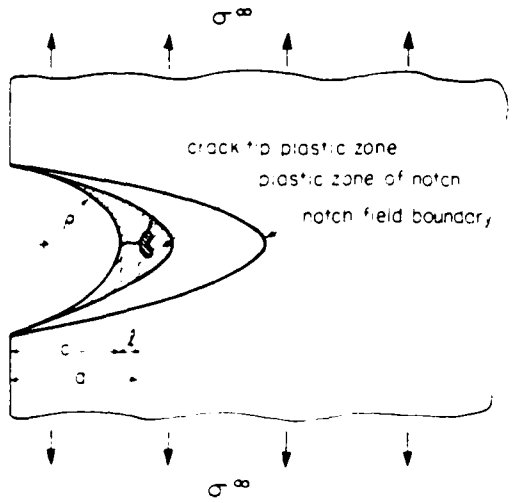

21 Schematic illustration of crack tip and notch tip plastic strain fields associated with growth of short crack of length l emanating from notch of depth c and root radius ρ

For elastic conditions, equation (29) reduces to

$$k_t = (\sigma\epsilon E)^{1/2}/\sigma^\infty \quad . \quad . \quad . \quad . \quad . \quad (30)$$

where σ and ϵ are the local stress and strain at the notch surface, respectively, σ^∞ is the nominal applied stress, and E is the elastic modulus.

Although elastic stress concentration factors are sometimes used in fatigue for conservative design in the presence of notches, k_t is generally replaced by k_f, the fatigue strength reduction factor; k_f can be considered as the effective stress concentration under fatigue loading conditions and is defined for finite life as

$$k_f = \frac{\text{unnotched bar endurance limit}}{\text{notched bar endurance limit}} \leq k_t \quad (31)$$

Values of k_f approach the theoretical values of k_t for larger notches and in higher strength materials, the degree of agreement being measured in terms of the so-called notch sensitivity index, defined as $(k_f - 1)/(k_t - 1)$. Although values of k_t are tabulated in handbooks (*see* e.g. Ref. 96), the determination of k_f generally involves experimental measurements or empirical predictions, such as the Peterson equation for iron-base wrought alloys,[97]

$$k_f = 1 + (k_t - 1)/[1 + (\alpha/\rho)] \quad . \quad . \quad (32)$$

where ρ is the notch root radius and α is an empirical constant that depends on the strength and ductility of the material. Typical values for α range from 0.01 for annealed steels to 0.001 for highly hardened steels.[2] Since such empirical equations are available only for steels, to avoid always measuring k_f experimentally the so-called 'local strain approach', essentially a modification of the Neuber rule for cyclic loading, has recently been developed (*see* e.g. Refs. 2, 98, 99). The values of k_f suggested by Morrow and co-workers[98] are determined from the relations

$$k_f = (k_\sigma k_\epsilon)^{1/2} \quad \text{(plastic)} \quad . \quad (33)$$

$$k_f = (\Delta\sigma\Delta\epsilon E)^{1/2}/\Delta\sigma^\infty \quad \text{(elastic)} \quad . \quad (34)$$

where $\Delta\sigma^{\infty}$, $\Delta\sigma$, and $\Delta\epsilon$ are the ranges of the nominal stress, local stress, and local strain, respectively. To compute k_f, equation (34), which is the equation of a rectangular hyperbola ($\Delta\sigma\Delta\epsilon$ = constant), must be solved simultaneously with the cyclic constitutive law, which similarly relates cyclic stresses to cyclic strains.

Fracture mechanics analyses, incorporating both analytical and numerical procedures (e.g. from equations (7) and (8)) have also been utilized by many authors to treat the problem of notches in fatigue. In particular, Barsom and McNicol,[37] Smith and Miller,[100] Dowling,[21,101] Kitagawa,[102] Lukáš and Klesnil,[103] El Haddad and co-workers,[91,104,105] and Tanaka and Nakai[64] have all attempted to characterize the growth of small cracks which are either fully or partially submerged in a notch tip plastic zone. Although not concerned specifically with the growth of short cracks, Barsom and McNicol[37] proposed the concept of a fatigue crack initiation threshold $\Delta K/\rho^{1/2}$, which is assumed to be a material constant for the initiation of 'engineering sized' cracks from notches of different root radii ρ (*see* Fig. 22). With the usual definition of the stress concentration factor k_t, however, the concept of an initiation threshold $\Delta K/\rho^{1/2}$ is really the notched bar fatigue limit $\Delta\sigma_e k_t$ expressed in fracture mechanics terms.[7] Smith and Miller,[100] on the other hand, assumed that a fatigue crack of length a growing in an unnotched specimen is comparable to a fatigue crack of length l growing from a notch when both have the same instantaneous velocity under identical conditions of bulk applied stress. They further suggested that the contribution e ($= a - l$) to a crack of length l growing from an edge notch of depth c and root radius ρ can be expressed as

$$e = 7.691\, l(c/\rho)^{1/2} \quad . \quad . \quad . \quad . \quad . \quad (35)$$

and that the extent of the notch field is equal to $0.13(c\rho)^{1/2}$. This estimate of the size of the notch field appears to be less accurate for fairly sharp notches, and is in disagreement with the predictions made by Dowling[21] for this regime (equation (9)).

An interesting aspect of crack growth from notches is that, after growing a short distance, cracks can arrest completely and become so-called non-propagating cracks (NPCs), as first demonstrated by Phillips,[106] Frost,[107] and Frost and Dugdale.[108] Since then, a number of other studies[64,89,91,100,103,109–111] have confirmed that NPCs exist, although the mechanism(s) by which a propagating crack becomes an NPC is not understood. Stress–strain life analyses, however, have revealed that NPCs form only at sharp notches, above the critical stress concentration factor k_t (*see* e.g. Refs. 100, 109, 111). This is illustrated in Fig. 23, where the long life fatigue strengths (i.e. fatigue limits) are plotted as functions of k_t. It is apparent from this figure that the threshold stress for crack initiation, i.e. the unnotched fatigue limit $\Delta\sigma_e$ divided by k_f or k_t, is less than the stress that would cause complete failure above the critical k_t for NPCs.

Fracture mechanics analyses of the plasticity of the notch field suggest that the condition for non-propagation involves either the long crack threshold stress intensity ΔK_0 applied to the short crack,[94] or a threshold strain intensity factor incorporating an intrinsic crack length (a_0) term.[89] As discussed below, the above models fail to explain physically why NPCs occur since the mere presence of a notch plastic zone does not obviously give rise to a driving force for crack growth which passes through a minimum.

Whether short cracks emanating from notches arrest or not, their growth, as compared to results obtained from conventional LEFM analyses of long cracks, is generally non-unique and significantly faster when characterized in terms of ΔK or K_{max}. An example of this behaviour is shown in Fig. 24, from the work of Leis and Forte,[110] where growth rates are plotted for cracks ~250 μm long propagating from notches of varying k_t, and compared to the growth rates of long cracks in an SAE 1015 mild steel. Hammouda and Miller[109] have analysed such behaviour in terms of notch plasticity theory, and argue that the total plastic shear displacement, which is taken as the sum of the shear displacement arising from (notch) bulk plasticity and from the local crack tip plastic zone for LEFM controlled growth, determines the growth

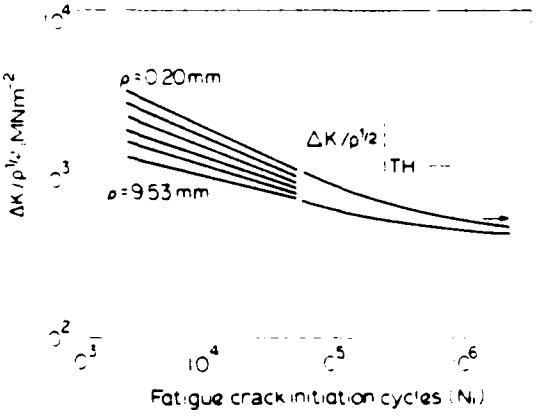

22 Correlation of fatigue life, based on initiation of engineering sized crack, with so-called fatigue crack initiation threshold $\Delta K/\rho^{1/2}$ based on results for HY130 steel, σ_0 = 1000 MNm^{-2}, double edge notched specimens of root radius ρ between 0.2 and 9.5 mm (Ref. 37)

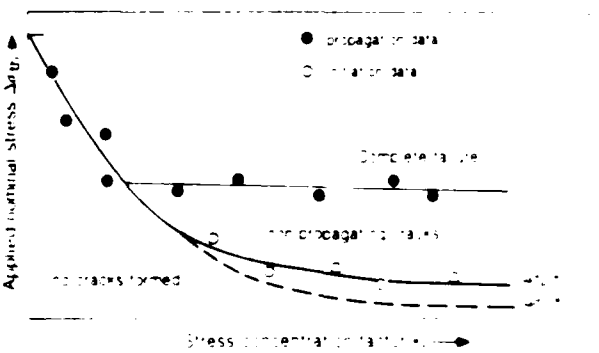

23 Threshold stress for crack initiation, i.e. unnotched fatigue limit $\Delta\sigma_e$ divided by k_f or k_t, as function of k_t (Ref. 111)

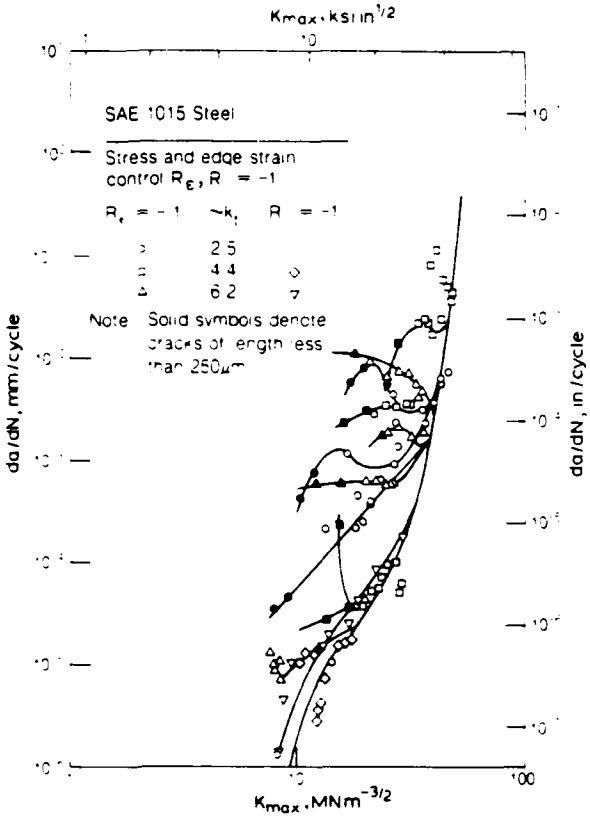

24 Propagation rate da/dN of cracks emanating from notches as function of maximum stress intensity factor K_{max} in 0.15%C mild steel; k_t is theoretical elastic stress concentration factor, R stress ratio, and R_ϵ edge strain ratio[110]

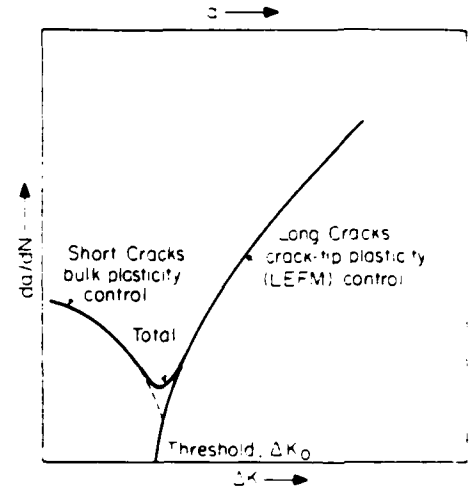

25 Elastic–plastic and linear elastic characterization of kinetics of crack growth for short crack propagation from notch, as shown in Fig. 21 (Ref. 109)

kinetics of such short cracks. If the crack is completely submerged in the notch tip plastic zone (*see* Fig. 21), bulk plasticity conditions dominate the behaviour. Hammouda and Miller estimate that the growth rates of the short cracks will decrease progressively until they arrest or merge with the long crack LEFM curve, where behaviour is dominated by local plasticity conditions within the crack tip plastic zone (*see* Fig. 25). Several continuum mechanics explanations have been advanced for such observations of growth rates of short cracks decreasing within the notch tip plastic zone. These explanations have been based on the total plastic shear displacement argument (*see* above),[109] on elastic–plastic analyses using the J parameter and the a_0 concept,[89] and on the idea that the size of the reversed plastic zone is a property of the material and is independent of crack length.[94] Such behaviour, however, is difficult to comprehend, particularly since there is a striking similarity between Figs. 25 and 14. In Fig. 14 is shown the progressive deceleration in short crack growth rates in the absence of a notch, which has been attributed to the impedance of growth at grain boundaries.[71] Thus it must be concluded that even though the precise mechanism for the deceleration of short crack growth and the formation of NPCs is unclear, factors such as notch tip plasticity, microplasticity, grain boundary blocking of slip bands, cessation of growth, crystallographic reorientation, deflection at grain boundaries, and crack closure may all play a significant role. In this regard it has been claimed that, since small cracks are capable of propagating below the long crack threshold ΔK_0 value, they may propagate for some distance until the combination of their size and the local stress causes them to arrest at or below the ΔK_0 value.[8] Although this is a convenient explanation of the behaviour shown in Figs. 14 and 25, the physical mechanisms that have been suggested for such behaviour do not follow from conventional elastic or elastic–plastic notch analyses. However, recent studies have suggested that the most general explanation involves the phenomenon of fatigue crack closure, and the variation of closure with crack length.[12,61] This is discussed in detail below.

Environmental and closure effects

The third definition of a short crack (*see* the introductory section), perhaps the most important from a design viewpoint, is the crack which is long compared to the scale of both the microstructure and the local plasticity, yet simply physically small, i.e. typically less than 0.5–1 mm long. Since both continuum mechanics and LEFM characterizations of the behaviour of such cracks would be expected to be valid, it is perhaps surprising to find that under certain circumstances[11,18,49,54,60] even physically short cracks grow faster than long cracks under a nominally identical driving force (i.e. at the same ΔK). This is not at all consistent with the concept of similitude, which forms the basis of fracture mechanics analyses of subcritical crack growth, and has been attributed primarily to two factors.[32]

The first of these is connected with the phenomenon of crack closure: interference and physical contact between mating fracture surfaces in the wake of the crack tip can, under positive loads during the fatigue cycle, lead to effective

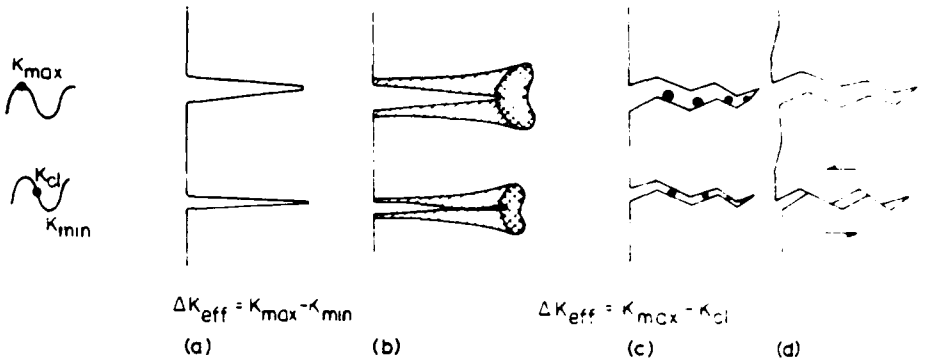

a no closure, and closure induced by: *b* cyclic plasticity; *c* corrosion deposits; *d* rough fracture morphology

26 Mechanisms of fatigue crack closure; ΔK_{eff} is effective stress intensity range, defined by $K_{max} - K_{cl}$, where K_{cl} is stress intensity at which two fracture surfaces come into contact ($K_{cl} \geq K_{min}$) (Ref. 119)

closure of the crack. Since the crack cannot propagate while it remains closed, the net effect of closure is to reduce the nominal stress intensity range ΔK, computed as $K_{max} - K_{min}$ from measurements of applied load and crack length, to some lower effective value ΔK_{eff} actually experienced at the crack tip, i.e. $\Delta K_{eff} = K_{max} - K_{cl}$, where K_{cl} is the stress intensity at closure ($\geq K_{min}$).[112] Several factors can lead to closure, such as the constraint of surrounding elastic material on the residual stretch in material elements previously plastically strained at the tip (plasticity induced closure),[112] the presence of corrosion debris within the crack (oxide induced closure),[113–116] and contact at discrete points between faceted or rough fracture surfaces where significant inelastic mode II crack tip displacements are present (roughness induced closure).[116–120] These mechanisms of crack closure are illustrated schematically in Fig. 26.

Plasticity induced closure, as first defined by Elber[112] from compliance measurements on fatigue cracks in aluminium alloys at high stress intensity ranges, is generally considered to play a dominant role under plane stress and is thus presumed to be of less importance at near-threshold levels where mostly plane strain conditions exist. In the latter case, the main contributions to the closure of fatigue cracks come from oxide deposits within the crack and from premature contact between the fracture surface asperities. Consideration of simple geometric models have led Suresh, Ritchie, and co-workers[119–122] to propose the following relationships for such closure:

$$(K_{cl}/K_{max})_{oxide} \approx (d_0^2 \beta/\pi s \delta_{max} \epsilon_0)^{1/2} \quad (36)$$

$$(K_{cl}/K_{max})_{roughness} \approx [2\gamma\nu/(1 + 2\gamma\nu)]^{1/2} \quad (37)$$

where d_0 is the maximum thickness of the excess oxide deposit located a distance $2s$ from the crack tip, δ_{max} is the maximum CTOD (mode I), ν is the ratio of mode II to mode I crack tip displacements, ϵ_0 is the yield strain (σ_0/E), γ is a non-dimensional roughness factor given by the ratio of the height of a fracture surface asperity to its width, and β is a constant of numerical value ~1/32.

Extensive studies of the behaviour of long cracks, particularly at near-threshold stress intensity levels, have revealed that such closure mechanisms determine to a large extent the effects on crack growth of load ratio,[114–116,121] yield strength,[116,124,125] grain size,[116,121] environment,[114–116,121,122,125] and variable amplitude cycling,[126–128] and even in the very existence of a threshold for no long crack growth.[116,121,125,129] However, such microscopic closure mechanisms are also particularly relevant to the behaviour of short cracks, simply because their action predominates in the wake of the crack tip. Since small cracks, by definition, have only a limited wake, it is to be expected that the effect of crack closure will be different for long and short cracks – that the short crack is likely to be less influenced by closure. Evidence that the extent of crack closure is a function of crack size has been reported by James and Morris[48] for the growth of short cracks in titanium alloys. By monitoring the surface CTOD at zero load for cracks from 50 to 500 μm long (*see* Fig. 27), these authors concluded that for cracks less than approximately 160 μm long the extent of crack

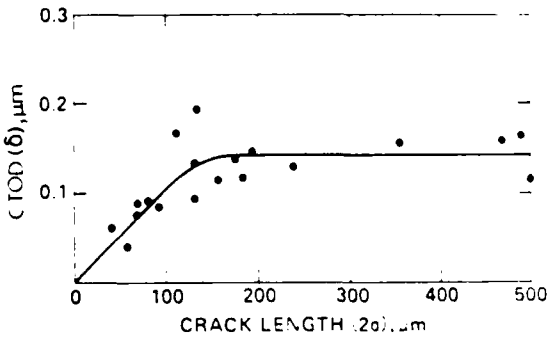

27 Variation of CTOD δ at zero load with length of small surface cracks in 6Al–2Sn–4Zn–6Mo titanium alloy (σ_0 = 1140 MNm^{-2}, primary α grain size ≈ 4 μm, β grain size ≈ 12 μm), showing reduction in crack closure with decreasing crack size[48]

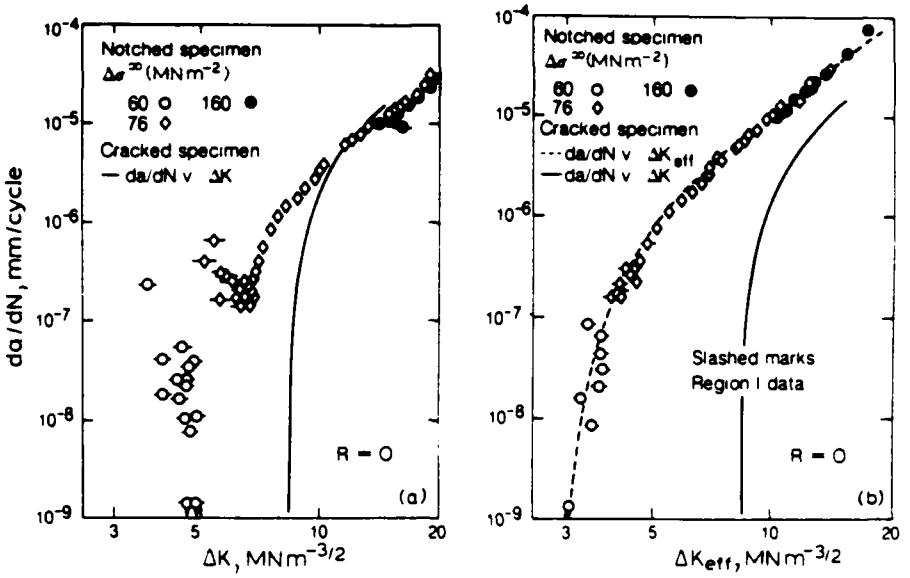

a da/dN *v.* nominal stress intensity range ΔK; *b* da/dN *v.* effective stress intensity range ΔK_{eff}, note that anomalous (sub-threshold) behaviour of short cracks is brought into direct correspondence with conventionally obtained data for long cracks once crack closure is accounted for

28 Variation of crack propagation rate with stress intensity ranges in JIM SM416, 0.17%C structural mild steel, σ_0 = 194 MNm^{-2} (Ref. 61)

closure, particularly that induced by roughness, decreased with decreasing crack length. A further influence of roughness-induced closure was found by McCarver and Ritchie,[60] who studied the crystallographic growth of long and physically short fatigue cracks in René 95 nickel-base superalloy. Threshold ΔK_{th} values for short cracks (a~0.01–0.20μm) at low mean stresses (R = 0.1) were found to be 60% smaller than for long cracks (a~25 mm), yet at high mean stresses (R = 0.7) where closure effects were minimal, this difference was not apparent. More recently, Tanaka and Nakai[61] have used compliance techniques to measure the extent of crack closure for small cracks emanating from notches in a low carbon steel and found a marked reduction in closure at short crack lengths. These authors claimed that the anomalous (sub-threshold) behaviour of short cracks (as shown in Figs. 14 and 25) could be brought into direct correspondence with conventional long crack data (*see* the next section) by analysing it in terms of ΔK_{eff} (*see* Fig. 28). Thus, at equivalent nominal ΔK levels, physically short cracks may be expected to propagate faster (and show lower thresholds) than corresponding long cracks simply because closure produces a smaller increase in effective stress intensity range at the crack tip in long cracks. Specific mechanisms for this effect are discussed in more detail in the next section.

Chemical and electrochemical effects can also increase the growth rate of small cracks, and this is particularly relevant to the growth of physically short cracks in aggressive environments.[11,53,54,57,130] Experiments by Gangloff[11,54] on high strength AISI 4130 steels tested in NaCl solution revealed the corrosion fatigue crack propagation rates of short cracks (0.1-0.8 mm) to be up to two orders of magnitude faster than corresponding rates for long cracks (25–60 mm) at the same ΔK level, although the behaviour in inert atmospheres was essentially similar (see Fig. 29). This phenomenon is not completely understood, but preliminary analyses have indicated that the effect could be attributable to differences in the local crack tip environment of long and short cracks, resulting mainly from the different electrochemically active surface-to-volume ratios of the cracks and from the influence of crack length on the solution renewal rate in the crack tip region.[11,54,57]

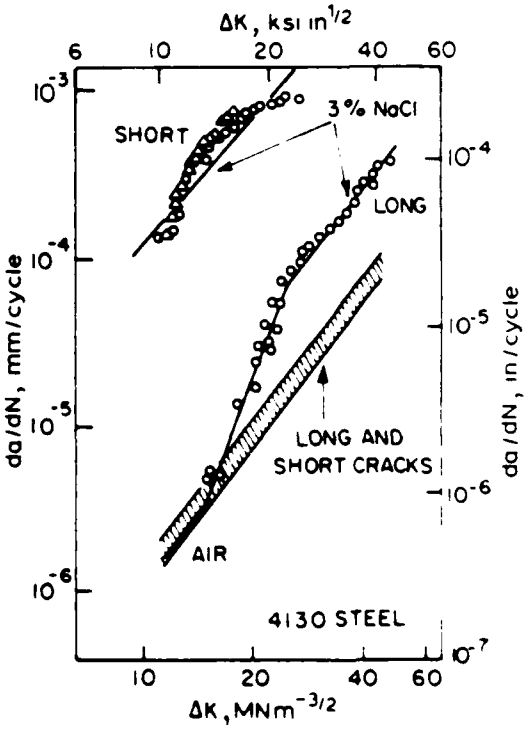

29 Fatigue crack propagation rate da/dN as function of ΔK for long (a ~ 50 mm) and physically short (a = 0.1–0.8 mm) cracks in AISI 4130 steel, σ_0 = 1300 MNm^{-2}, tested in moist air and in aqueous 3% NaCl solution[53]

DISCUSSION

From the above review of experimental results, it is apparent that short fatigue cracks may present difficulties in fatigue design simply because their growth behaviour cannot be predicted with certainty by using the analyses and methodologies developed for long cracks, for example by making use of LEFM results. It is also apparent that the use of these procedures can lead to overestimates of the lifetimes of components containing short cracks because, under the same nominal driving force, a short crack invariably propagates more quickly than a corresponding long crack. This problem, of 'lack of similitude', arises for a number of reasons, including:

(i) inappropriate fracture mechanics characterization of the crack driving force for short cracks subjected to near-tip and notch field plasticity effects
(ii) local microstructural features which do not substantially alter the growth of large cracks, but can interact strongly with small cracks because they are of comparable size
(iii) lack of similitude associated with crack extension mechanisms
(iv) crack closure effects
(v) differences in the local crack tip environments.

Each of these factors is now examined in turn.

Questions on the inappropriate use of LEFM to characterize the extension of short cracks have been central to the short crack problem (see e.g. Refs. 7–10, 12, 131, 132). In fact, it has often been claimed that the short crack problem arises simply when LEFM analyses become invalid,[131] although it is now clear that this is an oversimplification. Conventional LEFM approaches can be inappropriate for short cracks, even under nominally elastic conditions, since the use of the linear elastic singularity to characterize the local stresses on the basis of K_I (i.e. equation (3)) invariably involves neglecting all terms of order higher than $r^{-1/2}$ (Ref. 133 and 134). However, when $a \sim r_y$ such higher order terms can have an appreciable effect and therefore should be considered when comparing the behaviour of long and short cracks.[133,134] It is also well recognized that one of the main reasons for the breakdown in LEFM analysis for short cracks is the presence of excessive plasticity over distances comparable with the crack size in the vicinity of the crack tip. This problem has been partly resolved by the use of elastic–plastic fracture mechanics in methods based on the J-integral or on the crack tip opening displacement, as evidenced by the results obtained by Dowling[23] and shown in Fig. 20. It is now apparent that differences in the behaviour of long and short cracks as revealed by early studies can be traced to the fact that growth rates were compared at equivalent ΔK values, and that the use of this LEFM parameter did not provide an adequate characterization of the stress and strain fields at the tip of short cracks, where $a \sim r_y$. However, for short cracks emanating from notches, where initial growth occurs within the plastic zone of the notch (see Fig. 21), a continuum mechanics description of the behaviour is less clear. Certainly there is experimental evidence that such short cracks can propagate below the long crack threshold at progressively decreasing growth rates (see Fig. 25), and can even arrest to form non-propagating cracks,[106–110] but such behaviour can also occur in the absence of a notch and can be attributed to microstructural factors (see Fig. 14).[71] Certainly no linear elastic analysis of a short crack emanating from a notch (see e.g. Refs. 21, 100) has shown that the crack driving force (e.g. K_I) passes through a minimum as the crack begins to extend from the notch, and to the present authors' knowledge there is no formal elastic plastic analysis available which predicts a similar variation in crack driving force without having to incorporate crack closure effects.[12,64,135] Although there is no complete continuum mechanics analysis, it can be concluded that the anomalous growth rate of short cracks emanating from notches may result in part from the interaction of the short crack with microstructural features, and principally from crack closure.

With respect to microstructural features, it is generally accepted that the presence of microscopic discontinuities, such as grain boundaries, hard second phases, or inclusions, plays a somewhat minimal role in influencing the growth of long fatigue cracks[6] (at least for growth rates below $\sim 10^{-3}$ mm/cycle) because the behaviour is governed primarily by average bulk properties.[71] However, it is clear that this is not the case for small cracks whose length is comparable to the size of microstructural features. For example, for small cracks contained within a single grain, cyclic slip will be strongly influenced by the crystal orientation and the proximity of the grain boundary, resulting in locally non-linear crack extension.[19,71–74] There is now a large body of evidence showing that the growth of small cracks is impeded by the presence of grain boundaries (see e.g. Fig. 30) by such mechanisms as the blocking of slip bands[76] or containment of the plastic zone[19] within the grain, reorientation and reinitiation of the crack as it traverses the boundary,[19,71] and simple cessation of growth at the boundary.[19] Crack propagation has also been found to be halted by harder second phases: in duplex ferritic–martensitic steels, small cracks

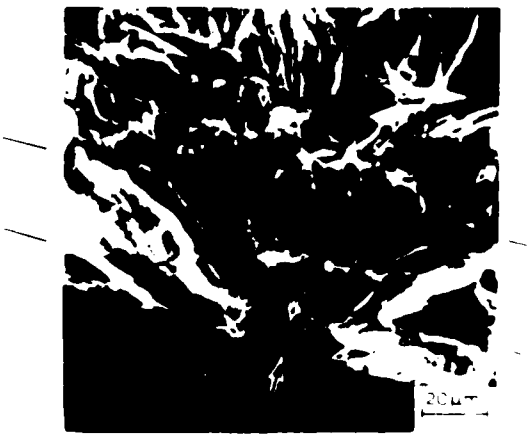

30 Changes in direction of crack advance when crack tip encounters grain boundaries in 7075 T6 aluminium alloy[71]

were observed to initiate and grow in the softer ferrite, only to arrest when they encountered the harder martensite.[136] Many of these effects can be explained by considering the mechanics of crack deflection.

Based on the theoretical analyses by Bilby *et al.*[137] and Cotterell and Rice,[138] recent studies by Suresh[81] have shown that alternatives to previous interpretations of the way in which a crack tip interacts with a grain boundary can be developed by considering the effect of crack deflection on the propagation of short fatigue cracks. For a short crack, the low restraint on cyclic slip promotes a predominantly crystallographic mode of failure. When a crack tip reaches a grain boundary, it tends to reorient itself in the adjacent grain to advance by the single shear mechanism, and can be considerably deflected by the grain boundary. This phenomenon is illustrated schematically in Fig. 31. The extent of deflection at the grain boundary is a function of the relative orientations of the most favourable slip systems in the adjoining crystals. For an elastic crack initially inclined at an angle θ_0 to the mode I growth plane and deflected at the first grain boundary through an angle θ_1 (see Fig. 31), approximate estimates of the local stress intensity factors yield the relation[81]

$$K_1/K_I = \cos^2\theta_0 \cos^3(\tfrac{1}{2}\theta_1) + 3\sin\theta_0 \cos\theta_0 \sin(\tfrac{1}{2}\theta_1)\cos^2(\tfrac{1}{2}\theta_1) \quad . \quad . \quad . \quad . \quad . \quad (38)$$

$$K_2/K_I = \cos^2\theta_0 \sin(\tfrac{1}{2}\theta_1)\cos^2(\tfrac{1}{2}\theta_1) - \sin\theta_0 \cos\theta_0 \cos(\tfrac{1}{2}\theta_1)[1 - 3\sin^2(\tfrac{1}{2}\theta_1)] \quad . \quad . \quad . \quad . \quad . \quad (39)$$

Here, K_1 and K_2 are the near-tip mode I and mode II stress intensity factors, respectively, immediately following deflection at the grain boundary, whereas K_I is the nominal mode I (far-field) value. For a typical short crack emanating from the surface at an angle of $\theta_0 \approx 45°$ and deflected at the grain boundary by $\theta_1 \approx 90°$, equations (38) and (39) yield $K_1 \approx 0.7K_I$ and $K_2 \approx 0.35K_I$. The effective driving force for coplanar growth can then be approximated as the square root of the sum of the squares of K_1 and K_2, such that $\Delta K_{eff} \approx 0.78\Delta K_I$. Thus consideration of crack deflection processes alone can account for a significant reduction in driving force as a crack tip interacts with a grain boundary when the way in which a short crack advances is characterized by LEFM. It has been postulated[81] that if the extent of deflection at the grain boundary is large, the effective cyclic stresses may be reduced to a value smaller than the true threshold for short crack advance (e.g. to the fatigue endurance limit) such that complete crack arrest will result (denoted by curve A in Fig. 32). If the effective cyclic stresses after deflection are above such threshold values, there would be no crack arrest (as denoted by curve B in Fig. 32) and only a temporary deceleration in growth rate. Although the numerical predictions of the deflection models can be subject to considerable uncertainties when used to characterize the mechanics of short cracks in metals and alloys, the mechanisms underlying crack deflection processes have been shown to provide a physically meaningful explanation not only for the role of microstructure in influencing short crack advance, but also for several fatigue characteristics of long cracks under constant[81] and variable amplitude[81,126–128] loading.

In addition to causing a reduction in the effective driving force, crack deflection mechanisms could play a major role in enhancing closure.[81,120] For example, the irreversibility of

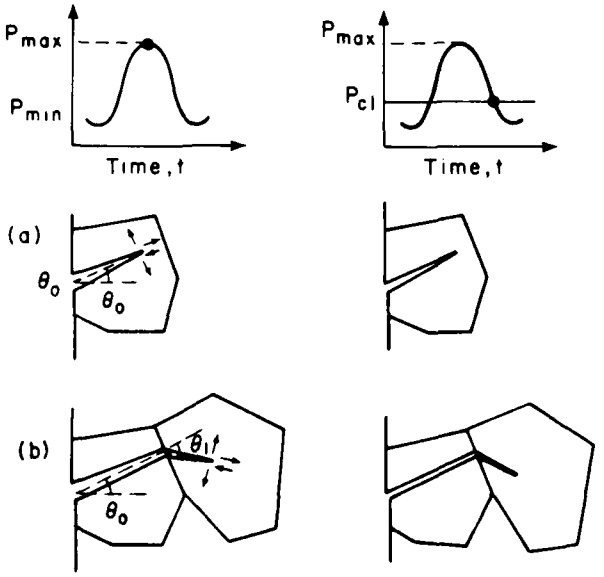

a propagation into first grain; *b* propagation across grain boundary

31 Growth and deflection of microstructurally short fatigue crack and the resultant crack tip displacements and closure; θ_0 is short crack initiation angle and θ_1 angle of deflection at first grain boundary[81]

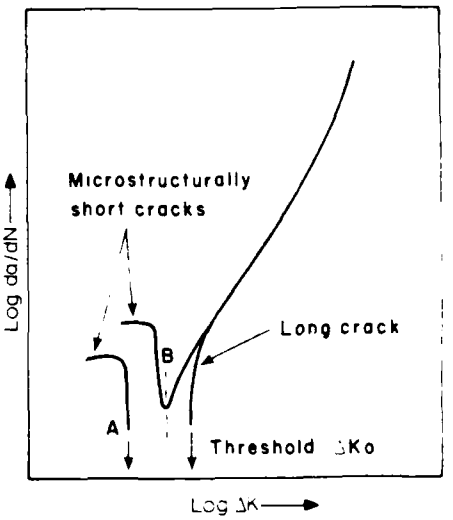

32 Variation of fatigue crack growth rate da/dN with ΔK for both long and microstructurally short fatigue cracks; note how growth rates for short cracks decrease progressively below long crack threshold ΔK_0 before arresting or merging with long crack data

slip steps and surface oxidation can lead to non-uniform tensile opening and shear displacements of short cracks.[12,81] Given the presence of serrated fracture surfaces and mode II crack tip displacements occurring after deflection, such non-uniformities in crack opening and sliding result in premature contact between asperities, leading to roughness induced closure (*see* Figs. 26 and 31). (An ideally elastic crack may not result in any roughness induced closure, irrespective of the extent of deflection.) Experimental measurements of crack closure made by Morris and co-workers[47-49] do indeed show that even short cracks (spanning only a few grain diameters) can close above the minimum load of the fatigue cycle (*see* Fig. 27).

A further factor which may contribute to differences in the behaviour of long and short cracks is the question of crack shape.[10] Even long cracks, running across many grains, are known to possess certain irregularities in their geometry (on a microscopic scale) that result from local interactions with microstructural features,[10] yet, at a given ΔK, the overall growth behaviour would be expected to be similar. However, on comparing a large crack with a small one this similarity would seem questionable. Moreover, the early stages of fatigue damage often involve the initiation of several small cracks, the subsequent growth of any of which is likely to be strongly influenced by the presence of the others.[37-40]

Differences in the behaviour of long and short cracks may also result from the fact that, at the same nominal ΔK, the crack extension mechanisms may be radically different. As pointed out by Schijve,[10] the restraint of the elastic surrounding on a small crack near a free surface is very different from that experienced at the tip of a long crack inside the material. For a small, grain sized crack, cyclic slip along the system with the highest critical resolved shear stress results in mixed mode II and mode I slip band cracking akin to Forsyth's stage I mechanism.[139] However, for a long crack, spanning many grains, maintaining such slip band cracking in a single direction in each grain is incompatible with maintaining a coherent crack front. The resulting increased restraint on cyclic plasticity will tend to activate further slip systems, leading to a non-crystallographic mode of crack advance by alternating or simultaneous shear, commonly referred to as striation growth (Forsyth's stage II).[139] At near-threshold levels where the extent of local plasticity can be small enough to be contained within a single grain, even long cracks may propagate via the single shear mechanism, the orientation of the slip band cracking changing at each grain boundary and leading to a faceted or zigzag crack path morphology (*see* Fig. 33).[117-120]

The occurrence of this shear mode of crack extension, with the related development of a faceted fracture surface, has a major influence on the magnitude of crack closure effects,[116-120] which may in turn lead to differences in the behaviour of long and short cracks (*see* Figs. 26 and 31).

The differences in fatigue characteristics resulting from crack closure arise from two main sources. First, since closure results from the constraint of surrounding elastic material on the plastic region surrounding the crack, the amount of closure experienced by a small crack at high stress amplitudes in a fully plastic specimen would be far less than that experienced by a larger crack at lower stress amplitudes in an elastic–plastic or nominally elastic specimen at the same (nominal) driving force. However, more importantly, differences between the effect of closure on long and short cracks result from the fact that such closure effects predominate in the wake of the crack tip. Since short cracks – by definition – possess a limited wake, it is to be expected that in general such cracks will be subjected to less closure. Thus, at the same nominal driving force, short cracks may experience a larger effective value than will the equivalent long crack. As outlined in the previous section, this can arise in two ways. In the first, with respect to plasticity induced closure, plastic deformation in the wake of the crack has to build up before it can be effective in reducing ΔK_{eff} (Ref. 112). From analogous studies of the role of dilatant inelasticity (inelasticity resulting from phase transformations) on reducing the effective stress intensity at the crack tip in ceramics,[110] it has been found that the full effect of this closure is felt only when the transformed zone extends into the wake of the crack by a distance of five times its forward extent. Although no comparable analysis has been carried out for plastic deformation in metals, it is to be expected that the role of the compressive stresses in the plastic zone encompassing the wake of the crack would be limited for small cracks of a length comparable to the forward extent of this zone (i.e. for $a \sim r_y$). It is believed[12,64,133] that this is one of the main reasons (at least from the perspective of continuum mechanics) for non-propagating cracks and also explains why microstructurally short cracks and cracks emanating from notches can propagate below the long crack threshold ΔK_0 (*see* Figs. 14 and 25). Essentially, they can initiate and grow at nominal stress intensities below ΔK_0 because of the absence of closure effects but, as they increase in length, the build-up of permanent residual plastic strains in their wake means that crack closure begins to have the effect of progressively decreasing the effective ΔK experienced at the crack tip, resulting in a progressive reduction in crack growth rate and sometimes complete arrest.

This notion, by which the anomalous behaviour of short cracks below the long crack threshold regime and in the strain field of notches (*see* e.g. Fig. 1) is related primarily to a decrease in crack closure effects at small crack sizes,[12,64,135] has recently been substantiated by both numerical[135] and experimental[64] studies. Newman[135] has demonstrated that by incorporating plasticity induced closure in finite element computational models of fatigue crack propagation, the progressively decreasing growth rates of short cracks emanating from notches could be predicted and shown to be in good agreement with experimental data on lower strength steel (*see* Fig. 34). Tanaka and Nakai[64] monitored the growth of similar short cracks in notched specimens of low strength steel at both $R = 0$ and 0.4 while simultaneously measuring the extent of crack closure. Their data, which

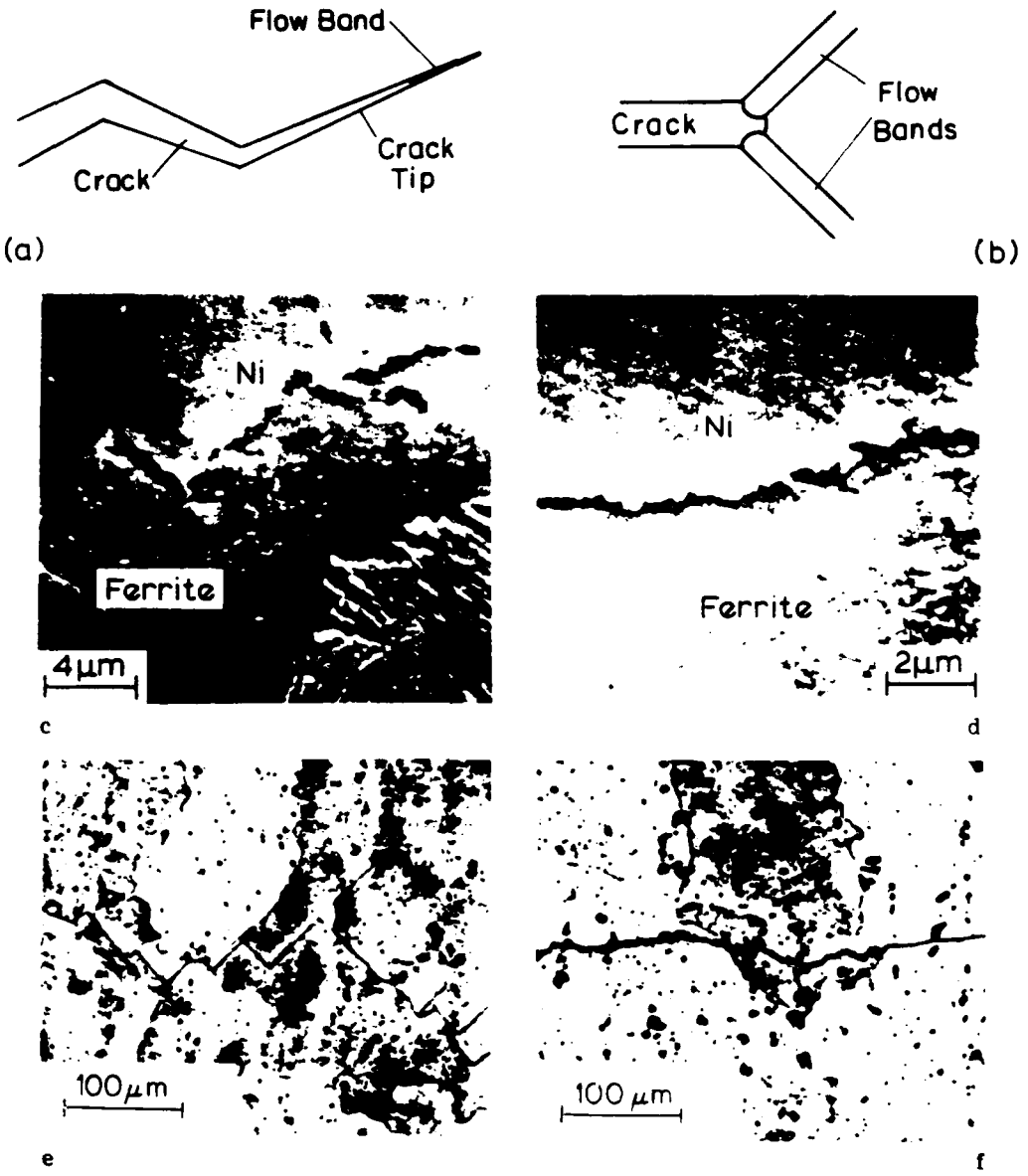

a, *c*, *e* near threshold, $r_y < d_g$, stage I, mixed modes I and II; *b*, *d*, *f* higher growth rates, $r_y > d_g$, stage II, mode I; *c*, *d*, fractographs of nickel-plated 1018 steel;[118] *e*, *f* sections of 7075 T6 aluminium alloy[10]

33 Crack opening profiles and morphologies of long fatigue cracks[120]

show the characteristic decreasing growth rate for short cracks when plotted in the usual way (in terms of a nominal ΔK), can be seen to coincide with the long crack data and to fall on a single smooth curve when reanalysed in terms of ΔK_{eff} incorporating the experimental K_{cl} measurements (*see* Fig. 28).

A similar situation can arise from the effect of roughness induced crack closure promoted by rough, irregular fracture surfaces, particularly if the crack extension mechanism involves a strong single shear (mixed mode II and mode I) component.[118–120] Since a crack of zero length can have no fracture surface and hence cannot undergo roughness induced closure, the development of such closure is expected to be a strong function of crack size,[47–49,120,133] as demonstrated by the experimental data obtained by James and Morris[48] and shown in Fig. 27. An estimate of the lower bound to the size of transition crack below which roughness induced closure is ineffective (at near-threshold levels) can be appreciated from Figs. 31 and 33 (Ref. 120). A long crack which encompasses several grains will, at near-threshold levels, have developed a faceted morphology and, as a result of the incompatibility between mating crack surfaces arising from the mode II crack tip displacements, will undergo roughness induced closure in the manner depicted in Fig. 26. The short crack, however, will not undergo such closure while its length remains less than a grain diameter since it will not have changed direction at a grain boundary, and accordingly will not have formed a faceted morphology, despite extension via the same single shear mechanism.

In general, since most of the results that show differences between the growth rates of long and short cracks have been obtained at low stress

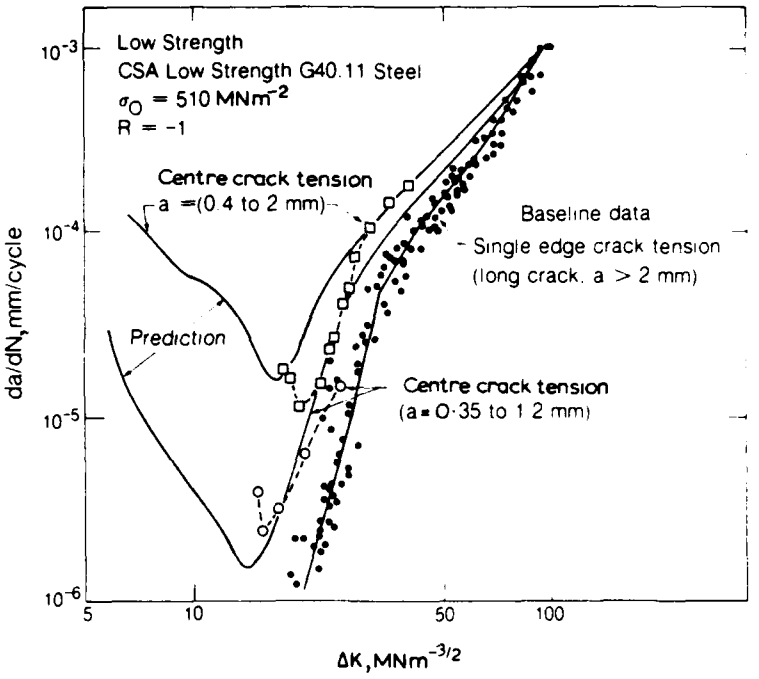

34 Comparison of experimental results and numerical predictions of crack propagation rates for small cracks in centre cracked tensile specimens of CSA G40.11 low strength structural steel σ_0 = 510 MNm^{-2}, subjected to high stress levels[135]

intensity ranges, and fatigue-crack propagation of long cracks in this near-threshold regime is known to be strongly influenced by crack closure effects, it seems most likely that the main reason for the faster growth of short cracks and the fact that they can propagate below the long crack threshold ΔK_0 is associated with the role of closure decreasing with crack size. Results obtained by Potter and Yee[141] on the behaviour of short cracks under variable amplitude loading are consistent with this notion, since the crack growth transients (i.e. accelerations and retardations) normally observed following overloads and spectrum loading sequences, which have been attributed — at least in part — to closure mechanisms (*see* e.g. Ref. 112), were largely absent for short cracks. In this regard it is useful to compare data for short and long cracks at high load ratios, since closure effects are then minimal even for long cracks. This has been done for crystallographic near-threshold fatigue in nickel-base alloys,[60] and the threshold for short cracks, despite being 60% smaller than the long crack threshold at $R = 0.1$, was approximately equal to the long crack threshold at $R = 0.7$.

Finally, large differences in the behaviour of long and short cracks can arise at stress intensities well outside the threshold regime, because of environmental factors.[11,54,130] As shown in Fig. 29, the results obtained by Gangloff[11,54] have demonstrated that corrosion fatigue crack growth rates of physically short cracks in AISI 4130 steel tested in aqueous NaCl solution can be one to two orders of magnitude faster than the corresponding growth rates of long cracks at the same ΔK value. This unique environmentally assisted propagation of short cracks was attributed to differing local crack tip environments as a function of crack size. Specifically, Gangloff argued that the local concentration of the embrittling species within the crack depends on the surface-to-volume ratio of the crack, on the diffusive and convective transport of the embrittling medium to the crack tip, and on the distribution and coverage of active sites for electrochemical reaction, all processes sensitive to crack depth, opening displacement, and crack surface morphology.[54,57] Analogous, yet less spectacular, environmental crack size effects may also arise in gaseous environments or in the presence of internally charged hydrogen where, for example, the presence of hydrogen may induce an intergranular fracture mode. The rough crack surfaces that tend to be produced by this failure mechanism would lead to roughness induced closure, which again directly influences the long crack phenomenon of a reduced ΔK_{eff} (see e.g. Ref. 142).

These differences in the behaviour of fatigue cracks of different size provide clear examples of how the fracture mechanics similitude concept can break down. The stress intensity, although adequately characterizing the mechanical driving force for crack extension, can account for neither the chemical activity of the crack tip environment nor the local interaction of the crack with microstructural features. Since these factors, together with the development of crack closure, are a strong function of crack size, it is actually unreasonable to expect the growth behaviour of long and short cracks to be identical. Thus, in the absence of the similitude relationship, the analysis and utilization of laboratory fatigue-crack propagation data to predict the performance of in-service components in which short cracks are present

becomes an extremely complex task; a task which demands an immediate and major effort from both researchers and practising engineers alike.

CONCLUDING REMARKS

The problem of short cracks must be recognized as one of the most important and challenging topics currently faced by researchers in fatigue. Not only is it a comparatively unexplored area academically, but it also raises doubts about the universal application to the characterization of sub-critical flaw growth of fracture mechanics, the misuse of which can result in overestimates of defect-tolerant lifetimes. It is an area that, represents an interface between the fracture mechanics methodologies dealing specifically with the macroscopic growth of fatigue cracks and the classical engineering mechanics methodologies dealing with total life and engineering concepts of (macro-) crack initiation (as depicted in Fig. 1). As discussed in the introductory section, the last process, of macrocrack initiation, is simply the growth of short cracks (microcracks). The process of the initiation of short cracks (microcrack initiation) has not been treated explicity in this paper as it has been the subject of several recent reviews (*see* e.g. Refs. 7, 143, 144). Suffice it to say that such small cracks tend to initiate at constituent particles (i.e. inclusions and intermetallics, as shown in Fig. 9) in commercial materials (*see* e.g. Refs. 39, 41, 145), whereas in pure metals and alloys their initiation is often associated with emerging planar slip bands *called persistent slip bands* (PSBs) (*see* e.g. Ref. 143, 144, 146, 147). In fcc metals, such small cracks appear to initiate via a crystallographic stage I mechanism along the PSB, as shown in Fig. 35 (Ref. 148), although the specific mechanisms of initiation and their relation to the PSBs vary markedly from material to material.[144]

In the present paper an attempt has been made to provide a critical overview of recent experimental studies on the growth of small fatigue cracks, and specifically to outline the mechanical, metallurgical, and environmental reasons, as to why the behaviour of such cracks should differ from the behaviour of long cracks. The intention has not been to present a formal analysis of each of these factors, since in most cases such an analysis is simply not possible, but rather to give a thorough review of the many interdisciplinary factors which may be relevant to the short crack problem. It has been concluded that differences in the behaviour of short and long cracks are to be expected, and that such differences can arise from a number of distinct phenomena:

(i) inadequate characterization of the mechanics of crack tip stress and deformation fields of short cracks, including the neglect of higher order terms for the elastic singularity and the presence of extensive local crack tip plasticity
(ii) notch tip stress and deformation field effects (for cracks emanating from notches)
(iii) the interaction, including deflection, of short cracks with microstructural features such as grain boundaries, inclusions, and second phases, of dimensions comparable in size with the crack length
(iv) differences in crack shape and geometry
(v) differences in crack extension mechanism
(vi) the effect of crack closure varying with crack length
(vii) differences in the local crack tip environments.

Each of these factors represents a formidable challenge in fatigue research because of the complex nature of both experimental and theoretical studies, yet they are of great importance to an understanding of the anomalous behaviour of short flaws. This problem will undoubtedly come to

35 Transmission electron micrograph of stage I small cracks propagating within persistent slip bands, showing ladder-like dislocation substructures in fatigued, polycrystalline, high purity copper. Insets show corresponding optical micrograph of cracks and electron diffraction pattern[148]

assume even greater significance in the future since, with improvements in the science and practice of non-destructive testing, the projected lifetime of a fatigue flaw in the short crack regime will become an increasingly larger proportion of the total life.

ACKNOWLEDGMENTS

The work was performed under Grant No. AFOSR-82-0181 from the US Air Force Office of Scientific Research to the University of California at Berkeley. The authors wish to thank Dr A. H. Rosenstein of AFOSR for his support and encouragement, Drs W. L. Morris and J. Lankford for kindly supplying original micrographs, and M. Penton for her help in preparing the manuscript. This review is an expanded version of a paper presented at the 55th Specialists Meeting of the AGARD Structural Materials Panel in Toronto, Canada, in September 1982.

REFERENCES

1. L. F. Coffin: in 'Fatigue and microstructure', (ed. M. Meshii), 1; 1979, Metals Park, Ohio, American Society for Metals.
2. M. R. Mitchell: in 'Fatigue and microstructure', (ed. M. Meshii), 385; 1979, Metals Park, Ohio, American Society for Metals.
3. J. E. Campbell, W. E. Berry, and C. E. Feddersen: 'Damage tolerant design handbook'; 1972, Columbus, Ohio, Metals and Ceramics Information Center, Battelle Columbus Laboratories.
4. S. T. Rolfe and J. M. Barsom: 'Fracture and fatigue control in structures: applications of fracture mechanics'; 1977, Englewood Cliffs, NJ, Prentice Hall.
5. H. H. Johnson and P. C. Paris: *Eng. Fract. Mech.*, 1968, **1**, 3.
6. R. O. Ritchie: *Int. Met. Rev.*, 1979, **24**, 205.
7. M. E. Fine and R. O. Ritchie: in 'Fatigue and microstructure', (ed. M. Meshii), 245; 1979, Metals Park, Ohio, American Society for Metals.
8. S. J. Hudak: *J. Eng. Mater. Technol. (Trans. ASME H)*, 1981, **103**, 26.
9. M. H. El Haddad, T. H. Topper, and B. Mukherjee: *J. Test. Eval.*, 1981, **9**, 65.
10. J. Schijve: in 'Fatigue thresholds', (ed. J. Backlund *et al.*), Vol. 2, 881; 1982, Warley, West Midlands, Engineering Materials Advisory Services Ltd.
11. R. P. Gangloff: in 'Advances in crack length measurement', (ed. C. J. Beevers), 175; 1983, Warley, West Midlands, Engineering Materials Advisory Services Ltd.
12. R. O. Ritchie and S. Suresh: in 'Behaviour of short cracks in airframe components', AGARD Conf. Proc. No. 328, 1-1; 1983, Neuilly sur Seine, Advisory Group for Aerospace Research and Development.
13. M. L. Williams: *J. Appl. Mech. (Trans. ASME E)*, 1957, **24**, 109.
14. G. R. Irwin: *J. Appl. Mech. (Trans. ASME)*, 1957, **24**.
15. P. C. Paris and F. Erdogan: *J. Basic Eng. (Trans. ASME D)*, 1963, **85**, 528.
16. J. R. Rice: in 'Fracture: an advanced treatise', (ed. H. Liebowitz), Vol. 2, 191; 1968, New York, Academic Press.
17. J. R. Rice: in 'Fatigue crack propagation', STP 415, 247; 1967, Philadelphia, Pa, American Society for Testing and Materials.
18. H. Tada, P. C. Paris, and G. R. Irwin: 'The stress analysis of cracks handbook'; 1973, Hellertown, Pa, Del Research Corp.
19. G. C. Sih: 'Handbook of stress intensity factors'; 1973, Bethlehem, Pa, Lehigh University.
20. D. P. Rooke and D. J. Cartwright: 'Compendium of stress intensity factors'; 1975, London, HMSO.
21. N. E. Dowling: *Fatigue Eng. Mater. Struct.*, 1979, **2**, 129.
22. R. O. Ritchie: *J. Eng. Mater. Technol. (Trans. ASME, H)*, 1983, **105**, 1.
23. J. W. Hutchinson: *J. Mech. Phys. Solids*, 1968, **16**, 13.
24. J. R. Rice and G. R. Rosengren: *J. Mech. Phys. Solids*, 1968, **16**, 1.
25. J. R. Rice: *J. Appl. Mech. (Trans. ASME)*, 1968, **35**, 379.
26. N. E. Dowling: in 'Cracks and fracture', STP 601, 19; 1976, Philadelphia, Pa, American Society for Testing and Materials.
27. N. E. Dowling and J. A. Begley: in 'Mechanics of crack growth', STP 590, 82; 1976, Philadelphia, Pa, American Society for Testing and Materials.
28. J. W. Hutchinson and P. C. Paris: in 'Elastic–plastic fracture', STP 668, 37; 1979, Philadelphia, Pa, American Society for Testing and Materials.
29. D. M. Parks: unpublished work, Yale University, 1978.
30. C. F. Shih: *J. Mech. Phys. Solids*, 1981, **29**, 305.
31. D. Broek and B. N. Leis: in 'Materials, experimentation and design in fatigue', (ed. F. Sherratt and J. B. Sturgeon), 129; 1981, Guildford, Westbury House.
32. R. O. Ritchie and S. Suresh: *Mater. Sci. Eng.*, 1983, **57**, L27.
33. C. J. Beevers (ed.): 'The measurement of crack length and shape during fracture and fatigue'; 1980, Warley, West Midlands, Engineering Materials Advisory Services Ltd.
34. C. J. Beevers (ed.): 'Advances in crack length measurement'; 1983, Warley, West Midlands, Engineering Materials Advisory Services Ltd.
35. ASTM Standard E647-83 on 'Test method for constant-load-amplitude fatigue crack growth rates above 10^{-8} m cycle', Annual Book of ASTM Standards, Section 3, 710; 1983, Philadelphia, Pa, American Society for Testing and Materials.
36. W. L. Morris, M. R. James, and O. Buck: in 'Nondestructive evaluation – microstructural characterization and reliability strategies', (ed. O. Buck and S. M. Wolf), 387; 1981, Warrendale, Pa, Metallurgical Society of AIME.
37. J. M. Barsom and R. C. McNicol: in 'Fracture toughness and slow stable cracking', STP

559, 183; 1974, Philadelphia, Pa, American Society for Testing and Materials.
38. Y. H. Kim, T. Mura, and M. E. Fine: *Metall. Trans.*, 1978, **9A**, 1679.
39. C. Y. Kung and M. E. Fine: *Metall. Trans.*, 1979, **10A**, 603.
40. W. L. Morris: *Metall. Trans.*, 1977, **8A**, 589.
41. W. L. Morris and O. Buck: *Metall. Trans.*, 1977, **8A**, 597.
42. W. L. Morris: *Metall. Trans.*, 1978, **9A**, 1345.
43. R. Chang, W. L. Morris, and O. Buck: *Scr. Metall.*, 1979, **13**, 191.
44. W. L. Morris: *Metall. Trans.*, 1979, **10A**, 5.
45. W. L. Morris: personal communication, Rockwell International Science Center, Thousand Oaks, Cal., 1983.
46. W. L. Morris: *Metall. Trans.*, 1980, **11A**, 1117.
47. W. L. Morris, M. R. James, and O. Buck: *Metall. Trans.*, 1981, **12A**, 57.
48. M. R. James and W. L. Morris: *Metall. Trans.*, 1983, **14A**, 153.
49. W. L. Morris, M. R. James, and O. Buck: *Eng. Fract. Mech.*, 1983, **18**, 871.
50. G. P. Sheldon, T. S. Cook, T. W. Jones, and J. Lankford: *Fatigue Eng. Mater. Struct.*, 1981, **3**, 219.
51. N. E. Dowling: in 'Cyclic stress–strain and plastic deformation aspects of fatigue crack growth', STP 637, 97; 1977, Philadelphia, Pa, American Society for Testing and Materials.
52. N. E. Dowling: in Proc. ASME 4th Natl Congr. on 'Pressure vessel and piping technology', Portland, Oreg., June 1983, American Society for Mechanical Engineers.
53. R. P. Gangloff: in 'Fatigue crack growth measurement and data analysis', (ed. Hudak and Bucci), STP 738, 120; 1981, Philadelphia, Pa, American Society for Testing and Materials.
54. R. P. Gangloff: *Res Mech. Lett.*, 1981, **1**, 299.
55. M. T. Resch, D. V. Nelson, J. C. Shyne, and G. S. Kino: in Ref. 34, p. 473.
56. W. Baxter: *Int. J. Fatigue*, 1983, **5**, 37.
57. R. P. Gangloff: in 'Embrittlement by the localized crack environment', (ed. R. P. Gangloff); 1984, Warrendale, Pa, Metallurgical Society of AIME, in the press.
58. B. Wiltshire and J. F. Knott: *Int. J. Fract.*, 1980, **16**, R21.
59. S. Usami and S. Shida: *Fatigue Eng. Mater. Struct.*, 1979, **1**, 471.
60. J. F. McCarver and R. O. Ritchie: *Mater. Sci. Eng.*, 1982, **55**, 63.
61. K. Tanaka and Y. Nakai: *Fatigue Eng. Mater. Struct.*, 1983, **6**, 315.
62. J. Byrne and T. V. Duggan: in 'Fatigue thresholds', (ed. J. Bäcklund *et al.*), Vol. 2, 753; 1982, Warley, West Midlands, Engineering Materials Advisory Services Ltd.
63. S. Suresh: *Eng. Fract. Mech.*, 1984, **20**, in the press.
64. K. Tanaka and Y. Nakai: *J. Eng. Mater. Technol. (Trans. ASME H)*, 1984, **106**, 192.
65. J. Lankford and D. L. Davidson: *Acta Metall.*, 1983, **31**, 1273.
66. J. Lankford and D. L. Davidson: *Fatigue Eng Mater Struct.*, 1983, **6**, 241.
67. F. Guiu, R. Dulniak, and B. C. Edwards: *Fatigue Eng. Mater Struct.*, 1982, **5**, 311.
68. S. Pearson: *Eng. Fract. Mech.*, 1975, **7**, 235.
69. O. N. Romaniv, V. N. Siminkovich, and A. N. Tkach: in 'Fatigue thresholds', (ed. J. Bäcklund *et al.*), Vol. 2, 799; 1982, Warley, West Midlands, Engineering Materials Advisory Services Ltd.
70. K. Tanaka, M. Hojo, and Y. Nakai: in 'Fatigue mechanisms: advances in quantitative measurement of fatigue damage', (ed. Lankford *et al.*), STP 811, 207; 1983, Philadelphia, Pa, American Society for Testing and Materials.
71. J. Lankford: *Fatigue Eng. Mater. Struct.*, 1982, **5**, 233.
72. J. Lankford: *Fatigue Eng. Mater. Struct.*, 1983, **6**, 15.
73. D. Taylor and J. F. Knott: *Fatigue Eng. Mater Struct.*, 1981, **4**, 147.
74. C. W. Brown and M. A. Hicks: *Fatigue Eng. Mater. Struct.*, 1983, **6**, 67.
75. Y. Nakai and K. Tanaka: in 'Proc. 23rd Japan congress on materials research', 1980, 106.
76. K. Tanaka, Y. Nakai, and M. Yamashita: *Int. J. Fract.*, 1981, **17**, 519.
77. R. O. Ritchie: *J. Eng. Mater. Technol (Trans. ASME H)*, 1977, **99**, 195.
78. J. Lankford: *Eng. Fract. Mech.*, 1977, **9**, 617.
79. S. Taira, K. Tanaka, and M. Hoshina: in 'Fatigue mechanisms', STP 675, 135; 1979, Philadelphia, Pa, American Society for Testing and Materials.
80. S. Taira, K. Tanaka, and Y. Nakai: *Mech. Res Commun.*, 1978, **5**, 375.
81. S. Suresh: *Metall. Trans.*, 1983, **14A**, 2375.
82. H. Kitagawa and S. Takahashi: in 'Proc. 2nd int. conf. on mechanical behavior of materials', 627; 1976, Metals Park, Ohio, American Society for Metals.
83. D. Taylor: *Fatigue Eng. Mater. Struct.*, 1982, **5**, 305.
84. M. H. El Haddad, K. N. Smith, and T. H. Topper: *J. Eng. Mater. Technol. (Trans. ASME H)*, 1979, **101**, 42.
85. R. C. Boettner, C. Laird, and A. J. McEvily: *Trans. AIME*, 1965, **233**, 379.
86. H. D. Solomon: *J. Mater.*, 1972, **7**, 299.
87. J. R. Haigh and R. P. Skelton: *Mater. Sci. Eng.*, 1978, **36**, 133.
88. M. S. Starkey and R. P. Skelton: *Fatigue Eng Mater. Struct.*, 1982, **5**, 329.
89. M. H. El Haddad, T. H. Topper, and K. N. Smith: *Eng. Fract. Mech.*, 1979, **11**, 573.
90. M. H. El Haddad, T. H. Topper, and K. N. Smith: *J. Test. Eval.*, 1980, **8**, 301.
91. M. H. El Haddad, N. E. Dowling, T. H. Topper, and K. N. Smith: *Int. J. Fract.*, 1980, **16**, 15.
92. H. Ohuchida, A. Nishioka, and S. Usami: in 'Proc. 3rd int. conf. on fracture', April 1973, Munich, Verein Deutscher Eisenhüttenlente, Vol. 5, V-443 A.
93. H. Ohuchida, S. Usami, and A. Nishioka: *Bull. Jpn Soc. Mech. Eng.*, 1975, **18**, 1185.
94. S. Usami: in 'Fatigue thresholds', (ed. J. Bäcklund *et al.*), Vol. 1, 205; 1982, Warley, West Midlands, Engineering Materials Advisory Services Ltd.
95. H. Neuber: *J. Appl. Mech. (Trans. ASME H)*, 1961, **28**, 544.
96. R. E. Peterson: 'Stress concentration factors'; 1974, New York, Wiley–Interscience.
97. R. E. Peterson: in 'Metal fatigue', ed. G. Sines

and J. L. Waisman), 293; 1959, New York, McGraw-Hill.
98. T. H. Topper, R. M. Wetzel, and J. Morrow: *J. Met.*, 1969, **4**, 200.
99. N. E. Dowling, W. R. Brose, and W. K. Wilson: 'Fatigue under complex loading – analysis and experiments', 55; 1977, Warrendale, Pa, Society of Automotive Engineers.
100. R. A. Smith and K. J. Miller: *Int. J. Mech. Sci.*, 1977, **19**, 11.
101. N. E. Dowling: in 'Fracture mechanics', STP 677, 247; 1979, Philadelphia, Pa, American Society for Testing and Materials.
102. H. Kitagawa: in 'Fatigue thresholds', (ed. J. Bäcklund *et al.*), Vol. 2, 1051; 1982, Warley, West Midlands, Engineering Materials Advisory Services Ltd.
103. P. Lukáš and M. Klesnil: *Mater. Sci. Eng.*, 1978, **34**, 61.
104. M. H. El Haddad, K. N. Smith, and T. H. Topper: in 'Fracture mechanics', STP 677, 274; 1979, Philadelphia, Pa, American Society for Testing and Materials.
105. T. H. Topper and M. H. El Haddad: in 'Fatigue thresholds', (ed. J. Bäcklund *et al.*), Vol. 2, 777; 1982, Warley, West Midlands, Engineering Materials Advisory Services Ltd.
106. C. E. Phillips: in 'Proc. colloq on fatigue', 1955, Stockholm, IUTUM, 210; 1956, Berlin, Springer.
107. N. E. Frost: *J. Mech. Eng. Sci.*, 1960, **2**, 109.
108. N. E. Frost and D. S. Dugdale: *J. Mech. Phys. Solids*, 1957, **5**, 182.
109. M. M. Hammouda and K. J. Miller: in 'Elastic–plastic fracture', STP 668, 703; 1979, Philadelphia, Pa, American Society for Testing and Materials.
110. B. N. Leis and T. P. Forte: in 'Fracture mechanics', STP 743, (ed. R. Roberts), 100; 1981, Philadelphia, Pa, American Society for Testing and Materials.
111. N. E. Frost, K. J. Marsh, and L. P. Pook: 'Metal fatigue'; 1974, Oxford, Clarendon Press.
112. W. Elber: in 'Damage tolerance in aircraft structures', STP 486, 230; 1971, Philadelphia, Pa, American Society for Testing and Materials.
113. K. Endo, K. Komai, and Y. Matsuda: *Mem. Fac. Eng., Kyoto Univ.*, 1969, **31**, 25.
114. R. O. Ritchie, S. Suresh, and C. M. Moss: *J. Eng. Mater. Technol. (Trans. ASME H)*, 1980, **102**, 293.
115. A. T. Stewart: *Eng. Fract. Mech.*, 1980, **13**, 463.
116. S. Suresh, G. F. Zamiski, and R. O. Ritchie: *Metall. Trans.*, 1981, **12A**, 1435.
117. N. Walker and C. J. Beevers: *Fatigue Eng. Mater. Struct.*, 1979, **1**, 135.
118. K. Minakawa and A. J. McEvily: *Scr. Metall.*, 1981, **15**, 633.
119. R. O. Ritchie and S. Suresh: *Metall. Trans.*, 1982, **13A**, 937.
120. S. Suresh and R. O. Ritchie: *Metall. Trans.*, 1982, **13A**, 1627.
121. S. Suresh, D. M. Parks, and R. O. Ritchie: in 'Fatigue thresholds', (ed. J. Bäcklund *et al.*), Vol. 1, 391; 1982, Warley, West Midlands, Engineering Materials Advisory Services Ltd.
122. S. Suresh and R. O. Ritchie: *Scr. Metall.*, 1983, **17**, 575.
123. R. A. Schmidt and P. C. Paris: in 'Progress in flaw growth and fracture toughness testing', STP 536, 79; 1973, Philadelphia, Pa, American Society for Testing and Materials.
124. R. O. Ritchie, S. Suresh, and P. K. Liaw: in 'Ultrasonic fatigue', (ed. J. M. Wells *et al.*), 433; 1982, Warrendale, Pa, Metallurgical Society of AIME.
125. S. Suresh and R. O. Ritchie: in 'Concepts of fatigue crack growth thresholds', (ed. D. L. Davidson and S. Suresh), 227; 1984, Warrendale, Pa, Metallurgical Society of AIME.
126. S. Suresh: *Scr. Metall.*, 1982, **16**, 995.
127. S. Suresh: *Eng. Fract. Mech.*, 1983, **18**, 577.
128. S. Suresh and A. K. Vasudévan: in 'Concepts of fatigue crack growth thresholds', ed. D. L. Davidson and S. Suresh); 361; 1984, Warrendale, Pa, Metallurgical Society of AIME.
129. R. J. Cooke, P. E. Irving, G. S. Booth, and C. J. Beevers: *Eng. Fract. Mech.*, 1975, **7**, 69.
130. B. F. Jones: *J. Mater. Sci.*, 1982, **17**, 499.
131. K. J. Miller: *Fatigue Eng. Mater. Struct.*, 1982, **5**, 223.
132. W. T. Chiang and K. J. Miller: *Fatigue Eng. Mater. Struct.*, 1982, **5**, 249.
133. A. Talug and K. Reifsnider: in 'Cyclic stress strain and plastic deformation aspects of fatigue crack growth', STP 637, 81; 1977, Philadelphia, Pa, American Society for Testing and Materials.
134. R. J. Allen and J. C. Sinclair: *Fatigue Eng. Mater. Struct.*, 1982, **5**, 343.
135. J. C. Newman, Jr: in 'Behaviour of short cracks in airframe components', AGARD Conf. Proc. No. 328, 6-1; 1983, Neuilly sur Seine, Advisory Group for Aerospace Research and Development.
136. T. Kunio and K. Yamada: in 'Fatigue mechanism', STP 675, 342; 1979, Philadelphia, Pa, American Society for Testing and Materials.
137. B. A. Bilby, C. E. Cardew, and I. C. Howard: in 'Fracture 1977', (ed. D. M. R. Taplin), Vol. 3, 197; New York, Pergamon.
138. B. Cotterell and J. R. Rice: *Int. J. Fract.*, 1980, **16**, 155.
139. P. J. E. Forsyth: in 'Crack propagation', 76; 1962, Cranfield, Bedfordshire, Cranfield Press.
140. R. M. McMeeking and A. G. Evans: *J. Am. Ceram. Soc.*, 1982, **65**, 242.
141. J. M. Potter and B. G. W. Yee: in 'Behaviour of short cracks in airframe components', AGARD Conf. Proc. No. 328, 4-1; 1983, Neuilly sur Seine, Advisory Group for Aerospace Research and Development.
142. K. A. Esaklul, A. G. Wright, and W. W. Gerberich: *Scr. Metall.*, 1983, **17**, 1073.
143. C. Laird: 'Fatigue and microstructure', (ed. M. Meshii), 149; 1979, Metals Park, Ohio, American Society for Metals.
144. H. Mughrabi: in 'Strength of metals and alloys', (ed. P. Haasen *et al.*), Vol. 3, 1615; 1980, New York, Pergamon.
145. G. Lutjering, H. Dicker, and D. Munz: in 'The microstructure and design of alloys', Vol. 1, 427; 1973, London, The Institute of

Metals and The Iron and Steel Institute.
146. P. Neumann: *Z. Metallkd.*, 1967, **58**, 780.
147. J. G. Antonopoulos, L. M. Brown, and A. T. Winter: *Philos. Mag.*, 1976, **34**, 549.
148. K. Katagiri *et al.*: *Metall Trans.*, 1977, **8A**, 1769.

Book review

The role of crack growth in metal fatigue, L. P. Pook, 210 × 148 mm, 157 pp, paperback, 1983, London, The Metals Society, UK **£15.00** (Members **£12.00**), Overseas **$30.00** (Members **$24.00**)

I thoroughly enjoyed this well written book. It is pitched at a relatively advanced level, so that the reader must have had some previous introduction to fracture mechanics and to metallurgy. But it is most refreshing to have a short account of metal fatigue based on such a wealth of practical experience, and from the standpoint of a mechanical engineer.

The book is not at all comprehensive: it is based largely on work at the National Engineering Laboratory, East Kilbride, and is very much concerned with the framework of fracture mechanics which treats the growth of cracks larger than the grain size. There is no mention of the Coffin–Manson 'law' and only a few sentences on the J-integral, so transatlantic readers may be disappointed. The process of crack nucleation by plastic flow in smooth specimens is scarcely mentioned. The book is really a welcome distillation of the earlier, much longer book by the NEL team of Frost, Marsh, and Pook.

Am I right in thinking that with the wide acceptance of the framework of fracture mechanics the next step is to incorporate into the design of structures features which will make the monitoring of cracks easier or even perhaps automatic, such as built-in ultrasonic transducers? This vision of design philosophy is hinted at in various places in the book, and is a current topic of discussion among workers in the field. If it comes about, it will be a spectacular vindication of the scientific view of fatigue as the cycle-by-cycle growth of a crack.

In the final chapter, Dr Pook suggests that the next step in understanding fatigue is likely to emerge from a fresh look at fatigue behaviour on an atomic or near-atomic scale. One cannot but agree. It is now up to those working in the area of crack nucleation and persistent slip to produce as readable a short account of their work as Dr Pook has produced of his, to demonstrate to mechanical engineers and designers that considerable understanding at this level has in fact emerged from recent work. I am certain that every scientist concerned with the phenomenon of fatigue will appreciate Dr Pook's exposition of his point of view.

L. M. BROWN

Report No. UCB/RP/84/A1018

ENVIRONMENTAL EFFECTS NOVEL TO THE PROPAGATION OF SHORT FATIGUE CRACKS

R. P. Gangloff

Exxon Research and Engineering Co., Annandale, NJ 08801

and

R. O. Ritchie

Department of Materials Science and Mineral Engineering
University of California, Berkeley, CA 94720

March 1984

IUTAM/ICF/ICM Conference on "Fundamentals of Deformation and Fracture"
Published in the Proceedings of the Eshelby Memorial Symposium,
University of Sheffield, April 1984,
B. A. Bilby and K. J. Miller, eds., Cambridge University Press, 1984

ENVIRONMENTAL EFFECTS NOVEL TO THE PROPAGATION OF SHORT FATIGUE CRACKS

R. P. Gangloff

Exxon Research and Engineering Co., Annandale, NJ 08801, U.S.A.

R. O. Ritchie

University of California, Berkeley, CA 94720, U.S.A.

ABSTRACT

Crack size and opening morphology dominate the mechanical and chemical driving forces for fatigue propagation in embrittling environments. Similitude based on a crack tip field parameter is compromised, particularly for small cracks (< 5 mm) which grow up to several orders of magnitude faster than projected and below apparent threshold conditions. Environment sensitive mechanical and chemical mechanisms which govern the growth of small cracks are reviewed. For the former the retarding effect of crack closure; originating from wake plasticity, surface roughness, deflection, corrosion debris or fluid pressure; increases with increasing crack size particularly within the near threshold regime. Data for high strength steel in H_2 demonstrate the importance of such mechanisms, however, precise models of crack size dependencies and systematic closure measurements are lacking. Considering the chemical driving force, the embrittling activity of the occluded crack differs from that of the bulk environment, and is geometry dependent. The deleterious influence of small crack size is demonstrated experimentally for steels in aqueous chloride solutions, and related quantitatively to crack opening shape and size effects on diffusion, convective mixing and electrochemical reaction. Small crack size promotes hydrogen embrittlement due to enhanced hydrolytic acidification and reduced oxygen inhibition. Chemical crack size effects are material and environment specific; criteria defining limiting crack sizes and opening shapes for K or J-based similitude do not exist.

1. INTRODUCTION

Fracture mechanics analyses of subcritical crack propagation are based on the fundamental notion that a characterizing parameter such as stress intensity (K) or the J integral describes remote loading and geometry effects on crack tip stress and strain distributions, and hence the kinetics of slow growth.(1-3) By similitude, cracks extend at equal rates when subjected to equal mechanical driving forces. Fracture mechanics scaling of laboratory data to predict component life is established, only in part, for fatigue and statically loaded cracks in benign and embrittling environments.(4-8) Recent investigations indicate that stress intensity-based similitude must be modified to account for plasticity,(9) crack motion,(10) closure,(11) deflection,(12) crack size,(13) and environment.(14)

Extensive data demonstrate that short cracks grow faster than projected and below apparent threshold conditions compared to long crack (25-50 mm) kinetics at constant stress intensity.(11,13,15-30) Typically for benign environments, the limiting crack size for deviations from K-based similitude increases from 10 μm for high strength alloys to about 1 mm for low strength materials, as reviewed from a mechanical perspective.(11,13,15-17,31)

In active environments rates of fatigue crack propagation are controlled by interrelated mechanical and chemical driving forces.(32,33) Critically, each driving force is crack size, shape and applied stress sensitive. The theses of this review are that small crack size influences uniquely the mass transport and reaction components of the chemical driving force, and that environmental modifications of the mechanical driving force are novel within the short crack regime. Mechanical and chemical factors which lead to breakdowns in similitude for small fatigue cracks, and which are traceable to environmental effects, are characterized separately.

Data establish the importance and complexity of small crack-embrittling environment interactions. Threshold stress versus crack size results in Fig. 1 indicate threshold stress intensity range (ΔK_o) control for long cracks, and constant stress or endurance limit control for very short cracks in 13Cr steel at two stress ratios (R).(20) While similar size dependencies are observed for moist air and liquid water, crack growth deviates from ΔK_o control at larger limiting crack sizes for the later environment. Embrittlement, evidenced by reduced stress, is promoted for decreased crack size and lower R. Geometry sensitive chemical and mechanical closure effects contribute to the trends depicted in Fig. 1. The potential for small crack chemical contributions to corrosion fatigue, independent of mechanical effects, is illustrated in Fig. 2.(21,24) Cracking in vacuum and moist air is defined

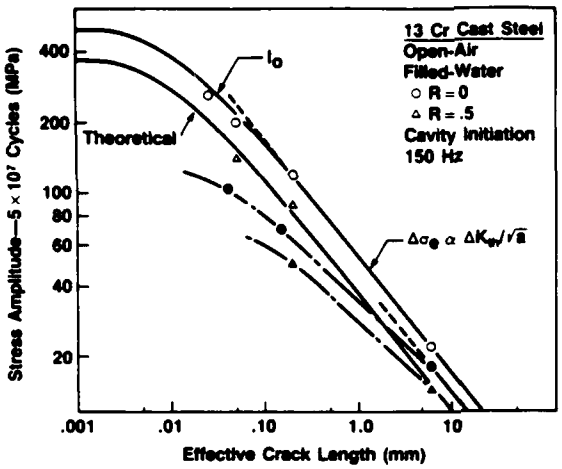

FIG. 1. Variation of fatigue threshold stress with crack length for cast 13Cr steel in air and water at two stress ratios. Note ΔK_o control for long cracks and endurance stress control for short cracks. After Usami and Shida (1979).

uniquely by ΔK, independent of crack size and applied stress. In contrast small cracks in aqueous NaCl grow up to 300 times faster than long cracks at constant ΔK. A multiplicity of da/dN-ΔK relations is observed; chemical embrittlement is enhanced for decreased crack size or reduced stress, and correlates with crack opening shape.(14) Data in Fig. 3 demonstrate the role of crack closure independent of chemical effects.(34-38) Based on long crack

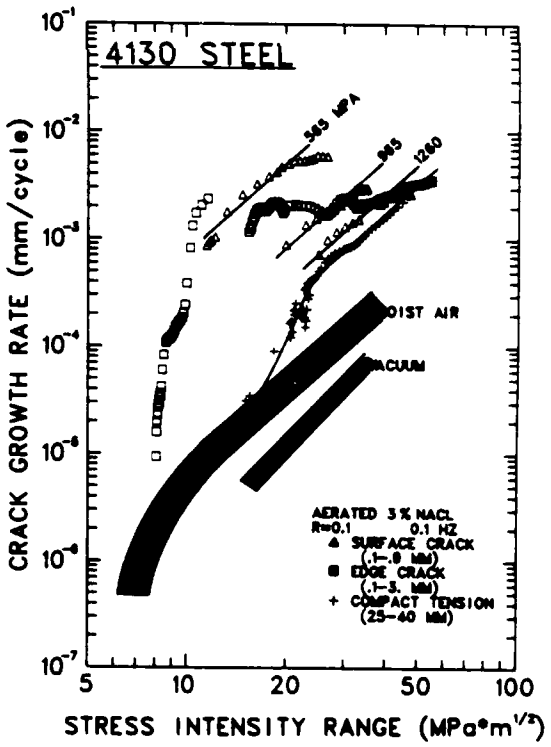

FIG. 2. Crack growth rate versus stress intensity range data for variably sized cracks in high strength (1330 MPa) 4130 steel. Note the accelerated growth of physically short cracks only in aqueous NaCl, and the stress dependence of small crack corrosion fatigue ($\Delta\sigma$ values are listed for surface cracks). After Gangloff (1984).

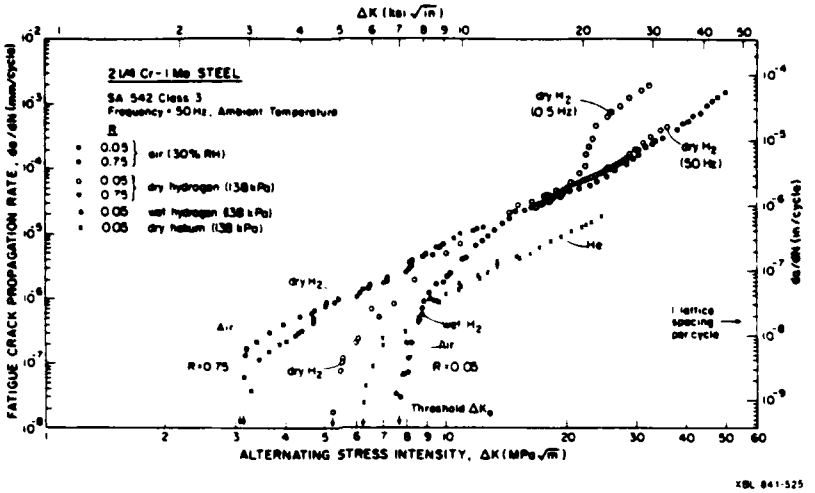

FIG. 3. Influence of load ratio and environment on fatigue propagation of long (~ 50 mm) cracks in low strength bainitic 2 1/4Cr-1Mo steel (σ_0 = 500 MPa) in moist air, dry helium and hydrogen gases at R = 0.05 and 0.75. Note the contrasting effect of environment at near-threshold and higher growth rates. After Suresh and Ritchie (1982).

measurements and applied stress intensity, hydrogen embrittlement predominates for high ΔK low frequency conditions, whereas closure dominates crack growth at high frequencies in the near-threshold regime. Reduced rates of growth correlate with low R and moist environments which promote corrosion debris and crack surface contact. Faster growth rates are observed for high R and environments such as He and H_2 which maintain clean crack surfaces.

Environment-assisted growth of small fatigue cracks; nucleated from corrosion pits, weld defects, scratches, porosity or inclusions; is an important failure mode often dominating total life.(39-44) In an example of a pipeline carrying H_2S contaminated oil,(39) 85% of an 87 year (predicted) fatigue life is associated with the growth of a 0.5 mm starting flaw to 1.0 mm. Accelerated short crack growth (e.g., Fig. 2) could reduce total life by 50 to 100 fold. To date, however, most life prediction analyses have scaled long crack data, without accounting for short crack-environment interactions.(45,46)

2. SMALL CRACK-ENVIRONMENT INTERACTIONS: MECHANICAL DRIVING FORCE

2.1 CONCEPT

Of the factors contributing to crack size similitude problems through effects on the mechanical driving force, local

plasticity, crack deflection and crack closure are of major importance as illustrated in Fig. 4.(11,13,15-20) Each of these processes can be modified strongly by an embrittling environment, for example through the role of adsorbed hydrogen in affecting dislocation behavior, or the enhancement of crack closure through crack surface corrosion products or roughness. We examine the influence of environment on the processes affecting the mechanical driving force, and highlight effects unique to small cracks.

2.2 ACTIVE CRACK TIP PLASTICITY

A primary reason for crack size effects is the inappropriate characterization of crack tip fields. Inaccuracies result from the use of linear elastic fracture mechanics to describe crack growth behavior in the presence of extensive local plasticity, i.e., where crack length (a) is comparable with the extent of the active plastic zone ahead of the crack tip, $r_y \sim (1/2\pi)(K_I/\sigma_0)^2$, or where the crack is embedded within the strain field of a notch (Fig. 4a). Plasticity effects may dominate at crack sizes below a limiting length ℓ_0, given by $1/\pi(\Delta K_0/\Delta\sigma_e)^2$, where ΔK_0 is the long crack threshold and $\Delta\sigma_e$ is the smooth bar fatigue limit.(25,47)

The extent of local plasticity is often influenced by environment.(48) There is clear experimental evidence that dissolved hydrogen can affect the flow stress of materials.(48,49) In high purity iron softening is observed at temperatures above 200 K, whereas hardening is seen at lower temperatures. In steels

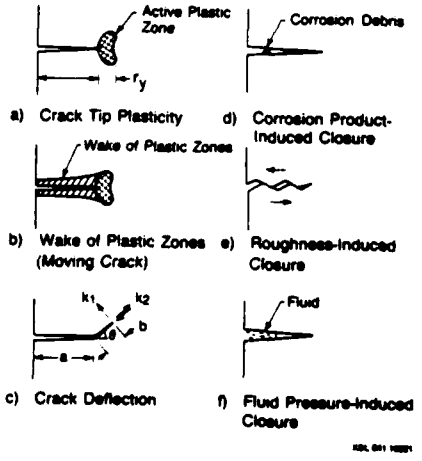

FIG. 4. Schematic illustrations of mechanisms for breakdowns in similitude relevant to small fatigue cracks in embrittling environments.

conversely, softening has been associated with single slip deformation and hardening with multiple slip, and the environmental influence declines with increasing alloy strength. The mechanisms for hydrogen effects on plasticity are imprecise.(48) Hydrogen segregation to dislocation cores enhances double kink nucleation on screw dislocations which facilitates movement. (The effect on edge dislocations may be exactly the reverse.) Softening may also result from the formation of voids induced by high fugacity hydrogen (i.e., during charging). Hardening is related to hydrogen atmospheres on dislocations or increased, hydrogen-stabilized vacancy concentrations, factors which may impede dislocation motion.

With respect to fatigue crack growth, in situ measurements in 7075-T651 aluminum alloys indicate decreased crack tip plasticity, in the form of reduced crack tip fracture strains, in water vapor compared to dry nitrogen and due to the embrittling effect of hydrogen.(50) Conversely, recent studies of aluminum show fatigue cracks to remain sharp when exposed to inert atmospheres, due to a Mode II + I opening, yet to become blunt in moist air where purely Mode I opening occurs.(28) The contributions of crack tip shape, closure, deflection and chemical embrittlement are not fully understood.

While a fundamental mechanism for environment-crack tip deformation interactions is not available, it is clear that environmental effects on plasticity and crack opening morphologies are crucial for the small crack regime.(28) To alleviate the problem of local plasticity, the use of non-linear elastic fracture mechanics, specifically involving the ΔJ parameter, has been suggested.(9,17,25) Data for short surface cracks in elastic-plastic low cycle fatigue samples correlated with conventional long crack results, through the use of ΔJ in place of ΔK as the generalized crack driving force.(12,25) In balance, however, this approach is imprecise for small cracks in elastically loaded material. The use of J is questionable for crack growth, since it is strictly defined for monotonic, increasing, proportional loading.(2,3) Environmental effects on material flow properties must be defined, and the resultant influence on small crack driving force quantified.

2.3 CRACK TIP WAKE PLASTICITY

In addition to active plasticity ahead of the crack, it is necessary to consider the enclave of prior plastic zone left behind the crack tip, particularly when crack size approaches the scale of local plasticity (Fig. 4b). Recent asymptotic analyses of monotonically loaded, Mode I non-stationary cracks indicate that the crack tip strain singularity weakens as the crack moves.(10) Specifically in the limit as $r \to 0$, the plastic strain distribution, $\gamma_p(r)$, is given in terms of an effective plastic zone size (r_y'),

Poisson's ratio (ν) and constant (m) as:

$$\gamma_p = \frac{m}{\sigma_o}\frac{dJ}{da} + \frac{1.88(2-\nu)\sigma_o}{E}\,\ell n\left(\frac{r'_y}{r}\right) \qquad (1)$$

Thus, due to wake plasticity behind the growing crack, crack tip strains decay as $\ell n(1/r)$, rather than as $1/\sqrt{r}$ or $1/r$ for a stationary crack in a linear elastic or perfectly plastic solid. This implies that at a fixed K_I or J, the plastic strains ahead of a stationary crack exceed those ahead of a slowly moving crack with its trailing wake of plasticity. More importantly since short cracks sized below r_y have by definition a limited wake, larger plastic strains must occur ahead of a moving short crack compared to the equivalent long crack at the same K_I or J. Recent in situ crack tip deformation measurements on growing fatigue cracks in 7075 aluminum alloy clearly show this to be the case. The strain distribution ahead of a long crack at low ΔK conforms to a $\ell n(1/r)$ singularity,(51) and corresponding crack tip strains and opening displacements for small cracks, 30 to 200 μm in length, are significantly higher.(18)

The effect of wake plastic zone on the mechanical crack driving force and the significance to the crack size similitude question is influenced by chemical factors since environment can affect plasticity. There is, however, no characterizing parameter currently available which considers wake plasticity effects as a function of material flow properties, and which describes driving force independent of crack size.

2.4 CRACK DEFLECTION

Crack deflection contributes to a lack of similitude by causing the near tip driving force to differ from the globally computed K_I or J (Fig. 4c).(15) In general Mode I crack growth data are correlated in terms of K_I or J assuming a linear crack oriented perpendicular to the maximum tensile stresses. Crack paths can, however, deflect out-of-plane due to metallurgical and environmental interactions such that the local driving force at the crack tip is reduced.(12) For an elastic crack deflected through an angle θ and subjected to tensile and shear loads, the local Mode I and Mode II stress intensity factors, k_1 and k_2, are given in terms of the nominal stress intensities, K_I and K_{II}, and angular functions $a_{ij}(\theta)$, as: (52)

$$k_1 = a_{11}(\theta)\,K_I + a_{12}(\theta)\,K_{II} \quad ,$$
$$k_2 = a_{21}(\theta)\,K_I + a_{22}(\theta)\,K_{II} \quad . \qquad (2)$$

For a simply kinked elastic crack, deflection through $\Theta = 45°$ yields $k_1 \approx 0.8K_I$ and $k_2 \approx 0.3K_I$. The 45° crack path deflection induces a significant Mode II shear component at the crack tip and reduces the effective driving force by roughly 15%.(12)

Fatigue crack deflection is promoted by microstructure in duplex structures,(12,53) and at lower ΔK levels where crack growth may be crystallographic, particularly for coarse planar slip materials.(54,55) The effect can be striking for microstructurally-small cracks where prolonged retardation periods or arrest are observed as such cracks encounter and reorient at grain boundaries.(12,26) The crack size dependence upon the mechanics of crack deflection (e.g., Eq. (2)) remains unsolved.

Environmental factors which induce a specific crack path morphology can have a major influence on the mechanical crack driving force through crack deflection. The branching of stress corrosion cracks under specific material/environment/crack velocity conditions,(56) the faceted or crystallographic nature of the fracture plane in certain materials during corrosion fatigue ("brittle" striations in aluminum alloys,(57)) and most importantly the development of intergranular facets and secondary cracks due to hydrogen embrittlement or active path corrosion (4,27,48,57) are examples of environment induced deflection.

The effect of crack deflection is not limited to modifying the local stress intensity for a stationary crack. Under cyclic loading, crack deflection induces irregular fracture surfaces and Mode II crack tip displacements. Such factors promote the development of crack closure, to a degree dependent upon crack length, thus further enhancing the discrepancy between local and global mechanical crack driving forces.

2.5 FATIGUE CRACK CLOSURE

Crack closure, or fracture surface contact, during cyclic loading is a major factor contributing to crack size similitude effects. At lower load ratios (below typically $R = 0.5$) where contact occurs at positive loads (i.e., the closure stress intensity, K_{cl}) during the cycle, the consequence of closure is to reduce the nominal driving force ($\Delta K = K_{max} - K_{min}$) to an effective value, $\Delta K_{eff} = K_{max} - K_{cl}$, where K_{max} and K_{min} are the maximum and minimum applied stress intensities. Crack growth rates decrease in response to the reduced driving force, but often correlate with ΔK_{eff}. Crack closure can result solely from cyclic plasticity,(58) or may be developed through several alternate mechanisms as illustrated in Fig. 4.(53) Closure processes include crack surface corrosion product formation, irregular fracture surface morphologies coupled with inelastic shear displacements, and fluid-induced pressure inside the crack. Whereas plasticity-induced

closure is significant at higher ΔK levels approaching plane stress, higher levels of closure may be developed at lower ΔK levels approaching ΔK_0 (plane strain) through the mechanisms depicted in Fig. 4.

All closure phenomena contribute to crack size similitude breakdown through modifications of the near-tip mechanical driving force and to a degree dependent upon crack size. Geometry is crucial because closure must act in the wake of the crack tip. Since short cracks have a restricted wake, growth rate retardations by crack closure mechanisms are limited. At equivalent nominal ΔK levels, short cracks may propagate faster than long cracks due to a higher effective stress intensity. This effect will diminish as closure develops with increasing crack length. Although there is a growing body of experimental evidence to support this notion,(11,19,59,60) with the exception of the fluid pressure-induced closure mechanism, few analytical models exist which incorporate the crack size dependence of closure. Furthermore, indirect, geometry dependent chemical effects on corrosion products and roughness characteristics have not been examined.

CLOSURE INDUCED BY CYCLIC PLASTICITY: Elastic constraint of material surrounding the plastic zone in the wake of the crack front affects material elements plastically deformed at the crack tip, and leads to interference between mating fracture surfaces. Although analyses showing the crack size dependence of closure are not available, recent experimental and numerical studies indicate that the effect of closure diminishes at small crack sizes.(11,19,59-61) Unpublished results by Heubaum and Fine on Van 80 steel (R_B 94) cycled in moist air show this particularly clearly, as reproduced in Fig. 5. High precision closure measurements, using a 0.05 μm sensitivity

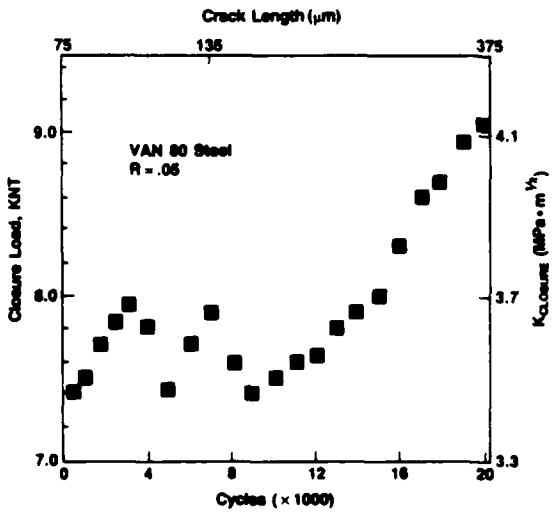

FIG. 5. Experimental evidence for increasing crack closure with increasing small crack size, based on compliance measurements for Van 80 steel cycled in moist air; R = 0.05, K_{max} = 9 to 20 MPa√m. After Heubaum and Fine (1984).

compliance gauge, establish that closure stress intensity (K_{cl}) increases by almost 20% for crack extension from 75 to 375 μm. Although small crack growth rates exceed those for long cracks based on constant ΔK, a unique growth rate-driving force law was reported for ΔK_{eff}.

CLOSURE INDUCED BY CORROSION PRODUCTS: Closure induced by corrosion products(33,53,62-65) is relevant to environmentally influenced crack growth when the size-scale of such debris approaches crack tip opening displacements (v) (Fig. 4d). The mechanism is most potent at low R and at near-threshold stress intensity ranges, especially in lower strength materials where fretting processes during the opening and closing of the crack enhance oxidation and excess deposit formation. The closure mechanism was demonstrated as significant for oxide films formed on alloy steel crack surfaces exposed to moist gases,(53,62-64) and for calcareous deposits produced on structural steel fatigue crack surfaces through electrochemical reactions with seawater.(33,66)

Corrosion product induced closure is modeled approximately in terms of the thickness of excess film (d) and the location of the maximum thickness from the crack tip (2ℓ) to yield:(67)

$$K_{cl} \approx \frac{d\,E}{4\sqrt{(\pi\ell)}\,(1 - \nu^2)} \quad , \tag{3}$$

For air formed oxide, measured values of d (0.01 to 0.2 μm) and 2ℓ (5μm) correspond to a closure K of about 1.5 MPa$\sqrt{m}$. Significant levels of K_{cl} tend to offset the embrittling influence of an aggressive environment which might otherwise accelerate crack growth. In material and environment systems where susceptibility to embrittlement is small, crack growth rates based on ΔK may appear slower in seemingly more corrosive environments (Fig. 3). To date, no analytical representation of the crack size dependence of reaction product closure has been derived. Apart from size effects on the mechanics of closure, the thickness and composition of reaction products are determined by mass transport and electrochemical reaction, processes which are crack geometry sensitive as developed in ensuing sections.

CLOSURE INDUCED BY FLUID PRESSURE: Environment may influence crack closure through the hydrodynamic wedging effect of fluids inside the crack during cyclic loading (Fig. 4f).(37,39,59) Fluids may induce an internal pressure relatable to a stress intensity (K^*_{max}) which opposes the opening and principally the closing of the crack, and which reduces the effective stress intensity range at the tip to $\Delta K_{eff} = K_{max} - K_{min} - K^*_{max}$. This mechanism results in frequency and viscosity sensitive fatigue crack growth rates in inert fluids. Trends in behavior with these variables are difficult to predict since higher viscosity fluids, which induce higher fluid pressures,

are kinetically limited in their ability to fully ingress into the crack.(59)

Experimental and theoretical analyses of fluid pressure closure provide estimates of K_{cl} as a function of frequency, viscosity and crack size.(38,59) Internal fluid pressure p(x) is distributed along a crack of depth, a, and average opening width, $\langle h \rangle$, according to:

$$p(x) = 6\eta\rho \frac{\dot{h}_{max}}{h^3_{max}} a^2 \, \ell n(1 - x/a), \quad \text{for } d/a = 1$$

$$\text{or} \quad p(x) = 6\eta\rho \frac{\langle \dot{h} \rangle}{\langle h \rangle^3} x(x - d), \quad \text{for } d/a < 1 \quad , \tag{4}$$

where ρ is fluid density and η is kinematic viscosity. The extent of fluid penetration (d) during a fatigue load cycle is time dependent and estimated based on capillary flow to be:

$$d^2(t) \sim \frac{\gamma \cos \beta}{3\eta\rho} \int_0^t \langle h \rangle dt \quad , \tag{5}$$

where β is the wetting angle and γ is surface tension. This analysis suggests that the magnitude of closure typically saturates at K_{cl}/K_{max} values approaching 0.5, based on fluid viscosities between 5 and 60,000 cS and growth rates between 10^{-6} and 10^{-3} mm/cycle, indicating that the mechanism is less potent than oxide or roughness-induced closure.(59)

Equations 4 and 5 predict that fluid pressure, and hence the degree of closure, are related to crack size and are diminished at smaller crack lengths. Predictions of closure stress intensity (K^*_{max}) due to fluid pressure, generated by oils of viscosities varying from 5 to 60,000 cS, are shown in Fig. 6 for a 2 1/4Cr-1Mo steel cycled at R = 0.05 and 50 Hz. K^*_{max} decreases as crack length approaches zero, and to a degree dependent upon viscosity. At a fixed nominal ΔK, the smaller crack experiences a higher effective driving force, and hence propagates at a faster speed.

CLOSURE INDUCED BY FRACTURE SURFACE ROUGHNESS: Environmental factors can influence the extent of crack closure through an effect on fracture morphology (Fig. 4e). Irregular fracture surfaces; produced by microbranching, intergranular separation or crystallographic cleavage, together with local mixed mode crack tip displacements; promote roughness induced closure during unloading.(34,35,64,68,69) K_{cl} is developed through premature contact of pronounced asperities. For example, in high strength steels where near-threshold growth rates are often lower in

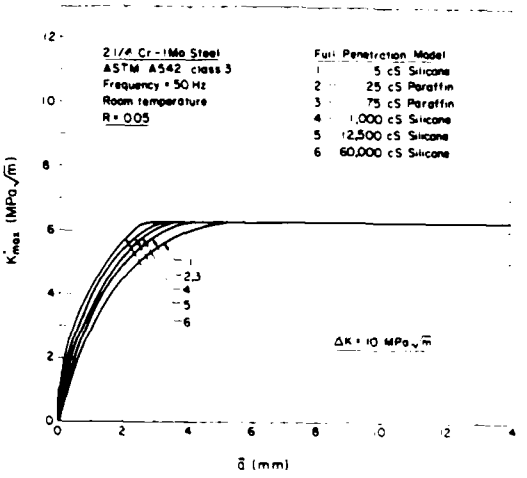

FIG. 6. Evidence for decreased K_{cl} at small crack lengths based on predictions of fluid-induced closure forces for crack propagation in silicone and paraffin oils. K^*_{max} is the stress intensity resulting from fluid pressure and is equivalent to K_{cl}. After Tzou, Hseuh, Evans and Ritchie (1984).

potentially embrittling gaseous hydrogen environments compared to moist air, the intergranular nature of hydrogen-induced fracture surfaces promotes fretting corrosion debris and asperity contact during cyclic loading, leading to closure of varying degrees in each environment.(36,60)

Roughness induced closure is modeled in terms of the extent of surface roughness, or the ratio of asperity height to width (γ), and the ratio of Mode II to Mode I crack tip displacements (μ):(68)

$$\frac{K_{cl}}{K_{max}} = \sqrt{\left(\frac{2\gamma\mu}{1+2\gamma\mu}\right)}. \qquad (6)$$

K_{cl} is significant at low R and for crack tip displacements comparable with asperity size.(68,69) Crack size may influence both the degree of fracture surface roughness through a chemical mechanism and the level of K_{cl} based on crack mechanics. The latter geometry effect has not been analyzed to date, while the former mechanism is considered in Section 3.

2.6 HYDROGEN ASSISTED GROWTH OF SMALL CRACKS IN STEEL

A novel small fatigue crack-environment interaction, traceable to the combined effects of mechanical closure and chemical transport, is summarized in Fig. 7 for 4340 steel (σ_o = 1030 MPa) stressed in either gaseous hydrogen or helium. At low R (Fig. 7a) 0.1 to 1 mm edge cracks grow five times faster than long (25-50 mm) cracks in compact tension specimens at constant ΔK and in H_2. Cracking in He is well defined by ΔK independent of crack size for this class of steels (e.g., Fig. 2 and Refs. 13,24,[illegible]).

AD-A182 949 FATIGUE BEHAVIOR OF LONG AND SHORT CRACKS IN ALUMINUM ALLOYS..(U) CALIFORNIA UNIV BERKELEY DEPT OF MATERIALS SCIENCE AND MINERA.. R O RITCHIE ET AL. 01 MAY 87 3/3

UNCLASSIFIED UCB/RP/87/A1047 AFOSR-TR-87-0872 F/G 11/6.1 NL

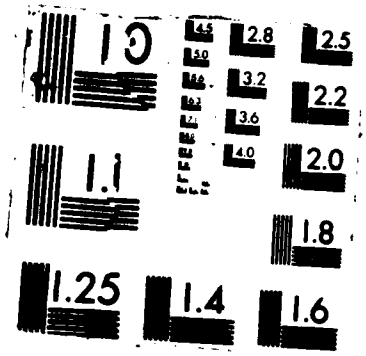
1.0
1.1
1.25
1.4
1.6
1.8
2.0
2.2
2.5
2.8
3.2
3.6
4.0
4.5
5.0

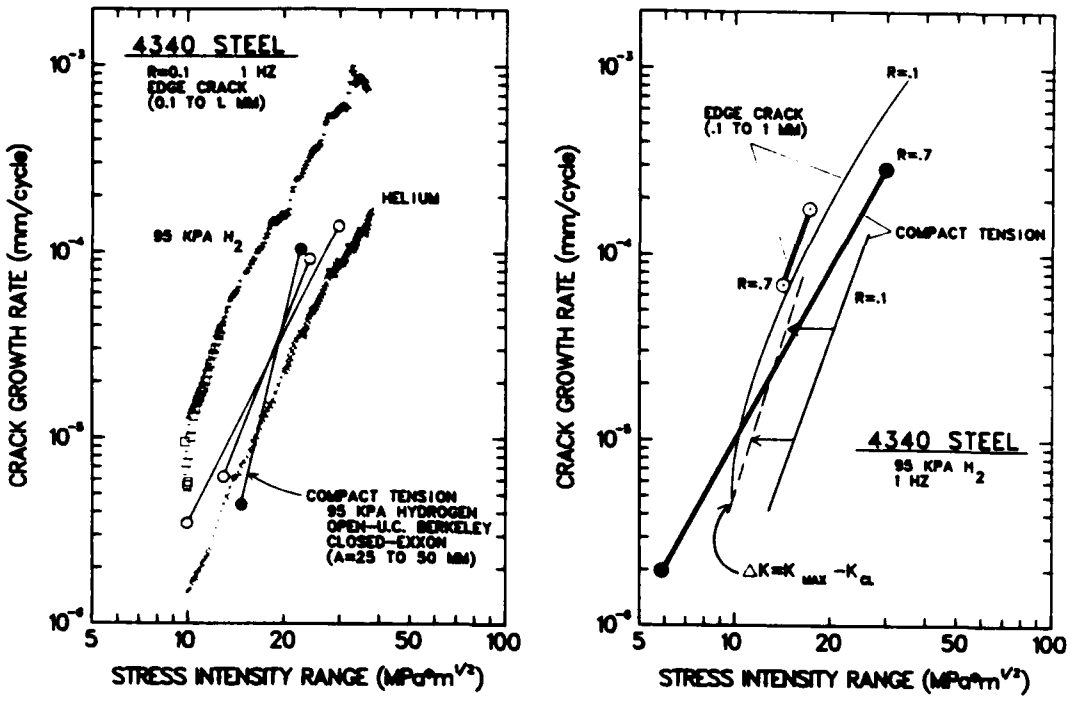

(a) (b)

FIG. 7. The effect of crack size on fatigue growth kinetics for 4340 steel (σ_0 = 1030 MPa) exposed to purified (95 kPa) H_2. (a) 0.1 to 1 mm edge and 25 to 50 mm compact tension cracks at R = 0.1. Note the accelerated growth of small cracks. (b) Edge and surface cracks for R = 0.7. Note the similar growth rates for long and short cracks at high R and the role of closure for long cracks at low R.

The breakdown in similitude for small cracks is also observed for higher strength (σ_0 = 1360 MPa) 4130 steel in H_2.(70) At the high R value where closure is minimized, growth rates for the long crack approach short crack speeds for H_2 (Fig. 7b). In contrast short crack growth rates in H_2 are equivalent at R = 0.1 and 0.7. When low R, long crack results are adjusted for closure based on ΔK_{eff} computed from compliance estimates of K_{cl}, the differences between long and short crack speeds become small as shown by the dashed line in Fig. 7b. Equivalent growth rates are observed for cycling from K_{min} to K_{max} and from K_{cl} to K_{max}, demonstrating the absence of damage for changing stress intensity below K_{cl}.

The crack size effect summarized in Fig. 7 is reasonably explained based on closure. Since crack geometry effects are

accounted for by applied ΔK for high strength alloys in inert environments, the origin of the closure variations must be environmental. Precise micromechanisms for such behavior are uncertain, but the results are consistent with a rougher intergranular fracture surface in hydrogen which both promotes crack deflection and roughness induced closure. This view is speculative. Crack closure was not estimated for short cracks, and no quantitative model exists to explain the crack size dependence of K_{cl} for given roughness. Additionally, roughness differences were not quantified for the cracks represented in Fig. 7.(69) Cracks produced in H_2 were only partially intergranular. Finally, the chemical driving force for embrittlement may be crack size sensitive, and contribute to or dominate mechanical closure.

3. SMALL CRACK-ENVIRONMENT INTERACTIONS: CHEMICAL DRIVING FORCE

3.1 CONCEPT

Crack size and opening shape effects on the chemical driving force for brittle crack growth compromise the stress intensity similitude concept for both static and cyclic stressing. It is unreasonable to assume apriori that a mechanics based crack tip field parameter will describe a chemical driving force. Local crack chemistry controls environment assisted subcritical cracking, and differs from that of the bulk due to enrichment (or depletion) of embrittling (or inhibiting) constituents.(71) The chemistry and embrittling activity of the occluded crack environment is geometry sensitive because of crack size and shape effects on mass transport by diffusion and convection, electrochemical potential and on reaction kinetics.(72-78)

Experiment and transport-reaction modeling are required to define the crack size range where geometry effects on crack chemistry are significant for a given material and environment. Chemical crack size effects are particularly relevant for small cracks because of: (a) the proximity of the crack tip to the bulk environment and applied potential,(73,76) (b) the crack size dependence of convective pumping,(78,79) (c) the large crack surface area to occluded solution volume ratio,(14,24) (d) the likelihood of tortuous crystallographic cracking influencing transport,(54) and (e) the sensitivity to localized environment enhanced plasticity.(26,28) Geometry effects may remain constant with increasing crack size beyond a saturation point,(29,57) consistent with demonstrations of ΔK similitude for aqueous environments.(4-7,50,80)

Chemical crack size effects are predicted for a wide range of embrittling environments. (24,72,73,76,77,81,82) Experimental

confirmations are, however, lacking because of the difficulties associated with isolating chemical and mechanical effects on similitude, and with monitoring the growth of small cracks.

3.2 GASEOUS ENVIRONMENTS

THEORETICAL MODELING: Gaseous environment enhanced fatigue crack propagation rates are controlled by the slow step in the sequence including gas transport, adsorption, diffusion, and chemical embrittlement.(29,32,72) For free molecular flow, collisions between gas molecules and crack walls dominate transport and impede the arrival rate of reactive species at the crack tip.(71,81) Local gas pressure is reduced below the bulk level, and embrittlement is decreased provided that gas transport is rate limiting.

Gas transport to the tip is crack size and opening shape sensitive. Impeded flow occurs when molecular mean free path (λ) exceeds crack opening displacement (ν), with impedance beginning for ν below about 100 λ.(72) Mean free path equals 0.1 μm for H_2, N_2, O_2 and H_2O at 300 K and 200 kPa pressure, and varies inversely with pressure and the square of molecular diameter. Considering an edge crack loaded to K = 10 MPa$\sqrt{m}$, crack mouth opening varies from 2 μm for a depth of 0.1 mm to 18 μm at a depth of 15 mm. For the 100 λ interaction criterion, impeded flow should occur over the entire length of the short crack, but over a much longer length for the deep crack. Crack geometry effects are more likely for lower gas pressure (e.g. λ = 20 μm at 5 kPa), for rough crack surfaces and for large molecules (λ = 2 mm for Cd at 5 kPa) relevant to solid metal embrittlement.(82)

Flow impedance (I) is approximated by:(72)

$$I = \left(\phi_1 \int_{a^*}^{a} dx/\nu_{max}^2\right)^{-1} = \phi_2 \sigma^2 a/\log \nu_{max}^* \qquad (7)$$

for a crack of length a along x, of mouth opening, ν, at a stress, σ, the constants ϕ_1 and ϕ_2 and molecular flow starting at a*. Impedance decreases as I increases from 0 to 1, and is time dependent during each stress cycle, $\sigma(t)$. The integral is solved in equation 7 for near tip displacements ($\alpha K/(a - x)$); alternate solutions are obtainable for the complete crack. While approximate, this analysis demonstrates that crack tip pressure and hence embrittling activity depends on stress, crack shape and size. K^2 (or $\sigma^2 a$) in equation 7 results from the assumed form of $\nu(x)$ between a* and a, and is not relatable to a mechanical driving force. ΔK-based similitude is predicted for those long crack cases where changes in log ν_{max}^* due to increasing a, have only a mild effect on I, and for those gases where subsequent steps in the reaction sequence are fast compared to transport.(83) Alternately, within the short

crack regime and at constant K, increasing a results in decreasing I and increasing impedance until crack length equals a*. A multiplicity of growth rates would be projected, and ΔK-based similtude compromised.

EXPERIMENTAL CONFIRMATIONS: Experimental evidence of unique small crack-gas environment interactions is limited, since studies of embrittlement have not focused on either small crack growth kinetics or similitude. Typically, ΔK and crack size vary simultaneously, complicating interpretation. Wei and coworkers reported that constant ΔK loading produced constant crack growth rates independent of crack size for long (> 25mm) cracks in an aluminum alloy in water vapor, supporting similitude.(32) Systemmatic studies of this sort must be extended to variable crack size and shape.

Anomalously rapid growth kinetics for small cracks growing in moist air are not relatable to chemical influences because experiments were not conducted in an inert environment to isolate mechanical effects.(11,13,15-17,31). Lankford demonstrated rapid growth rates for small cracks in an aluminum alloy exposed to moist air at constant ΔK.(28) A larger crack size effect was reported for pure N_2, indicating that water vapor transport and reaction did not dominate the crack size-environment interaction.(28) Holder demonstrated that small fatigue cracks in steel grew at anomalously fast rates at low ΔK compared to extrapolated long crack kinetics for moist air, but not in an inert reference environment.(23) Impeded molecular flow, shielding the long crack tip from embrittling H_2O molecules, was invoked. Experiments were, however, limited and flow impedance was not modeled.

Geometry sensitive gas transport may contribute to the effect of crack size on hydrogen assisted fatigue crack propagation rates, Fig. 7a. 1 to 100 λ equals 0.1 to 10 μm for H_2 at 300 K and 100 kPa. Crack mouth opening displacement at maximum load varies from 0.1 to 7 μm for the small crack geometries and from 40 to 200 μm for the compact tension conditions indicated in Fig. 7a. Larger flow impedances (Equation 7) are expected for the long crack. This simple analysis does not consider surface roughness enhanced molecule-wall collisions, and mass transport due to convection or surface diffusion. If flow impedance caused the chemical crack size effect at low R, then growth rates should be crack size independent at high R where the long crack tip is open and accessible to the bulk environment. A stress ratio effect is observed only for the long crack, (Fig. 7b). Gas transport control is not, however, unambiguously identified because data are equally well explained based on crack closure. Determination of the effect of hydrogen pressure on the magnitude of the crack size effect at constant ΔK would differentiate between impeded gas transport, proportional to $P_{H_2}^{-1}$, and crack closure, independent of P_{H_2}.

3.3 AQUEOUS ENVIRONMENTS

STATIC LOADING: DATA AND THEORY Small crack-environment interactions during static loading provide a basis for understanding more complex chemical crack size effects in fatigue. Superposition concepts relate the environmental effect for each loading mode.(84)

Experimental evidence for chemical crack size effects on stress corrosion cracking is virtually nonexistent. Static load growth rate data, presented in Fig. 8a for 0.1 to 2 mm deep elliptical surface and through thickness edge cracks in 4130 steel (σ_0 = 1330 MPa) exposed to 3% NaCl, show Stage I, K-independent (Stage II) kinetics for replicate specimens. Critically, small cracks grow at faster plateau rates and at stress intensities well

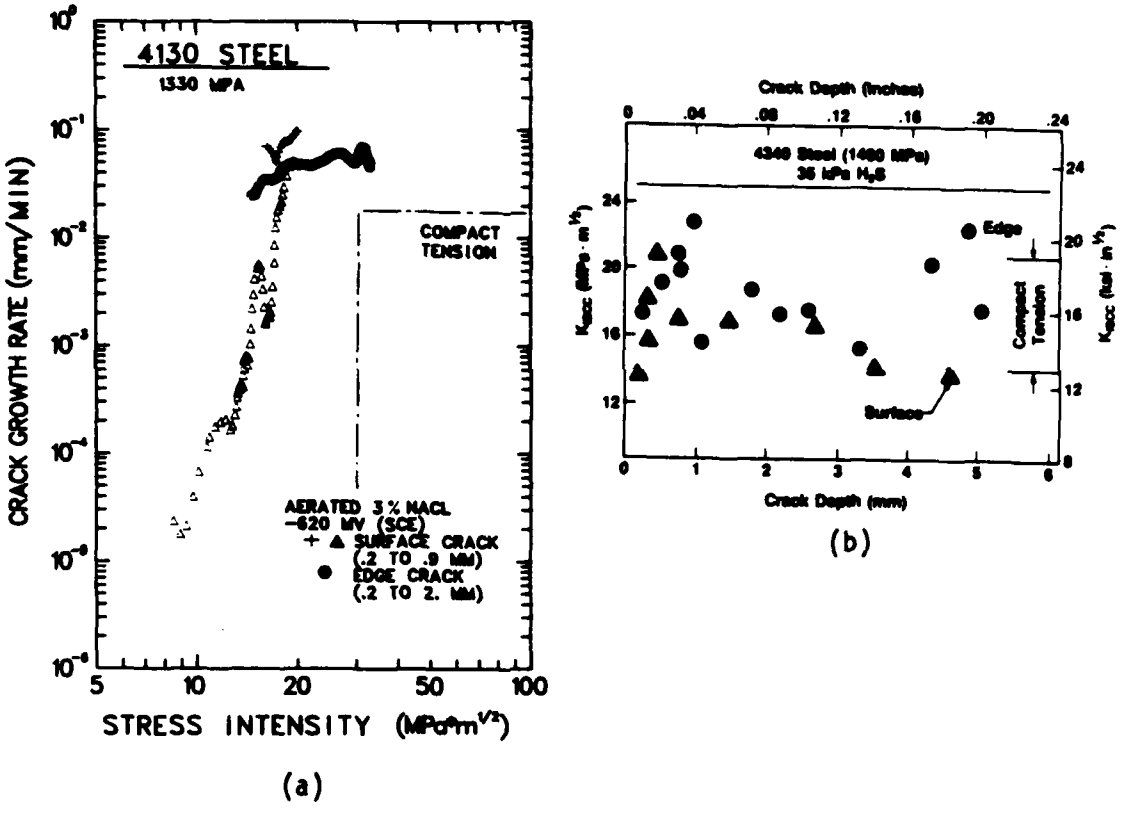

FIG. 8. Crack size effects on static load embrittlement of high strength steels. (a) Growth rate - K data for 0.1 to 2.0 mm deep cracks in 4130 steel (σ_0 = 1330 MPa) exposed to aqueous NaCl. Note the rapid rates of growth for small cracks; after Gangloff (1984). (b) Threshold stress intensity versus crack size for surface and edge flawed specimens of 4340 steel (σ_0 = 1480 MPa) exposed to gaseous H_2S. Note the crack size independence of K_{ISCC} supporting similitude; after Clark (1976).

below the threshold (K_{ISCC}), compared to literature data for long (> 20 mm) cracks in similar steels at constant strength.(85) Shahinian and Judy (7) report constant K_{ISCC} for 3.6 to 10 mm deep elliptical surface flaws and deep cracks in cantelever beam specimens for two strength levels (σ_o = 890 and 1410 MPa) of 4340 steel in 3.5% NaCl.

The crack size effect portrayed in Fig. 8a is traceable to geometry effects on the electrochemical processes which contribute to embrittlement. Cracks at either size scale would not grow in an inert environment at the K levels examined, and crack closure and corrosion product wedging are not relevant. Crack size has no influence on K_{ISCC} for gaseous H_2S embrittlement of a similar steel (Fig. 8b).(85) While embrittlement in aqueous NaCl and gaseous H_2S is attributable to hydrogen, crack geometry only influences solution transport and electrochemical reactions, and hence the level of embrittling hydrogen developed, for the former environment. Specifically, acidic conditions and embrittling hydrogen are produced in the occluded crack exposed to saltwater based on iron and chrome dissolution, water hydrolysis to produce H^+ and cathodic hydrogen and oxygen reductions.(65,86,87) Turnbull and coworkers modeled the geometry dependence of crack potential, pH, dissolved O_2, and cation concentrations leading to hydrogen production; and based on charge and concentration driven diffusional supply of the relevant electrochemical reactions.(55,73,74,89) The material, crack geometry and K conditions of Fig. 8a were analyzed to yield the results listed in Table I. Crack tip acidification (pH), the current density for H^+ reduction (i_H) and the concentration of embrittling hydrogen adsorbed into the metal near the crack tip (C_H) increase significantly with decreasing crack size. Hydrogen reduction is promoted for small cracks through an indirect influence of a reduction in dissolution product concentration by enhanced diffusion. Model predictions are qualitatively consistent with crack growth rate data in Fig. 8a because K_{ISCC} decreases with increasing C_H.

TABLE I

MODEL PREDICTIONS OF LOCALIZED CRACK CHEMISTRY

	CRACK TIP CHEMISTRY*		
CRACK SIZE	pH	Potential (mV-SCE)	i_H A/cm^2 ($\propto C_H^2$)
0.25 mm Deep 0.5 μm Wide	4.1	-638	5×10^{-7}
38 mm Deep 250 μm Wide	8.0	-664	3×10^{-8}

*E_{CORR} = -600mV-SCE Bulk pH = 6.0
K = 10 MPa√m

Model predictions and growth rate data for alternate stress corrosion cracking systems have not been compared to establish the importance of crack size. Doig and Flewitt(76) and Turnbull(73,79) predict that crack propagation rates controlled by anodic dissolution increase with decreasing crack size as shown in Fig. 9 for low alloy steel in a boiling caustic solution. Changing crack size between 0.1 and 2 mm significantly influences crack growth rate, while the effect saturates for larger crack sizes. Applied stress intensity is constant, but growth rate changes with crack size due to a chemical influence. Small cracks are sensitive to embrittlement because of relatively small potential differences between tip and surface, and because of enhanced elimination of dissolution products. Both phenomena promote rates of dissolution.

Smyrl and Newman(88) predict that diffusion supplies a propagating stress corrosion crack tip only for depths less than a_c, given by the ratio of diffusivity (D) to crack speed. For $a > a_c$, crack growth is length dependent at constant applied K, while short cracks propagate at faster rates which are not diffusion limited. For example, a_c equals 1 mm for typical values of D (10^{-3} mm^2/sec) and crack speed (10^{-3}mm/sec., Figure 8). Charnock and Taunt(89) demonstrated that solute penetration by diffusion into the occluded crack solution is proportional to $\sqrt{\nu}$ for a slowly moving crack with chemically reactive crack walls. Environment transport to the crack tip is enhanced for stress and geometry factors which increase crack opening.

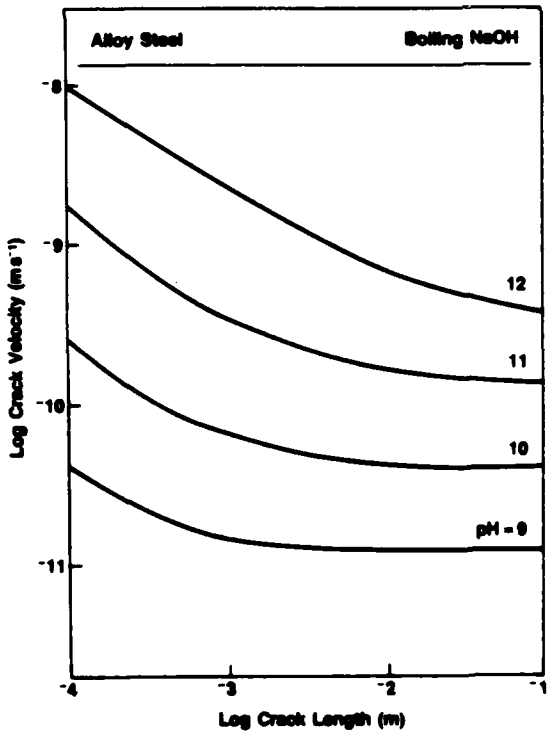

FIG. 9. Predicted effect of crack size on static load growth rates controlled by crack tip anodic dissolution for low alloy steel in boiling NaOH at constant crack opening. After Doig and Flewitt (1983).

CYCLIC LOADING: EXPERIMENTAL RESULTS Small fatigue crack-environment interactions have been investigated only for low alloy steels exposed to aqueous chloride solutions, a system relevant to many applications including offshore structures.(33,65,80,90,91) Specific data are summarized in Table II, where comparisons between short and long crack growth kinetics indicate marked compromises in similitude.

Important trends are apparent based on the data contained in Table II.

i) Small corrosion fatigue cracks always grow faster (between 1.2 and 300 times) than projected based on long crack kinetics at low to moderate ΔK and R values. Crack size influences corrosion fatigue growth rates comparably to well recognized variables.(80)

ii) The size regime for small crack-environment interactions is below about 3 mm. Results are, however, insufficient to exclude a size effect for deeper cracks.

iii) The magnitude of the small crack effect decreases with increasing a at constant $\Delta\sigma$ (increasing ΔK), with increasing $\Delta\sigma$ at constant a and with increasing R. Crack opening shape, approximated by mouth displacement, correlates a, $\Delta\sigma$, ΔK and R effects.(14,24) Stress effects are not universally observed.(29,30)

TABLE II
SMALL FATIGUE CRACK—ENVIRONMENT INTERACTION FOR STEELS IN WATER

Material	σ_y (MPa)	Environment	Crack Size (mm)	Rate Defined By ΔK?	$\frac{da/dN\ Short}{da/dN\ Long}$ @ ΔK Constant	"Short" Crack Regime (mm)	Mechanical Effect Considered	Comments	Ref
AISI 4130 (.3C-.9Cr-.2Mo)	1330	3% NaCl	.1 to 40	Yes-Air No-NaCl	1.2 to 300	.1 to >2.5	Yes	Small crack growth retarded by increased σ_{max}, described by V.	21,24
HY-130 (.1C-.5Cr-5Ni)	—	3% NaCl	.4 to 2.5	Yes-Air No-NaCl	1.0 to 2.5	.4 to 1.0	Yes	ΔK described cracking at a> 1-3 mm; σ_{max} not important.	29
HY-130	930	3% NaCl	.1 to 40	Yes-Air No-NaCl	4.0	.1 to >1.0	Yes	σ_{max} not important.	30
HY-130	930	Seawater	>.5	Yes	1.0	—	Yes	Limited Data.	92
13Cr (.03C-12.5Cr-6Ni)	770	Water	?	No	4.0 @R = 0 High @R = .8	?	No	High frequency, near-ΔK_o data. Size effect intensified at high R. $\Delta\sigma_{th}(a)$ in Fig.1.	20
Q1N (.17C-1.3Cr-2.4Ni)	825	Seawater	.5-6	No	1.0 to 4.0	.5 to 2.0	No	Crack size effect eliminated at $\Delta K > 30$ MPa-m$^{\frac{1}{2}}$ and R .5. K, σ,a interactions, reference environment not considered.	22
BS-4360 (.19-1.17 Mn)	370	Seawater	1-7	Yes-Air No-Seawater	1.0 to 3.0	1.0-3.0	Yes	Crack size effect eliminated for air, cathodic polarization	90
8N6 (.3C-.67Mn)	380	Seawater	>.5	No	1.0 to 3.0	.5 to 2.0	No	Limited Data.	92

iv) The magnitude of the small crack effect decreases with decreasing yield strength, however, a systematic study has not been performed. This trend is consistent with a general decline in both environment sensitivity and the effects of R, frequency and environment activity with decreasing strength.(80,85)

v) The mechanism for the crack size effect is chemical for high strength steels, based on measured crack growth rates in benign environments and on the unlikely occurrence of mechanical effects on similitude for a > 0.1 mm. Mechanical effects may contribute to the rapid growth of short cracks in low strength steels. Studies in an inert environment have not been conducted to separate chemical and mechanical effects for such steels.

vi) Compliance measurements have not been reported for small cracks in embrittling environments. Environment enhanced plasticity, corrosion product and roughness induced closure contributions to retarded cracking cannot be assessed.

vii) The effects of cyclic frequency, electrochemical potential and bulk solution composition on the kinetics of small corrosion fatigue cracks have not been investigated extensively.(14,90)

viii) Small crack corrosion fatigue studies are impeded by problems in crack monitoring,(27) by the low frequencies and ΔK levels of interest,(90) by the possibility of net section yielding (9,25) and by small differences in growth rates, which are none-the-less relevant to long term component integrity.(90,92)

CYCLIC LOADING: THEORETICAL ANALYSES Early explanations for the rapid growth of small corrosion fatigue cracks were based on enhanced environment access to the crack tip.(22,23,54,90) The proximity concept is, however, overly simplistic. Recent results for 4130 steel demonstrate that small crack growth rates decrease with increasing stress and with decreasing crack size for very small cracks; embrittlement decreases as crack opening increases. (14,21,24) Tortuous, Stage I fatigue cracking is often not observed for aqueous environments. The proximity concept implies diffusional flow, however, precise transport mechanisms are not specified. Turnbull(57) demonstrates that mass transport is not necessarily impeded by increased crack depth because of the increasingly important contribution of convection. Finally, the proximity concept does not specify the chemical mechanism for brittle crack

extension. Impeded transport of an inhibiting species to the crack tip will, for example, result in enhanced crack propagation.

Modeling is required to define the effects of crack geometry on the chemical driving force for embrittlement. Mass transport by diffusion and convection determines crack chemistry,(57) which dictates transient reactions with straining crack surfaces,(29) which, in turn, control brittle crack advance. A detailed theory does not exist.(71) Elements of the problem are, however, developed from a hydrogen embrittlement perspective, and are relevant to corrosion fatigue by dissolution and film rupture. For steel in an aqueous solution, hydrogen is produced by hydrolysis within the occluded, pulsating crack.(86,93) The time and cycle dependent corrosion fatigue components to the total crack growth rate, da/dN_{CF}, are defined by (14,29,32,65):

$$\frac{da}{dN_{CF}} = \phi C_H(\sigma,a,t)\ \Delta K^2, \qquad (8)$$

where ϕ is a constant. The chemical driving force is represented by the concentration of adsorbed hydrogen (C_H) which is crack size, stress and time dependent. The mechanical driving force is accounted for by ΔK^2.

If convective mixing is ignored, then modeling of the static crack provides a description of $C_H(\sigma,a,t)$,(57,73,79) with enhanced acidification and hydrogen discharge predicted for decreased crack size (Table I). Since hydrogen embrittlement is probable for the conditions represented in Table II, (65,86,93) this result provides a reasonable explanation for the rapid growth of small corrosion fatigue cracks. For 4130 steel the crack size effect on corrosion fatigue, Fig. 2, is predicted in part based on linear superposition of stress corrosion growth rates for "short" and "long" cracks (Fig. 8a) combined with growth rates for a benign environment.(24) This comparison adds credence to the applicability of the static crack model for hydrogen production.

Crack size dependent convection effects cannot, however, be ignored.(57,74,75,77,78) Considering hydrolysis, no model exists to describe convection effects on electrode potential, pH and metal ion concentrations within a pulsating crack. The importance of crack geometry dependent convection is illustrated by analyses of dissolved O_2 supply and reduction within a crack. Static cracks are presumed to be fully oxygen depleted due to cathodic reduction dominating diffusional supply; O_2 does not affect C_H.(73,74) Convection provides an additional source of oxygen which consumes protonic hydrogen during each load cycle. C_H and da/dN_{CF} are reduced for decreased acidification traceable to "oxygen inhibition".

Perfect mixing analysis of O_2 supply and reaction demonstrates that depletion, and by inference the effect of O_2 on corrosion fatigue, are reduction rate, cyclic frequency, crack size and opening shape dependent. Taunt and Charnock(77) analyzed solute supply and reaction within a crack as a function of load cycles for a variety of rate expressions. Turnbull(74) focused a similar analysis on O_2 depleted at a rate proportional to instantaneous concentration. Each model demonstrates that ΔK similitude is compromised. These approaches were modified(14) to predict the concentration of dissolved $O_2(C_0)$ within small cracks for square wave fatigue loading in aqueous chloride at a frequency of $1/\tau$ and O_2 reduction at a rate given by αC_0. The result is:

$$C_0 = C_B (1 - R) \exp \left(\frac{- \alpha A_c \tau a^*}{2V_{max}}\right) \qquad (9)$$

where C_B = bulk solution oxygen concentration, A_c = crack surface area, V_{max} = crack solution volume at K_{max}, and a^* = geometric constant. For a wedge crack, the ratio of A_c to V_{max} equals $4/\nu_{max}$. As such C_0 depends exponentially on $-1/\nu_{max}$, a parameter which is crack depth sensitive at constant ΔK. (Typically, $\nu_{max} \alpha (\sigma_{max} a) \alpha (K_{max}\sqrt{a})$.) Physically, depletion is controlled by the ratio of active crack surface area available for reaction, a^*A_c, to the occluded solution volume, V_{max}, which supplies reactant. Small cracks are distinguished by a large surface to occluded solution volume ratio, and hence by extremely low values of C_0 compared to long cracks at constant ΔK. Equation 9 is plotted in Fig. 10 as a function of edge crack depth for constant ΔK, frequency and reaction rate conditions. C_0/C_B is on the order of 10^{-40} for 0.1 mm deep cracks, and rises rapidly to values between 10^{-4} and 10^{-2} for cracks deeper than 5 mm.(14)

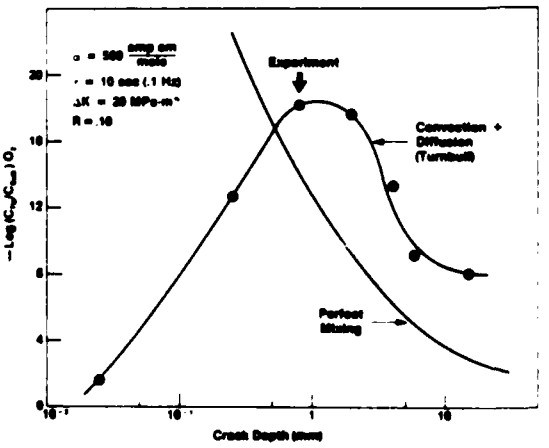

FIG. 10. Analytical predictions of the effect of edge crack length on dissolved oxygen content at constant ΔK. Modeling includes O_2 depletion by cathodic reduction and O_2 supply by either perfect convective mixing (Gangloff, 1984) or diffusion and laminar convection (Turnbull, 1983).

The unique chemical character of small cracks is confirmed by relating perfect mixing to brittle corrosion fatigue. Specifically, the hydrogen ion concentration remaining at the end of a square wave load cycle is calculated based on O_2 reduction to consume H^+ and produce OH^-. O_2 modified acidification is related to C_H and corrosion fatigue crack growth rate through equation 8 to yield either:(16)

$$\text{LOG}\,\frac{da}{dN_{CF}} = \phi + \alpha\tau(a^*/\nu_{max}) \qquad (10)$$

at constant ΔK, or the normalized equation listed and plotted in Fig. 11. (Rates are normalized by an absolute brittle crack growth rate (da/dN_{CF-ABS}) independent of O_2 inhibition to account for the mechanical influence of ΔK^2.) The extent of O_2 inhibition increases as the normalized growth rate parameter decreases from 1.0 to 0. Physically, increased crack length results in increased crack solution volume to active surface area, increased O_2 reduction persisting to longer times during loading, decreased hydrogen production and hence in reduced rates of brittle corrosion fatigue.

The perfect mixing analysis of O_2 inhibition is consistent with experimental results. The logarithm of corrosion fatigue crack growth rate for 4130 steel in saltwater (Fig. 2) varies linearly with reciprocal maximum crack mouth opening as shown in Fig. 11 and predicted by equation 10. The O_2 reduction rate constant inferred from least squares slope analysis is of the correct order. Similar good agreement is observed at constant ΔK without normalization.(14) Considering Fig. 11, compact tension cracking produces small changes in ν_{max} (squares) compared to the results for 0.5 to 3 mm deep edge and surface cracks. The retarding influences

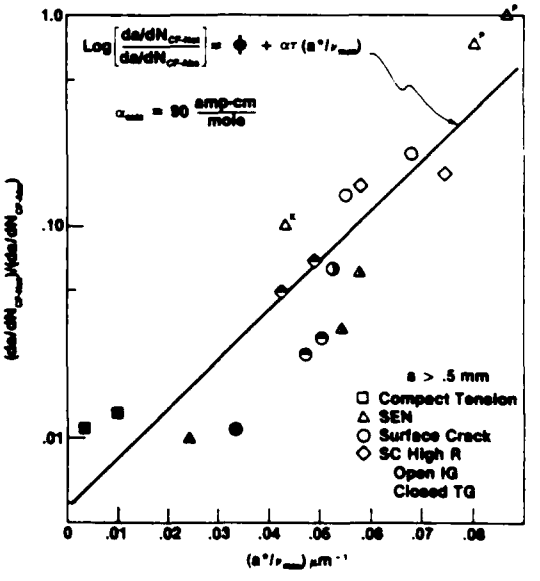

FIG. 11. Experimental data and analytical prediction for the effect of crack shape, given by reciprocal crack mouth opening at maximum load, on corrosion fatigue crack growth rate for 4130 steel in 3% NaCl. Fracture mechanics similitude predicts a horizontal line at 1.0. After Gangloff (1984).

of increased stress, produced by increased R, increased $\Delta\sigma$ or instantaneous stress increases; and of increased crack size are accounted for by maximum crack opening shape. A brittle fracture mode transition occurs with decreasing da/dN_{CF} and correlates with $(\nu_{max})^{-1}$ indicative of a chemical crack size effect. Intergranular cracking (open symbols) at small ν_{max} is replaced progressively by brittle transgranular fracture (filled symbols) at increased ν_{max}. Many of the trends represented for lower strength steels in Table II are consistent with maximum crack mouth opening displacement control and perhaps O_2 inhibition. Small cracks grow at the fastest rates when sized below 1 mm and when stressed at low ΔK and R. Cracking is retarded by increased a, ΔK or R, or equivalently, by increased crack mouth opening.

While the breakdown in ΔK similitude and the correlation between da/dN_{CF} and crack opening are well established in Fig. 11, the O_2 inhibition model is speculative. Acidification differences may contribute to crack size effects, Table I. Experiments with deoxygenated solutions are inconclusive for 4130 steel,(14) relevant values of α are uncertain and may exceed 15 amp-m/mole,(74,75,79) and perfect mixing may provide an inaccurate description of mass transport. Turnbull argues that mass transport within a slowly cycled (< 1 Hz) corrosion fatigue crack is viscous-laminar.(57) Turbulence is expected and perfect mixing is relevant only when crack surface contact occurs. For viscous flow, a transition crack size (a_T) is defined:

$$a_T = \frac{\sqrt{(D/f)}}{1 - R^{(.5 \text{ to } 1.0)}} , \qquad (11)$$

where f is cyclic frequency and the exponent depends on precise crack shape. Diffusion dominates mass transport for cracks sized below a_T, while deeper cracks are supplied predominantly by convection. a_T equals between 0.1 and 0.2 mm for oxygen dissolved in water and a loading frequency of 0.1 Hz.

Crack size, ΔK, frequency, R and chemical reaction rate influence crack chemistry, as illustrated by analysis of diffusional/laminar convectional O_2 supply and cathodic reduction.(57,75,79) A typical prediction is presented in Fig. 10 and compared to the perfect mixing approximation for the same conditions. Note that perfect mixing provides an upper bound on dissolved O_2 within the crack. At very small crack depths, O_2 is enriched significantly due to diffusion. As crack size increases, O_2 diffusion decreases and convection increases. C_0 is minimized, and further increases in crack depth result in increased dissolved O_2 due to convection. The comparison between crack growth rate data and perfect mixing theory, Fig. 11, is for small cracks sized above 0.5 mm to avoid the complicating effects of diffusion. Crack growth rates at constant ΔK for 4130 steel in saltwater exhibit a maximum

at a = 0.8 mm, and decline with increasing and decreasing crack size.(14) The complex effect of crack size on crack chemistry illustrated in Figure 10 may be general. The minimum value of C_0 represents that crack depth where transport of either a bulk specie to the tip or a crack tip reaction product to the bulk is most effectively impeded. Modeling further indicates that, for the long crack convection dominated regime, concentration increases with decreasing O_2 reduction rate and increasing ΔK, R and frequency. Variable effects on the location of the maximum in Figure 10 have not been analyzed in detail. Experimental evidence for crack size effects of the type predicted in Fig. 10 is lacking.

4. SUMMARY

When analyzing the growth of small fatigue cracks in embrittling gaseous and aqueous environments, ΔK or ΔJ based similitude concepts must be examined. Data confirm that small crack geometry effects are not wholly accounted for by a crack tip field parameter. Crack size and opening shape must be considered as variables, and crack closure phenomena characterized experimentally. Unfortunately, it is not possible to provide general criteria which define limiting crack size and shape for ΔK similitude from an environmental perspective. Crack size effects are material and environment specific, and may vary with alloy strength, cyclic frequency, temperature, applied potential or gas pressure. Theoretical analyses of the mechanical and chemical origins of the driving force for brittle crack growth clearly establish the potential for novel small crack-environment interactions. Refined analyses are required, however, to fully define crack geometry effects. Experimental tools exist to assess the importance of crack size effects for specific corrosion fatigue applications.

Understanding of small crack effects is limited for technologically important, low strength alloys in gas, water, chloride or caustic environments, and for both static and cyclic loading. Deleterious chemical crack size effects are documented for high strength steel in aqueous chloride and gaseous hydrogen, and mechanistic understanding is forthcoming. Complicating plasticity and wake, roughness and corrosion debris induced closure effects are unlikely. In contrast research is required for low strength structural steels. Crack size effects are suggested experimentally and hydrogen is known to embrittle such alloys, albeit less severely compared to high strength steels. Environment enhanced plasticity and closure mechanisms are particularly relevant for lower strength alloys. As such, the range of interactions considered in this review may impact corrosion fatigue and produce complex crack size effects. For alternate environments, the potential exists for crack geometry effects on localized chemistry. For example, the chloride conditions described in previous sections were unbuffered and at the free corrosion potential. Transport of buffering species, as

encountered in seawater or inhibited solutions, and the response of crack tip potential and electrochemical reactions to applied potential, as encountered in cathodic protection, are likely to be crack geometry sensitive. Crack geometry effects related to anodic dissolution and film rupture are largely undefined. The research challenge exists to isolate, measure and model such geometry sensitive processes.

ACKNOWLEDGEMENTS

This work was supported by the Corporate Research Science Laboratories of the Exxon Research and Engineering Company (for R.P.G.), and under Grant No. AFOSR-82-0181 from the U.S. Air Force Office of Scientific Research (for R.O.R.).

REFERENCES

(1) Williams, M. L. (1957). Journal of Applied Mechanics, Trans. ASME, 24, 104-109.
(2) Hutchinson, J. R. (1968). J. Mech. Phys. Solids, 16, 13-31.
(3) Rice, J. R. & Rosengren, G. F. (1968). J. Mech. Phys. Solids, 16, pp. 1-12.
(4) McEvily, A. J. & Wei, R. P. (1973). Corrosion Fatigue: Chemistry Mechanics and Microstructure, eds. O. Deveraux, A. J. McEvily and R. W. Staehle, pp. 381-395, Houston: NACE.
(5) Brown, B. F. (1968). Met. Rev., No. 129, 171-183.
(6) Novak, S. R. & Rolfe, S. T. (1970). Corrosion, 26, 121-130.
(7) Shahinian, P. & Judy, Jr., R. W. (1976). Stress Corrosion: New Approaches, ASTM STP 610, ed. H. L. Craig, Jr., pp. 128-142, Philadelphia: ASTM.
(8) Hertzberg, R. W. (1983). Deformation and Fracture Mechanics of Engineering Materials, pp. 519-618, New York: John Wiley and Sons.
(9) Dowling, N. E. (1977). Cyclic Stress-Strain and Plastic Deformation Aspects of Fatigue Crack Growth, ASTM STP 637, pp. 97-121, Philadelphia: ASTM.
(10) Rice, J. R., et al. (1980). Fracture Mechanics, 12th Conf., ASTM STP 700, pp. 189-221, Philadelphia: ASTM.
(11) Suresh, S., & Ritchie, R. O. (1984). Int. Metals Reviews, 25, in press.
(12) Suresh, S. (1983). Metall. Trans. A, 14A, 2375-2385.
(13) Hudak, S. J. (1981). J. Eng. Matls. Technol., Trans. ASME, Ser. H, 103, 26-35.
(14) Gangloff, R. P. (1984). Embrittlement by the Localized Crack Environment, ed. R. P. Gangloff, Warrendale, PA: TMS-AIME, in press.
(15) Ritchie, R. O., & Suresh, S. (1983). Mater. Sci. Eng., 57, 127-130.
(16) Miller, K. J. (1982). Fat. Eng. Matls. Struc., 5, 223-232.

(17) Leis, B. N., et al. (1983). Air Force Wright Aeronautical Labs, Report No AFWAL-TR-83-4019, Wright-Patterson AFB, Ohio.
(18) Lankford, J. & Davidson, D. L. (1984). Fatigue Crack Growth Threshold: Concepts, eds. D. L. Davidson and S. Suresh, Warrendale, PA: TMS-AIME,in press.
(19) Tanaka, K. & Nakai, Y. (1983). Fat. Eng. Matls. Struc., 5, 315-327.
(20) Usami, S. & Shida, S. (1979). Fat. Eng. Matls. Struc., 1, 471-481.
(21) Gangloff, R. P. (1981). Res. Mech. Let., 1, 299-306.
(22) Jones, B. F. (1982). J. Matl. Sci., 17, 499-507.
(23) Holder, R. (1977). Proc. Conf. on Influence of Environment on Fatigue, pp. 37-41, London: Institit. Mech. Engr.
(24) Gangloff, R. P. (1984). Metall. Trans. A, submitted for publication.
(25) El Haddad, M. H., et al. (1980). Int. J. Fract., 16, 15-30.
(26) Lankford, J. (1982). Fat. Eng. Matls. Struc., 5, 233-248.
(27) Gangloff, R. P. (1982). Advances in Crack Length Measurement, ed. C. J. Beevers, pp. 175-221, London: EMAS.
(28) Lankford, J. (1983). Fat. Eng. Matls. Struc., 6, 5-31.
(29) Wei, R. P., et al. (1984). Embrittlement by the Localized Crack Environment, ed. R. P. Gangloff, Warrendale, PA: TMS-AIME, in press.
(30) Hudak, S. J. & Gangloff, R. P. (1984). unpublished research.
(31) Miller, K. J. (1984). Proc. This Conference, Cambridge: Cambridge University Press.
(32) Wei, R. P. & Simmons, G. W. (1981). Int. J. Frac., 17, 235-247.
(33) Scott, P. M. (1984). Corrosion Fatigue Mechanics, Metallurgy, Electrochemistry and Engineering, ASTM STP, Philadelphia, PA: ASTM, in press.
(34) Walker, N. & Beevers, C. J. (1979). Fat. Eng. Matls. Struc., 1, 135-148.
(35) Minakawa, K. & McEvily, A. J. (1981). Scripta Metall., 15, 633-636.
(36) Toplosky, J. & Ritchie, R. O. (1981). Scripta Metall., 15, 905-908.
(37) Endo, K. et al. (1972). Bull. JSME, 25, 439-445.
(38) Tzou, J.-L., et al. (1984). Acta Met, submitted for publication.
(39) Vosikovsky, O. & Cooke, R. J. (1978). Int. J. Pres. Ves. & Piping, 5, 113-129.
(40) Kesten, M. & Windgasser, K.-F. (1981). Hydrogen Effects in Metals, eds. I. M. Bernstein and A. W. Thompson, pp. 1017-1025, Warrendale, PA: TMS-AIME.
(41) Maddox, S. J. (1974). Weld. Res. Suppl., 53, 4015-4095.
(42) Chauhan, P. & Roberts, B. W. (1979). Metall. Matl. Tech., 131-136.
(43) Bennett, J. A. & Mindlin, H. (1973). J. Test. Eval., 1, 152-161.
(44) Jack, A. R. & Paterson, A. N. (1977). Proc. Inst. Mech. Engr. Conf. Fat., paper C107/77, pp. 75-83, London: IMECHE.
(45) Muller, M. (1982). Metall. Trans. A, 13A, 648-655.

(46) Hoeppner, D. W. (1979). Fatigue Mechanisms, ASTM STP 675, ed. J. T. Fong, pp. 841-870, Philadelphia: ASTM.
(47) Kitagawa, H. & Takahasi, S. (1976). Proc. 2nd Intl. Conf. on Mech. Beh. Matls., pp. 627-663, Metals Park, Ohio: ASM.
(48) Lynch, S. (1983). Advances in the Mechanics and Physics of Surfaces, eds. R. M. Latanision and T. E. Fischer, pp. 265-364, New York: Harwood Academic Publishers.
(49) Hirth, J. P. (1980). Metall. Trans. A, 11A, 861-874.
(50) Davidson, D. L. & Lankford, J. (1983). Fat. Eng. Matls. Struc., 6, 241-256.
(51) Lankford, J. (1983). Mechanical Behavior of Materials - IV, eds. J. Carlsson and N. G. Ohlson, 1, pp. 3-29, Oxford: Pergamon Press.
(52) Bilby, B. A., et al. (1977). Fracture (ICF-4), ed. D. M. R. Taplin, 3, pp. 197-212, Waterloo, Canada: Univ. of Waterloo Press.
(53) Suresh, S. & Ritchie, R. O. (1984). Fatigue Crack Growth Threshold: Concepts, eds. D. L. Davidson and S. Suresh, Warrendale, PA:TMS-AIME, in press.
(54) Tomkins, B. (1977). Proc. Conf. on Influence of Environment on Fatigue, pp.111-115, London: IMECHE.
(55) Forsyth, P. J. E. (1962). Crack Propagation, p. 76, Cranfield College of Aeronautics: Cranfield Press.
(56) Tu, L. K. L. & Seth, B. B. (1978). J. Test Eval., 6, 66-74.
(57) Stubbington, C. A. (1963). Metallurgica, 68, 109-121.
(58) Elber, W. (1971) Damage Tolerance in Aircraft Structures, ASTM STP 486, pp. 230-242, Philadelphia, PA: ASTM.
(59) Tzou, J.-L., et al. (1984). Acta Met., submitted for publication.
(60) Morris, W. L., et al. (1981). Eng. Fract. Mech., 18, 871-977.
(61) Newman, J. C. (1983). Behavior of Short Cracks in Airframe Components, vol. CP 328, pp. 7.1-7.16, Advisory Group for Aeronautical Research and Development.
(62) Ritchie, R. O., et al. (1980). J. Eng. Matls. Tech., Trans. ASME, Ser. H, 102, 293-299.
(63) Stewart, A. T. (1980). Eng. Fract. Mech., 13, 463-478.
(64) Suresh, S., et al. (1981). Metall. Trans. A, 12A, 1435-1443.
(65) Scott, P. M., et al. (1983). Corros. Sci., 23, 559-575.
(66) Hartt, W. H., & Rajpathak, S. S. (1983). "Formation of Calcareous Deposits Within Simulated Fatigue Cracks in Seawater," Corrosion/83, Paper No. 62, Houston: NACE.
(67) Suresh, S., et al. (1982). Fatigue Thresholds, eds. J. Backlund, A. Blom and C. J. Beevers, 1, pp. 391-408, Warley, U.K: EMAS.
(68) Suresh, S. & Ritchie, R. O. (1982). Metall. Trans. A, 13A, 1627-1631.
(69) Esaklul, K. A., et al. (1983). Scripta Met., 17, 1073-1078.
(70) Gangloff, R. P. (1984). unpublished research.
(71) Embrittlement by the Localized Crack Environment (1984). ed. R. P. Gangloff, Warrendale, PA: TMS-AIME, in press.
(72) Lawn, B. R. (1977). Mat. Sci., 13, 277-283.

(73) Turnbull, A. & Thomas, J. G. N. (1982). J. Electrochem. Soc., 129, 1412-1422.
(74) Turnbull, A. (1980). Br. Corros. J., 15, 162-171.
(75) Turnbull, A. (1982). Corros. Sci., 22, 877-893.
(76) Doig, P. & Flewitt, P. E. J. (1983). Metall. Trans. A, 14A, 978-983.
(77) Taunt, R. J. & Charnock, W. (1978). Matl. Sci. Engr., 35, 219-228.
(78) Hartt, W. H., et al. (1978). Corrosion Fatigue Technology, ASTM STP 642, eds. H. C. Craig, Jr., T. W. Crooker, and D. W. Hoeppner, pp. 5-18, Philadelphia: ASTM.
(79) Turnbull, A. (1983). National Physical Laboratory Report No. NPL DMA (D) 363, England.
(80) Jaske, C. E., et al. (1981). MCIC Report 81-42, Columbus, Ohio: Battelle.
(81) Snowdon, K. V. (1963). J. Appl. Phys., 34, 3150-1.
(82) Gangloff, R. P. (1984). Liquid and Solid Metal Induced Embrittlement, ed. M. H. Kamdar, Warrendale, PA: TM AIME, in press.
(83) Bradshaw, F. J. (1967). Scripta Met., 1, 41-43.
(84) Wei, R. P. & Gao, Ming (1983). Scripta Met., 17, 959-962.
(85) Carter, C. S. (1977). Stress Corrosion Cracking and Corrosion Fatigue of Medium and High Strength Steel, Boeing Co. Report, Seattle, Washington.
(86) Brown, B. F. (1976). Stress Corrosion Cracking and Hydrogen Embrittlement of Iron Based Alloys, eds. J. Hockmann, J. Slater, R. D. McCright and R. W. Staehle, pp. 747-750, Houston: NACE.
(87) Sandoz, G., et al. (1970). Corros. Sci., 10, 839-845.
(88) Smyrl, W. H. & Newman, J. (1974). J. Electrochem. Soc., 121, 1000-1007.
(89) Charnock, W. & Taunt, R. J. (1978). Metall. Trans. A, 9A, 880-881.
(90) Bardal, E., et al. (1978). Proc. Conf. European Offshore Steel Research, pp. 415-436, London: Welding Institute.
(91) Cotton, H. C. (1979). Proc. Inst. Mech. Engrs., 193, 193-206.
(92) Jones, B. F. (1984). Embrittlement by the Localized Crack Environment, ed. R. P. Gangloff, Warrendale, PA: TMS-AIME, in press.
(93) Barsom, J. M. (1971). Int. J. Frac. Mech., 7, 164-182.

END

9-87

DTIC